Brain connectivity network models based on multi-modal MRI to study brain reorganization of prenatal origin using intrauterine growth restriction as a model

Dafnis Batallé Bolaño

Brain connectivity network models based on multi-modal MRI to study brain reorganization of prenatal origin using intrauterine growth restriction as a model

Dafnis Batallé Bolaño

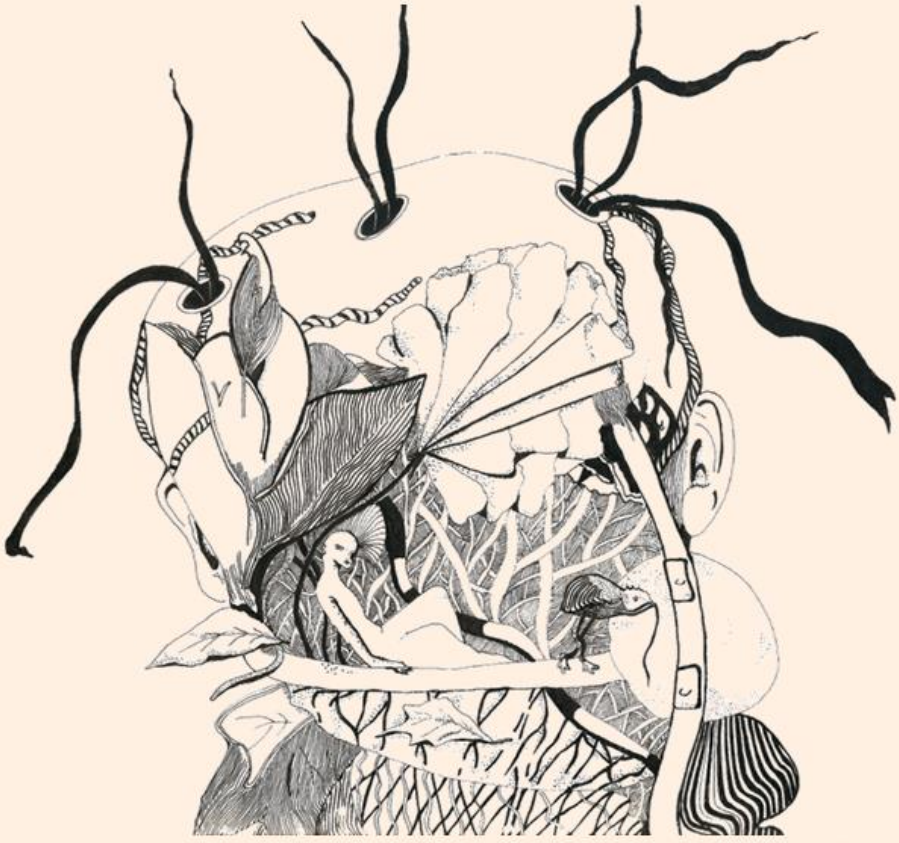

Universitat de Barcelona

DOCTORAL THESIS

Programa de Doctorat en Biomedicina
Universitat de Barcelona

Brain connectivity network models based on multi-modal MRI to study brain reorganization of prenatal origin using intrauterine growth restriction as a model

Dafnis BATALLÉ BOLAÑO

Supervised by

Dr. Elisenda EIXARCH ROCA

Prof. Eduard GRATACÓS SOLSONA

Fetal and Perinatal Medicine Research Group

Hospital Clínic – IDIBAPS – University of Barcelona

2014

CLÍNIC BARCELONA Hospital Universitari

fetal iD FETAL MEDICINE RESEARCH CENTER

IDIBAPS

Cover art illustration by Salomé Bolaño.

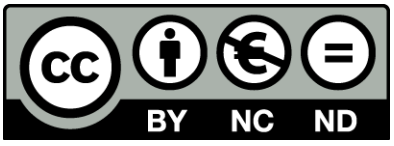

Barcelona, July 2014

This thesis is submitted by Dafnis Batallé Bolaño for the PhD degree of Doctor in Biomedicine of the University of Barcelona, including the mention of "International Doctor" under the direction of Eduard Gratacós Solsona, MD, PhD, Professor of Obstetrics and Gynecology at University of Barcelona and Elisenda Eixarch Roca, MD, PhD, Senior Researcher at Fetal and Perinatal Medicine Research Group, Hospital Clínic, University of Barcelona.

The co-directors declare that Dafnis Batallé Bolaño has conducted under their supervision the studies presented in this thesis at the Fetal and Perinatal Medicine Research Group, IDIBAPS, Hospital Clínic, University of Barcelona. The Thesis has been structured following the normative for PhD theses as a compendium of publications for the degree of Doctor in Biomedicine of the University of Barcelona, and consists in three articles published in first quartile international peer-reviewed journals and one ready for its publication:

- Altered small-world topology of structural brain networks in infants with intrauterine growth restriction and its association with later neurodevelopmental outcome
  Batalle D, Eixarch E, Figueras F, Munoz-Moreno E, Bargallo N, Illa M, Acosta-Rojas R, Amat-Roldan I, Gratacos E
  2012, Neuroimage 60, 1352-1366
  ISI 2012 IF = 6.252, 2/14 (NeuroImage), 20/144 (Neurosciences)

- Normalization of similarity-based individual brain networks from gray matter MRI and its association with neurodevelopment in infants with intrauterine growth restriction
  Batalle D, Munoz-Moreno E, Figueras F, Bargallo N, Eixarch E, Gratacos E
  2013, Neuroimage 83C, 901-911.
  ISI 2012 IF = 6.252, 2/14 (NeuroImage), 20/144 (Neurosciences)

- Long-term reorganization of structural brain networks in a rabbit model of intrauterine growth restriction
  Batalle D, Muñoz-Moreno E, Arbat-Plana A, Illa M, Figueras F, Eixarch E, Gratacos E
  2014, Neuroimage, *In Press*
  ISI 2012 IF = 6.252, 2/14 (NeuroImage), 20/144 (Neurosciences)

- Altered resting-state whole-brain functional brain networks of neonates with intrauterine growth restriction
  Batalle D, Muñoz-Moreno E, Tornador C, Bargallo N, Deco G, Eixarch E, Gratacos E
  Ready to be submitted.

The co-directors confirm that Dafnis Batallé substantially contributed to all the studies presented. He participated into the study design, pre- and post-processed the data, developed algorithms and scripts, analyzed the results, wrote first drafts and revised the final version of all the presented papers.

The co-directors also confirm that none of the co-authors has used, or is going to use any of the articles here presented in another PhD Thesis.



Prof. Eduard Gratacós Solsona Dr. Elisenda Eixarch Roca Dafnis Batallé Bolaño

“This is the greatest damn thing about the universe.
That we can know so much, recognize so much,
dissect, do everything, and we can’t grasp it.”

Henry Miller

TABLE OF CONTENTS

ABBREVIATIONS

AAL: anatomical automatic labeling

ADHD: attention deficit hyperactive disorder

ASD: autism spectrum disorder

BOLD: blood-oxygen-level dependent

BSID-III: Bayley scale for infant and toddler development, third edition

CSF: cerebrospinal fluid

DSI: diffusion spectrum imaging

DTI: diffusion tensor imaging

FA: fractional anisotropy

FD: fiber density

fMRI: functional magnetic resonance imaging

FN: fiber number

GA: gestational age

GFA: general fractional anisotropy

GM: gray matter

ICA: independent component analysis

IUGR: intrauterine growth restriction

MRI: magnetic resonance imaging

NBAS: neonatal behavioral assessment scale

RSN: resting state networks

WM: white matter

1. STRUCTURE

This PhD Thesis is mainly structured in four projects, covering brain networks of different modalities (structural, diffusion and functional MRI) and different sets of population representing the evolution of IUGR at different ages (neonates, one-year-old infants, and an animal model of long-term IUGR equivalent to pre-adolescent age). With these means, we aimed to assess systematically the information that can be obtained from the analysis of brain networks of IUGR, and to propose potential biomarkers of altered neurodevelopment in such population. Each project has led to a publication accepted, or ready to be submitted, in international peer-reviewed journals:

- **PROJECT 1: Brain networks of diffusion MRI in one-year-old infants with IUGR**

  Altered small-world topology of structural brain networks in infants with intrauterine growth restriction and its association with later neurodevelopmental outcome

  Batalle D, Eixarch E, Figueras F, Muñoz-Moreno E, Bargallo N, Illa M, Acosta-Rojas R, Amat-Roldan I, Gratacos E

  2012, Neuroimage 60, 1352-1366

- **PROJECT 2: Brain networks of GM morphology similarity in one-year-old infants with IUGR**

  Normalization of similarity-based individual brain networks from gray matter MRI and its association with neurodevelopment in infants with intrauterine growth restriction

  Batalle D, Muñoz-Moreno E, Figueras F, Bargallo N, Eixarch E, Gratacos E

  2013, Neuroimage 83C, 901-911.

- **PROJECT 3: Brain networks of diffusion MRI in a rabbit model of IUGR at pre-adolescent age**

  Long-term reorganization of structural brain networks in a rabbit model of intrauterine growth restriction

  Batalle D, Muñoz-Moreno E, Arbat-Plana A, Illa M, Figueras F, Eixarch E, Gratacos E

  2014, Neuroimage, *In Press*

- **PROJECT 4: Brain networks of functional MRI in neonates with IUGR**

  Altered resting-state whole-brain functional brain networks of neonates with intrauterine growth restriction

  Batalle D, Muñoz-Moreno E, Tornador C, Bargallo N, Deco G, Eixarch E, Gratacos E

  Ready to be submitted.

Supplementary results that cover brain networks from diffusion MRI in neonatal subjects and brain networks from functional MRI in one-year-old infants are also provided for the sake of completeness. A general introduction and a summary of the methodology used are included prior to the presentation of the results, which consist in a copy of each published paper. A section summarizing the results obtained in the four projects and a general discussion and conclusions of the projects are included as well.

2. GENERAL INTRODUCTION

2.1. Intrauterine growth restriction

Intrauterine growth restriction (IUGR) due to placental insufficiency affects 5-10% of all pregnancies and it is a leading cause of fetal morbidity and mortality (Jarvis et al., 2003; Kady and Gardosi, 2004). Reduction of placental blood flow results in sustained exposure to hypoxemia and undernutrition (Baschat, 2004) and this has profound consequences on the developing brain (Rees et al., 2011). A substantial number of studies have described associations between IUGR and neurodevelopmental and cognitive dysfunctions in neonatal period (Bassan et al., 2011; Figueras et al., 2009), childhood (Bassan et al., 2011; Eixarch et al., 2008; Feldman and Eidelman, 2006; Geva et al., 2006a; Geva et al., 2006b; Leitner et al., 2007; McCarton et al., 1996; Scherjon et al., 2000), and adulthood (Løhaugen et al., 2013). Hence, the characterization of underlying brain alterations supporting this dysfunctions and the prediction of the subset of the population with a higher risk of altered neurodevelopmental outcomes are among the challenges of modern fetal medicine and pediatrics. Importantly, the development of imaging biomarkers is an urgent clinical and experimental need (Ment et al., 2009). However, this goal is hampered by the limited understanding of the brain reorganization processes leading to poor neurodevelopment in IUGR children and the lack of suitable imaging biomarkers in fetal or early life

2.2. Magnetic Resonance Imaging

Magnetic resonance imaging (MRI) is a non-invasive technique that allows studying tissue properties and structures based on their response to radio-frequency pulses. Acquisition parameters can be tuned to obtain different contrast in the images, highlighting specific features of the tissue. Since the seminal work of Carr (Carr, 1953), Damadian (Damadian, 1971), Lauterbur (Lauterbur, 1973) and Mansfield (Mansfield and Maudsley, 1977), MRI has significantly evolved into one of the main imaging techniques applied widely both for clinical practice and research. Briefly, generation of images from magnetic resonance is based on the detection of radio-frequency signal of excited nuclei in response to radio frequency pulses applied at a given frequency of resonance. MRI acquisition requires submitting the tissue to a constant strong magnetic field. Importantly, given the good contrast provided

between gray matter (GM) and white matter (WM), and its non-invasive nature, during the last decades MRI has become one of the main techniques used to obtain neuroimaging data and has been a useful tool to improve scientific understanding of structure and function of the brain.

Typical MRI techniques rely on the spin-lattice relaxation time (T1) or spin-spin relaxation time (T2) in order to obtain an anatomical map of the tissue under study. Given that different tissues have different magnetic properties (relaxation times), they gave different intensities in the acquired images. These contrast images have been widely used to identify different regions and tissues of the brain in a manual or automatic manner, allowing the systematic study of different features of the brain including volume and shape of different areas in health and disease. But MRI has huge potential besides anatomical mapping using "classical" MRI neuroimaging, and in the last decades two different specific MRI techniques have arisen, being demonstrated to be very relevant for the better understanding of brain structure and function: diffusion MRI and functional MRI.

2.2.1. Diffusion MRI

Based on the work of Stejskal and Tanner (Stejskal and Tanner, 1965), that defined an experiment to measure diffusion by means of magnetic resonance, Le Bihan developed the idea that diffusion of liver tumors would result in low values due to movement restriction of water molecules (Le Bihan and Breton, 1985). This seminal idea evolved into what today is known as diffusion MRI, a technique that allows measuring the restriction of water diffusion at each point (voxel) of different tissue, but especially important for the study of the brain, where myelinated WM strongly restricts water diffusion. Besides using the information obtained with diffusion MRI to assign contrasts in cross sectional images, mathematical models of the restriction of water diffusion can be applied in order to reconstruct neural tracts. The most used of these models up today has been diffusion tensor imaging (DTI). This model describes the diffusion in each point (voxel) by a second order symmetric tensor: the diffusion tensor, providing information about the diffusion direction and amount. From this tensor, the *anisotropy* or *isotropy* of the diffusion of the water in a

given tissue can be assessed, a feature that has been related with the myelination and density of axons in WM tissue (Pierpaoli and Basser, 1996). There are different ways of measuring anisotropy, being one of the most common parameter the fractional anisotropy (FA) (Basser and Pierpaoli, 1996). Diffusion tensor model assumes a Gaussian distribution for diffusion, an assumption that fails when modeling different fiber population crossing at the same point. For this reason, other techniques have been developed to characterize the diffusion in each point of the brain with a higher angular resolution (Hagmann et al., 2006), involving both different diffusion models and advanced acquisition protocols. This is the case of Q-Ball imaging (Tuch, 2004), or diffusion spectrum imaging (DSI) (Wedeen et al., 2005), that overcome some of the limitations of DTI, including the ability to solve fibers crossings in the same point. Besides the model or acquisition scheme used, one of the main advantages of modeling diffusion is the possibility to obtain useful information of the structural connectivity of the brain, being diffusion orientation related to WM fiber tract pathways. Therefore, using the diffusion information at each voxel, a three-dimensional map of streamlines associated to WM fiber trajectories can be estimated, what is known as a *tractography*. Importantly, integrating the information of the estimated streamlines with anatomical information of the regions of the brain it is possible to generate a structural brain network.

2.2.2. Functional MRI

In the other hand, roughly based on 19th century ideas of Angelo Mosso of measuring the redistribution of blood during emotional and intellectual activity (Sandrone et al., 2014), three studies in the 1990s suggested the use of a blood-oxygen-level dependent (BOLD) signal to assess blood flow at each point of the brain, associating these measures with neuronal activation (Bandettini et al., 1992; Kwong et al., 1991; Ogawa et al., 1990). These experiments lead to the technique today known as functional MRI (fMRI). The main idea is to use statistical models to assess changes in magnetization between tissues with high and low level of oxygen. Briefly, hemoglobin behaves as a diamagnetic material when is oxygenated but as a paramagnetic material when is deoxygenated. In the presence of an external magnetic field, atomic spins of paramagnetic material align with the field direction,

observing an increase in the magnetic signal, while atomic spins of diamagnetic material aligns perpendicularly to the magnetic field, observing a decrease in the measured signal. Measuring this BOLD signal among several instants of time allows to obtain time series of the evolution of oxygenation-deoxygenation at each point of the brain, which has been associated with neural activity (Logothetis et al., 2001). fMRI studies of health and disease have proliferated during the last years, using a variety of techniques in order to statistically assess brain activity individually and at group level. Importantly, one of the techniques with highest success has been the use of block and event-related designs (Donaldson and Buckner, 2001), allowing to assess the spatial specific brain activations produced by a cognitive or emotional response based on the comparison of baseline versus activity conditions. Of notably importance was the developing of resting-state fMRI (rs-fMRI), based on the evaluation of regional interactions that are produced when the brain is not performing an explicit task. This technique has its fundamentals on the seminal study of Biswal and colleagues showing low frequency fluctuations in resting brain with a high degree of temporal correlation and suggesting its association with functional connectivity of the brain (Biswal et al., 1995). Posterior analysis of these signals with different techniques, including independent component analysis (ICA), showed the existence of anti-correlated differentiated spatial relations between different areas of the brain suggesting the existence of functional brain networks active at rest, including the well-known default mode network (Fox et al., 2005). Importantly, low-frequency fluctuations have also been used to model whole-brain functional brain networks based on partial correlations of averaged BOLD signal (Salvador et al., 2005).

2.3. Magnetic Resonance Imaging in IUGR

With the significant advance of MRI in the recent years, the brain alterations and reorganization underlying neurodevelopmental alterations associated with IUGR are starting to be elucidated. It has been suggested that brain reorganization starts in utero, where different patterns of cortical development (Egaña-Ugrinovic et al., 2013) and altered quantitative MRI texture (Sanz-Cortes et al., 2013) have been shown in IUGR, being related with later altered neurodevelopment. At neonatal period IUGR has been reported to have

decreased volume in GM (Tolsa et al., 2004) and hippocampus (Lodygensky et al., 2008) and discordant patterns of gyrification (Dubois et al., 2008). Persistence of structural changes at one year of age has also been described, demonstrating reduced volumes of GM in the temporal, parietal, frontal, and insular regions (Padilla et al., 2011) and decrease in fractal dimension of both GM and WM which correlates with specific developmental difficulties (Esteban et al., 2010). Studies on IUGR later in life have reported changes in regional brain volumes and cortical thickness in 4 to 7-year-old children (De Bie et al., 2011), reduced volumes for thalamus and cerebellar white matter (Martinussen et al., 2009), and thinning of corpus callosum together with a general WM reduction (Skranes et al., 2005) in adolescents. However, despite these studies are useful to demonstrate disease-related differences, the ability to use MRI information to generate individual predictive biomarkers in IUGR is limited, existing a necessity to better characterize the brain reorganization underlying neurodevelopmental and cognitive dysfunctions in IUGR.

2.4. Brain Networks based in MRI

The use of brain network models based in different modalities of MRI is an emerging approach to extract information associated with brain organization. Based on anatomical and diffusion MRI acquisitions it is possible to obtain structural brain networks, while functional brain networks are obtained from fMRI. In addition, the use of graph theory analyses of brain networks from both a structural and a functional origin has been a useful tool to characterize brain organization by use of a few comprehensible parameters. Graph theory tools have been proposed to allow quantifying brain network infrastructure (average degree and strength), integration (global efficiency) and segregation (local efficiency) of the global functioning of a brain network (Rubinov and Sporns, 2009). Of further interest is the ability to explore regional differences by assessing graph theory characteristics of the regional networks associated to a given region.

2.4.1. Structural brain networks

Diffusion MRI brain networks are based in the assessment of the structural macroscopic connectivity of the brain obtained from the reconstruction of WM tracts with a

tractography. This approach has been coined “connectomics” (Hagmann, 2005), and allows exhaustively mapping inter-regional structural connectivity within the brain to build a graph model of its neural circuitry known as brain network or connectome (Sporns et al., 2005). Particularly, connectomics extracts a number of "image features" after intensive processing that integrates structural information of the individual, related to anatomical brain regions and neuronal connectivity, to compute adjacency matrices that represent brain networks or graph models of a particular subject brain. Connectomics has been successfully utilized to construct structural brain networks in healthy populations (Gong et al., 2009; Hagmann et al., 2008; Iturria-Medina et al., 2008), being its network properties associated with sex and brain size (Yan et al., 2010), intelligence (Li et al., 2009), and specific cognitive abilities in old age (Wen et al., 2011). It also has been used to report altered group network topology features in adults and adolescents suffering different pathologies such as schizophrenia (Wang et al., 2012), Alzheimer's disease (Lo et al., 2010; Wee et al., 2010), multiple sclerosis (Shu et al., 2011), and early blindness (Shu et al., 2009). These studies suggest the potential of brain networks based in diffusion MRI to develop biomarkers for disease diagnosis and treatment effects monitoring. Concerning the use of brain network analysis in pediatric subjects, it has been applied to assess normal development of the human brain during infancy with a longitudinal cohort of 2 weeks, 1 year and 2 years of age (Yap et al., 2011) and childhood and adolescence in subjects from 2 to 18 years of age (Hagmann et al., 2010). However, no studies in infants with perinatal conditions had been conducted prior to the first study presented in this thesis (**PROJECT 1**).

Whether brain reorganization produced by IUGR persists at long-term (adolescence and adult period) and whether connectomic analysis could be a suitable tool to characterize the patterns induced by this condition is still unknown. Indeed, the assessment of long-term effects produced by IUGR in the human brain is a challenging task, limited by the influence of uncontrolled environmental factors (Hall and Perona, 2012) and the difficulty of obtaining sufficiently large sample sizes. Notwithstanding, the induction of IUGR in rabbit models has been proven to reproduce major features of human IUGR (Bassan et al., 2000; Eixarch et al., 2009; Eixarch et al., 2011). Importantly, white matter maturation process in

rabbit is closer to humans than other species, since it starts in intrauterine period (Derrick et al., 2007). Hence, albeit their obvious limitations, the rabbit model of IUGR may be a useful tool to analyze long-term brain remodeling associated to this condition. Importantly, animal models could play a key role in the definition of image biomarkers for early diagnosis that are critical to demonstrate changes after the application of experimental therapies, especially when those should be tested in fetuses or neonates. Besides highly reproducible experimental conditions, high quality MRI with long acquisition times can be performed in isolated whole brain preparations. Using this IUGR rabbit model, regional brain changes in fractional anisotropy, correlated with poorer outcome in neurobehavioral tests has been reported in newborns (Eixarch et al., 2012), some of them persisting in preadolescent period, where changes in the connectivity of anxiety, attention and memory networks has also been shown (Illa et al., 2013). With the recent development of an MRI rabbit brain atlas (Muñoz-Moreno et al., 2013), the possibility to obtain whole brain structural networks based on diffusion MRI arises. This opens the opportunity to assess long-term network reorganization associated with functional impairments without *a priori* hypothesis, taking advantage of the huge potential of graph theory measures to characterize brain functioning and organization (Bassett and Bullmore, 2009). Hence, we were able to assess long-term brain reorganization produced by IUGR with a rabbit animal model (**PROJECT 3**), complementing the first study in one-year-old infants with IUGR presented in this thesis.

Although the use of diffusion MRI is being more frequently applied, this technique is still not very common in clinical practice compared with conventional anatomical T1 acquisitions. In addition, the requirement of higher acquisition times and the extreme sensitivity to motion artifacts of diffusion MRI is critical when scanning subjects where control of movements cannot be ensured, such as fetuses or infants. Based on the concept that correlations of GM features such as volume or cortical thickness across groups of individuals are associated with brain connectivity (He et al., 2007), anatomical T1 acquisitions have been used to obtain group connectomes that allow a better understanding of brain circuitry in health and disease (Bassett et al., 2008; Fan et al., 2011; He et al., 2008). However, in order to develop individual biomarkers, it is indispensable to

extract individual brain networks, which typically requires diffusion and/or functional MRI. Recently, a number of published reports have suggested approaches to extract individual brain networks based on the analysis of the similarities of GM features (Raj et al., 2010; Tijms et al., 2013; Tijms et al., 2012; Zhou et al., 2011). These methodologies can benefit from the power of brain network analysis to predict individual neurological outcome, albeit using conventional T1 acquisitions. To which extent these networks resemble anatomical brain networks is an issue that remains to be elucidated. But regardless of whether the brain networks reconstructed resemble actual anatomical networks or just serve to analyze cortical pattern similarities, this approach has the potential to become a powerful tool in clinical practice if it allows obtaining features associated with the neurological outcome of different diseases. Its potential to assess alterations in a condition of perinatal origin is demonstrated in the second study presented in this thesis (**PROJECT 2**).

2.4.2. Functional brain networks

Several studies have demonstrated the feasibility to use rs-fMRI to characterize the functional organization of the healthy neonatal brain, opening the opportunity to also characterize the alterations in brain organization produced by pathologies of prenatal origin such as IUGR. Using ICA, the emergence of synchronized spontaneous low-frequency fMRI BOLD signals exhibiting resting state networks spatially matching some of those previously described in the adult brain has been demonstrated in studies of cross-sectional term and preterm infants both during light sedation and natural sleep (Fransson et al., 2009; Fransson et al., 2007). Both ICA and seed-based correlation approaches have also been used in longitudinal studies of preterm and term infants showing the emergence of connections partially or completely matching several resting state networks (RSN) during neonatal development, including the default mode network (Doria et al., 2010; Gao et al., 2009; Lin et al., 2008; Smyser et al., 2010). Notwithstanding, studies considering whole-brain functional brain networks of the neonatal brain are scarce in the literature. Neonatal networks composed of selected ROIs were studied by Gao et al. (Gao et al., 2009), while voxel-wise networks obtained in a normalized space were obtained by Fransson et al. (Fransson et al., 2011), showing the presence of cortical hubs and sub-networks associated

to those hubs. In the present thesis, we present a study based on partial correlations of the rs-fMRI BOLD signals averaged into 90 brain regions of neonatal subjects for the first time, allowing the assessing of functional brain reorganization produced by IUGR at neonatal age (**PROJECT 4**).

3. HYPOTHESIS AND OBJECTIVES

3.1. Hypothesis

The main hypothesis of this PhD Thesis is that abnormal neurodevelopment in children who had suffered IUGR has a substrate in their structural and functional connectivity organization.

The specific hypotheses are:

1. Structural brain networks from diffusion MRI can characterize the structural brain reorganization produced by IUGR at one year of age, being associated with neurodevelopmental alterations observed later in life.
    a. Techniques to obtain brain networks from diffusion MRI can be adapted to pediatric population.
    b. Infants with IUGR present a structural brain reorganization that can be assessed with global and regional graph theory features.
    c. Changes in structural brain connectivity at one year of age produced by IUGR are associated with neurodevelopmental alterations observed later in life.

2. Individual structural brain networks based on morphology features of GM from anatomical MRI can demonstrate differences produced by IUGR, being associated with neurodevelopmental alterations observed later in life.
    a. Existing techniques to obtain structural brain networks based on morphology features of GM can be adapted to pediatric population.
    b. These techniques can be further developed in order to obtain networks of a fixed size for all individuals, based on an anatomical atlas.
    c. The brain networks obtained with this technique can assess differences in the brain organization produced by IUGR.
    d. Changes in network features obtained with this technique are associated with neurodevelopmental alterations observed later in life.

3. Structural brain networks based on diffusion MRI can characterize brain reorganization persisting at long-term in a rabbit model of IUGR, being associated with neurobehavioral performance.
    a. Techniques to obtain structural brain networks from diffusion MRI can be adapted to pre-adolescent rabbit.
    b. Structural brain reorganization produced by IUGR can be assessed at pre-adolescence period in a rabbit model of IUGR.
    c. Changes in structural brain connectivity at pre-adolescence age can be associated with neurobehavioral outcomes in a rabbit model of IUGR.

4. Functional brain reorganization produced by IUGR can be assessed at neonatal age with functional brain networks obtained with acquisition during natural sleep, being associated with neurobehavioral outcomes.
    a. Methods to obtain whole-brain functional brain networks based in an anatomical atlas can be adapted to neonatal age.
    b. Global and regional functional brain network features can assess the functional reorganization produced by IUGR at neonatal age.
    c. Changes in functional brain connectivity can be associated to altered neurobehavior.

3.2. Objectives

The main objective of this PhD thesis is to use graph theory features of brain networks in order to assess brain reorganization produced by perinatal brain damage and to associate this reorganization with abnormal neurodevelopment.

The specific objectives are:

1. To assess the structural brain reorganization of one-year-old infants who suffered IUGR and its association with neurodevelopmental alterations observed later in life.
    a. To adapt state-of-the-art techniques to a pediatric population.
    b. To assess differences in global and regional structural network features in a one-year-old population who suffered IUGR when compared with controls.
    c. To associate structural network features obtained at one year of age with altered neurodevelopment at two years of age.

2. To assess the alterations in structural brain networks based on morphology features of GM from anatomical MRI in one-year-old infants who suffered IUGR and its association with neurodevelopmental alterations observed later in life.
    a. To adapt existing techniques to a pediatric population.
    b. To further develop existing techniques in order to obtain networks of a fixed size for all the individuals based on a brain atlas (AAL).
    c. To characterize alterations in global and regional brain network features obtained with this technique in a one-year-old population of infants who suffered IUGR.
    d. To associate the network features obtained with this technique with altered neurodevelopment at two years of age.

3. To assess the alterations in structural brain networks based on diffusion MRI in a rabbit model of IUGR at long-term and its association with neurobehavioral performance.

   a. To adapt existing techniques to the rabbit brain at pre-adolescence age.
   b. To characterize alterations in global and regional structural network features of the long-term rabbit model of IUGR in pre-adolescent period.
   c. To associate structural network features obtained in the rabbit model of IUGR with altered neurobehavioral scores.

4. To characterize functional brain network reorganization produced by IUGR at neonatal age and its association with altered neurobehavior.
   a. To adapt methods used in adulthood to neonatal population in order to obtain whole-brain functional brain networks based on a brain atlas (AAL).
   b. To characterize alterations in global and regional functional brain network features in a population of neonates who suffered IUGR.
   c. To associate functional network features obtained with altered neurobehavior.

4. SUMMARY OF THE METHODOLOGY

Most of the methodology of the present Ph.D. Thesis is transversal in several of the projects; however, having to be adapted for the specific population and MRI modality used. This is the case of brain parcellation (adapted to one-year-old infants, neonates and rabbit animal model), brain network computation and graph theory analysis (slightly different depending on the use of structural, diffusion or functional MRI). Here the most important points of the methodology used are summarized.

4.1. Subjects

This Ph.D. Thesis is part of a larger prospective research program on IUGR involving fetal assessment and short- and long-term postnatal follow-up at Hospital Clínic of Barcelona. In this context, the present thesis uses the existent large database of MRI data of our research group that includes more than 100 IUGR and 100 control fetuses appropriate for gestational age born between October 2007 and December 2010 that were scanned at one year of age. Structural and diffusion MRI acquisitions of this population were used for **PROJECT 1** and **PROJECT 2**. In addition, from April of 2012, our group started a new protocol to acquire neonatal brain MRI during natural sleep, having acquired around 30 controls and 30 subjects with IUGR having structural, diffusion, and/or functional MRI. 13 controls and 20 IUGR with a successful anatomical and functional MRI acquisition of this population were used for **PROJECT 4**. IUGR was defined as a fetal estimated weight below 10th centile according to local reference standards (Figueras et al., 2008) confirmed at birth. Control subjects were defined as fetuses with fetal estimated weight between the 10th and 90th customized centiles according to local reference (Figueras et al., 2008) confirmed at birth and were sampled from our general pregnant women population. Pregnancies were dated according to the first-trimester crown-rump length measurements (Robinson and Fleming, 1975). Infants with chromosomal, genetic, or structural defects and signs of intrauterine infection or neonatal early onset sepsis as defined by positive blood culture within the first 72 h of life were excluded. Neonatal data were prospectively recorded including: gestational age (GA), birth weight, gender, Apgar at 5 min, umbilical artery pH and neonatal complications including late-onset sepsis, necrotizing enterocolitis and chronic lung disease (defined as oxygen need at 36 weeks postmenstrual age). Maternal education was recorded

as low, intermediate or high educational level. Maternal smoking status during pregnancy and breastfeeding were also recorded. Growth parameters (weight, length, body mass index and head circumference) were recorded at 12 months and were normalized for local standards (Sobradillo et al., 2004). In **PROJECT 2** and **PROJECT 4** only subjects with late-onset IUGR were included, defined as those infants meeting the requirements to be considered IUGR as previously described, and in addition, were delivered after 34 weeks of pregnancy.

PROJECT 3 is based on a rabbit animal model of IUGR that our group has developed (Eixarch et al., 2009; Eixarch et al., 2011). Briefly, IUGR was induced by means of a ligation of 40-50% of uteroplacental vessels at 25 days of gestation. Cesarean section was performed at 30 days of gestation and living pups were obtained. On the 70th postnatal day, which is considered to be equivalent to pre-adolescense period in humans in terms of sexual maturity, neurobehavioral tests were applied and the rabbits were sacrificed thereafter. The brains were collected and fixed with 4% paraformaldehyde phosphate-buffer saline (PBS) and ex-vivo MRI acquisition was performed, including anatomical and diffusion MRI sequences with 126 gradient direction, which allowed to perform a high angular tractography reconstruction, with Q-Ball (Tuch, 2004).

4.2. Neurobehavioral and neurodevelopmental assessment

In **PROJECT 1** and **PROJECT 2** neurodevelopment during early infancy was assessed at 24 months of corrected age with the Bayley scale for infant and toddler development, third edition (BSID-III), which evaluates five distinct scales: cognitive; language; motor; socio-emotional behavior; and adaptive behavior. The scales have scores with a mean of 100 and S.D. of 15. Abnormal BSID-III is defined as a score below 85 in any of the five different scales (Anderson et al., 2010).

In **PROJECT 4** neurobehavioral outcome of newborns was assessed with neonatal behavioral assessment scale (NBAS) (Nugent and Brazelton, 2000), which evaluates cortical and subcortical functions in 35 items grouped into 6 clusters: habituation, motor, social-interactive, organization of state, regulation of state, autonomous nervous system and

attention (Sagiv et al., 2008). Cluster scores were defined as abnormal if they have a z-score below minus one. NBAS severity score was defined as the number of abnormal NBAS clusters for each subject.

In the rabbit animal model of IUGR (**PROJECT 3**), neurobehavior was assessed at +70 postnatal days by means of the Open Field Behavioral Task which evaluates anxiety and attention and the Object Recognition Task that evaluates short-term memory as well as attention (Illa et al., 2013).

4.3. Automatic brain segmentation

In human subjects (**PROJECT 1, 2 and 4**) Anatomical Automatic Labeling (AAL) atlas (Tzourio-Mazoyer et al., 2002) was used to parcellate each subject brain. It has recently been adapted to a pediatric population (Shi et al., 2011) and is available online (http://bric.unc.edu/ideagroup/free-softwares/unc-infant-0-1-2-atlases/). In order to automatically parcellate each subject brain using this atlas, we have used a customized software implementing a consistent version (Tristan-Vega and Arribas, 2007) of a block matching algorithm (Warfield et al., 2002), allowing to obtain an elastic transformation matching the template with each subject anatomical T1 or T2 volume. The labels of AAL atlas were propagated to each structural MRI acquisition of our subjects using this elastic transformation, and transformed to diffusion native space with the previously calculated affine transformation. Discrete labeling values were preserved by nearest neighbor interpolation for both transformations.

In order to automatically parcellate rabbit brain MRI acquisitions (**PROJECT 3**), we have used an MRI atlas developed by our group, including 44 regions of cortical and deep GM (Muñoz-Moreno et al., 2013). The same block matching algorithm used to register human brain volumes was also used in the animal model, being able to estimate an elastic transformation matching the rabbit brain atlas with each individual.

4.4. Connectivity inference and brain network construction

The connectivity inference between regions of the brain was performed with different techniques depending on the MRI modality used. The gold standard to obtain structural brain networks is tractography from diffusion MRI data which estimate white matter tracts that connect each pair of cortical regions. We used DTI reconstruction for human subjects (**PROJECT 1**) and Q-Ball for the experimental animal model (**PROJECT 3**).

Structural connectivity has also been inferred from conventional anatomical MRI (T1 weighted volumes) by means of the correlation of morphological features, specifically by inter-individual correlation of cortical thickness or GM volumes of each pair of regions (He et al., 2007). This approach has the advantage of allowing the construction of brain networks from a much simpler and faster acquisition, but the inconvenient of only allowing obtaining group brain networks, which makes it unpractical for individualized prediction of abnormal neurodevelopment. Notwithstanding, recently it has been proposed an approach to obtain individual structural brain networks from morphological features (Raj et al., 2010; Tijms et al., 2012). One of the objectives of the proposed PhD thesis was to adapt and implement Tijms' methodology in our one-year-old infants' data with some novel modifications in order to normalize the size of the brain network obtained based on an anatomical atlas, and hence being able to fairly compare between subjects (**PROJECT 2**).

Functional resting-state brain networks have been previously calculated in pediatric population from the analysis and correlation of resting-state functional BOLD MRI time series (Doria et al., 2010; Fransson et al., 2011; Fransson et al., 2007; Smyser et al., 2011), however, to the best of our knowledge, it has never been performed a whole brain connectivity network based on pair-to-pair regional correlation of a neonatal or infant population (hence allowing a graph theory characterization). In the present Ph.D. Thesis, we adapted the methodology used with this goal in adults (Zeng et al., 2012) to our neonatal population, in order to assess the effects of IUGR in the neonatal functional brain network (**PROJECT 4**). Briefly, T2-weighted volumes were skull-striped (Smith, 2002) and segmented into WM, GM and cerebrospinal fluid (CSF) (Ashburner and Friston, 2005) using neonatal

tissue probability maps (Shi et al., 2011). AAL atlas (Tzourio-Mazoyer et al., 2002) adapted to neonatal population in a T2-weighted template (Shi et al., 2011) was used to parcellate each subject' brain into 90 regions based on an elastic transformation. Image preprocessing included correction of intra-volume time differences and inter-volume geometric displacements, regression of head motion effects in the signal, average of time series corresponding to each ROI and band pass filtering (0.01 – 0.15 Hz). Network edges were calculated as the partial correlation coefficients obtained between the average signals of each pair of ROIs excluding the effects of the signal of the other 88 ROIs.

4.5. Network analysis

Network analysis of structural brain networks enables a refinement of image features obtained from MRI. As brain networks are defined by nodes (regions) and edges that connect pairs of nodes, which are represented mathematically by adjacency matrices or graphs (Hagmann et al., 2007), it is possible to characterize every subject structural brain network with a set of graph theory measures (or equivalently, network features) that summarize the behavior of a network. We mainly studied average degree, global efficiency and local efficiency of each subject brain network at a global level, and nodal degree, betweenness centrality and nodal efficiency of all the nodes of each subject at a regional level. For both global and regional network features, we used the definitions of Rubinov and Sporns (2009) and Brain Connectivity Toolbox (Rubinov and Sporns, 2009) to calculate most of them. Briefly, *N* was defined as the set of all nodes in the network, and *n* as the number of nodes, (i, j) was the link between nodes *i* and *j* and a_{ij} the connection status between node *i* and *j*: $a_{ij} = 1$ when link (i, j) exists and zero otherwise. w_{ij} is defined as the weight of the link (i, j) in weighted networks.

Degree of a node *i* was calculated as $k_i = \sum_{j \in N} a_{ij}$. Shortest path length between nodes *i* and *j* was defined for binary networks as $d_{ij} = \sum a_{uv} \in g_{i \leftrightarrow j}$, where $g_{i \leftrightarrow j}$ is the shortest path (geodesic) between *i* and *j*. Shortest path length was generalized for weighted

networks as $d_{ij}^{w} = \sum a_{uv} \in g_{i \leftrightarrow j}^{w} f(w_{uv})$, where f is a map from weight to length (in our case an inverse map) and $g_{i \leftrightarrow j}^{w}$ is the shortest weighted path between *i* and *j*. Number of triangles around a node *i* was defined as $t_i = \frac{1}{2} \sum_{j,h \in N} a_{ij} a_{ih} a_{jh}$.

Clustering coefficient of a node was defined as the fraction of triangles around that individual node, and is equivalent to the fraction of the node's neighbors that are also neighbors of each other (Watts and Strogatz, 1998). The clustering coefficient of a network, C_p, was defined as the average of each node clustering coefficient (Watts and Strogatz, 1998) :

$$C_p = \frac{1}{n} \sum_{i \in N} C_i = \frac{1}{n} \sum_{i \in N} \frac{2t_i}{k_i \left(k_i - 1 \right)}$$

Characteristic path length of a network, L_p, was defined as the average shortest path length between all pair of nodes (Watts and Strogatz, 1998):

$$L_p = \frac{1}{n} \sum_{i \in N} L_i = \frac{1}{n} \sum_{i \in N} \frac{\sum_{j \in N, j \neq i} d_{ij}}{n-1}$$

Normalized clustering coefficient of a network, γ, and normalized characteristic path length, λ, were defined as $\gamma = \frac{C_p}{C_{p_{rand}}}$ and $\lambda = \frac{L_p}{L_{p_{rand}}}$ respectively, were $C_{p_{rand}}$ and $L_{p_{rand}}$ are the mean clustering coefficient and characteristic path length of matched random networks that preserve the same number of nodes and degree distribution as the real networks (Maslov and Sneppen, 2002).

Global efficiency was defined as the average inverse shortest path length (Latora and Marchiori, 2001):

$$E_{glob} = \frac{1}{n} \sum_{i \in N} \frac{\sum_{j \in N, j \neq i} d_{ij}^{-1}}{n-1},$$

Generalized to weighted networks as:

$$E_{glob} = \frac{1}{n}\sum_{i\in N}\frac{\sum_{j\in N, j\neq i}\left(d_{ij}^{W}\right)^{-1}}{n-1}$$

Nodal efficiency of a node *i* was defined as the inverse of the harmonic mean of the minimum path length between that index node and all other nodes in the network (Achard and Bullmore, 2007):

$$E_{nodal}(i) = \frac{1}{k_i\left(k_1-1\right)}\sum_{j,h\in N, j\neq i} a_{ij}a_{ih}\left[d_{jh}(N_i)\right]^{-1}$$

Where $d_{jh}(N_i)$ is the length of the shortest path between *j* and *h*, which contains only neighbors of *i*.

Local efficiency was defined as the average of Nodal Efficiency of each node:

$$E_{loc} = \frac{1}{n}\sum_{i\in N}E_{nodal}(i) = \frac{1}{n}\sum_{i\in N}\frac{1}{k_i\left(k_i-1\right)}\sum_{j,h\in N,[j,h]\neq i} a_{ij}a_{ih}\left[d_{jh}(N_i)\right]^{-1}$$

Generalized to weighted networks as (Rubinov and Sporns, 2009):

$$E_{local}^{w} = \frac{1}{n}\sum_{i\in N}\frac{1}{k_i\left(k_i-1\right)}\sum_{j,h\in N, j\neq i} w_{ij}w_{ih}\left[d_{jh}^{w}(N_i)\right]^{\frac{1}{3}}$$

Importantly, in order to disentangle brain organization from network infrastructure and be able to study pure organizational components of brain networks, different approaches of network normalization were performed, including normalization by the total energy of each network (neutralizing differences in strength), normalization at each level of cost (neutralizing differences in network density), and a novel approach that normalizes by cost and energy at the same time presented in **PROJECT 4**. Particularly, in order to assess the topology of weighted networks independently of its cost, a set of cost thresholds were applied to each individual weighted network, obtaining a binary network at each cost level (Achard and Bullmore, 2007). This approach allows comparing networks with the same

number of binary connections, and therefore, comparing network features independently of their cost. This approach, however, increases the number of comparisons and the complexity of the results interpretation, as the clinical groups must be compared on each cost threshold level. In order to disentangle connectivity strength from topology in a single value for each graph theory feature, Ginestet et al. (2011) demonstrated the usefulness of integrating each network feature over the entire cost regime. The cost-integrated version of a topological metric $T(\cdot)$ is defined as (Ginestet et al., 2011):

$$T_{CI}(G) = \frac{1}{N_I} \sum_{t=1}^{N_I} T\left(\gamma(G, k_t)\right)$$

Where G is a given weighted graph, $\gamma(G,k)$ is the graph G binarized at cost k_t and N_I is the cardinal of network costs assessed.

With the goal to assess the pure weighted organizational characteristic of the network topology, normalized weighted networks were also calculated for each weighting approach. This normalization was performed by means of dividing each connection weight by the total weight on the network. Hence, normalized weights were calculated as $\mathrm{w}_{\mathrm{X}}^{\mathrm{N}}(\mathrm{i},\mathrm{j}) = \mathrm{w}_{\mathrm{X}}(\mathrm{i},\mathrm{j}) / \sum_{\forall \mathrm{i},\mathrm{j}} \mathrm{w}_{\mathrm{X}}(\mathrm{i},\mathrm{j})$, where "X" is the weighting of the network. By this means, each normalized weight $\mathrm{w}_{\mathrm{X}}^{\mathrm{N}}(\mathrm{i},\mathrm{j})$ corresponds to the percentage of connection weight used in the link between *i* and *j* relative to the total amount of weights in the network. This way the measures performed on normalized weighted networks were independent to the total amount of connectivity strength each subject had, and then assessing only its distribution of weights.

Finally, the effect of differences in strength and density were neutralized at the same time by means of a combination of both methods, obtaining the weighted network at each network cost and normalizing it as described in the strength normalization approach.

5. RESULTS

5.1. PROJECT 1: COPY OF PUBLISHED PAPER

Altered small-world topology of structural brain networks in infants with intrauterine growth restriction and its association with later neurodevelopmental outcome

Batalle D, Eixarch E, Figueras F, Muñoz-Moreno E, Bargallo N, Illa M, Acosta-Rojas R, Amat-Roldan I, Gratacos E

2012, Neuroimage 60, 1352-1366

NeuroImage 60 (2012) 1352–1366

Contents lists available at SciVerse ScienceDirect

NeuroImage

journal homepage: www.elsevier.com/locate/ynimg

Altered small-world topology of structural brain networks in infants with intrauterine growth restriction and its association with later neurodevelopmental outcome

Dafnis Batalle [a,b], Elisenda Eixarch [a,b], Francesc Figueras [a,b], Emma Muñoz-Moreno [a,b], Nuria Bargallo [c], Miriam Illa [a,b], Ruthy Acosta-Rojas [a,b], Ivan Amat-Roldan [a,b], Eduard Gratacos [a,b,*]

[a] Department of Maternal–Fetal Medicine, Institut Clinic de Ginecologia, Obstetricia i Neonatologia (ICGON), Hospital Clinic and Institut d'Investigacions Biomediques August Pi i Sunyer (IDIBAPS), University of Barcelona, Barcelona, Spain
[b] Centro de Investigacion Biomedica en Red de Enfermedades Raras (CIBERER), Barcelona, Spain
[c] Department of Radiology, Centre de Diagnostic per la Imatge, Hospital Clinic, Barcelona, Spain

ARTICLE INFO

Article history:
Received 10 October 2011
Revised 23 December 2011
Accepted 7 January 2012
Available online 18 January 2012

Keywords:
Fetal growth restriction
Brain reorganization
Postnatal development
Diffusion MRI
Connectomics
Bayley Scale for Infant and Toddler Development

ABSTRACT

Intrauterine growth restriction (IUGR) due to placental insufficiency affects 5–10% of all pregnancies and it is associated with a wide range of short- and long-term neurodevelopmental disorders. Prediction of neurodevelopmental outcomes in IUGR is among the clinical challenges of modern fetal medicine and pediatrics. In recent years several studies have used magnetic resonance imaging (MRI) to demonstrate differences in brain structure in IUGR subjects, but the ability to use MRI for individual predictive purposes in IUGR is limited. Recent research suggests that MRI in vivo access to brain connectivity might have the potential to help understanding cognitive and neurodevelopment processes. Specifically, MRI based connectomics is an emerging approach to extract information from MRI data that exhaustively maps inter-regional connectivity within the brain to build a graph model of its neural circuitry known as brain network. In the present study we used diffusion MRI based connectomics to obtain structural brain networks of a prospective cohort of one year old infants (32 controls and 24 IUGR) and analyze the existence of quantifiable brain reorganization of white matter circuitry in IUGR group by means of global and regional graph theory features of brain networks. Based on global and regional analyses of the brain network topology we demonstrated brain reorganization in IUGR infants at one year of age. Specifically, IUGR infants presented decreased global and local weighted efficiency, and a pattern of altered regional graph theory features. By means of binomial logistic regression, we also demonstrated that connectivity measures were associated with abnormal performance in later neurodevelopmental outcome as measured by Bayley Scale for Infant and Toddler Development, Third edition (BSID-III) at two years of age. These findings show the potential of diffusion MRI based connectomics and graph theory based network characteristics for estimating differences in the architecture of neural circuitry and developing imaging biomarkers of poor neurodevelopment outcome in infants with prenatal diseases.

Introduction

Intrauterine growth restriction (IUGR) due to placental insufficiency affects 5–10% of all pregnancies and it is a leading cause of fetal morbidity and mortality (Jarvis et al., 2003; Kady and Gardosi, 2004). Reduction of placental blood flow results in sustained exposure to hypoxemia and undernutrition (Baschat, 2004) and this has profound consequences on the developing brain (Rees et al., 2011). A substantial number of studies have described associations between IUGR and short (Bassan et al., 2011; Figueras et al., 2009) and long-term neurodevelopmental and cognitive dysfunctions (Bassan et al., 2011; Eixarch et al., 2008; Feldman and Eidelman, 2006; Geva et al., 2006a,b; Leitner et al., 2007; McCarton et al., 1996; Scherjon et al., 2000). Prediction of neurodevelopmental outcomes in IUGR is among the clinical challenges of modern fetal medicine and pediatrics. This goal is currently hampered by the limited understanding of the brain reorganization processes leading to poor neurodevelopment in IUGR children and the lack of suitable imaging biomarkers in fetal or early life.

Abbreviations: AAL, Anatomical automatic labeling; BSID-III, Bayley scale for infant development, third edition; CA, Corrected age; DTI, Diffusion tensor imaging; FA, Fractional anisotropy; FN, Fiber number; GA, Gestational age; GM, Gray matter; IUGR, Intrauterine growth restriction; MRI, Magnetic resonance imaging; WM, White matter.

* Corresponding author at: Maternal–Fetal Medicine Department and Research Centre, Hospital Clinic, Universitat de Barcelona, Sabino de Arana 1, 08028 Barcelona, Spain. Fax: +34 93 227 5612.
E-mail addresses: dbatalle@clinic.ub.es (D. Batalle), eixarch@clinic.ub.es (E. Eixarch), ffiguera@clinic.ub.es (F. Figueras), emunozm@clinic.ub.es (E. Muñoz-Moreno), bargallo@clinic.ub.es (N. Bargallo), miriamil@clinic.ub.es (M. Illa), eracosta@clinic.ub.es (R. Acosta-Rojas), iamat@clinic.ub.es (I. Amat-Roldan), egratacos@clinic.ub.es (E. Gratacos).

1053-8119/$ – see front matter © 2012 Elsevier Inc. All rights reserved.
doi:10.1016/j.neuroimage.2012.01.059

In recent years several studies have used magnetic resonance imaging (MRI) to demonstrate differences in brain structure in IUGR subjects. Studies in term neonates have reported decreased volume in gray matter (Tolsa et al., 2004) and hippocampus (Lodygensky et al., 2008), and major delays in cortical development, with discordant patterns of gyrification and a pronounced reduction in cortical expansion (Dubois et al., 2008). Persistence of structural changes at 1-year of age has been recently reported demonstrating reduced volumes of gray matter (GM) in the temporal, parietal, frontal, and insular regions (Padilla et al., 2011) and decrease in fractal dimension of both gray and white matter (WM) which correlate with specific developmental difficulties (Esteban et al., 2010). Despite these studies are useful to demonstrate disease-related differences, the ability to use MRI information to generate individual predictive biomarkers in IUGR is limited.

Recent research suggests that MRI in vivo access to brain connectivity might help understanding cognitive and neurodevelopment processes (Sporns et al., 2005). Connectomics (Hagmann, 2005) is an emerging approach to extract information from different modalities, including MRI data, exhaustively mapping inter-regional connectivity within the brain to build a graph model of its neural circuitry known as brain network or connectome (Bullmore and Sporns, 2009; Sporns et al., 2005). Particularly, connectomics extracts a number of "image features" after intensive processing that integrates structural information of the individual, related to anatomical brain regions and neuronal connectivity, to compute adjacency matrices that represent brain networks or graph models of a particular subject brain. Connectomics provides a framework to compare architecture of brain circuits among different individuals in a direct and elegant manner. In order to assess brain organization, graph theory tools have been proposed to allow quantifying brain network infrastructure, integration and segregation of the global functioning of a brain network (Rubinov and Sporns, 2009). Of further interest is the ability to explore regional differences by assessing graph theory characteristics of the regional networks associated to a given region.

Connectomics has been successfully utilized in different sets of data, including functional MRI, structural MRI and diffusion MRI, to report altered group connectivity parameters in adults and adolescents undergoing diseases such as schizophrenia (Alexander-Bloch et al., 2010; Bassett et al., 2008; Liu et al., 2008), Parkinson's disease (Wu et al., 2009), Alzheimer's disease (He et al., 2008, 2009a; Lo et al., 2010), attention deficit hyperactivity disorder (Wang et al., 2009), and in non-clinical samples as in the study of synesthesia (Hänggi et al., 2011). These studies suggest the potential of MRI based connectomics to develop biomarkers for disease diagnosis and treatment effects monitoring. Among the above MRI modalities diffusion imaging can be of particular interest for the study of the developing brain. Diffusion MRI allows non-invasively assessing in-vivo WM fiber orientation in the brain. In recent years diffusion MRI based connectomics has been used to construct structural brain networks in healthy populations (Gong et al., 2009; Hagmann et al., 2008; Iturria-Medina et al., 2008), being its network properties associated with sex and brain size (Yan et al., 2010), intelligence (Li et al., 2009) and specific cognitive abilities in old age (Wen et al., 2011) and to report altered group network topology features in Alzheimer's disease (Lo et al., 2010; Wee et al., 2010), multiple sclerosis (Shu et al., 2011), schizophrenia (Wang et al., 2012) and early blindness (Shu et al., 2009). Connectomics from diffusion MRI has been applied to assess normal development of the human brain during childhood and adolescence, including subjects from 2 to 18 years of age (Hagmann et al., 2010). Diffusion MRI connectomics in younger children has been used to study a healthy longitudinal cohort of 2 weeks, 1 year and 2 years of age (Yap et al., 2011), but no studies in infants with perinatal conditions have been conducted.

In the present study, we evaluated the hypothesis that diffusion MRI based connectomics could determine quantifiable changes resulting from the existence of brain reorganization in children who suffered IUGR. We used diffusion MRI based connectomics to obtain structural brain networks in one year old infants with and without growth restriction. We analyzed global and regional graph theory features of brain networks explored in previous studies such as infrastructure, integration, segregation and centrality. We evaluated the ability of diffusion MRI based connectomics to demonstrate group differences in global brain network features and localize altered regional networks. Finally, we also explored whether brain network features at one year would be associated with neurodevelopmental outcome at two years of age.

Methods

Subjects

This study was part of a larger prospective research program on IUGR involving fetal assessment and short- and long-term postnatal follow-up at Hospital Clinic (Barcelona-Spain). The study design involved recruitment of a consecutive sample of 83 fetuses: 42 IUGR singleton infants and 41 control fetuses appropriate for gestational age. All individuals were born between October 2007 and November 2009. IUGR was defined as a fetal estimated weight below 10th centile according to local reference standards (Figueras et al., 2008) confirmed at birth. Control subjects were defined as fetuses with fetal estimated weight between the 10th and 90th customized centiles according to local reference (Figueras et al., 2008) confirmed at birth and were sampled from our general pregnant women population during the same period. Pregnancies were dated according to the first-trimester crown-rump length measurements (Robinson and Fleming, 1975). Infants with chromosomal, genetic, or structural defects and signs of intrauterine infection or neonatal early onset sepsis as defined by positive blood culture within the first 72 h of life were excluded from this study. Neonatal data were prospectively recorded including: gestational age (GA), birth weight, gender, Apgar at 5 min, umbilical artery pH and neonatal complications including late-onset sepsis, necrotizing enterocolitis and chronic lung disease (defined as oxygen need at 36 weeks postmenstrual age). Maternal education was recorded as low, intermediate or high educational level. Maternal smoking status during pregnancy and breastfeeding were also recorded. Growth parameters (weight, length, body mass index and head circumference) were recorded at 12 months and were normalized for local standards (Sobradillo et al., 2004). The study protocol was approved by the local Ethics Committee, and written informed consent was obtained from the parents or legal guardians of all participants.

Neurodevelopmental assessment

Neurodevelopmental outcome was assessed at 21 months of corrected age (CA) ($\pm$3 months) with the Bayley Scale for Infant and Toddler Development, Third edition (BSID-III), which evaluates five distinct scales: cognitive; language; motor; socio-emotional behavior; and adaptive behavior. The scales have scores with a mean of 100 and S.D. of 15. Abnormal BSID-III was defined as a score below 85 in any of the five different scales (Anderson et al., 2010). All developmental examinations were performed by a single trained psychologist examiner with previous experience with the BSID-III. The examiner was not informed about the infant medical history.

MRI data acquisition

Children were scanned at 12$\pm$2 months CA, during natural sleep. Structural MRI and diffusion MRI were performed using a TIM TRIO 3.0 T whole body MR scanner (Siemens, Germany). Diffusion images were acquired by using a single-shot Echo-Planar Imaging (SE-EPI) sequence covering 30 diffusion directions with a b-value of 1000 s/

mm^2. All acquired images covered the whole brain, with 3-mm slice thickness with no interslice gap, 40 axial slices and in-plane acquisition matrix of 122×122 with a field of view (FoV) set to 200×200 mm which resulted in a voxel dimension of $1.64\times1.64\times3$ mm^3, repetition time (TR) = 9300 ms, echo time (TE) = 94 ms. An additional image without diffusion weight ($b=0$ s/mm^2) was also acquired. High resolution structural T1 weighted images were obtained by a Magnetization Prepared Rapid Acquisition Gradient Echo (MPRAGE) sequence with the following parameters: 0.9-mm slice thickness with no interslice gap, 192 sagittal slices, in-plane acquisition matrix of 256×256, FoV = 220×220 mm^2, which resulted in a voxel dimension of $0.86\times0.86\times0.9$ mm^3, TR = 2050 ms, TE = 2.41 ms and inversion time (TI) = 1050 ms. All acquired MRI structural and diffusion images were visually inspected for apparent or aberrant artifacts, and subjects excluded accordingly. In addition, structural T2 weighted images were also acquired in order to exclude WM abnormalities. Diffusion weighted images were corrected for eddy currents effects and simple head motions using FMRIB's Diffusion Toolbox (FSL 4.1; www.fmrib.ox.ac.uk/fsl).

White matter brain network construction

The methodology to compute individual connectivity based on MRI acquisitions was composed by a comprehensive integration of standard protocols (Fig. 1).

White matter, gray matter and cerebrospinal fluid segmentation

3D structural volumes were segmented into WM, GM and cerebrospinal fluid (CSF) using the unified segmentation model (Ashburner and Friston, 2005) available at the SPM software (SPM8 release, www.fil.ion.ucl.ac.uk/spm/). The SPM8 software was slightly modified to better fit an infant brain. Since the original software package uses default tissue probability maps derived from adult brains, we replaced the original templates by specific one year old infant a priori tissue probability maps (Altaye et al., 2008) (available at irc.cchmc.org/software/infant.php) which could fit better with the anatomical brain features of the patients included in the study.

Structural 3D volume of each subject was registered to its correspondent b_0 volume (in the diffusion native space) using IRTK (www.

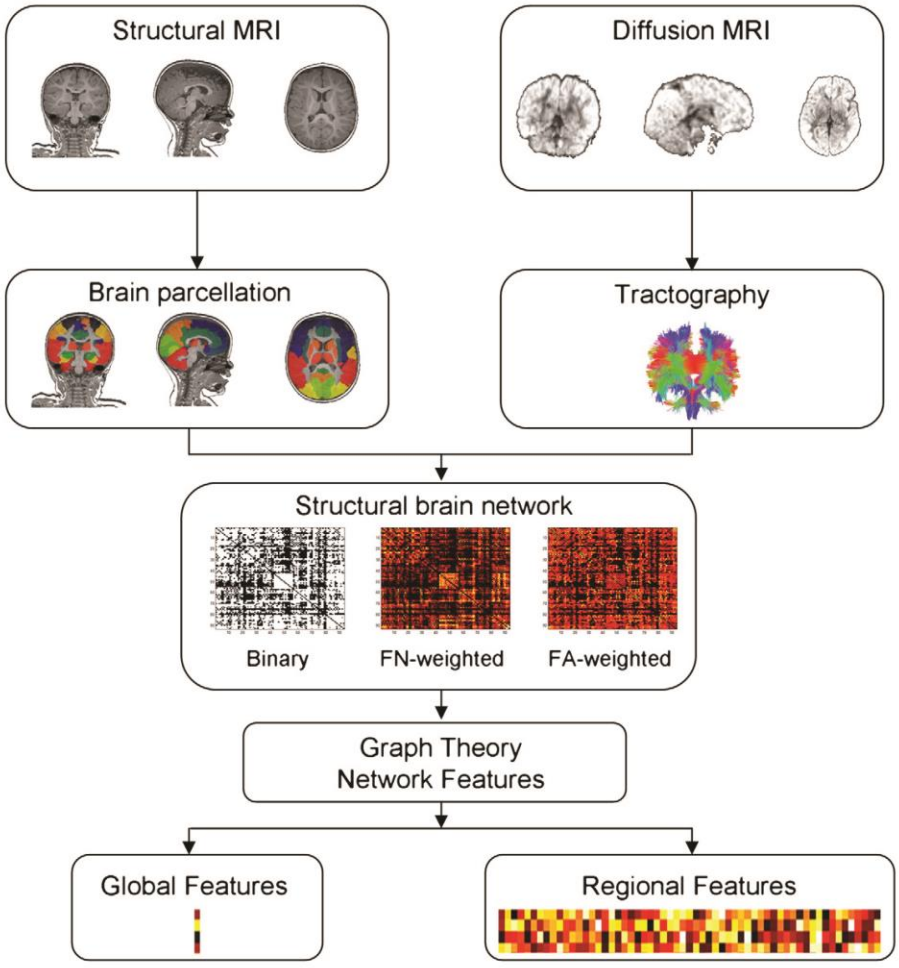

Fig. 1. Methodological scheme. By means of automatic parcellation and tractography, structural and diffusion MRI data of each subject is integrated into adjacency matrices (connectomes) and global and regional brain network features are extracted.

doc.ic.ac.uk/~dr/software/) to perform a 3D voxel-based affine registration maximizing normalized mutual information of each pair of images (Maes et al., 1997; Studholme et al., 1999). The transformation obtained for each subject was used to transform WM, GM and CSF to the diffusion native space.

Network node definition

Anatomical Automatic Labeling (AAL) atlas (Tzourio-Mazoyer et al., 2002), has recently been adapted to a one year old population (Shi et al., 2011) and is available online (http://bric.unc.edu/ideagroup/free-softwares/unc-infant-0-1-2-atlases/). In order to automatically parcellate each subject brain using this atlas, we have used a customized software implementing a consistent version (Tristan-Vega and Arribas, 2007) of a block matching algorithm (Warfield et al., 2002), allowing to obtain an elastic transformation matching the template with each subject anatomical T1 volume. The labels of AAL atlas were propagated to each structural MRI acquisition of our subjects using this elastic transformation, and transformed to diffusion native space with the previously calculated affine transformation. Discrete labeling values were preserved by nearest neighbor interpolation for both transformations. The original atlas is composed by 90 cortical and sub-cortical regions and 16 cerebellar regions. In order to simplify the analysis, we merged the cerebellar regions into right cerebellum, left cerebellum and vermix, resulting into a total of 93 regions per subject brain (Table 1), each of which corresponded to a node in the brain network.

Table 1
Regions of interest used as nodes in structural brain networks, corresponding to the regions defined in AAL atlas.

Anatomical regions	Label	Anatomical regions	Label
Precentral gyrus	PRE	Lingual gyrus	LING
Superior frontal gyrus, dorsolateral	F1	Superior occipital gyrus	O1
Superior frontal gyrus, orbital	F1O	Middle occipital gyrus	O2
Middle frontal gyrus	F2	Inferior occipital gyrus	O3
Middle frontal gyrus, orbital part	F2O	Fusiform gyrus	FUSI
Inferior frontal gyrus, opercular part	F3OP	Postcentral gyrus	POST
Inferior frontal gyrus, triangular part	F3T	Superior parietal gyrus	P1
Inferior frontal gyrus, orbital part	F3O	Inferior parietal, but supramarginal and angular gyri	P2
Rolandic operculum	RO	Supramarginal gyrus	SMG
Supplementary motor area	SMA	Angular gyrus	AG
Olfactory cortex	OC	Precuneus	PQ
Superior frontal gyrus, medial	F1M	Paracentral lobule	PCL
Superior frontal gyrus, medial orbital	F1MO	Caudate nucleus	CAU
Gyrus rectus	GR	Lenticular nucleus, putamen	PUT
Insula	IN	Lenticular nucleus, pallidum	PAL
Anterior cingulate and paracingulate gyri	ACIN	Thalamus	THA
Median cingulate and paracingulate gyri	MCIN	Heschl gyrus	HES
Posterior cingulate gyrus	PCIN	Superior temporal gyrus	T1
Hippocampus	HIP	Temporal pole: superior temporal gyrus	T1P
Parahippocampal gyrus	PHIP	Middle temporal gyrus	T2
Amygdala	AMYG	Temporal pole: middle temporal gyrus	T2P
Calcarine fissure and surrounding cortex	V1	Inferior temporal gyrus	T3
Cuneus	Q	Cerebellum	CER
		Vermis	VER

White matter tractography

A deterministic tractography was performed for each subject diffusion data using a diffusion tensor imaging (DTI) based fiber tracking algorithm with log-Euclidean metrics (Fillard et al., 2007), available on MedINRIA 1.9 (www-sop.inria.fr/asclepios/software/MedINRIA/). A relatively low Fractional Anisotropy (FA) threshold of 0.1 was chosen as stopping criterion for the fiber tract algorithm in order to ensure that the fiber tracts invade the WM-GM interface. Note that the preprocessing prior to the tractography includes a joint tensor field estimation and regularization that reduce the noise in the estimated DTI volume used to compute the tractography (Fillard et al., 2007).

Network edge definition

Tractography generated in the previous step was integrated to the anatomical parcellation in diffusion space in order to construct the inter-cortical brain network. Similarly to Shu et al. (2011), we characterized each brain network with a binary adjacency matrix and two weighted matrices. Specifically, two nodes (regions) i and j were considered to be connected by an edge e_{ij}, when there exist at least one fiber bundle f with end-points in i and j WM–GM interface, with self-loops excluded. Some authors proposed to establish a threshold of a minimum number of fiber bundles connecting two ROIs to consider them connected by an edge (Li et al., 2009; Lo et al., 2010; Shu et al., 2009, 2011) in order to minimize false positives that may be introduced into individual networks due to the noisy nature of the acquisitions. However, it has been suggested that the use of different thresholds does not significantly influence the resulting network analysis in case–control studies (Li et al., 2009; Lo et al., 2010; Shu et al., 2011). Analyses applying a fiber threshold from 1 to 5 fiber bundles were performed, but we focused in the analysis of unthresholded networks, as it was considered to be a more objective criterion preserving the whole structure of the connectivity in each individual. Network edge weights were defined according to two different criteria: fiber number (FN) connecting each pair of regions, and mean FA along all the fibers connecting a pair of region, hence obtaining two weighted adjacency matrices in addition to the binary one.

Network analysis

Network analysis of structural brain networks enables a refinement of image features obtained from MRI. As brain networks are defined by nodes (regions) and edges that connect pairs of nodes, which are represented mathematically by adjacency matrices or graphs (Hagmann et al., 2007), it is possible to characterize every subject structural brain network with a set of graph theory measures (or equivalently, network features) that summarize the behavior of a network. Particularly, we characterized each of the three brain network classes computed for each subject (binary, FN-weighted and FA-weighted) at two levels: global and regional.

At a global level, network infrastructure (i.e. mean degree), segregation (i.e. local efficiency) and integration (i.e. global efficiency) were characterized by means of standard measures as described in Supplementary material. At a regional level, a node based analysis was performed to extract the way in which these elements were embedded in the network (Rubinov and Sporns, 2009) by a set of network features of each node and its associated regional network. In that sense, in the network of a subject, a regional network associated to a given node was defined as the new network composed by the neighbors of that node, that is, by the nodes that are connected to that node. Nodes i and j are considered neighbors in a network if there exist an edge e_{ij} that connect both nodes (Rubinov and Sporns, 2009). Therefore, the definition of regional networks was based on its network topology, that is, in the connections among regions no matter how distant were from each other, not in anatomical and/or contiguity criteria. Specifically, regional network infrastructure (i.e., nodal degree), regional

network functional integration (i.e., nodal efficiency), and centrality of the node (i.e., betweenness centrality) were assessed.

In summary, the global level analysis included: average degree, global efficiency and local efficiency of each subject structural brain network. Regional level analysis included nodal degree, betweenness centrality and nodal efficiency of all the nodes of each subject structural brain network. For both global and regional network features the definitions of Rubinov and Sporns (2009) were applied and Brain Connectivity Toolbox (Rubinov and Sporns, 2009) was used to calculate most of them. Global, local and nodal efficiencies were calculated in both their binary and weighted versions according to the brain network considered.

Small-worldness

"Small-world" network model was originally characterized by (Watts and Strogatz (1998)), relating network clustering coefficient C_p, and characteristic path length L_p. According Watts and Strorgatz criterion, small-world networks have L_p comparable to a random equivalent network but a higher C_p. Specifically, C_p and L_p of each network were compared with equivalent random networks with the same size and degree distribution.

A more general criterion that characterizes small-world networks in terms of efficiency was also used. Following these criteria, a network can be considered to follow a small-world model if it accomplishes both following conditions (Achard and Bullmore, 2007):

$$E_{glob}^{latt} < E_{glob} < E_{glob}^{rand} \text{ and } E_{loc}^{rand} < E_{loc} < E_{loc}^{latt}$$

where E_{glob}^{latt} and E_{loc}^{latt} are the global and local efficiency of a lattice (regular) equivalent of the network, and E_{glob}^{rand} and E_{loc}^{rand} are the global and local efficiency of an equivalent random network. It can be seen as a network with an optimal balance between local processing and global integration (Sporns and Tononi, 2001).

In addition, the principal hubs, defined as the 10% of regions (nodes) with the highest degree for each subject, were also calculated.

Association with abnormal neurodevelopment at two years of age

Regional connectivity risk index of abnormal neurodevelopment

Due to the relatively reduced sample size, in order to avoid overfitting of the predictive models (Michel et al., 2012), a procedure to reduce the regional feature space was undertaken. Hence, in a previous step, regional connectivity features that predicted better neurodevelopment at 2-years were selected and reduced to a single index. In brief, a scheme was defined to integrate the complex process of regional brain reorganization into a single score, defined as 'regional connectivity risk index'. To this end, a leave-one-out cross validation strategy was followed to obtain a blind score integrating the relevant regional features of each IUGR infant. The scheme for the generation of this index was built according to the following steps (Fig. 2):

(1) Feature selection based on keeping those features with higher individual discriminative power of the normal/abnormal BSID-III (dicotomic value) for the training set. Specifically, those features with an absolute value two-sample *t*-test one standard deviation above the mean for the training set were selected.
(2) Computation of the nonlinear regression model that better classified the training set using the features selected in step (1) by means of a regression tree (Breiman et al., 1984).
(3) Calculation of the 'regional connectivity risk index' (probability of abnormal BSID-III) and blind classification (using a 0.5 cutoff on the probability of abnormal BSID-III) of the test sample by applying the regression tree estimated in step (2).

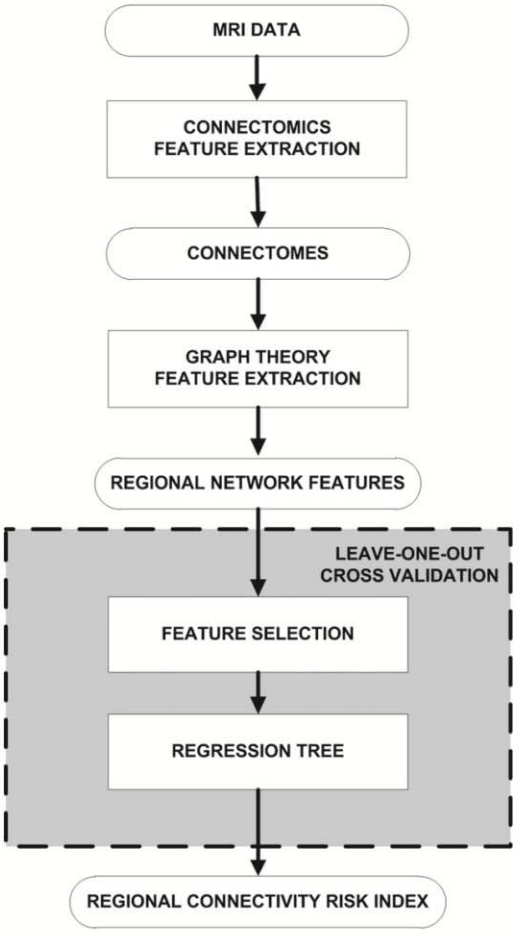

Fig. 2. Learning algorithm scheme to obtain a 'regional connectivity risk index' that integrates regional network features associated to abnormal neurodevelopment.

Subsequently, the performance of this 'regional connectivity risk index' to achieve a blind classification of the neurodevelopmental status (normal or abnormal) was evaluated.

Association of network features and clinical data to neurodevelopmental scores on BSID-III in 2 year IUGR children

Three blocks of data were established: clinical–epidemiological features (gender, smoking status, breastfeeding, GA and weight centile at birth), global network features and the regional connectivity risk index as defined in the Regional connectivity risk index of abnormal neurodevelopment section.

In order to assess the association of the three blocks of data with neurodevelopmental scores in IUGR, a binomial logistic regression with two different approaches was then conducted. In the first approach the independent association power of each block binomial logistic regression was evaluated based on an enter method. In the second approach, the three blocks were consecutively entered as predictors into a binomial logistic regression with a backward step-wise selection criterion in order to assess the best predictive model for BSID-III abnormal performance. Removal testing in backward step-wise selection was based on the probability of the likelihood-ratio statistic based on the maximum partial likelihood estimates. p value for variable removal was set at 0.15.

Statistical analysis

Statistical comparisons among groups were performed by general linear models with gender, maternal education level, smoking during pregnancy and breastfeeding as cofactors and GA as a covariate. Due to the exploratory nature of these analyses, significance was declared at $p<0.05$ (uncorrected). In addition, the results of each regional feature were corrected for multiple comparisons with a False Discovery Rate (FDR) approach (Benjamini et al., 2006) in order to control alpha error to 5%. The software package SPSS 18.0 (SPSS, Chicago, IL) was used for the statistical analyses. All computational algorithms were implemented using MATLAB (2007b, The MathWorks Inc., Natick, MA).

Results

Basic clinical features in the study population

Structural MRI evaluation revealed the presence of anomalies in 8 IUGR (two increased cisterna magna, four ventricular dilatations and two WM lesions) and in 5 controls (two increased cisterna magna and three ventricular dilatations) that were excluded from the final analysis. In addition, 4 controls and 10 IUGR did not pass quality criteria concerning motion artifacts or correct tractography reconstruction that prevented performing further analysis. Thus, the final sample included 24 IUGR infants and 32 control infants.

As expected, anthropometric measurements at birth normalized for local standards were significantly lower in IUGR group (Table 2). No significant differences were found in GA at birth, gender distribution, Apgar score at 5 min, umbilical artery pH and rate of neonatal complications among groups. No postnatal corticosteroids were administered to any individual included in our study. Maternal smoking status during pregnancy was increased in IUGR group ($p=0.005$). Regarding BSID-III neurodevelopmental test, IUGR infants showed a trend to worse scores than the control group in all scales, although the differences were statistically significant only for cognitive ($p=0.029$), motor ($p=0.018$) and language ($p=0.002$) clusters (Table 2). Proportion of abnormal BSID-III in IUGR groups was non-significantly higher when compared with control group (47.1% vs. 27.3%, $p=0.201$).

Table 2
Neonatal data, demographic characteristics, growth parameters, and BSID-III scores in the study groups. Mean (±SD). Variables with $p<0.05$ are highlighted in bold.

	Controls n = 32	IUGR n = 24	p[a]
Neonatal data			
GA at delivery	34.8 (5.8)	36.6 (3.1)	0.173
Birth weight centile	54 (23.9)	5.5 (5.5)	<**0.001**
Length at birth centile	59.1 (23.3)	11.6 (11.8)	<**0.001**
Cephalic perimeter at birth centile	43.5 (25.1)	13.2 (17.2)	<**0.001**
Gender distribution (male/female)	17/15	15/9	0.483
Apgar 5 min	9 (2.5)	9.5 (1.7)	0.395
Umbilical artery pH	7.27 (0.07)	7.24 (0.09)	0.122
Neonatal complications	3.1% [1/32]	4.2% [1/24]	0.835
Demographic characteristics			
Maternal age [years]	31.3 (4.1)	32.2 (4.0)	0.426
Maternal education less than high school	25.8%	33.3%	0.542
Breastfeeding longer than 4 months	67.7%	59.1%	0.518
Smoking during pregnancy	12.5%	45.8%	**0.005**
Corrected age at MR [months]	12.8 (1.5)	13.2 (1.6)	0.382
Corrected age at BSID-III [months]	20.2 (3.5)	21.7 (3.0)	0.155
Growth parameters at 12 months			
Weight z-score	−0.52 (0.82)	−1.06 (0.85)	**0.024**
Height z-score	−0.17 (1.17)	−1.01 (0.97)	**0.008**
Body mass index (BMI) z-score	−0.49 (1.05)	−0.52 (0.91)	0.079
Cephalic perimeter z-score	−0.50 (1.05)	−1.09 (1.30)	0.891
BSID-III scores			
Cognitive score [b]	108.8 (12.5)	104.3 (9.4)	**0.029**[c]
Language score [b]	102.1 (19.0)	91.3 (12.5)	**0.002**[c]
Motor score [b]	106.9 (14.2)	100.7 (9.6)	**0.018**[c]
Social emotional score [d]	117.4 (30.2)	108.6 (23.7)	0.514[c]
Adaptive behavior score [d]	92.9 (17.0)	89.5 (18.8)	0.469[c]

[a] Student's *t*-test for independent samples or Pearson's Chi^2 test.
[b] Controls n = 22/IUGR n = 17.
[c] General Lineal Model significance among groups corrected for clinical covariables and cofactors.
[d] Controls n = 18/IUGR n = 16.

Small-worldness

Graph theoretical analysis on the adjacency matrices representing structural brain networks of our subjects, showed that 1-year old children structural brain networks are a small-world network of neural tracts. The comparison among local and global efficiencies of the structural brain networks and its random and lattice equivalents showed that all our population fulfilled a small-world criterion, having an intermediate global and local efficiency compared to its random and regular equivalent networks (Table 3). Using classical small-world criteria, a small-world behavior was also observed (Supplementary Table 1).

Hubs of IUGR and controls, defined as the 10% of nodes with higher degree, were identified for each group separately (Table 4). Similar hubs on both groups were found, mainly precuneus and cerebellum of each hemisphere.

Global connectivity characteristics

The analyses of unthresholded networks show that general linear models of average degree, binary global efficiency and binary local efficiency did not show statistically significantly differences between cases and controls (Figs. 3A–C). FN-weighted global and local efficiency were not significantly different in cases and controls, but there was a trend of reduced values in IUGR (Figs. 3D and E). FA-weighted global efficiency was significantly decreased in IUGR (group effect: $F=7.15$ $p=0.012$, Fig. 3F). FA-weighted local efficiency was also significantly lower in the IUGR group (group effect: $F=5.99$ $p=0.020$, Fig. 3G). Further analyses with fiber threshold from 1 to 5 are included in Supplementary Table 2.

Disrupted regional connectivity

Analysis of regional connectivity revealed statistically significant differences in IUGR at multiple levels on the set of features evaluated (Table 5, Fig. 4). For instance, differences in nodal degree were mainly observed in parietal and occipital lobe whereas all regions in temporal lobe and cerebellum demonstrated differences in betweenness centrality. Binary nodal efficiency showed most of the differences in temporal and parietal lobe and cerebellum while frontal lobe and subcortical gray nuclei were the most affected in FN-weighted nodal efficiency. Finally, FA-weighted nodal efficiency presented significant differences in multiple regions of frontal lobe and sub-cortical gray matter, almost all regions included in parietal and occipital lobe and in whole cerebellum and central region.

Association with abnormal neurodevelopment at two years of age

Regional connectivity risk index of abnormal neurodevelopment

Most discriminant regional connectivity features are shown in Fig. 5 and Supplementary Table 3. Specifically, features selected in more than 90% of leave-one-out iterations included characteristics of frontal regions (right and left precentral gyrus, left superior frontal gyrus, left superior and middle frontal gyrus orbital part, left superior frontal gyrus medial orbital part, right inferior frontal gyrus triangular

Table 3
Controls, IUGR and their equivalent random and lattice networks binary global and local efficiency. Mean (±SD).

Fiber threshold	Group	Random global efficiency	Global efficiency	Lattice global efficiency	Random local efficiency	Local efficiency	Lattice local efficiency
1	Controls	0.8191 (0.0178)	0.8191 (0.0181)	0.8191 (0.0178)	0.8598 (0.0148)	0.8766 (0.0098)	0.8978 (0.0053)
	IUGR	0.8178 (0.0147)	0.8178 (0.0151)	0.8177 (0.0148)	0.8610 (0.0128)	0.8766 (0.0089)	0.8984 (0.0048)
2	Controls	0.7629 (0.0159)	0.7626 (0.0162)	0.7624 (0.0161)	0.8155 (0.0143)	0.8501 (0.0071)	0.8835 (0.0040)
	IUGR	0.7595 (0.0141)	0.7592 (0.0145)	0.7589 (0.0142)	0.8154 (0.0135)	0.8499 (0.0082)	0.8838 (0.0037)
3	Controls	0.7301 (0.0137)	0.7290 (0.0145)	0.7285 (0.0142)	0.7862 (0.0142)	0.8355 (0.0065)	0.8766 (0.0041)
	IUGR	0.7263 (0.0140)	0.7253 (0.0145)	0.7247 (0.0143)	0.7849 (0.0135)	0.8358 (0.0070)	0.8762 (0.0038)
4	Controls	0.7072 (0.0122)	0.7055 (0.0132)	0.7042 (0.0134)	0.7637 (0.0142)	0.8255 (0.0061)	0.8708 (0.0042)
	IUGR	0.7041 (0.0128)	0.7023 (0.0134)	0.7008 (0.0133)	0.7664 (0.0125)	0.8272 (0.0069)	0.8715 (0.0037)
5	Controls	0.6899 (0.0111)	0.6872 (0.0123)	0.6849 (0.0126)	0.7460 (0.0138)	0.8179 (0.0063)	0.8660 (0.0055)
	IUGR	0.6869 (0.0127)	0.6841 (0.0135)	0.6818 (0.0139)	0.7462 (0.0145)	0.8201 (0.0073)	0.8659 (0.0055)

part, right gyrus rectus right supplementary motor area), occipital regions (right middle occipital gyrus, left inferior occipital gyrus, left calcarine fissure and surrounding cortex) and subcortical gray matter (right and left caudate, right putamen and thalamus).

The regional connectivity risk index obtained blindly for each subject in the leave-one-out learning algorithm also allowed us to blindly classify each IUGR subject into normal or abnormal BSID-III performance with an accuracy of 82.4%, with a sensitivity of 87.5% and a specificity of 77.8%.

Table 4
Principal hubs in controls and IUGR and its frequency (%) of selection at different fiber thresholds.

Fiber threshold	Controls hubs	Frequency (%)	IUGR hubs	Frequency (%)
1	PQ (L)	93.8	PQ (L)	87.5
	PQ (R)	84.4	PQ (R)	79.2
	CER (L)	84.4	CER (L)	75.0
	CER (R)	71.9	CER (R)	75.0
	CAU (L)	53.1	P1 (R)	50.0
	P1 (R)	46.9	F2 (R)	45.8
	CAU (R)	34.4	CAU (L)	41.7
	AG (R)	31.3	F2 (L)	37.5
	THA (L)	21.9	CAU (R)	33.3
2	PQ (L)	90.6	PQ (L)	87.5
	PQ (R)	84.4	PQ (R)	87.5
	CER (L)	84.4	CER (L)	83.3
	CER (R)	65.6	CER (R)	75.0
	CAU (L)	56.3	CAU (R)	54.2
	CAU (R)	43.8	P1 (R)	45.8
	P1 (R)	34.4	F2 (R)	41.7
	T1P (L)	31.3	CAU (L)	41.7
	F2 (L)	28.1	F2 (L)	33.3
3	PQ (L)	93.8	PQ (R)	91.7
	CER (L)	87.5	PQ (L)	87.5
	PQ (R)	84.4	CER (L)	75.0
	CER (R)	68.8	CER (R)	66.7
	CAU (R)	53.1	F2 (L)	58.3
	CAU (L)	50.0	CAU (R)	54.2
	F2 (L)	28.1	F2 (R)	50.0
	O2 (R)	28.1	CAU (L)	41.7
	AG (R)	28.1	F1 (R)	33.3
4	PQ (L)	87.5	PQ (L)	91.7
	PQ (R)	87.5	PQ (R)	91.7
	CER (L)	84.4	CER (L)	70.8
	CER (R)	68.8	CER (R)	70.8
	CAU (R)	53.1	F2 (R)	58.3
	CAU (L)	50.0	CAU (R)	54.2
	F2 (R)	31.3	F2 (L)	41.7
	P1 (R)	28.1	CAU (L)	41.7
	T2 (R)	28.1	T2 (R)	41.7
5	PQ (L)	90.7	PQ (L)	91.7
	PQ (R)	87.5	PQ (R)	79.2
	CER (L)	84.4	CER (L)	75.0
	CER (R)	75.0	CER (R)	75.0
	CAU (R)	53.1	F2 (L)	58.3
	CAU (L)	50.0	F2 (R)	54.2
	F2 (R)	31.3	CAU (R)	41.7
	F2 (L)	28.1	T2 (R)	41.7
	P1 (R)	28.1	F1 (R)	33.3

(L) refers to left hemisphere and (R) to right hemisphere.

Predictive model including clinical and MRI data

Binomial logistic regression was used to assess the predictive value of clinical data, global connectivity features and regional connectivity risk index with abnormal BSID-III performance in IUGR group (Table 6). The regression model based on clinical information (weight centile, GA, gender, maternal education level, mother smoking status during pregnancy and breastfeeding) was not significantly associated with abnormal neurodevelopment. The binomial logistic regression with global connectivity features (average degree and binary, FN-weighted and FA-weighted global and local efficiency) showed an accuracy of 76.5%, with a sensitivity of 87.5% and a specificity of 66.7%. The model had a Chi-square = 9.81 with p = 0.199 and a Nagelkerke R^2 of 0.59. None of the global connectivity features had a significant contribution by itself. Finally, previously calculated regional connectivity risk index achieved an accuracy of 82.4%, with 87.5% of sensitivity and 77.8% of specificity. The regression model was significant with a Chi-square = 7.17, p = 0.007 and a Nagelkerke R^2 of 0.46.

In an exploratory analysis, in order to find the best performing combination of predictive variables, binary logistic regression with a backwards stepwise method was applied, entering the data in three consecutive blocks: clinical–epidemiological features, global connectivity and regional connectivity risk index (Table 7). In the first block, all clinical data were discarded by the step-wise process. Entering global connectivity data in the second block leaded to a six step process in which only average degree and binary global efficiency remained. However, the model was not significant. When regional connectivity risk index was added in a third block, accuracy of the classification increased to 88.2% (sensitivity 87.5, specificity 88.9%) with a significant model (Chi-square = 11.38, p = 0.010, Nagelkerke R^2 = 0.65).

Discussion

This study describes the use of diffusion MRI based connectomics in one-year-old infants, with particular focus on the analysis of structural brain networks. The study provides evidence that diffusion MRI based connectomics can demonstrate large-scale brain reorganization of the structural brain network in one year old children who suffered IUGR by means of global as well as regional brain network feature analysis. Finally, it was demonstrated that structural brain network features evaluated at one year could predict later neurodevelopment in 2-year old children.

Small-worldness of structural brain networks

Overall, graph theory characterization showed the small-worldness of one year old brain networks based on diffusion MRI structural connectivity. These findings are in accordance with recent studies on structural brain networks based on diffusion MRI on adults (Gong et al.,

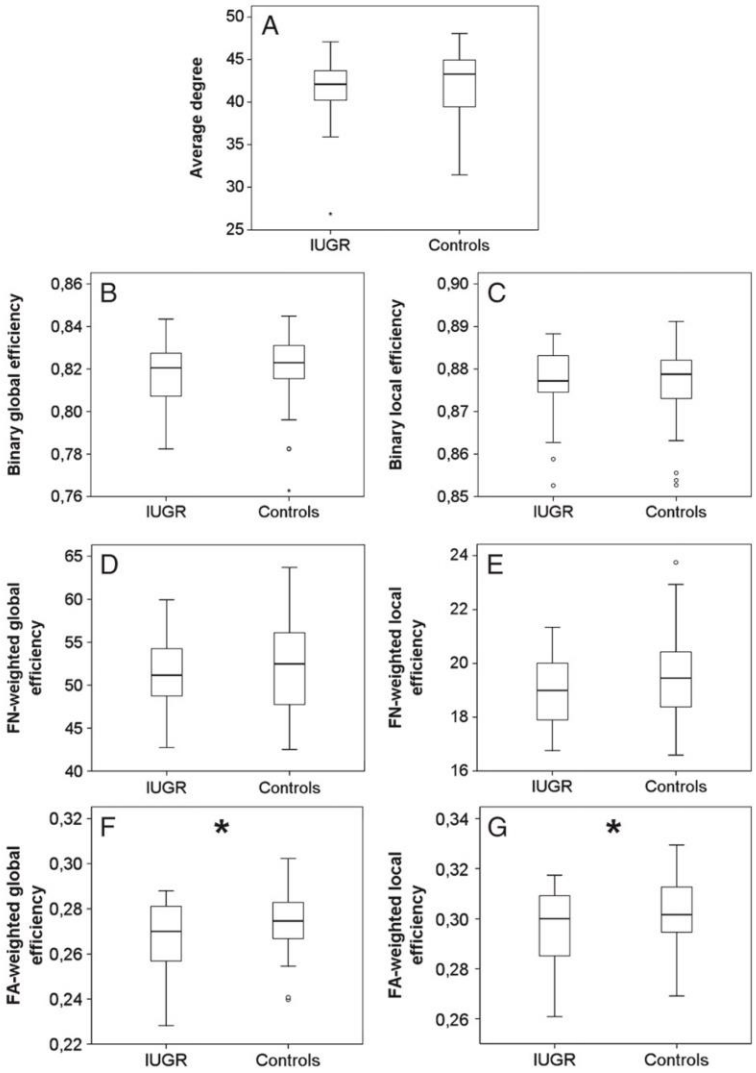

Fig. 3. Global characteristics of control and IUGR groups. (A) Average degree, (B) binary global efficiency, (C) binary local efficiency, (D) FN-weighted global efficiency, (E), FN-weighted local efficiency, (F) FA-weighted global efficiency and (G) FA-weighted local efficiency. *$p<0.05$.

2009; Hagmann et al., 2008), late developing brain (Hagmann et al., 2010) and brain networks based on regional volumes correlations in early developing brain (Fan et al., 2011). The results are indicative of a high connectivity organization and efficiency already at one year of age. Random networks communicate every pair of nodes with relatively few intermediate steps, but have a lack of organization. On the contrary, lattice networks have a high level of organization but a poor average capability to efficiently communicate a given pair of nodes. Small-world networks present a balance between both kinds of networks (Sporns and Tononi, 2001) and have been reported in a wide range of networks present in nature as well as in man-made systems (Bullmore and Sporns, 2009).

Interestingly, we identified precuneus as one of the principal hubs in our one-year-old population, which is in line with previously reported results in infants (Yap et al., 2011) and in adults (Gong et al., 2009; Hagmann et al., 2008; Tomasi and Volkow, 2011).

Global structural brain network features

There is increasing agreement that network features indicate differences in brain organization (Bassett and Bullmore, 2009). Consequently, global brain network features may be a useful approach to identify which kind and at which level of complexity brain reorganization occurs. By means of weighted measures of efficiency, alterations in global and local efficiency were observed. These findings might suggest brain reorganization of the WM connectivity without significant changes in the total amount of connections. The results suggest that FA-weighted approach could be a more sensitive parameter to reveal brain reorganization due to IUGR. This is in line with previous studies suggesting the value of weighted metrics of brain networks to assess subtle differences in neurodegenerative and psychiatric conditions (Lo et al., 2010; Shu et al., 2011; Wang et al., 2012; Wee et al., 2010). In addition, weighted measures seem to correlate better with intelligence

measured by IQ score in normal subjects (Li et al., 2009). Lower global efficiency has been described in multiple sclerosis (Shu et al., 2011), schizophrenia (Wang et al., 2012), Alzheimer's disease (Lo et al., 2010) and early blindness (Shu et al., 2009). A few studies have evaluated global efficiency in relation with normal neurodevelopment. A pattern of increasing values with increasing age from 2 to 18 years of age has been described (Hagmann et al., 2010), while similar global efficiency values were measured in neonates, one-year-old and two-year-old infants (Yap et al., 2011).

FA-weighted local efficiency was also significantly lower in the IUGR group. The clinical implications of local efficiency are still undefined. While some have reported decreased local efficiency in schizophrenia (Alexander-Bloch et al., 2010; Wang et al., 2010), multiple sclerosis (He et al., 2009b; Shu et al., 2011) and children with severe reading difficulties (Vourkas et al., 2010), others found increased local efficiency in attention deficit hyperactivity disorder (Wang et al., 2009). Late developing brains (2–18 years) show decreasing clustering coefficients, and hence decreasing local efficiency, with increasing age (Hagmann et al., 2010). An increase in diffusion MRI local efficiency values has been observed during the first years of life (Yap et al., 2011).

Regional structural brain network features

Analysis of regional brain network features allowed extracting information of the topological changes on each region and its associated network. Regional characteristics were altered following a diffuse pattern along the whole brain, which included multiple areas as frontal, temporal, parietal and occipital lobes, subcortical GM nuclei, insular cortex and cerebellum. Frontal and temporal areas showed changes in all regional features, although alterations in frontal areas were found mainly in FN-weighted nodal efficiency. Frontal and temporal areas are involved in the regulation of functions previously reported to be abnormal in IUGR children, including short-term memory (Geva et al., 2006a), learning abilities (Geva et al., 2006b), attention (Heinonen et al., 2010) and social skills (Eixarch et al., 2008). Fronto-temporal areas have also been related with attention deficit hyperactivity disorder (Kobel et al., 2010), which is present in higher proportion in children who suffered IUGR (Heinonen et al., 2010). Parietal areas showed differences mainly in nodal degree and FA-weighted nodal efficiency. These findings are consistent with the poorer performance in BSID-III motor domain observed in IUGR children. Previous studies have linked worst motor performance with reduced GM in parietal areas of IUGR (Padilla et al., 2011). Occipital areas were altered mainly on FA-weighted nodal efficiency, but also on nodal degree in a less spread pattern. This result is consistent with previous findings where parieto-occipital and inferior occipital regional vulnerability to IUGR has been demonstrated (Thompson et al., 2007). Some subcortical GM nuclei including amygdala, putamen, pallidum and thalamus were also found altered, by regional features, mainly by FN-weighted nodal efficiency. Interestingly, striatal injury has been related to perinatal disorders, including IUGR, suggesting that it could be a risk factor of behavioral disturbances (Toft, 1999) and specific alterations in the cortico-striato-thalamic network have been associated with cognitive disorders, including Tourette syndrome (Makki et al., 2009), bipolar disorder (Chen et al., 2006) and attention deficit hyperactivity disorder (Castellanos et al., 1994; Faraone and Biederman, 1998). Finally, cerebellum alterations in nodal degree and weighted nodal efficiency were found. These findings are in line with previously described decreases in cerebellar WM in IUGR infants (Padilla et al., 2011) and with alterations in cerebellar neuron population in animal models of IUGR (Mallard et al., 2000).

Association with abnormal neurodevelopment at two years of age

In this study IUGR infants showed significantly worse performance in cognitive, motor and language scores on the BSID-III areas. These findings are in line with previous data in IUGR infants and children (Bassan et al., 2011; Eixarch et al., 2008; Feldman and Eidelman, 2006; Geva et al., 2006a,b; Jarvis et al., 2003; Leitner et al., 2007; Marsal, 2002; McCarton et al., 1996; Scherjon et al., 2000). The results of this study provide evidence that graph theory features of structural brain network at one year of age carry relevant individual information related with adverse neurodevelopment measured one year later by BSID-III. Specifically, we have shown that global network connectivity features were associated to abnormal neurodevelopment. Furthermore, regional connectivity features allowed to blindly classify abnormal neurodevelopment in IUGR with an accuracy of 82.4%. By means of an exploratory backward step-wise logistic regression, we also demonstrated that mean degree and binary global efficiency in combination with regional connectivity risk index, increased the association power, to 88.2%, and achieved a very high goodness of fit of the model (Nagelkerke $R^2 = 0.65$). These results are in line with previous studies relating neurofunction with diffusion MRI based structural brain network features. Thus, global efficiency has been previously demonstrated to be associated with intelligence (Li et al., 2009), and regional features of brain networks selected by means of a learning algorithm have been related successfully to mild cognitive impairment in studies attempting to develop early biomarkers for Alzheimer's disease (Wee et al., 2010). The data here reported and previous studies suggest that combining global and regional characteristics could help to improve the understanding of neurofunctional mechanisms underlying structural connectivity. In addition, further studies linking structural and functional networks would be very helpful in order to better understand the intricate link between structural and functional connectivity in the infant brain. Combined analysis of both substrates is warranted in future studies to advance in the understanding of brain reorganization and its relation with altered neurobehavior due to IUGR and other prenatal condition. Several studies have demonstrated the feasibility of the estimation of resting-state functional MRI networks in infants, and revealed some of the principal functional hubs in the developing brain (Doria et al., 2010; Fransson et al., 2007, 2010; Smyser et al., 2010, 2011). The link between functional and structural networks has been scarcely investigated. There is preliminary evidence that structural connections are predictive of functional connections (Honey et al., 2010), but specific studies in the developing brain are lacking.

Strengths and limitations of the study

One of the most noteworthy strengths of the current study is that it was performed in well-defined cohorts diagnosed prenatally and followed prospectively. While most perinatal and demographic characteristics were not significantly different among groups, the results were corrected for a substantial number of potential confounders.

Notwithstanding, some issues must be noted concerning the methodology followed. The techniques used on a series of complex analyses, and due to their relative novelty there is a lack of 'gold standards' in the literature. Brain parcellation in young infants is a controversial subject and tissue segmentation in infant brains is considered a challenging task due to the isointense developmental pattern which results in a poor differentiation between GM and WM (Paus et al., 2001). To minimize this limitation we used high quality T1 weighted 3-Tesla Magnetic Resonance images and to guide the segmentation we used appropriate brain tissue probability maps (Altaye et al., 2008) and a pediatric atlas (Shi et al., 2011). In addition, each scan was reviewed to determine if the results of the tissue segmentation were accurate (Knickmeyer et al., 2008). A drawback of DTI tractography reconstruction is that it is highly sensitive to motion artifacts during acquisition. This prevented us to analyze a remarkable number of subjects. It is also well known that DTI is not able to encode multi-directional diffusion information, which may lead to errors in regions with a high amount of crossing fibers. Other techniques such as Q-Ball Imaging (QBI) (Tuch, 2004) or Diffusion Spectrum Imaging (DSI) (Wedeen et al., 2005) should be

Table 5
Regions with statistically significant differences in nodal degree, betweenness centrality, binary nodal efficiency, FN-weighted nodal efficiency and FA-weighted nodal efficiency in IUGR compared with controls.

ROI	Nodal degree	Betweenness centrality	Binary nodal efficiency	FN-weighted nodal efficiency	FA-weighted nodal efficiency
PRE (L)	N.S.	N.S.	N.S.	N.S.	**p = 0.025 F = 5.507**
PRE (R)	N.S.	N.S.	N.S.	N.S.	**p = 0.027 F = 5.393**
F1 (L)	N.S.	N.S.	N.S.	N.S.	N.S.
F1 (R)	N.S.	N.S.	N.S.	N.S.	N.S.
F1O (L)	N.S.	N.S.	N.S.	N.S.	N.S.
F1O (R)	N.S.	N.S.	N.S.	N.S.	N.S.
F2 (L)	N.S.	N.S.	N.S.	p = 0.023 F = 5.650	**p = 0.032 F = 5.024**
F2 (R)	N.S.	N.S.	N.S.	N.S.	N.S.
F2O (L)	N.S.	N.S.	N.S.	p = 0.023 F = 5.721	N.S.
F2O (R)	N.S.	N.S.	N.S.	p = 0.009 F = 7.603	N.S.
F3OP (L)	N.S.	N.S.	N.S.	N.S.	**p = 0.021 F = 5.870**
F3OP (R)	N.S.	N.S.	N.S.	N.S.	N.S.
F3T (L)	N.S.	N.S.	N.S.	N.S.	N.S.
F3T (R)	N.S.	N.S.	N.S.	p = 0.013 F = 6.922	N.S.
F3O (L)	p = 0.012 F = 7.133	p = 0.006 F = 8.578	p = 0.020 F = 5.930	p = 0.019 F = 6.097	N.S.
F3O (R)	N.S.	N.S.	N.S.	N.S.	N.S.
RO (L)	N.S.	N.S.	N.S.	N.S.	p = 0.035 F = 4.814
RO (R)	N.S.	N.S.	N.S.	N.S.	p = 0.038 F = 4.667
SMA (L)	N.S.	N.S.	N.S.	N.S.	**p = 0.027 F = 5.377**
SMA (R)	N.S.	N.S.	N.S.	p = 0.033 F = 4.977	N.S.
OC (L)	N.S.	N.S.	N.S.	N.S.	N.S.
OC (R)	N.S.	N.S.	N.S.	**p = 0.003 F = 10.618**	N.S.
F1M (L)	N.S.	N.S.	N.S.	N.S.	**p = 0.021 F = 5.895**
F1M (R)	N.S.	N.S.	N.S.	N.S.	N.S.
F1MO (L)	N.S.	N.S.	N.S.	N.S.	N.S.
F1MO (R)	N.S.	N.S.	N.S.	N.S.	N.S.
GR (L)	N.S.	N.S.	N.S.	N.S.	N.S.
GR (R)	N.S.	N.S.	N.S.	N.S.	N.S.
IN (L)	N.S.	N.S.	N.S.	N.S.	N.S.
IN (R)	N.S.	N.S.	N.S.	N.S.	N.S.
ACIN (L)	N.S.	N.S.	N.S.	N.S.	N.S.
ACIN (R)	N.S.	N.S.	N.S.	N.S.	N.S.
MCIN (L)	N.S.	N.S.	N.S.	p = 0.020 F = 6.020	N.S.
MCIN (R)	N.S.	p = 0.010 F = 7.387	p = 0.023 F = 5.679	N.S.	p = 0.037 F = 4.742
PCIN (L)	N.S.	N.S.	N.S.	N.S.	N.S.
PCIN (R)	N.S.	N.S.	N.S.	N.S.	N.S.
HIP (L)	N.S.	N.S.	N.S.	N.S.	N.S.
HIP (R)	N.S.	N.S.	N.S.	N.S.	N.S.
PHIP (L)	N.S.	N.S.	N.S.	N.S.	N.S.
PHIP (R)	N.S.	N.S.	N.S.	N.S.	N.S.
AMYG (L)	N.S.	N.S.	N.S.	N.S.	p = 0.035 F = 4.839
AMYG (R)	N.S.	N.S.	N.S.	N.S.	N.S.
V1 (L)	N.S.	N.S.	N.S.	N.S.	**p = 0.003 F = 10.644**
V1 (R)	N.S.	N.S.	N.S.	N.S.	**p = 0.005 F = 8.950**
Q (L)	N.S.	N.S.	N.S.	N.S.	**p = 0.001 F = 14.081**
Q (R)	N.S.	N.S.	N.S.	N.S.	**p = 0.013 F = 6.975**
LING (L)	N.S.	N.S.	N.S.	N.S.	**p = 0.003 F = 10.601**
LING (R)	N.S.	N.S.	N.S.	p = 0.024 F = 5.562	**p = 0.008 F = 7.843**
O1 (L)	N.S.	N.S.	N.S.	N.S.	**p = 0.005 F = 8.999**

(continued on next page)

Table 5 (*continued*)

ROI	Nodal degree	Betweenness centrality	Binary nodal efficiency	FN-weighted nodal efficiency	FA-weighted nodal efficiency
O1 (R)	p = 0.035 F = 4.830	N.S.	N.S.	N.S.	**p = 0.005** **F = 9.038**
O2 (L)	p = 0.039 F = 4.634	N.S.	N.S.	N.S.	**p = 0.010** **F = 7.395**
O2 (R)	p = 0.028 F = 5.319	N.S.	N.S.	N.S.	**p < 0.001** **F = 16.938**
O3 (L)	N.S.	N.S.	N.S.	N.S.	**p = 0.007** **F = 8.289**
O3 (R)	N.S.	N.S.	N.S.	N.S.	**p = 0.004** **F = 9.551**
FUSI (L)	N.S.	N.S.	N.S.	N.S.	**p = 0.008** **F = 8.105**
FUSI (R)	N.S.	N.S.	N.S.	N.S.	N.S.
POST (L)	p = 0.006 F = 8.499	N.S.	N.S.	N.S.	**p = 0.008** **F = 7.948**
POST (R)	N.S.	p = 0.015 F = 6.540	p = 0.043 F = 4.437	N.S.	**p = 0.007** **F = 8.340**
P1 (L)	**p < 0.001** **F = 15.774**	N.S.	N.S.	N.S.	**p = 0.003** **F = 10.659**
P1 (R)	N.S.	N.S.	N.S.	N.S.	**p = 0.004** **F = 9.322**
P2 (L)	p = 0.022 F = 5.736	N.S.	N.S.	N.S.	**p = 0.003** **F = 10.711**
P2 (R)	N.S.	N.S.	N.S.	N.S.	**p = 0.006** **F = 8.515**
SMG (L)	N.S.	N.S.	N.S.	N.S.	**p = 0.008** **F = 7.866**
SMG (R)	N.S.	p = 0.009 F = 7.757	p = 0.012 F = 7.064	N.S.	N.S.
AG (L)	p = 0.017 F = 6.288	N.S.	N.S.	N.S.	**p = 0.007** **F = 8.395**
AG (R)	p = 0.046 F = 4.301	N.S.	N.S.	p = 0.012 F = 7.128	**p = 0.006** **F = 8.560**
PQ (L)	N.S.	p = 0.046 F = 4.307	p = 0.016 F = 6.513	N.S.	**p = 0.005** **F = 9.156**
PQ (R)	N.S.	N.S.	N.S.	N.S.	**p = 0.012** **F = 7.040**
PCL (L)	N.S.	N.S.	N.S.	N.S.	**p = 0.012** **F = 7.040**
PCL (R)	N.S.	N.S.	p = 0.025 F = 5.542	N.S.	N.S.
CAU (L)	N.S.	N.S.	N.S.	N.S.	N.S.
CAU (R)	N.S.	N.S.	N.S.	N.S.	N.S.
PUT (L)	N.S.	N.S.	N.S.	p = 0.043 F = 4.445	p = 0.036 F = 4.799
PUT (R)	N.S.	N.S.	N.S.	**p = 0.001** **F = 13.440**	N.S.
PAL (L)	N.S.	N.S.	N.S.	p = 0.025 F = 5.556	N.S.
PAL (R)	N.S.	N.S.	N.S.	p = 0.014 F = 6.738	N.S.
THA (L)	N.S.	N.S.	N.S.	N.S.	N.S.
THA (R)	N.S.	N.S.	N.S.	p = 0.035 F = 4.814	**p = 0.016** **F = 6.449**
HES (L)	N.S.	N.S.	N.S.	N.S.	**p = 0.028** **F = 5.271**
HES (R)	N.S.	p = 0.031 F = 5.061	p = 0.012 F = 7.131	N.S.	p = 0.041 F = 4.506
T1 (L)	N.S.	p = 0.037 F = 4.710	p = 0.011 F = 7.235	N.S.	**p = 0.016** **F = 6.432**
T1 (R)	N.S.	**p < 0.001** **F = 17.798**	p = 0.001 F = 14.411	N.S.	N.S.
T1P (L)	N.S.	N.S.	N.S.	**p = 0.002** **F = 11.304**	N.S.
T1P (R)	N.S.	N.S.	N.S.	p = 0.029 F = 5.225	N.S.
T2 (L)	p = 0.028 F = 5.305	p = 0.005 F = 9.172	p = 0.005 F = 9.263	N.S.	**p = 0.024** **F = 5.616**
T2 (R)	N.S.	**p < 0.001** **F = 15.620**	p = 0.001 F = 12.612	N.S.	**p = 0.010** **F = 7.516**
T2P (L)	p = 0.046 F = 4.285	p = 0.042 F = 4.468	N.S.	p = 0.027 F = 5.332	N.S.
T2P (R)	N.S.	N.S.	N.S.	N.S.	N.S.
T3 (L)	N.S.	p = 0.038 F = 4.647	p = 0.006 F = 8.652	N.S.	**p = 0.004** **F = 9.339**
T3 (R)	N.S.	N.S.	N.S.	N.S.	

Table 5 (*continued*)

ROI	Nodal degree	Betweenness centrality	Binary nodal efficiency	FN-weighted nodal efficiency	FA-weighted nodal efficiency
					p = 0.017
					F = 6.273
CER (L)	p = 0.023	N.S.	N.S.	**p < 0.001**	**p = 0.011**
	F = 5.657			**F = 15.467**	**F = 7.346**
CER (R)	p = 0.042	N.S.	N.S.	**p < 0.001**	**p = 0.003**
	F = 4.471			**F = 19.769**	**F = 10.630**
VER	p = 0.026	N.S.	N.S.	p = 0.006	**p = 0.016**
	F = 5.453			F = 8.539	**F = 6.467**

Features that maintain significance after False Discovery Rate controlling alpha error to 0.05 are highlighted in bold. (L) refers to left hemisphere, (R) to right hemisphere. N.S. for Not Significant.

used to solve this issue and provide more accurate WM tractography reconstruction in future studies. Current limitations of DTI based tractography, and the noisy nature of the acquisitions, may result in the inclusion of spurious connections in individual networks. However, it must be noted that we did not perform an analysis directly based on edges, but measured network topology features. This approach is robust against noise as it integrates overall information of the individual networks, and therefore, minimizes the effect of spurious connections. How the connectivity between regions must be quantified is also an issue to be addressed. Binarization of the obtained network implies a loss of information of the connectivity pattern, and some authors propose different measures to quantify connections based on diffusion MRI as the number of fiber bundles, density of fibers or average measures of diffusion along the tract (Hagmann et al., 2007; Li et al., 2009; Wee et al., 2010). However, how the weight of a connection must be quantified, and its correlation with the anatomical substrate in which transfer of neural signals yields is still an open question (Li et al., 2009; Shu et al., 2009). It must be noted that average degree, and therefore the network cost, were non-significantly different between groups in the unthresholded networks, which supports that similar network density of WM connections were calculated throughout all the population, minimizing the chances of differences in network cost causing some of the observed differences.

It is also worth noticing that the proportion of control subjects with abnormal Bayley scores may seem relatively high (27%). Part of the control population was composed by prematurely born infants, which by definition are associated with increased rates of neurodevelopmental delay (Darlow et al., 2009). While we cannot exclude that this may have hampered the demonstration of some differences, correction for prematurity was important to ensure that differences are most likely the consequence of intrauterine growth restriction. Finally, we acknowledge that the relatively reduced sample size used in the present study prevents to generalize the set of altered features that predict an abnormal BSID-III performance. Larger sample sizes will help to estimate the generality of the identified regions in future studies and the robustness of the learning algorithm.

Conclusion

In conclusion, MRI connectomics is an emerging technique that is suitable for the assessment of brain reorganization in IUGR infants by means of global and regional graph theory based network features,

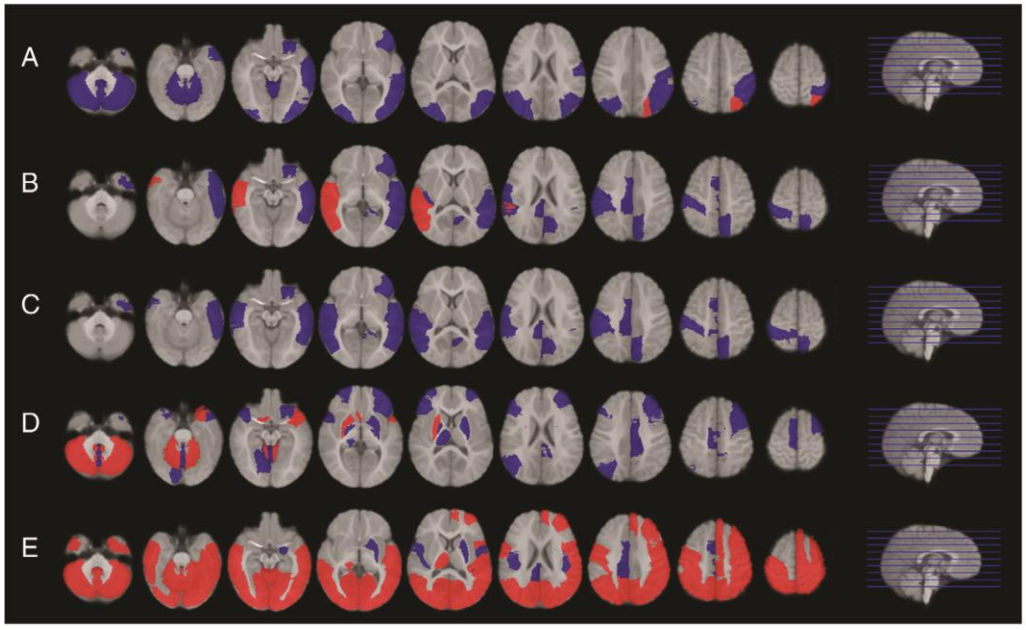

Fig. 4. Altered regional features in IUGR. In blue, regional characteristics showing statistically significant differences ($p<0.05$) in IUGR. In red, those regional characteristics that remained statistically significant after False Discovery Rate controlling alpha error at 5%. (A) Nodal degree, (B) betweenness centrality, (C) binary nodal efficiency, (D) FN-weighted nodal efficiency and (E) FA-weighted nodal efficiency. (For interpretation of the references to color in this figure legend, the reader is referred to the web version of this article.)

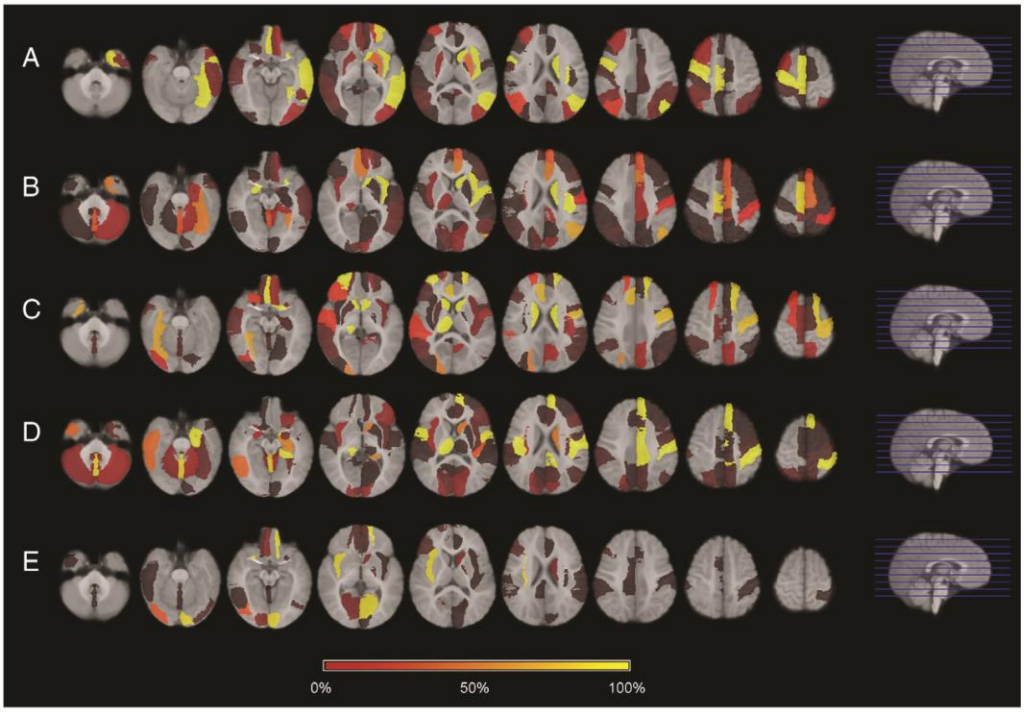

Fig. 5. Regional features associated with an abnormal BSID-III outcome in IUGR expressed as the frequency (%) of selection in the leave-one-out algorithm. (A) Nodal degree, (B) betweenness centrality, (C) binary nodal efficiency, (D) FN-weighted nodal efficiency and (E) FA-weighted nodal efficiency.

which are related to different levels of organizational complexity. We could demonstrate altered brain network topology in one-year-old IUGR infants and its association with abnormal performance in neurodevelopmental scales (BSID-III) at two years of age. Larger studies are required to validate the results here reported. However, the findings show the potential of diffusion MRI based connectomics and graph theory based network analysis for extracting features that characterize the individual architecture of neural circuitry. Hence, this methodology holds as a promising candidate for the

Table 6
Binomial logistic regression (enter method) of abnormal Bayleys performance using three blocks of predictors: clinical characteristics, global connectivity features, and regional connectivity risk index.

	B	S.E.	Wald	df	Sig.
Clinical characteristics (Cox and Snell R^2: 0.155; Nagelkerke R^2: 0.207; model significance: $p = 0.825$)					
Maternal education	−0.610	1.646	0.137	1	0.711
Smoking status	0.791	1.292	0.375	1	0.540
Gender	0.404	1.238	0.106	1	0.744
Breastfeeding more than 4 months	1.081	1.394	0.602	1	0.438
GA	−0.135	0.246	0.300	1	0.584
Weight centile	−0.021	0.300	0.005	1	0.945
Constant	3.953	9.952	0.158	1	0.691
Global connectivity features (Cox and Snell R^2: 0.439; Nagelkerke R^2: 0.585; model significance: $p = 0.199$)					
Mean degree	1.601	1.452	1.216	1	0.270
Binary global efficiency	−491.020	672.818	0.533	1	0.466
Binary local efficiency	274.691	621.901	0.195	1	0.659
FN-weighted global efficiency	0.894	1.016	0.775	1	0.379
FN-weighted local efficiency	−4.375	4.024	1.182	1	0.277
FA-weighted global efficiency	−537.727	1046.374	0.264	1	0.607
FA-weighted local efficiency	688.091	1061.576	0.420	1	0.517
Constant	68.287	124.702	0.300	1	0.584
Regional connectivity features (Cox and Snell R^2: 0.344; Nagelkerke R^2: 0.459; model significance: $p = 0.007$)					
Regional connectivity risk index	3.348	1.443	5.384	1	0.020
Constant	−1.805	1.014	3.170	1	0.075

Table 7
Binomial logistic regression (step-wise backward method) of abnormal Bayleys performance in three consecutive blocks including clinical characteristics, global connectivity features, and regional connectivity risk index. Results are the last step of the backward algorithm.

Number of steps	Variables remaining in the step	B	S.E.	Wald	Sig. in the equation	Sig. of the model change if removed
Block1: clinical characteristics (Cox and Snell R^2: 0.000; Nagelkerke R^2: 0.000; model significance: $p = 0.229$)						
7	Constant	−0.118	0.486	0.059	0.808	–
Block2: clinical characteristics + global connectivity features (Cox and Snell R^2: 0.250; Nagelkerke R^2: 0.333; model significance: $p = 0.087$)						
6	Mean degree	0.361	0.305	1.402	0.236	0.105
	Binary global efficiency	−94.774	61.936	2.342	0.126	0.050
	Constant	62.155	41.914	2.199	0.138	–
Block3: clinical characteristics + global connectivity features + regional connectivity risk index (Cox and Snell R^2: 0.488; Nagelkerke R^2: 0.651; model significance: $p = 0.010$)						
1	Mean degree	0.757	0.527	2.069	0.150	–
	Global efficiency	−150.857	97.979	2.371	0.124	–
	Regional connectivity risk index	4.238	2.177	3.790	0.052	0.011
	Constant	89.089	61.150	2.123	0.145	–

development of imaging biomarkers of poor neurodevelopmental outcome in infants at risk due to prenatal diseases.

Acknowledgments

This work was supported by grants: Obra Social "la Caixa", Barcelona, Spain; The Cerebra Foundation for the Brain-Injured Child, Carmarthen, Wales, UK; The Thrasher Research Fund, Salt Lake City, USA; Rio Hortega and Sara Borrell grants from Carlos III Institute of Health, Spain (CM08/00105, to E.E., CM11/00032 to M.I. and CD11/00048 to E.M.); Emili Letang fellowship by Hospital Clinic, Barcelona, Spain (to M.I.) and Marie Curie Industry-Academia Partnerships and Pathways (IAPP) (FP7-PEOPLE-2007-3-1-IAPP 217911 uVOLUMES, to I.A.). The Image Registration Toolkit was used under license from Ixico Ltd.

Appendix A. Supplementary data

Supplementary data to this article can be found online at doi:10.1016/j.neuroimage.2012.01.059.

References

Achard, S., Bullmore, E., 2007. Efficiency and cost of economical brain functional networks. PLoS Comput. Biol. 3, e17.
Alexander-Bloch, A.F., Gogtay, N., Meunier, D., Birn, R., Clasen, L., Lalonde, F., Lenroot, R., Giedd, J., Bullmore, E.T., 2010. Disrupted modularity and local connectivity of brain functional networks in childhood-onset schizophrenia. Front. Syst. Neurosci. 4, 147.
Altaye, M., Holland, S.K., Wilke, M., Gaser, C., 2008. Infant brain probability templates for MRI segmentation and normalization. NeuroImage 43, 721–730.
Anderson, P.J., De Luca, C.R., Hutchinson, E., Roberts, G., Doyle, L.W., 2010. Underestimation of developmental delay by the new Bayley-III Scale. Arch. Pediatr. Adolesc. Med. 164, 352–356.
Ashburner, J., Friston, K.J., 2005. Unified segmentation. NeuroImage 26, 839–851.
Baschat, A.A., 2004. Pathophysiology of fetal growth restriction: implications for diagnosis and surveillance. Obstet. Gynecol. Surv. 59, 617–627.
Bassan, H., Stolar, O., Geva, R., Eshel, R., Fattal-Valevski, A., Leitner, Y., Waron, M., Jaffa, A., Harel, S., 2011. Intrauterine growth-restricted neonates born at term or preterm: how different? Pediatr. Neurol. 44, 122–130.
Bassett, D.S., Bullmore, E.T., 2009. Human brain networks in health and disease. Curr. Opin. Neurol. 340–347.
Bassett, D.S., Bullmore, E., Verchinski, B.A., Mattay, V.S., Weinberger, D.R., Meyer-Lindenberg, A., 2008. Hierarchical organization of human cortical networks in health and schizophrenia. J. Neurosci. 28, 9239–9248.
Benjamini, Y., Krieger, A.M., Yekutieli, D., 2006. Adaptive linear step-up procedures that control the false discovery rate. Biometrika 93, 491–507.
Breiman, L., Friedman, J.H., Olshen, R.A., Stone, C.G., 1984. Classification and Regression Trees. CRC Press, Boca Raton, FL.
Bullmore, E., Sporns, O., 2009. Complex brain networks: graph theoretical analysis of structural and functional systems. Nat. Rev. Neurosci. 10, 186–198.
Castellanos, F.X., Giedd, J.N., Eckburg, P., Marsh, W.L., Vaituzis, A.C., Kaysen, D., Hamburger, S.D., Rapoport, J.L., 1994. Quantitative morphology of the caudate nucleus in attention deficit hyperactivity disorder. Am. J. Psychiatry 151, 1791–1796.
Chen, C.H., Lennox, B., Jacob, R., Calder, A., Lupson, V., Bisbrown-Chippendale, R., Suckling, J., Bullmore, E., 2006. Explicit and implicit facial affect recognition in manic and depressed states of bipolar disorder: a functional magnetic resonance imaging study. Biol. Psychiatry 59, 31–39.
Darlow, B.A., Horwood, L.J., Wynn-Williams, M.B., Mogridge, N., Austin, N.C., 2009. Admissions of all gestations to a regional neonatal unit versus controls: 2-year outcome. J. Paediatr. Child Health 45, 187–193.
Doria, V., Beckmann, C.F., Arichi, T., Merchant, N., Groppo, M., Turkheimer, F.E., Counsell, S.J., Murgasova, M., Aljabar, P., Nunes, R.G., Larkman, D.J., Rees, G., Edwards, A.D., 2010. Emergence of resting state networks in the preterm human brain. Proc. Natl. Acad. Sci. U. S. A. 107, 20015–20020.
Dubois, J., Benders, M., Borradori-Tolsa, C., Cachia, A., Lazeyras, F., Ha-Vinh Leuchter, R., Sizonenko, S.V., Warfield, S.K., Mangin, J.F., Hüppi, P.S., 2008. Primary cortical folding in the human newborn: an early marker of later functional development. Brain 131, 2028–2041.
Eixarch, E., Meler, E., Iraola, A., Illa, M., Crispi, F., Hernandez-Andrade, E., Gratacos, E., Figueras, F., 2008. Neurodevelopmental outcome in 2-year-old infants who were small-for-gestational age term fetuses with cerebral blood flow redistribution. Ultrasound Obstet. Gynecol. 32, 894–899.
Esteban, F.J., Padilla, N., Sanz-Cortes, M., de Miras, J.R., Bargallo, N., Villoslada, P., Gratacos, E., 2010. Fractal-dimension analysis detects cerebral changes in preterm infants with and without intrauterine growth restriction. NeuroImage 53, 1225–1232.
Fan, Y., Shi, F., Smith, J.K., Lin, W., Gilmore, J.H., Shen, D., 2011. Brain anatomical networks in early human brain development. NeuroImage 54, 1862–1871.
Faraone, S.V., Biederman, J., 1998. Neurobiology of attention-deficit hyperactivity disorder. Biol. Psychiatry 44, 951–958.
Feldman, R., Eidelman, A.I., 2006. Neonatal state organization, neuromaturation, mother–infant interaction, and cognitive development in small-for-gestational-age premature infants. Pediatrics 118, e869–e878.
Figueras, F., Meler, E., Iraola, A., Eixarch, E., Coll, O., Figueras, J., Francis, A., Gratacos, E., Gardosi, J., 2008. Customized birthweight standards for a Spanish population. Eur. J. Obstet. Gynecol. Reprod. Biol. 136, 20–24.
Figueras, F., Oros, D., Cruz-Martinez, R., Padilla, N., Hernandez-Andrade, E., Botet, F., Costas-Moragas, C., Gratacos, E., 2009. Neurobehavior in term, small-for-gestational age infants with normal placental function. Pediatrics 124, e934–e941.
Fillard, P., Pennec, X., Arsigny, V., Ayache, N., 2007. Clinical DT-MRI estimation, smoothing, and fiber tracking with log-Euclidean metrics. IEEE Trans. Med. Imaging 26, 1472–1482.
Fransson, P., Skiold, B., Horsch, S., Nordell, A., Blennow, M., Lagercrantz, H., Aden, U., 2007. Resting-state networks in the infant brain. Proc. Natl. Acad. Sci. U. S. A. 104, 15531–15536.
Fransson, P., Aden, U., Blennow, M., Lagercrantz, H., 2010. The functional architecture of the infant brain as revealed by resting-state FMRI. Cereb. Cortex 21, 145–154.
Geva, R., Eshel, R., Leitner, Y., Fattal-Valevski, A., Harel, S., 2006a. Memory functions of children born with asymmetric intrauterine growth restriction. Brain Res. 1117, 186–194.
Geva, R., Eshel, R., Leitner, Y., Valevski, A.F., Harel, S., 2006b. Neuropsychological outcome of children with intrauterine growth restriction: a 9-year prospective study. Pediatrics 118, 91–100.
Gong, G., He, Y., Concha, L., Lebel, C., Gross, D.W., Evans, A.C., Beaulieu, C., 2009. Mapping anatomical connectivity patterns of human cerebral cortex using in vivo diffusion tensor imaging tractography. Cereb. Cortex 19, 524–536.
Hagmann, P., 2005. From Diffusion MRI to Brain Connectomics. Signal Processing Institute. Ecole Polytechnique Fédérale de Lausanne (EPFL), Lausane.
Hagmann, P., Kurant, M., Gigandet, X., Thiran, P., Wedeen, V.J., Meuli, R., Thiran, J.P., 2007. Mapping human whole-brain structural networks with diffusion MRI. PLoS One 2, e597.
Hagmann, P., Cammoun, L., Gigandet, X., Meuli, R., Honey, C., Wedeen, V.J., Sporns, O., 2008. Mapping the structural core of human cerebral cortex. PLoS Biol. 6e, 159.
Hagmann, P., Sporns, O., Madan, N., Cammoun, L., Pienaar, R., Wedeen, V.J., Meuli, R., Thiran, J.P., Grant, P.E., 2010. White matter maturation reshapes structural connectivity in the late developing human brain. Proc. Natl. Acad. Sci. U. S. A. 107, 19067–19072.
Hänggi, J., Wotruba, D., Jancke, L., 2011. Globally altered structural brain network topology in grapheme-color synesthesia. J. Neurosci. 31, 5816–5828.
He, Y., Chen, Z., Evans, A.C., 2008. Structural insights into aberrant topological patterns of large-scale cortical networks in Alzheimer's disease. J. Neurosci. 28, 8148–8159.
He, Y., Chen, Z., Gong, G., Evans, A., 2009a. Neuronal networks in Alzheimer's disease. Neuroscientist 15, 333.
He, Y., Dagher, A., Chen, Z., Charil, A., Zijdenbos, A., Worsley, K., Evans, A., 2009b. Impaired small-world efficiency in structural cortical networks in multiple sclerosis associated with white matter lesion load. Brain 132, 3366–3379.
Heinonen, K., Raikkonen, K., Pesonen, A.K., Andersson, S., Kajantie, E., Eriksson, J.G., Wolke, D., Lano, A., 2010. Behavioural symptoms of attention deficit/hyperactivity disorder in preterm and term children born small and appropriate for gestational age: a longitudinal study. BMC Pediatr. 10, 91.
Honey, C.J., Thivierge, J.P., Sporns, O., 2010. Can structure predict function in the human brain? NeuroImage 52, 766–776.
Iturria-Medina, Y., Sotero, R.C., Canales-Rodríguez, E.J., Alemán-Gómez, Y., Melie-García, L., 2008. Studying the human brain anatomical network via diffusion-weighted MRI and graph theory. NeuroImage 40, 1064–1076.
Jarvis, S., Glinianaia, S.V., Torrioli, M.G., Platt, M.J., Miceli, M., Jouk, P.S., Johnson, A., Hutton, J., Hemming, K., Hagberg, G., Dolk, H., Chalmers, J., 2003. Cerebral palsy and intrauterine growth in single births: European collaborative study. Lancet 362, 1106–1111.
Kady, S., Gardosi, J., 2004. Perinatal mortality and fetal growth restriction. Best Pract. Res. Clin. Obstet. Gynaecol. 18, 397–410.
Knickmeyer, R.C., Gouttard, S., Kang, C., Evans, D., Wilber, K., Smith, J.K., Hamer, R.M., Lin, W., Gerig, G., Gilmore, J.H., 2008. A structural MRI study of human brain development from birth to 2 years. J. Neurosci. 28, 12176–12182.
Kobel, M., Bechtel, N., Specht, K., Klarhöfer, M., Weber, P., Scheffler, K., Opwis, K., Penner, I.-K., 2010. Structural and functional imaging approaches in attention deficit/hyperactivity disorder: does the temporal lobe play a key role? Psychiatry Res. 183, 230–236.
Leitner, Y., Fattal-Valevski, A., Geva, R., Eshel, R., Toledano-Alhadef, H., Rotstein, M., Bassan, H., Radianu, B., Bitchonsky, O., Jaffa, A.J., Harel, S., 2007. Neurodevelopmental outcome of children with intrauterine growth retardation: a longitudinal, 10-year prospective study. J. Child Neurol. 22, 580–587.
Li, Y., Liu, Y., Li, J., Qin, W., Li, K., Yu, C., Jiang, T., 2009. Brain anatomical network and intelligence. PLoS Comput. Biol. 5, e1000395.
Liu, Y., Liang, M., Zhou, Y., He, Y., Hao, Y., Song, M., Yu, C., Liu, H., Liu, Z., Jiang, T., 2008. Disrupted small-world networks in schizophrenia. Brain 131, 945–961.
Lo, C.Y., Wang, P.N., Chou, K.H., Wang, J., He, Y., Lin, C.P., 2010. Diffusion tensor tractography reveals abnormal topological organization in structural cortical networks in Alzheimer's disease. J. Neurosci. 30, 16876–16885.
Lodygensky, G.A., Seghier, M.L., Warfield, S.K., Tolsa, C.B., Sizonenko, S., Lazeyras, F., Hüppi, P.S., 2008. Intrauterine growth restriction affects the preterm infant's hippocampus. Pediatr. Res. 63, 438–443.

Maes, F., Collignon, A., Vandermeulen, D., Marchal, G., Suetens, P., 1997. Multimodality image registration by maximization of mutual information. IEEE Trans. Med. Imaging 16, 187–198.
Makki, M.I., Govindan, R.M., Wilson, B.J., Behen, M.E., Chugani, H.T., 2009. Altered fronto-striato-thalamic connectivity in children with Tourette syndrome assessed with diffusion tensor MRI and probabilistic fiber tracking. J. Child Neurol. 24, 669–678.
Mallard, C., Loeliger, M., Copolov, D., Rees, S., 2000. Reduced number of neurons in the hippocampus and the cerebellum in the postnatal guinea-pig following intrauterine growth-restriction. Neuroscience 100, 327–333.
Marsal, K., 2002. Intrauterine growth restriction. Curr. Opin. Obstet. Gynecol. 14, 127–135.
McCarton, C.M., Wallace, I.F., Divon, M., Vaughan Jr., H.G., 1996. Cognitive and neurologic development of the premature, small for gestational age infant through age 6: comparison by birth weight and gestational age. Pediatrics 98, 1167–1178.
Michel, V., Gramfort, A., Varoquaux, G., Eger, E., Keribin, C., Thirion, B., 2012. A supervised clustering approach for fMRI-based inference of brain states. Pattern Recognit. 45 (6), 2041–2049.
Padilla, N., Falcon, C., Sanz-Cortes, M., Figueras, F., Bargallo, N., Crispi, F., Eixarch, E., Arranz, A., Botet, F., Gratacos, E., 2011. Differential effects of intrauterine growth restriction on brain structure and development in preterm infants: a magnetic resonance imaging study. Brain Res. 1382, 98–108.
Paus, T., Collins, D.L., Evans, A.C., Leonard, G., Pike, B., Zijdenbos, A., 2001. Maturation of white matter in the human brain: a review of magnetic resonance studies. Brain Res. Bull. 54, 255–266.
Rees, S., Harding, R., Walker, D., 2011. The biological basis of injury and neuroprotection in the fetal and neonatal brain. Int. J. Dev. Neurosci. 29, 551–563.
Robinson, H.P., Fleming, J.E., 1975. A critical evaluation of sonar "crown-rump length" measurements. Br. J. Obstet. Gynaecol. 82, 702–710.
Rubinov, M., Sporns, O., 2009. Complex network measures of brain connectivity: uses and interpretations. NeuroImage 52, 1059–1069.
Scherjon, S., Briet, J., Oosting, H., Kok, J., 2000. The discrepancy between maturation of visual-evoked potentials and cognitive outcome at five years in very preterm infants with and without hemodynamic signs of fetal brain-sparing. Pediatrics 105, 385–391.
Shi, F., Yap, P.T., Wu, G., Jia, H., Gilmore, J.H., Lin, W., Shen, D., 2011. Infant brain atlases from neonates to 1- and 2-year-olds. PLoS One 6, e18746.
Shu, N., Liu, Y., Li, J., Li, Y., Yu, C., Jiang, T., 2009. Altered anatomical network in early blindness revealed by diffusion tensor tractography. PLoS One 4, e7228.
Shu, N., Liu, Y., Li, K., Duan, Y., Wang, J., Yu, C., Dong, H., Ye, J., He, Y., 2011. Diffusion tensor tractography reveals disrupted topological efficiency in white matter structural networks in multiple sclerosis. Cereb. Cortex 21, 2565–2577.
Smyser, C.D., Inder, T.E., Shimony, J.S., Hill, J.E., Degnan, A.J., Snyder, A.Z., Neil, J.J., 2010. Longitudinal analysis of neural network development in preterm infants. Cereb. Cortex 20, 2852–2862.
Smyser, C.D., Snyder, A.Z., Neil, J.J., 2011. Functional connectivity MRI in infants: exploration of the functional organization of the developing brain. NeuroImage 56, 1437–1452.
Sobradillo, B., Aguirre, A., Aresti, U., Bilbao, C., Fernandez-Ramos, C., Lizarraga, A., Lorenzo, H., Madariaga, L., Rica, I., Ruiz, I., Sanchez, E., Santamaria, C., Serrano, J., Zabala, A., Zurimendi, B., Hernandez, M., 2004. Curvas y tablas de crecimiento (Estudios longitudinal y transversal). Fundacion Faustino Orbegozo Eizaguirre Bilbao.
Sporns, O., Tononi, G., 2001. Classes of network connectivity and dynamics. Complexity 7, 28–38.
Sporns, O., Tononi, G., Kotter, R., 2005. The human connectome: a structural description of the human brain. PLoS Comput. Biol. 1, e42.
Studholme, C., Hill, D.L.G., Hawkes, D.J., 1999. An overlap invariant entropy measure of 3D medical image alignment. Pattern Recognit. 32, 71–86.
Thompson, D.K., Warfield, S.K., Carlin, J.B., Pavlovic, M., Wang, H.X., Bear, M., Kean, M.J., Doyle, L.W., Egan, G.F., Inder, T.E., 2007. Perinatal risk factors altering regional brain structure in the preterm infant. Brain 130, 667–677.
Toft, P.B., 1999. Prenatal and perinatal striatal injury: a hypothetical cause of attention-deficit-hyperactivity disorder? Pediatr. Neurol. 21, 602–610.
Tolsa, C.B., Zimine, S., Warfield, S.K., Freschi, M., Sancho Rossignol, A., Lazeyras, F., Hanquinet, S., Pfizenmaier, M., Hüppi, P.S., 2004. Early alteration of structural and functional brain development in premature infants born with intrauterine growth restriction. Pediatr. Res. 56, 132–138.
Tomasi, D., Volkow, N.D., 2011. Functional connectivity hubs in the human brain. NeuroImage 57, 908–917.
Tristan-Vega, A., Arribas, J.I., 2007. A fast B-spline pseudo-inversion algorithm for consistent image registration. Proceedings of the International Conference on Computer Analysis Images and Patterns (CAIP), Vienna, Austria, pp. 768–775.
Tuch, D.S., 2004. Q-ball imaging. Magn. Reson. Med. 52, 1358–1372.
Tzourio-Mazoyer, N., Landeau, B., Papathanassiou, D., Crivello, F., Etard, O., Delcroix, N., Mazoyer, B., Joliot, M., 2002. Automated anatomical labeling of activations in SPM using a macroscopic anatomical parcellation of the MNI MRI single-subject brain. NeuroImage 15, 273–289.
Vourkas, M., Micheloyannis, S., Simos, P.G., Rezaie, R., Fletcher, J.M., Cirino, P.T., Papanicolaou, A.C., 2010. Dynamic task-specific brain network connectivity in children with severe reading difficulties. Neurosci. Lett. 488, 123–128.
Wang, L., Zhu, C., He, Y., Zang, Y., Cao, Q., Zhang, H., Zhong, Q., Wang, Y., 2009. Altered small-world brain functional networks in children with attention-deficit/hyperactivity disorder. Hum. Brain Mapp. 30, 638–649.
Wang, L., Metzak, P.D., Honer, W.G., Woodward, T.S., 2010. Impaired efficiency of functional networks underlying episodic memory-for-context in schizophrenia. J. Neurosci. 30, 13171–13179.
Wang, Q., Su, T.P., Chou, K.H., Chen, I.Y., Jiang, T., Lin, C.P., 2012. Anatomical insights into disrupted small-world networks in schizophrenia. NeuroImage 59, 1085–1093.
Warfield, S.K., Guimond, A., Roche, A., Bharatha, A., Tei, A., Talos, F., Rexilius, J., Ruiz-Alzola, J., Westin, C.F., Haker, S., Angenent, S., Tannenbaum, A., Jolesz, F., Kilkinis, R., 2002. Advanced nonrigid registration algorithms for image fusion. In: Mazziotta, J.C., Toga, A.W. (Eds.), Brain Mapping: The Methods. Elsevier, pp. 661–690.
Watts, D.J., Strogatz, S.H., 1998. Collective dynamics of 'small-world' networks. Nature 393, 440–442.
Wedeen, V.J., Hagmann, P., Tseng, W.Y., Reese, T.G., Weisskoff, R.M., 2005. Mapping complex tissue architecture with diffusion spectrum magnetic resonance imaging. Magn. Reson. Med. 54, 1377–1386.
Wee, C.Y., Yap, P.T., Li, W., Denny, K., Browndyke, J.N., Potter, G.G., Welsh-Bohmer, K.A., Wang, L., Shen, D., 2010. Enriched white matter connectivity networks for accurate identification of MCI patients. NeuroImage 54, 1812–1822.
Wen, W., Zhu, W., He, Y., Kochan, N.A., Reppermund, S., Slavin, M.J., Brodaty, H., Crawford, J., Xia, A., Sachdev, P., 2011. Discrete neuroanatomical networks are associated with specific cognitive abilities in old age. J. Neurosci. 31, 1204–1212.
Wu, T., Wang, L., Chen, Y., Zhao, C., Li, K., Chan, P., 2009. Changes of functional connectivity of the motor network in the resting state in Parkinson's disease. Neurosci. Lett. 460, 6–10.
Yan, C., Gong, G., Wang, J., Wang, D., Liu, D., Zhu, C., Chen, Z.J., Evans, A., Zang, Y., He, Y., 2010. Sex- and brain size-related small-world structural cortical networks in young adults: a DTI tractography study. Cereb. Cortex 21, 449–458.
Yap, P.T., Fan, Y., Chen, Y., Gilmore, J.H., Lin, W., Shen, D., 2011. Development trends of white matter connectivity in the first years of life. PLoS One 6, e24678.

Supplementary Material

1.-Graph Theory definitions and formulation

General graph measures

We used definitions and nomenclature compiled by Rubinov and Sporns (2009). Briefly, *N* was defined as the set of all nodes in the network, and *n* as the number of nodes, (i, j) was the link between nodes *i* and *j* and a_{ij} the connection status between node *i* and *j*: $a_{ij} = 1$ when link (i, j) exists and zero otherwise. w_{ij} is defined as the weight of the link (i, j) in weighted networks.

Degree of a node *i* was calculated as $k_i = \sum_{j \in N} a_{ij}$. Shortest path length between nodes *i* and *j* was defined for binary networks as $d_{ij} = \sum a_{uv} \in g_{i \leftrightarrow j}$, where $g_{i \leftrightarrow j}$ is the shortest path (geodesic) between *i* and *j*. Shortest path length was generalized for weighted networks as $d_{ij}^{w} = \sum a_{uv} \in g_{i \leftrightarrow j}^{w} f(w_{uv})$, where f is a map from weight to length (in our case an inverse map) and $g_{i \leftrightarrow j}^{w}$ is the shortest weighted path between *i* and *j*. Number of triangles around a node *i* was defined as $t_i = \frac{1}{2} \sum_{j,h \in N} a_{ij} a_{ih} a_{jh}$.

Clustering coefficient and characteristic path length

Clustering coefficient of a node was defined as the fraction of triangles around that individual node, and is equivalent to the fraction of the node's neighbors that are also neighbors of each other (Watts and Strogatz, 1998). The clustering coefficient of a network, C_p, was defined as the average of each node clustering coefficient (Watts and Strogatz, 1998) :

$$C_p = \frac{1}{n} \sum_{i \in N} C_i = \frac{1}{n} \sum_{i \in N} \frac{2t_i}{k_i (k_i - 1)}$$

Characteristic path length of a network, L_p, was defined as the average shortest path length between all pair of nodes (Watts and Strogatz, 1998):

$$L_p = \frac{1}{n}\sum_{i\in N} L_i = \frac{1}{n}\sum_{i\in N}\frac{\sum_{j\in N, j\neq i} d_{ij}}{n-1}$$

Normalized clustering coefficient of a network, γ, and normalized characteristic path length, λ, were defined as $\gamma = \frac{C_p}{C_{p_{rand}}}$ and $\lambda = \frac{L_p}{L_{p_{rand}}}$ respectively, were $C_{p_{rand}}$ and $L_{p_{rand}}$ are the mean clustering coefficient and characteristic path length of matched random networks that preserve the same number of nodes and degree distribution as the real networks (Maslov and Sneppen, 2002).

Global and Local Efficiency

Global efficiency was defined as the average inverse shortest path length (Latora and Marchiori, 2001):

$$E_{glob} = \frac{1}{n}\sum_{i\in N}\frac{\sum_{j\in N, j\neq i} d_{ij}^{-1}}{n-1},$$

Generalized to weighted networks as:

$$E_{glob} = \frac{1}{n}\sum_{i\in N}\frac{\sum_{j\in N, j\neq i}\left(d_{ij}^{W}\right)^{-1}}{n-1}$$

Nodal efficiency of a node *i* was defined as the inverse of the harmonic mean of the minimum path length between that index node and all other nodes in the network (Achard and Bullmore, 2007):

$$E_{nodal}(i) = \frac{1}{k_i\left(k_1-1\right)}\sum_{j,h\in N, j\neq i} a_{ij}a_{ih}\left[d_{jh}(N_i)\right]^{-1}$$

Where $d_{jh}(N_i)$ is the length of the shortest path between *j* and *h*, which contains only neighbors of *i*.

Local efficiency was defined as the average of Nodal Efficiency of each node:

$$E_{loc} = \frac{1}{n}\sum_{i\in N} E_{nodal}(i) = \frac{1}{n}\sum_{i\in N}\frac{1}{k_i\left(k_i-1\right)}\sum_{j,h\in N,[j,h]\neq i} a_{ij}a_{ih}\left[d_{jh}(N_i)\right]^{-1}$$

Generalized to weighted networks as (Rubinov and Sporns, 2009):

$$E^{w}_{local} = \frac{1}{n}\sum_{i\in N}\frac{1}{k_i\left(k_i-1\right)}\sum_{j,h\in N, j\neq i} w_{ij}w_{ih}\left[d^{w}_{jh}(N_i)\right]^{-\frac{1}{3}}$$

REFERENCES

Achard, S., Bullmore, E., 2007. Efficiency and cost of economical brain functional networks. PLoS Comput Biol 3, e17.
Latora, V., Marchiori, M., 2001. Efficient behavior of small-world networks. Phys Rev Lett 87, 198701.
Maslov, S., Sneppen, K., 2002. Protein interaction networks beyond artifacts. FEBS Lett 530, 255-256.
Rubinov, M., Sporns, O., 2009. Complex network measures of brain connectivity: uses and interpretations. Neuroimage 52, 1059-1069.
Watts, D.J., Strogatz, S.H., 1998. Collective dynamics of 'small-world' networks. Nature 393, 440-442.

2.- Supplementary Tables

Supplementary Table 1. Mean λ, γ and σ small-world parameters at different fiber thresholds in controls and IUGR .

Fiber Threshold	Group	λ	γ	σ
1	Controls	1.0001	1.0474	1.0473
	IUGR	1.0001	1.0437	1.0436
2	Controls	1.0013	1.1113	1.1099
	IUGR	1.0015	1.1103	1.1086
3	Controls	1.0040	1.1719	1.1671
	IUGR	1.0038	1.1754	1.1709
4	Controls	1.0066	1.2271	1.2190
	IUGR	1.0069	1.2240	1.2156
5	Controls	1.0099	1.2754	1.2627
	IUGR	1.0104	1.2817	1.2685

Supplementary Table 2. Average (± SD) global characteristics of control and IUGR.

Fiber Threshold	Group	Mean degree	Binary global efficiency	Binary local efficiency	FN weighted global efficiency	FN weighted local efficiency	FA weighted global efficiency	FA weighted local efficiency
1	Controls	58.7 (3.3)	0.819 (0.018)	0.877 (0.010)	52.507 (5.602)	19.454 (1.810)	0.274 (0.015)	0.303 (0.015)
	IUGR	58.5 (2.8)	0.818 (0.015)	0.877 (0.009)	51.777 (4.172)	18.956 (1.260)	0.268 (0.016)	0.297 (0.015)
		p=0.088 F=3.101	p=0.088 F=3.089	p=0.162 F=2.045	p=0.110 F=2.700	p=0.065 F=3.637	p=0.012 F=7.153	p=0.020 F=5.986
2	Controls	48.4 (3.0)	0.763 (0.016)	0.850 (0.007)	52.507 (5.602)	24.546 (2.401)	0.256 (0.015)	0.298 (0.015)
	IUGR	47.8 (2.7)	0.759 (0.015)	0.850 (0.008)	51.777 (4.172)	24.210 (1.536)	0.250 (0.014)	0.292 (0.015)
		p=0.053 F=4.037	p=0.053 F=4.039	p=0.241 F=1.424	p=0.110 F=2.700	p=0.172 F=1.952	p=0.009 F=7.612	p=0.019 F=6.101
3	Controls	42.4 (2.6)	0.729 (0.014)	0.835 (0.007)	52.507 (5.602)	28.335 (2.747)	0.245 (0.014)	0.295 (0.015)
	IUGR	41.7 (2.6)	0.725 (0.014)	0.836 (0.007)	51.777 (4.172)	28.104 (1.715)	0.239 (0.014)	0.289 (0.014)
		p=0.027 F=5.362	p=0.028 F=5.288	p=0.636 F=0.0228	p=0.110 F=2.700	p=0.304 F=1.090	p=0.008 F=8.092	p=0.018 F=6.169
4	Controls	38.2 (2.3)	0.705 (0.013)	0.825 (0.006)	52.507 (5.602)	31.436 (2.976)	0.237 (0.014)	0.292 (0.015)
	IUGR	37.6 (2.4)	0.702 (0.014)	0.827 (0.007)	51.777 (4.172)	31.207 (1.851)	0.231 (0.014)	0.287 (0.014)
		p=0.017 F=6.338	p=0.018 F=6.857	p=0.960 F=0.003	p=0.110 F=2.700	p=0.414 F=0.684	p=0.006 F=8.729	p=0.015 F=6.541
5	Controls	35.1 (2.1)	0.687 (0.014)	0.818 (0.006)	52.507 (5.602)	34.110 (3.192)	0.231 (0.013)	0.290 (0.015)
	IUGR	34.6 (2.3)	0.684 (0.014)	0.820 (0.007)	51.777 (4.172)	33.885 (1.978)	0.225 (0.013)	0.285 (0.014)
		p=0.014 F=6.798	p=0.013 F=6.857	p=0.981 F=0.001	p=0.110 F=2.700	p=0.513 F=0.438	p=0.006 F=8.826	p=0.016 F=6.398

Significance calculated from general linear model with gender, maternal education level, smoking during pregnancy and breastfeeding as cofactors and GA as a covariate.

Supplementary Table 3. Selection frequencies of the most discriminant regional features. Selection frequency for each regional feature is computed from its ratio of selection in the leave-one-out cross validation used in the learning algorithm to obtain the 'connectivity risk index' that better associates with abnormal neurodevelopment.

ROI	Nodal Degree frequency of selection (%)	Betweenness Centrality frequency of selection (%)	Binary Nodal Efficiency frequency of selection (%)	FN-weighted Nodal Efficiency frequency of selection (%)	FA-weighted Nodal Efficiency frequency of selection (%)
PRE (L)	0	5,9	88,2	11,8	0
PRE (R)	100	5,9	0	0	0
F1 (L)	0	5,9	94,1	5,9	0
F1 (R)	0	0	52,9	0	0
F1O (L)	41,2	29,4	29,4	0	100
F1O (R)	0	0	17,6	5,9	11,8
F2 (L)	0	5,9	0	5,9	0
F2 (R)	35,3	0	0	0	0
F2O (L)	94,1	11,8	11,8	0	0
F2O (R)	41,2	0	100	0	0
F3OP (L)	0	0	11,8	0	0
F3OP (R)	0	0	0	0	0
F3T (L)	0	11,8	0	17,6	0
F3T (R)	5,9	0	11,8	0	11,8
F3O (L)	0	0	0	29,4	0
F3O (R)	11,8	5,9	52,9	0	0
RO (L)	5,9	100	35,3	100	0
RO (R)	0	5,9	0	100	0
SMA (L)	5,9	64,7	11,8	5,9	0
SMA (R)	100	94,1	23,5	5,9	0
OC (L)	0	0	100	0	0
OC (R)	0	0	0	5,9	0
F1M (L)	0	58,8	5,9	100	0
F1M (R)	5,9	11,8	0	0	0
F1MO (L)	11,8	29,4	5,9	5,9	11,8
F1MO (R)	23,5	70,6	0	0	11,8
GR (L)	23,5	17,6	35,3	0	0
GR (R)	100	5,9	100	0	29,4
IN (L)	100	100	23,5	17,6	5,9
IN (R)	0	29,4	5,9	35,3	94,1
ACIN (L)	5,9	70,6	0	11,8	5,9
ACIN (R)	0	0	88,2	5,9	0
MCIN (L)	11,8	35,3	0	100	0
MCIN (R)	0	0	0	0	5,9
PCIN (L)	17,6	0	0	0	0
PCIN (R)	0	0	5,9	0	0
HIP (L)	0	5,9	11,8	76,5	0
HIP (R)	0	0	0	0	0
PHIP (L)	0	35,3	0	100	0
PHIP (R)	0	0	0	0	0
AMYG (L)	0	5,9	0	23,5	0
AMYG (R)	11,8	100	0	35,3	0
V1 (L)	0	5,9	0	5,9	94,1
V1 (R)	0	0	0	0	23,5
Q (L)	0	29,4	0	29,4	5,9
Q (R)	0	17,6	0	17,6	0
LING (L)	0	0	5,9	0	0
LING (R)	0	0	0	0	0
O1 (L)	0	0	0	0	0

O1 (R)	0	5,9	70,6	29,4	0
O2 (L)	35,3	0	0	0	0
O2 (R)	5,9	0	5,9	0	0
O3 (L)	0	0	0	0	11,8
O3 (R)	0	0	41,2	0	58,8
FUSI (L)	100	70,6	0	17,6	0
FUSI (R)	0	0	82,4	0	0
POST (L)	0	47,1	0	100	5,9
POST (R)	11,8	0	0	0	0
P1 (L)	23,5	5,9	0	0	0
P1 (R)	0	5,9	0	17,6	0
P2 (L)	17,6	0	5,9	0	0
P2 (R)	23,5	5,9	11,8	0	0
SMG (L)	0	0	11,8	0	5,9
SMG (R)	0	5,9	0	11,8	5,9
AG (L)	100	82,4	11,8	11,8	0
AG (R)	52,9	11,8	0	0	0
PQ (L)	0	5,9	35,3	11,8	0
PQ (R)	5,9	0	0	5,9	0
PCL (L)	0	11,8	0	11,8	0
PCL (R)	94,1	23,5	17,6	0	0
CAU (L)	100	100	100	70,6	23,5
CAU (R)	0	0	100	0	0
PUT (L)	64,7	5,9	0	5,9	0
PUT (R)	29,4	0	11,8	0	0
PAL (L)	5,9	5,9	5,9	0	11,8
PAL (R)	0	0	0	0	0
THA (L)	0	0	0	5,9	0
THA (R)	0	29,4	100	100	0
HES (L)	0	0	23,5	58,8	5,9
HES (R)	0	5,9	0	5,9	0
T1 (L)	0	5,9	0	5,9	0
T1 (R)	5,9	0	52,9	5,9	0
T1P (L)	0	0	0	0	0
T1P (R)	0	0	0	0	0
T2 (L)	100	17,6	0	0	0
T2 (R)	17,6	0	17,6	0	0
T2P (L)	29,4	5,9	0	5,9	0
T2P (R)	0	0	0	0	0
T3 (L)	23,5	0	0	0	0
T3 (R)	0	5,9	0	64,7	5,9
CER (L)	0	35,3	0	35,3	0
CER (R)	0	5,9	0	29,4	0
VER	0	58,8	11,8	94,1	5,9

(L) refers to left hemisphere and (R) to right hemisphere.

5.2. PROJECT 2: COPY OF PUBLISHED PAPER

Normalization of similarity-based individual brain networks from gray matter MRI and its association with neurodevelopment in infants with intrauterine growth restriction

Batalle D, Munoz-Moreno E, Figueras F, Bargallo N, Eixarch E, Gratacos E

2013, Neuroimage 83C, 901-911.

NeuroImage 83 (2013) 901–911

Contents lists available at SciVerse ScienceDirect

NeuroImage

journal homepage: www.elsevier.com/locate/ynimg

Normalization of similarity-based individual brain networks from gray matter MRI and its association with neurodevelopment in infants with intrauterine growth restriction

Dafnis Batalle [a,*], Emma Muñoz-Moreno [a], Francesc Figueras [a,b,c], Nuria Bargallo [d,e], Elisenda Eixarch [a,b,c], Eduard Gratacos [a,b,c]

[a] Fetal and Perinatal Medicine Research Group, Institut d'Investigacions Biomediques August Pi i Sunyer (IDIBAPS), Barcelona, Spain
[b] Maternal-Fetal Medicine Department, ICGON, Hospital Clínic, Universitat de Barcelona, Barcelona, Spain
[c] Centro de Investigación Biomédica en Red de Enfermedades Raras (CIBERER), Barcelona, Spain
[d] Centre de Diagnòstic per la Imatge Clínic (CDIC), Hospital Clínic, Barcelona, Spain
[e] Clinical Imaging Research, Institut d'Investigacions Biomediques August Pi i Sunyer (IDIBAPS), Barcelona, Spain

ARTICLE INFO

Article history:
Accepted 16 July 2013
Available online 22 July 2013

Keywords:
Brain morphology
Children
Connectome
Graph theory
Neurodevelopment
Bayley Scale for Infant and Toddler Development

ABSTRACT

Obtaining individual biomarkers for the prediction of altered neurological outcome is a challenge of modern medicine and neuroscience. Connectomics based on magnetic resonance imaging (MRI) stands as a good candidate to exhaustively extract information from MRI by integrating the information obtained in a few network features that can be used as individual biomarkers of neurological outcome. However, this approach typically requires the use of diffusion and/or functional MRI to extract individual brain networks, which require high acquisition times and present an extreme sensitivity to motion artifacts, critical problems when scanning fetuses and infants. Extraction of individual networks based on morphological similarity from gray matter is a new approach that benefits from the power of graph theory analysis to describe gray matter morphology as a large-scale morphological network from a typical clinical anatomic acquisition such as T1-weighted MRI. In the present paper we propose a methodology to normalize these large-scale morphological networks to a brain network with standardized size based on a parcellation scheme. The proposed methodology was applied to reconstruct individual brain networks of 63 one-year-old infants, 41 infants with intrauterine growth restriction (IUGR) and 22 controls, showing altered network features in the IUGR group, and their association with neurodevelopmental outcome at two years of age by means of ordinal regression analysis of the network features obtained with Bayley Scale for Infant and Toddler Development, third edition. Although it must be more widely assessed, this methodology stands as a good candidate for the development of biomarkers for altered neurodevelopment in the pediatric population.

Introduction

In recent years, the potential of brain magnetic resonance imaging (MRI) to detect brain alterations that can be related to a different range of neurological pathologies has been clearly demonstrated (Bassett and Bullmore, 2009; Eliez and Reiss, 2000; Horsfield and Jones, 2002). An additional area of importance in the application of the different modalities of MRI has been the development of connectomics (Hagmann, 2005) to extract features of the macroscopic circuitry of the connections of the brain, which has been called "the connectome" (Sporns et al., 2005). In particular, the use of graph theory analyses on brain networks has been a useful tool to characterize brain function by use of a few comprehensible parameters. For example, different sets of data, including functional MRI and diffusion MRI, have been used to extract macroscopic brain networks and analyze network features in healthy adults, adolescents and infants (Gong et al., 2009; Hagmann et al., 2008, 2010; Iturria-Medina et al., 2008; Yap et al., 2011) and to report altered group connectivity parameters in a wide range of neurological, neurobehavioral and neurodegenerative diseases by means of connectomic analysis (Alexander-Bloch et al., 2010; Liu et al., 2008; Lo et al., 2010; Shu et al., 2009, 2011; Wang et al., 2009; Wu et al., 2009). Importantly, connectomics and graph theory features are potential tools to develop biomarkers to predict neurological outcomes in adult (He et al., 2009; Li et al., 2009; Wee et al., 2010; Wen et al., 2011) and perinatal diseases (Batalle et al., 2012; Tymofiyeva et al., 2012).

However, although the use of diffusion and functional MRI are being more frequently applied, these techniques are still not very common in

Abbreviations: AAL, automated anatomical labeling; BSID-III, Bayley scale for infant development, third edition; CSF, cerebrospinal fluid; FDR, False Discovery Rate; GA, gestational age; GM, gray matter; IUGR, intrauterine growth restriction; MRI, magnetic resonance imaging; WM, white matter.

* Corresponding author at: Fetal and Perinatal Medicine Research Group, Hospital Clínic, IDIBAPS, Sabino de Arana 1, Helios III, 08028 Barcelona, Spain. Fax: +34 93 227 9336.
E-mail addresses: dbatalle@clinic.ub.es (D. Batalle), emunozm@clinic.ub.es (E. Muñoz-Moreno), figueras@clinic.ub.es (F. Figueras), bargallo@clinic.ub.es (N. Bargallo), eixarch@clinic.ub.es (E. Eixarch), gratacos@clinic.ub.es (E. Gratacos).

1053-8119/$ – see front matter © 2013 Elsevier Inc. All rights reserved.
http://dx.doi.org/10.1016/j.neuroimage.2013.07.045

clinical practice compared with conventional anatomical T1 acquisitions. In addition, the requirement of higher acquisition times and the extreme sensitivity to motion artifacts of diffusion and functional MRI is critical when scanning subjects where control of movements cannot be assured, such as fetuses or infants. Based on the concept that correlations of gray matter (GM) features such as volume or cortical thickness across groups of individuals are associated with brain connectivity (He et al., 2007), anatomical T1 acquisitions have been used to obtain group connectomes that allow for a better understanding of brain circuitry in health and disease (Bassett et al., 2008; Fan et al., 2011; He et al., 2008). However, in order to develop individual biomarkers, it is indispensable to extract individual brain networks, which typically requires diffusion and/or functional MRI. Recently, a number of published reports have suggested approaches to extract individual brain networks based on the analysis of the similarities of GM features (Raj et al., 2010; Tijms et al., 2012, 2013; Zhou et al., 2011). These methodologies can benefit from the power of brain network analysis to predict individual neurological outcome, albeit using conventional T1 acquisitions. To what extent these networks resemble anatomical brain networks is an issue that still remains to be elucidated. Regardless of whether the brain networks reconstructed resemble actual anatomical networks or just serve to analyze cortical pattern similarities, this approach has the potential to become a powerful tool in clinical practice if it allows obtaining features associated with the neurological outcome of different diseases.

In the present paper we extend the work of Tijms et al. (2012) that allows the generation of individual morphology similarity-based structural brain networks from MRI. Specifically, we propose a methodology that allows normalization of the large-scale networks obtained to a common framework, so that each subject network has the same network size, which has some clear advantages in order to perform comparative analyses (van Wijk et al., 2010). We prove the feasibility and utility of this approach by applying it to a specific disease. Namely, we used late-onset intrauterine growth restriction (IUGR) as a disease model for several reasons. First, it is a prevalent disease that affects around 7% of pregnancies in developed countries (WHO, 2012), and is thus a major public health issue. Late-onset IUGR is the most prevalent form and it has clearly been demonstrated to be associated with an increased risk of neurodevelopmental disorders in offspring (Bassan et al., 2011; Eixarch et al., 2008; Figueras et al., 2009; McCowan et al., 2002). Secondly, IUGR is a chronic condition which produces brain reorganization, more than overt brain damage (Rees et al., 2011), and this requires the use of advanced analysis of non-conventional brain imaging techniques to be identified (Gratacos, 2012). Finally, the early detection of infants with a high risk of neurodevelopmental problems is a challenge to modern medicine. Diagnosis in perinatal or very early life would open a window of opportunity for the treatment of these patients, which would have a strong impact on modifying clinical practice.

Here, we extracted the individual brain networks of 63 one year old infants, 41 who suffered prenatal late-onset IUGR and 22 controls, based on GM morphological similarities. Based on the analysis of the networks obtained, we tested the hypothesis that alterations in the brain network topology produced by IUGR can be assessed by GM morphology similarity based brain networks, and that network features obtained are associated with abnormal neurodevelopment later in life. Although the differences obtained were not so evident as those demonstrated by means of brain networks derived from diffusion MRI in a similar population of IUGR infants (Batalle et al., 2012), we were able to demonstrate alterations in the organization of late-onset IUGR extracted brain network topology. In addition, we provide evidence of the association of the obtained network features with neurodevelopmental scores. The proposed methodology stands as a potential candidate to develop quantitative imaging biomarkers for the prediction of the high risk of altered neurodevelopment in subjects who suffered perinatal damage and, importantly, it could be extended to other pathologies.

Materials and methods

Subjects

This study was part of a larger prospective research program on IUGR involving fetal assessment and short- and long-term postnatal follow-up at Hospital Clinic (Barcelona, Spain). The study protocol was approved by the local Ethics Committee, and written informed consent was obtained from the parents or legal guardians of all participants. The study included a sample of 84 singleton pregnancies with 51 late-onset IUGR and 33 control fetuses. Late-onset IUGR was defined as those fetuses with an estimated fetal weight (EFW) below the 10th centile according to local reference standards confirmed at birth (Figueras et al., 2008) delivered after 34 weeks of pregnancy. Control subjects were defined as fetuses with EFW between the 10th and 90th customized centiles according to local reference (Figueras et al., 2008) confirmed at birth. Pregnancies were dated according to the first-trimester crown-rump length measurements (Robinson and Fleming, 1975). Infants with chromosomal, genetic, or structural defects and signs of intrauterine infection or neonatal early onset sepsis were excluded from this study. Neonatal data were prospectively recorded including: gestational age (GA), birth weight, cephalic perimeter, gender, and neonatal complications including late-onset sepsis, necrotizing enterocolitis and chronic lung disease (defined as oxygen need at 36 weeks postmenstrual age). Maternal education was recorded as elementary or less, high school, undergraduate degree, and graduate/post-graduate degree. Maternal smoking status during pregnancy and breastfeeding were also recorded.

MRI data acquisition

Children were scanned at 12 ± 2 months corrected age, during natural sleep without sedation (Padilla et al., 2012). The scan was performed with a TIM TRIO 3.0 T whole body MR scanner (Siemens, Germany). High resolution structural T1-weighted images were obtained by a Magnetization Prepared Rapid Acquisition Gradient Echo (MPRAGE) sequence with the following parameters: 0.9-mm slice thickness with no interslice gap, 192 sagittal slices, in-plane acquisition matrix of 256×256, FoV $= 220 \times 220$ mm^2, TR $= 2050$ ms, TE $= 2.41$ ms and inversion time (TI) $= 1050$ ms. T1 acquisition time was 5 min 52 s. In addition, structural T2-weighted images were also acquired in order to exclude white matter (WM) abnormalities. All acquired images were visually inspected for apparent or aberrant artifacts, and subjects excluded accordingly. Prior to any further analyses, all the anatomical acquisitions were manually realigned to a common orientation aligning anterior and posterior commissure in the sagittal plane (pitch), and using the medial longitudinal fissure to align coronal (roll) and axial plane (yaw).

Brain segmentation and parcellation

The methodology performed to segment and parcel the brain in a similar population was previously described in Batalle et al. (2012). Briefly, the acquired images of each subject were first skull-stripped (Smith, 2002). All the resulting brain volumes were segmented into WM, GM and cerebrospinal fluid (CSF) using the unified segmentation model (Ashburner and Friston, 2005) available with the SPM software (SPM8 release, www.fil.ion.ucl.ac.uk/spm/). The default tissue probability maps of SPM were replaced by a specific one year old infant template (Shi et al., 2011). Each subject brain was regionally parceled in the native space with an atlas based on the Anatomical Automatic Labeling (AAL) atlas of 116 regions (Tzourio-Mazoyer et al., 2002), recently adapted to a one year old population (Shi et al., 2011). In order to automatically parcel each subject's brain using this atlas, we used a customized software implementing a consistent version (Tristan-Vega and Arribas, 2007) of a block matching algorithm (Warfield et al., 2002), obtaining an elastic transformation matching the template with each

Table 1
Regions of interest used as nodes in structural brain networks, corresponding to the regions defined in AAL atlas.

Anatomical regions	Label	Anatomical regions	Label
Precentral gyrus	PRE	Lingual gyrus	LING
Superior frontal gyrus, dorsolateral	F1	Superior occipital gyrus	O1
Superior frontal gyrus, orbital	F1O	Middle occipital gyrus	O2
Middle frontal gyrus	F2	Inferior occipital gyrus	O3
Middle frontal gyrus, orbital part	F2O	Fusiform gyrus	FUSI
Inferior frontal gyrus, opercular part	F3OP	Postcentral gyrus	POST
Inferior frontal gyrus, triangular part	F3T	Superior parietal gyrus	P1
Inferior frontal gyrus, orbital part	F3O	Inferior parietal, but supramarginal and angular gyri	P2
Rolandic operculum	RO	Supramarginal gyrus	SMG
Supplementary motor area	SMA	Angular gyrus	AG
Olfactory cortex	OC	Precuneus	PQ
Superior frontal gyrus, medial	F1M	Paracentral lobule	PCL
Superior frontal gyrus, medial orbital	F1MO	Caudate nucleus	CAU
Gyrus rectus	GR	Lenticular nucleus, putamen	PUT
Insula	IN	Lenticular nucleus, pallidum	PAL
Anterior cingulate and paracingulate gyri	ACIN	Thalamus	THA
Median cingulate and paracingulate gyri	MCIN	Heschl gyrus	HES
Posterior cingulate gyrus	PCIN	Superior temporal gyrus	T1
Hippocampus	HIP	Temporal pole: superior temporal gyrus	T1P
Parahippocampal gyrus	PHIP	Middle temporal gyrus	T2
Amygdala	AMYG	Temporal pole: middle temporal gyrus	T2P
Calcarine fissure and surrounding cortex	V1	Inferior temporal gyrus	T3
Cuneus	Q	Cerebellum	CER
		Vermis	VER

subject's anatomical T1 volume. The labels of the AAL atlas were propagated to each structural MRI acquisition of our subjects using this elastic transformation, with discrete labeling values preserved by nearest neighbor interpolation. The original atlas is composed of 90 cortical and sub-cortical regions and 26 cerebellar regions. In order to simplify the analysis, we merged the cerebellar regions into right cerebellum, left cerebellum and vermis, resulting in a total of 93 regions per subject brain (Table 1).

Extraction of brain networks

In the present study we followed the methodology proposed by Tijms et al. (2012) to extract individual structural morphology brain networks from MRI and extended it in order to normalize these networks to a common comparable framework based on the regional AAL parcellation previously performed. Fig. 1 shows a schematic overview of the methodology. Firstly, the GM segmentation of each individual was divided in cubes of $5 \times 5 \times 5$ voxels. We only considered non-empty cubes, which we defined as those with at least 50% of the voxels in the cube containing GM. The chosen size of $5 \times 5 \times 5$ corresponds to $4.3 \times 4.3 \times 4.5$ mm^3, slightly inferior to the cube size selected by Tijms et al. ($6 \times 6 \times 6$ mm^3), but that in our opinion maintains a good compromise between capturing the cortical folding of the brain (taking into account the smaller brain size of our subjects), and producing a reasonably detailed network, with a computationally manageable amount of cubes for each individual. Specifically, we obtained an average of 7426.6 (standard deviation = 652.2) cubes per subject. Each cube represents a node v of what we called the "weighted raw network" (WRN) of each individual, that is the network which every edge represents the similarity between each pair of cubes. In order to construct the edges of the raw network, we quantified the structural morphology similarity of two nodes v_i and v_j based on its correlation coefficient r_{ij} (Tijms et al., 2012):

$$r_{ij} = \frac{\sum_{k=1}^{n}\left(v_{ik}-\overline{v_i}\right)\left(v_{jk}-\overline{v_j}\right)}{\sqrt{\sum_{k=1}^{n}\left(v_{ik}-\overline{v_i}\right)^2}\sqrt{\sum_{k=1}^{n}\left(v_{jk}-\overline{v_j}\right)^2}} \quad (1)$$

Where v_{ik} is the kth element of the n voxels of the cube v_i and $\overline{v_i}$ is the mean value of all the voxels belonging to the cube v_i. The correlation coefficient was calculated for rotations of 90° and reflections over all axes of each cube, and the maximum correlation value and its corresponding p-value was taken. Finally, the "binary raw network" (BRN) of each individual was obtained by a binarization of the WRN considering only the significant correlations after a Bonferroni correction. Thus far, we have obtained a BRN of each individual similarly to Tijms et al. (2012). However, due to the methodological design, each subject would have a BRN with a different size (number of nodes), which is critical in order to compare the network features of clinical groups, given that most of the typical network features vary depending on changes in network size (van Wijk et al., 2010). For this reason, we normalized BRN based on the previously obtained AAL parcellation of each subject's brain, resulting in all subjects having the same number of nodes (93), corresponding to the different ROIs of the AAL atlas. To perform the normalization, a ROI of the AAL was assigned to each BRN node (cube), defined as the ROI to which most of the voxels of such cube belong to (mode). Each ROI constituted a node v^{norm} of what we defined as the "weighted normalized network" (WNN). Each pair of WNN nodes v_i^{norm} and v_j^{norm} were considered to be connected with a weight w_{ij} corresponding to the ratio of actual significant correlations by the total possible connections between all the BRN nodes belonging to the ROIs i and j:

$$w_{ij} = \frac{\sum_{k=1}^{N_i}\sum_{l=1}^{N_j} p_{kl}^{sig}}{N_i N_j} \quad (2)$$

Where p_{kl}^{sig} is 1 when $p_{kl}^{bonf} < 0.05$ and 0 otherwise, p_{kl}^{bonf} is the Bonferroni corrected significance of the correlation between cubes v_k and v_l, and N_i and N_j is the number of BRN nodes (cubes) belonging to ROI i and j respectively. Note that the weight obtained is bounded between 0 and 1 ($w_{ij} \in [0,1]$). Self-connections were excluded (i.e.: $w_{ii} = 0 \; \forall \; i$).

It is worth noting that in this study, we use the term "connections" to refer to brain network edges indicating statistically similar gray matter morphology of two cubes, in a similar way

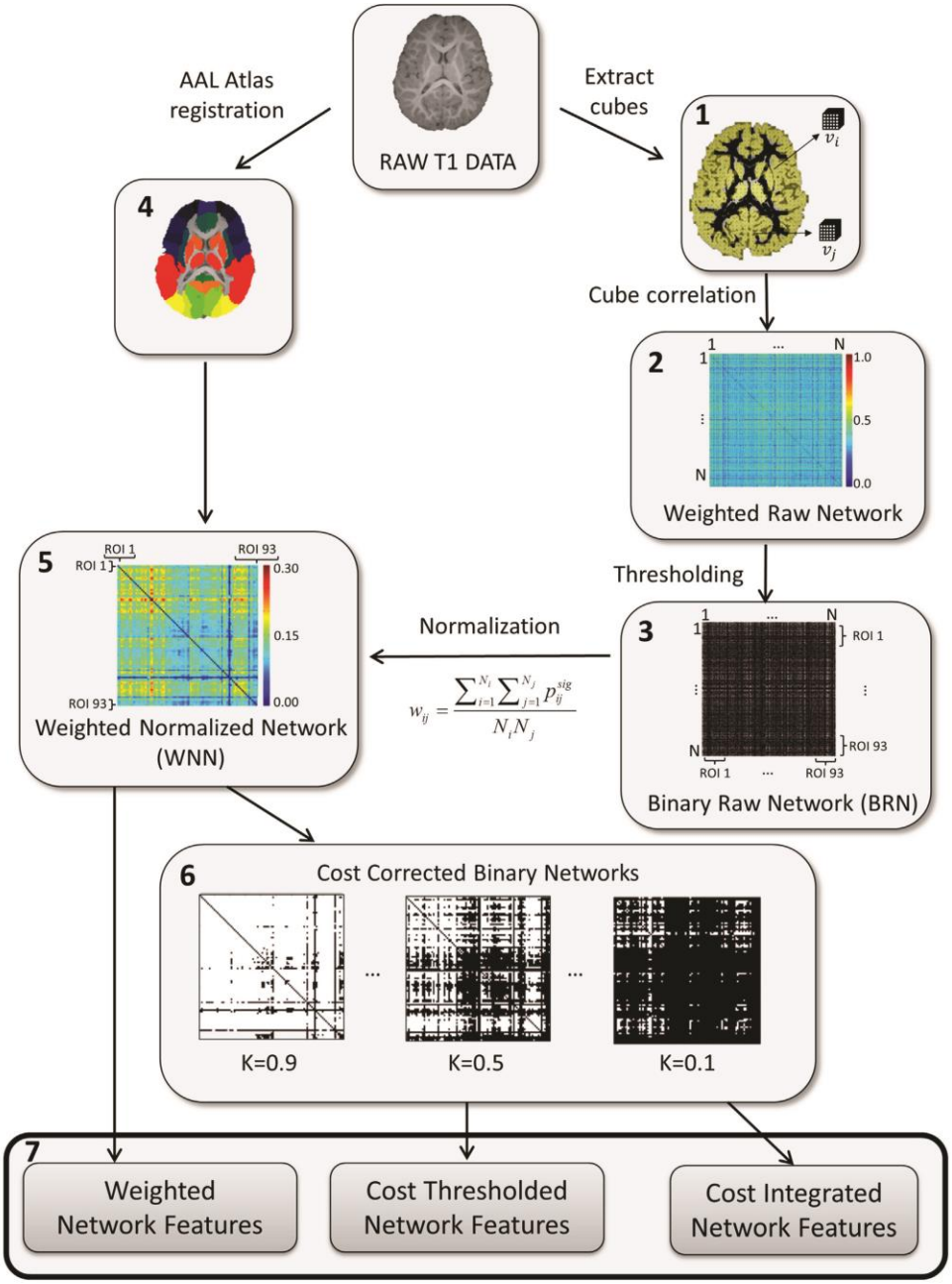

Fig. 1. General methodological scheme. (1) The GM segmentation of each individual was divided into cubes of 5 × 5 × 5 voxels. (2) The morphological similarity of each pair of cubes was calculated by its correlation coefficient obtaining the weighted raw network (WRN) of each subject. (3) Each WRN was thresholded considering only significant correlations after a Bonferroni correction, obtaining the binary raw network (BRN) of each subject. (4) Each subject brain volume was parceled in 93 ROIs corresponding to AAL atlas. (5) Information of BRN and anatomical parcellation of each subject was integrated in the weighted normalized network (WNN). (6) Cost correction of WNN was applied in order to obtain a set of binary networks corresponding to the whole range of network costs from 1 to 0 at steps of 0.01. (7) Weighted network features were obtained directly from WNN and cost-thresholded and cost-integrated network features were obtained from previously computed cost corrected binary networks.

than used previously by Tijms et al. (2012), but it must not be confused with anatomical connections. In the same line, "individual structural morphology brain networks" is used to refer to the brain networks obtained with this methodology, as the networks obtained are strongly associated with the similarity of local thickness and folding structure of different parts of the cortex, but

its relation with underlying brain connectivity still must be elucidated.

Network analysis

Graph theory measures

We mostly used definitions and nomenclature compiled by Rubinov and Sporns (2009). Briefly, N was defined as the set of all nodes in the network, and n as the number of nodes; (i,j) was the link between nodes i and j; and a_{ij} the connection status between node i and j: $a_{ij} = 1$ when link (i,j) exists and zero otherwise. w_{ij} is defined as the weight of the link (i,j) in weighted networks, normalized between 0 and 1, where a higher weight indicated a higher "connectivity" between nodes i and j. Degree of a node i was calculated as $k_i = \sum_{j \in N} a_{ij}$. Directly related to the average degree of a network, we defined the network cost K as the ratio of actual links present on a network divided by all the possible links:

$$K = \frac{1}{n(n-1)} \sum_{i,j \in N} a_{ij} \tag{3}$$

Weighted degree of a node is often called nodal strength and is calculated as the sum of all neighboring link weights of a given node: $k_i^w = \sum_{j \in N} w_{ij}$. Its average value along all nodes for a given network is a measure directly related to the energy of a network and was called average network strength.

Shortest path length between nodes i and j was defined for binary networks as $d_{ij} = \sum a_{uv} \in g_{i \leftrightarrow j}$, where $g_{i \leftrightarrow j}$ is the shortest path (geodesic) between i and j. Shortest path length was generalized for weighted networks as $d_{ij}^w = \sum a_{uv} \in g_{i \leftrightarrow j}^w f(w_{uv})$, where f is a map from weight to length (in our case an inverse map) and $g_{i \leftrightarrow j}^w$ is the shortest weighted path between i and j.

Global efficiency was defined as the average inverse shortest path length (Latora and Marchiori, 2001):

$$E_{glob} = \frac{1}{n} \sum_{i \in N} \frac{\sum_{j \in N, j \neq i} d_{ij}^{-1}}{n-1} \tag{4}$$

Generalized to weighted networks as:

$$E_{glob} = \frac{1}{n} \sum_{i \in N} \frac{\sum_{j \in N, j \neq i} \left(d_{ij}^W\right)^{-1}}{n-1} \tag{5}$$

Nodal efficiency of a node i was defined as the inverse of the harmonic mean of the minimum path length between that index node and all other nodes in the network (Achard and Bullmore, 2007):

$$E_{nodal}(i) = \frac{1}{k_i(k_i-1)} \sum_{j,h \in N, [j,h] \neq i} a_{ij} a_{ih} \left[d_{jh}(N_i)\right]^{-1} \tag{6}$$

Where $d_{jh}(N_i)$ is the length of the shortest path between j and h, which contains only neighbors of i.

Local efficiency was defined as the average of nodal efficiency of each node:

$$E_{loc} = \frac{1}{n} \sum_{i \in N} E_{nodal}(i) = \frac{1}{n} \sum_{i \in N} \frac{1}{k_i(k_i-1)} \sum_{j,h \in N, [j,h] \neq i} a_{ij} a_{ih} \left[d_{jh}(N_i)\right]^{-1} \tag{7}$$

Generalized to weighted networks as (Rubinov and Sporns, 2009):

$$E_{loc}^w = \frac{1}{n} \sum_{i \in N} \frac{1}{k_i(k_i-1)} \sum_{j,h \in N, [j,h] \neq i} \left(w_{ij} w_{ih} \left[d_{jh}^w(N_i)\right]^{-1}\right)^{\frac{1}{3}} \tag{8}$$

Levels of analysis: weighted, cost level thresholding and cost integration measures

We analyzed the obtained networks with three different approaches. The first and straightforward approach is to directly apply weighted versions of graph theory measures to the obtained WNN. However, some authors suggest that some of these measures could be closely associated with the average network strength and degree (Ginestet et al., 2011; van Wijk et al., 2010). Therefore, in order to assess the topology of weighted networks independently of its strength and cost, a set of cost level thresholds was applied to each individual weighted network, obtaining a binary network at each cost level (Ginestet et al., 2011). This second approach allows comparing networks with the same number of binary connections, and therefore, comparing network features independently of their cost. This approach, however, increases the number of comparisons and the complexity of the results interpretation, as the clinical groups must be compared at each cost threshold level. Finally, in order to disentangle connectivity strength from topology in a single value for each graph theory feature, Ginestet et al. (2011) demonstrated the usefulness of integrating each network feature over the entire cost regime. The cost-integrated version of a topological metric $T(\cdot)$ is defined as (Ginestet et al., 2011):

$$T_{CI}(G) = \frac{1}{N_l} \sum_{t=1}^{N_l} T(\gamma(G, k_t)) \tag{9}$$

Where G is a given weighted graph, $\gamma(G,k)$ is the graph G binarized at cost k_t and N_l is the cardinal of network costs assessed.

To summarize, for each individual network we computed three features: network average strength, global efficiency and local efficiency. Each of these network features was calculated in its weighted form, binarized at a cost threshold from 0 to 1 at steps of 0.01 and cost-integrated along the entire cost regime. In addition, regional analysis of network features was also performed, assessing nodal strength and nodal weighted efficiency for each network node.

Neurodevelopmental assessment

Neurodevelopmental outcome of each subject was assessed at 21 ± 2 months of corrected age with the Bayley Scale for Infant and Toddler Development, Third edition (BSID-III), which evaluates five distinct scales: cognitive, language, motor, socio-emotional behavior and adaptive behavior. The scales have scores with a mean of 100 and S.D. of 15. Abnormal Bayley was defined as a score below 85 in any of the five different scales (Anderson et al., 2010). Bayley's severity score was defined as the sum of scales below 85, being in a range from 0 to 5. All developmental examinations were performed by a single trained psychologist examiner with previous experience with the BSID-III. The examiner was not informed about the infant's medical history.

Statistical analysis

Group differences

Differences in total GM volume and regional AAL regions were assessed by means of general linear model with gender, maternal education, smoking during pregnancy and breastfeeding as cofactors and GA as covariate. In order to assess the differences in the topology of the extracted networks in the IUGR group when compared with controls, statistical comparisons among groups were also performed by means of general linear model with the same cofactors and covariates as previously, but including total GM volume as covariate to exclude GM size as a factor explaining the differences found. This was performed at the three levels of network analysis: weighted, cost level thresholding and cost integration measures. Multiple comparisons correction was

applied for regional analysis, including the results after a False Discovery Rate (FDR) over the 93 regions assessed (Benjamini et al., 2006).

Association with neurodevelopment

In order to assess the association of graph theory features obtained from the networks extracted for one-year-old children with late-onset IUGR with the neurodevelopmental scores obtained by the same children at two years of age, we followed two different approaches.

In the first approach, we computed a general linear model with normal/abnormal Bayley as independent variables and the previously analyzed network features (weighted and cost-integrated average strength, global and local efficiency) as dependent variables; gender, education, smoking during pregnancy and breastfeeding as cofactors; and GA and weight percentile as covariables. This way we assessed if there was a significant difference in the network features between IUGR children with abnormal values in their neurodevelopmental tests when compared with those with normal values, and therefore, if graph theory features obtained with the proposed methodology at one year of age have the potential to discriminate those children that will have an abnormal neurodevelopment one year after an MRI scan.

In the second approach, we assessed the association of the obtained network features with the severity of the abnormal neurodevelopment, and to which extent they added information to the clinical data. In order to do so, we first did an ordinal regression of the Bayley's severity score with the clinical data and then added graph theory features to the model in order to assess to what extent there is a better association. Note that association with neurodevelopment was performed only in the IUGR group, and weight percentile was added to clinical data as it may be relevant when group is not taken into account.

Results

Sample

Structural MRI evaluation revealed the presence of anomalies in 6 IUGR (two increased cisterna magna, one ventricular dilatation, one WM lesions and one thin corpus callosum) and in 2 controls (two increased cisterna magna) that were excluded from the final analysis. In addition, 9 controls and 4 IUGR did not pass quality criteria concerning motion artifacts that prevented performing further analysis. Thus, the final sample included 41 IUGR infants and 22 control infants.

As expected, anthropometric measurements at birth were significantly lower in the IUGR group: birth weight centile: 53.5 (32.9) vs. 2.3(2.7) $p < 0.001$, and cephalic perimeter at birth centile: 38.9 (25.1) vs. 12.7 (16.0), $p < 0.001$. GA at delivery was significantly lower in the IUGR group: 39.5 (1.5) vs. 38.1(1.6), $p = 0.003$. No significant differences were found in gender distribution: male/female 10/12 vs. 26/15, $p = 0.170$. No neonatal complications occurred among groups. No differences were observed in demographic characteristics including maternal age, maternal education and breastfeeding. However, maternal smoking status during pregnancy was increased in the IUGR group: 4.5% vs. 31.7%, $p = 0.023$. For the BSID-III neurodevelopmental test, IUGR infants showed lower scores than the control group in all scales without reaching statistical significance: Cognitive: 102.8 (15.5) vs. 99.1 (16.5), $p = 0.533$; Language: 98.8 (19.0) vs. 90.1 (17.1),$p = 0.798$; Motor: 107.1(15.8) vs. 96.5 (15.1), $p = 0.307$; Socio-emotional: 118.0 (28.6) vs. 106.6 (26.6), $p = 0.264$; Adaptive behavior: 91.4 (15.8) vs. 86.4 (16.8), $p = 0.412$. The proportion of abnormal BSID-III scores in late-onset IUGR was 60% and the distribution of Bayley's severity scores based on the number of scales affected was: one scale 42.9%, two scales 38.1%, three scales 9.5%, four scales 0%, and five scales 9.5%.

Concerning MRI acquisition, general lineal model showed reduced GM volume in the IUGR group ($p = 0.006$). Regional volume analysis also revealed differences in individual regions (Supplementary Material), but none of them were significant after FDR correction.

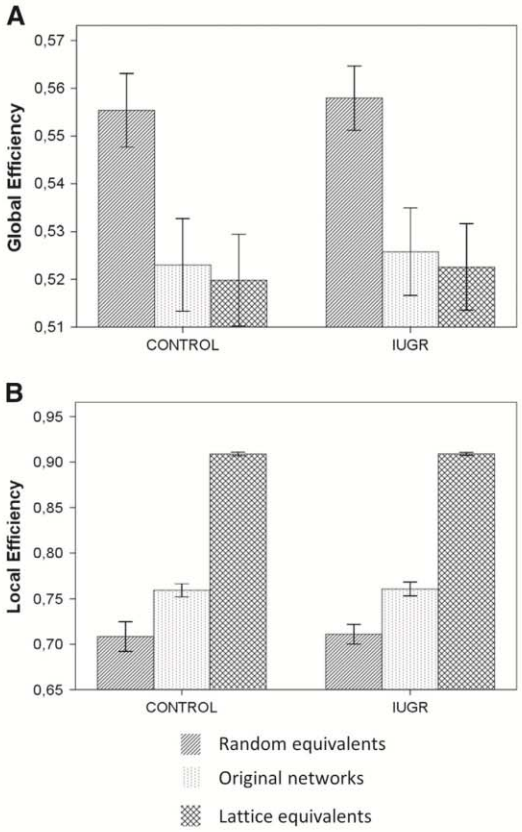

Fig. 2. Small-worldness. (A) Global and (B) local efficiency of the binary raw networks obtained compared with the values obtained for their random and lattice network equivalents.

Small-worldness

We calculated the BRN random and lattice equivalents of each subject that preserve degree distribution and compared their global and local efficiency with the original network. The original networks have an intermediate value of global and local efficiency when compared with their random and lattice equivalent, both at individual and group level, a typical characteristic of small-world networks (Fig. 2). However, the values of global and local efficiency of the original WNN and its random and lattice equivalents were virtually identical. Thus, the evaluation of small-worldness in WNN rendered unconclusive results.

Analysis of network features in IUGR

Compared with controls, analysis of global weighted features of WNN in IUGR showed no significant differences in network average strength ($p = 0.296$ $F = 1.130$), global efficiency ($p = 0.198$ $F = 1.727$) and local efficiency ($p = 0.247$ $F = 1.391$).

In order to analyze WNN independently of its network cost, thresholding and binarizing of WNN along a range of cost-levels from 0 to 1 at 0.01 steps was performed. Binary network features were analyzed at each cost level, obtaining no significant differences for average strength, some differences on local efficiency, but several in global efficiency, as shown in Fig. 3.

Integration of binary network features along the whole range of cost-levels allowed us to obtain a single representative value of each

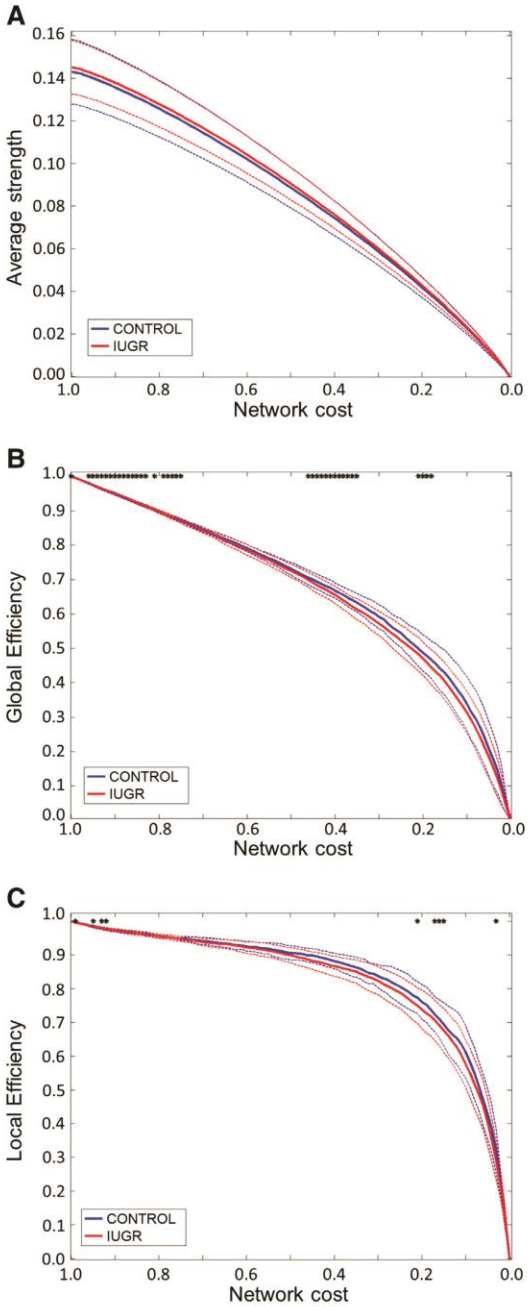

Fig. 3. Cost-thresholded network features. Control and IUGR cost-thresholded network features estimated from binarized weighted normalized networks at steps of 0.01 of network cost. (A) Average strength, (B) global efficiency and (C) local efficiency. Solid line corresponds to the mean across individuals and dashed lines to mean ± standard deviation. *p < 0.05.

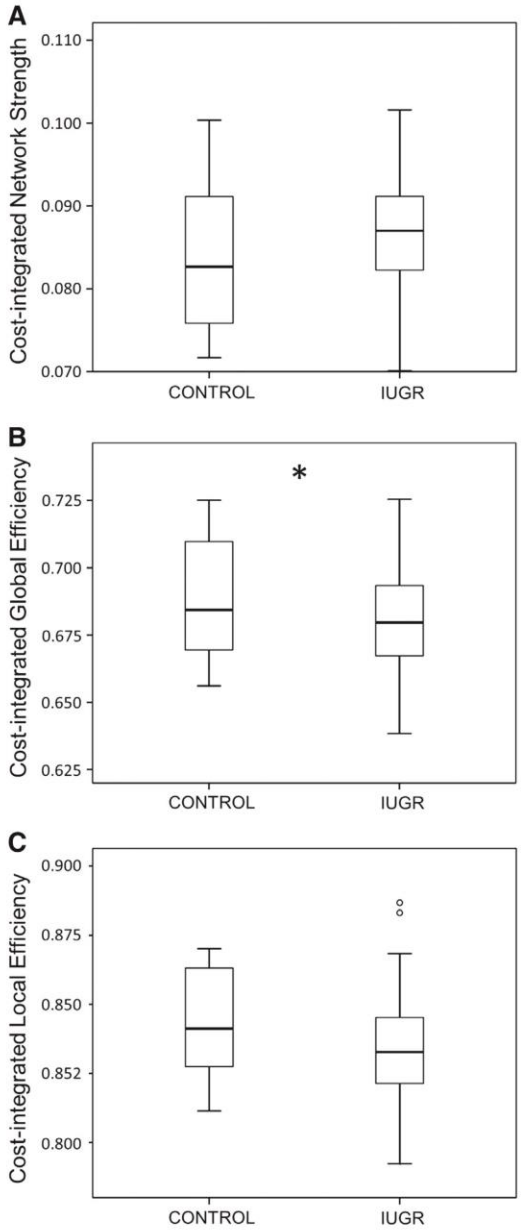

Fig. 4. Cost-integrated network features. Box plot of control and IUGR cost-integrated features. (A) Average strength, (B) global efficiency and (C) local efficiency. *p < 0.05.

binary feature that is independent of the network cost (Fig. 4). No significant difference was found on cost-integrated average strength ($p = 0.348$ $F = 0.906$) when compared with control group. Similarly, local efficiency was also not significantly different between controls and cases, although a tendency could be observed ($p = 0.076$ $F = 5.176$). However, global efficiency was significantly reduced in the IUGR group ($p = 0.030$ $F = 5.176$).

Regional network analysis of IUGR weighted networks showed differences in different regions when compared with controls. Specifically, we found alterations in left superior frontal gyrus orbital part (F1O), right parahippocampal gyrus (PHIP), left lingual gyrus (LING), left supramarginal gyrus (SMG), left angular gyrus (AG) and vermis (VER) weighted nodal efficiency and/or nodal strength (Fig. 5). However, none of them were significant after a false discovery rate correction.

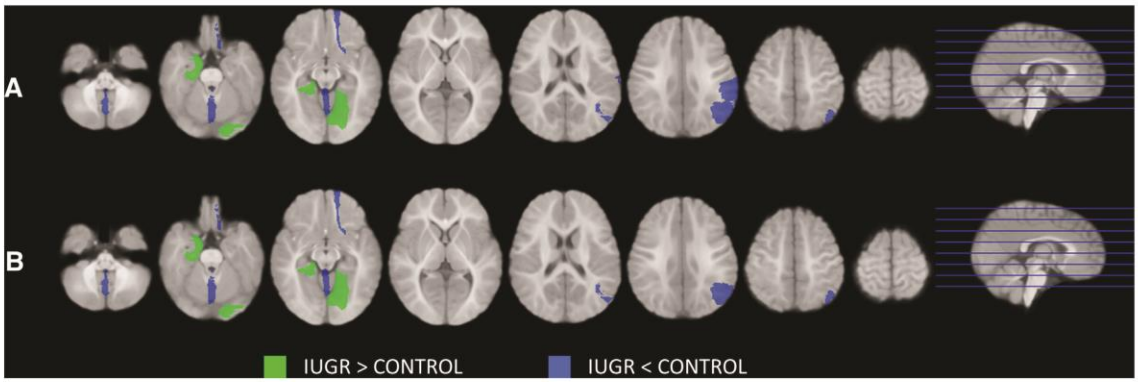

Fig. 5. Regional network features. (A) Nodal strength and (B) nodal efficiency features altered in IUGR group. Regional features highlighted in green are increased in IUGR group and those in blue are decreased.

Association with abnormal neurodevelopment in IUGR

A multivariate general linear model with the previously analyzed, weighted- and cost-integrated network features as dependent variables, and clinical features as covariables, showed no significant differences for any of the network features independently, but did show a multivariate statistically significant difference between normal and abnormal Bayley (Wilks' Lambda of 0.125, $p = 0.036$, $F = 5.815$). This demonstrated a discernibly different configuration of network features between IUGR cases with normal and abnormal Bayley.

In addition, an ordinal regression of Bayley's severity score with clinical data (GA, weight centile, gender, maternal education, smoking during pregnancy and breastfeeding) and the same ordinal regression with the addition of network features (weighted and cost integrated global efficiency, local efficiency and average strength) was also performed, demonstrating that the ordinal regression with only clinical data does not significantly fit Bayley's severity score ($p = 0.154$ $Chi^2 = 11.947$ Nagelkerke $R^2 = 0.309$, $df = 8$), but the addition of network features significantly changed the model ($p = 0.023$ $Chi^2 = 14.703$, $df = 6$), such that the resulting model was statistically significant ($p = 0.029$ $Chi^2 = 25.650$ Nagelkerke $R^2 = 0.555$, $df = 14$), demonstrating significant association of network features as a group and significantly adding information to the clinical data.

Discussion

This study, to the best of our knowledge, describes for the first time the use of individual similarity-based brain networks extracted from GM using standard T1-weighted MRI acquisitions in a pediatric population. To do so, we proposed a methodology in order to normalize the large-scale networks obtained to a common framework defined by an anatomical atlas, and applied it to a pediatric population of one-year-old infants who had suffered late-onset IUGR. Based on the networks extracted using this methodology, we demonstrated that late-onset IUGR children had an altered network topology compared with controls, and that the network features obtained are associated with the neurodevelopmental outcomes of the IUGR group at two years of age.

Individual networks obtained from GM morphology similarities

Obtaining brain networks from standard T1 anatomical acquisitions has a series of advantages compared with those reconstructed from other modalities such as diffusion or functional MRI, mainly reduced acquisition times, which is crucial in the study of several pathologies, especially in the pediatric population. There is a broad range of studies in the literature that obtained brain networks from T1 anatomical acquisitions by means of correlation of GM features, such as volume or cortical thickness, across groups of individuals. In this way, it has been possible to obtain a single brain network corresponding to a group of subjects. This line of research has been relevant to study alterations in brain organization produced by certain pathologies (Bassett et al., 2008; Bernhardt et al., 2011; He et al., 2008; Liu et al., 2008), and to improve understanding of the organization of the brain during neurodevelopment (Fan et al., 2011). However, this kind of approach is not useful to develop individual biomarkers predictive of neurological outcome as it generates only one brain network per group of individuals. Hence, developing methodologies that are able to extract individual networks from standard T1 MRI acquisitions is very relevant for clinical practice. The proposed methodology to extract individual networks benefits from the analytical power of graph theory and network models to describe GM similarities in the brain. However, it is very important to note that the extent to which the networks obtained resemble anatomical brain connectivity is an issue that requires deeper study. This issue aside, some studies have proposed that covariation of cortical morphology may be related to cortical connectivity (Andrews et al., 1997; Gong et al., 2011; Kennedy et al., 1998). Furthermore, in large-scale similarity-based networks, Tijms et al. (2012) found some similarities between the values of clustering and small world coefficients with resting-state functional MRI and morphological inter-subject correlation networks. Taking into account that some of the subjects analyzed in the present paper have available diffusion MRI included in a previous study (Batalle et al., 2012), we have performed correlations of the global graph theory features obtained with the ones generated from diffusion MRI in 10 control subjects (Supplementary Material). In this reduced sample we found correlations between weighted global and local efficiency of GM morphology similarity based brain networks with binary and weighted efficiencies obtained from diffusion MRI based brain networks. Yet even if some of the correlations found may indicate an association of the networks found in this study with underlying structural brain connectivity, it is still not clear to which extent the networks obtained in the present study resemble actual neuronal connections.

Disrupted network features in IUGR

Network features obtained with the proposed methodology in late-onset IUGR showed several differences when compared with controls when the weighted networks were binarized for the whole range of network cost. These differences are confirmed by the integration of the values along the entire cost regime, which has been proven to be a

robust measure of disentangling network topology from network cost in a single value (Ginestet et al., 2011). However, when applying the weighted versions of the features assessed directly on the weighted network, no differences were found. This can be explained as weighted measures and thresholded binary cost measures along the whole rank of network cost are assessing different aspects of network topology and are therefore complementary measures. Nodal network features revealed a pattern of mild alterations distributed along the whole brain, including regions of the frontal, occipital and parietal cortex, however, the significance of these findings is hampered after correction for multiple comparisons. Interestingly, a previous study of MRI based connectomics on IUGR babies (Batalle et al., 2012) also found decreased global and local efficiency in IUGR group, and some of the regional alterations found in the present study, as is the case of lingual gyrus, supramarginal gyrus, angular gyrus and vermis. We acknowledge that the meaning of these findings is unclear. We speculate that these differences could reflect a subtle pattern of alterations in cortical morphology produced by brain reorganization. This notion is in line with previous studies demonstrating structural differences in early and late-onset IUGR. Studies in preterm neonates have reported a decreased volume in cortical GM (Tolsa et al., 2004) and hippocampus (Lodygensky et al., 2008), and major delays in cortical development with discordant patterns of gyrification and a pronounced reduction in cortical expansion (Dubois et al., 2008). Persistence of structural changes at one year of age in IUGR babies has been reported, which demonstrate reduced volumes of GM in the temporal, parietal, frontal and insular regions (Padilla et al., 2011) and decreases in the fractal dimension of both gray and white matter, which correlate with specific neurodevelopmental difficulties in a similar population (Esteban et al., 2010). Note that the importance of the relationship between the network features obtained by individual GM similarity-based networks and fractal dimension has been previously suggested as there is a resemblance in both methodologies (Tijms et al., 2012). Recently published data has also demonstrated a reduced global cortical surface and volume as well as regional changes in cortical thickness, especially in the frontal region, in children after late-onset IUGR (De Bie et al., 2011) such that these regional changes are also present in the adolescent population (Martinussen et al., 2005).

Association of network features obtained with abnormal Bayley's scales in IUGR

Concerning the neurodevelopmental tests, late-onset IUGR showed lower results in all Bayley's scales, although reduced sample size prevented us from finding significant differences. Nevertheless, an association between IUGR and long-term neurodevelopmental and cognitive dysfunctions has been previously demonstrated (Bassan et al., 2011; Feldman and Eidelman, 2006; Geva et al., 2006a,b; Leitner et al., 2007; McCarton et al., 1996; Scherjon et al., 1993) as was the case with studies focusing on late-onset cases (Bassan et al., 2011; Eixarch et al., 2008; Figueras et al., 2009; McCowan et al., 2002). Our results demonstrated that network features of brain networks extracted from GM standard T1-weighted acquisitions at one year of age are related with neurodevelopment later in life. Association between network features in the IUGR population has previously been reported using diffusion MRI based brain networks (Batalle et al., 2012). In the present study, the combination of clinical data with global features was associated with the number of abnormal Bayley's scales, giving additional information about the severity of the neurodevelopmental delay. In our opinion, it is highly relevant that the network features extracted with the present methodology are related with neurodevelopmental outcome in IUGR children, suggesting the potential of this methodology to generate biomarkers able to detect altered neurodevelopment. This is especially relevant to clinical practice as the early detection of abnormal neurodevelopment would open a window of opportunity to apply interventional strategies.

Methodological considerations

Some methodological considerations must also be discussed. First of all, it is worth noting that brain parcellation and tissue segmentation in GM and WM in the infant brain is a critical issue due to the isointense developmental pattern which results from poor differentiation of tissues (Paus et al., 2001). However, the use of high quality T1 weighted 3-T MRI minimizes this effect. In addition, it is worth noting that to improve the reliability of the results obtained we used appropriated brain tissue probability maps of one-year-old infants for tissue segmentation and a pediatric atlas for brain parcellation (Shi et al., 2011). Each scan was reviewed to exclude those cases with apparent movement artifacts. In addition, brain tissue segmentation was individually analyzed to determine if the results of the tissue segmentation were accurate. The acquisition protocol during natural sleep (Padilla et al., 2012) allowed us to obtain good quality imaging without the use of sedation and, consequently, we obtained a very high ratio of successful acquisitions, taking into account the difficulty of acquiring MRI in such a young pediatric population. Due to the characteristics of the methodological approach proposed, it is reasonable to think that different brain orientation could have some effects on the obtained brain networks. To address this effect all the subjects were manually realigned previously to any further analyses, minimizing any possible influence of the patient orientation in the obtained networks. In addition we have assessed the effect on the network stability of minor head rotations ($\pm 10°$ at 2 degree steps in each axis) in the networks extracted (Supplementary Material), showing that the intra-subject variability provoked by head rotations is lower than inter-subject variability, hence observing the relatively high stability of the networks to this effect.

Some differences between the methodology proposed here and the methods presented by Tijms et al. (2012) should also be noted. Although Tijms et al. (2012) opted for a false discovery rate approach in order to obtain the BRN, thereby correcting the significance for the high amount of voxels analyzed, we opted for a more restrictive approach, using a Bonferroni correction, by which we obtained a relatively high amount of significant correlations while minimizing the amount of false positives. In order to correct cube correlation for rotation, we used 90 degree steps instead of 45. Note that it is possible to perform correlations of cubes rotated 45° without interpolation only if the cubes have a size of three voxels. For cubes of $5 \times 5 \times 5$ voxels, as in our case, the center of some rotated voxels would fall outside the boundaries of a voxel of the other cube, making it necessary to interpolate. It is our belief that decreasing false negatives in the extracted BRN does not justify the artifacts of partial volume effects and the interpolation needed to correct rotations by 45°. Note that the modifications performed in the methodology proposed by Tijms et al. (2012) are all very conservative: in the worst case increasing false negatives in the BRN obtained, but minimizing the number of false positives.

Strengths and limitations

One of the main strengths of this methodology is the straightforward adaptation of the proposed method to different population groups where MRI is a challenge and where connectomics based on diffusion and/or functional MRI is extremely difficult to perform, such as the pediatric population. Anatomical reconstruction of fetal structural acquisitions is becoming increasingly used in the literature (Kim et al., 2010; Kuklisova-Murgasova et al., 2012; Studholme, 2011). Hence, although the networks obtained are not so detailed and they lack a clear anatomical interpretation compared with those obtained with other techniques, adapting and assessing the proposed methodology to the fetal population seems a good opportunity to obtain biomarkers based on network features at the prenatal age and is a feasible alternative until diffusion and functional MRI protocols during fetal life become reliable and standardized.

Some limitations of the proposed methodology should also be noted. By its design, the methodology presented does not discriminate between GM to CSF or GM to WM boundaries, thus a connection could be considered between two cubes that have similar GM pattern without taking into account if they are adjacent to WM or CSF. However, it must be stressed that, even if the area occupied by WM and/or CSF in a pair of cubes is identical, a connection will not be established if GM pattern between the two cubes is different.

Another key issue that can be considered a limitation of this study is the possible resemblance (or not) of the networks obtained with actual underlying brain circuitry. Some hints on the validity of the networks obtained have been shown in the original article presenting the theoretical base of this methodology (Tijms et al., 2012), comparing the individual networks obtained to resting state and conventional GM morphology inter-subject correlation networks. In addition, in the present study some correlations of the network features obtained with a reduced sample of 10 subjects with diffusion MRI based networks has also been shown (Supplementary Material). However, the evidence available is not enough to state that there is an actual underlying brain circuitry explaining the connections obtained with the present methodology. Further studies are necessary to compare the individual networks obtained from GM morphology similarities to those networks obtained from standard diffusion and/or functional MRI in larger samples to clarify this issue. This is an extremely important remark when interpreting the results obtained, but is not so relevant from the point of view of purely developing neurological outcome biomarkers. Being able to show differences in the network features obtained between controls and cases may not directly indicate a different topology of brain circuitry, but may instead be showing subtle differences in cortical patterns that may not be detected by other less sensitive techniques. We can only hypothesize that the differences found can be partially explained not only by differences in brain connectivity that modulate cortical morphology (Gong et al., 2011; Van Essen, 1997), but also by differences in cortical structure produced by other reasons, such as changes in the distribution and/or density of neuronal bodies as occurs in animal models of chronic hypoxia (Fagel et al., 2006). In any case, in the sense used in the present paper, networks represent the similarities between regions of the brain (nodes) giving the weight of this similarity to the links connecting them. Whether these links, or what is the same, the morphological similarity between regions of the brain, describe or not an underlying circuitry is certainly unknown. However, to our understanding, the relevance of the technique and results here presented lies on the fact that differences in a pathological group have been demonstrated with this methodology and, importantly, a correlation between the features of the extracted networks from a simple T1 acquisition with the neurodevelopmental tests performed one year later has been found. This data show the potential of the proposed methodology to find image biomarkers in a different set of pathologies, but especially in the pediatric population, independently of whether or not the networks obtained with the presented methodology correspond with true underlying brain circuitries.

Conclusions

The methodology presented here proposes a solution for the problem of having different network sizes in individual large-scale networks obtained from GM MRI as published by Tijms et al. (2012). To the best of our knowledge, the present paper is the first work exploring the use of individual networks based on GM features in a pediatric population. Specifically, we applied the methodology proposed in a pediatric population who suffered perinatal mild brain reorganization, which is one of the target groups that can benefit from this kind of analysis. In this population, we were able to objectively demonstrate statistically significant differences between controls and children who suffered late-onset IUGR, supporting the notion that these children, although suffering a mild chronic insult, present patterns of brain organization that are different from their healthy counterparts. A noteworthy feature is that the network features obtained were successfully associated with abnormal neurodevelopmental scores, adding statistically relevant information to clinical data, nowadays the standard for the evaluation of neurological outcome in IUGR. Although this methodology must be more widely assessed, it stands as a good candidate for the development of biomarkers for altered neurodevelopment in the pediatric population.

Funding

This work was supported by grants: Obra Social "la Caixa", Barcelona, Spain; The Cerebra Foundation for the Brain-Injured Child, Carmarthen, Wales, UK; The Thrasher Research Fund, Salt Lake City, USA; The People Programme (Marie Curie Actions) of the European Union's Seventh Framework Programme FP7 under REA Grant Agreement number 217911 (u-Volumes); and Sara Borrell grants from Carlos III Institute of Health, Spain (grant number CD11/00048 to E.M.).

Acknowledgments

The authors would like to acknowledge Prof. Alberto Prats-Galino for useful discussions on the design of the methodology. The images used in this study were acquired in the Medical Imaging Core Facility of Institut d'Investigacions Biomèdiques August Pi i Sunyer (IDIBAPS), Barcelona, Spain.

Conflict of interest

The authors have no conflicts of interest to declare.

Appendix A. Supplementary data

Supplementary data to this article can be found online at http://dx.doi.org/10.1016/j.neuroimage.2013.07.045.

References

Achard, S., Bullmore, E., 2007. Efficiency and cost of economical brain functional networks. PLoS Comput. Biol. 3, e17.
Alexander-Bloch, A.F., Gogtay, N., Meunier, D., Birn, R., Clasen, L., Lalonde, F., Lenroot, R., Giedd, J., Bullmore, E.T., 2010. Disrupted modularity and local connectivity of brain functional networks in childhood-onset schizophrenia. Front. Syst. Neurosci. 4, 147.
Anderson, P.J., De Luca, C.R., Hutchinson, E., Roberts, G., Doyle, L.W., 2010. Underestimation of developmental delay by the new Bayley-III Scale. Arch. Pediatr. Adolesc. Med. 164, 352–356.
Andrews, T.J., Halpern, S.D., Purves, D., 1997. Correlated size variations in human visual cortex, lateral geniculate nucleus, and optic tract. J. Neurosci. 17, 2859–2868.
Ashburner, J., Friston, K.J., 2005. Unified segmentation. Neuroimage 26, 839–851.
Bassan, H., Stolar, O., Geva, R., Eshel, R., Fattal-Valevski, A., Leitner, Y., Waron, M., Jaffa, A., Harel, S., 2011. Intrauterine growth-restricted neonates born at term or preterm: how different? Pediatr. Neurol. 44, 122–130.
Bassett, D.S., Bullmore, E.T., 2009. Human brain networks in health and disease. Curr. Opin. Neurol. 22, 340–347.
Bassett, D.S., Bullmore, E., Verchinski, B.A., Mattay, V.S., Weinberger, D.R., Meyer-Lindenberg, A., 2008. Hierarchical organization of human cortical networks in health and schizophrenia. J. Neurosci. 28, 9239–9248.
Batalle, D., Eixarch, E., Figueras, F., Munoz-Moreno, E., Bargallo, N., Illa, M., Acosta-Rojas, R., Amat-Roldan, I., Gratacos, E., 2012. Altered small-world topology of structural brain networks in infants with intrauterine growth restriction and its association with later neurodevelopmental outcome. Neuroimage 60, 1352–1366.
Benjamini, Y., Krieger, A.M., Yekutieli, D., 2006. Adaptive linear step-up procedures that control the false discovery rate. Biometrika 93, 491–507.
Bernhardt, B.C., Chen, Z., He, Y., Evans, A.C., Bernasconi, N., 2011. Graph-theoretical analysis reveals disrupted small-world organization of cortical thickness correlation networks in temporal lobe epilepsy. Cereb. Cortex 21, 2147–2157.
De Bie, H.M., Oostrom, K.J., Boersma, M., Veltman, D.J., Barkhof, F., Delemarre-van de Waal, H.A., van den Heuvel, M.P., 2011. Global and regional differences in brain anatomy of young children born small for gestational age. PLoS One 6, e24116.
Dubois, J., Benders, M., Borradori-Tolsa, C., Cachia, A., Lazeyras, F., Ha-Vinh Leuchter, R., Sizonenko, S.V., Warfield, S.K., Mangin, J.F., Hüppi, P.S., 2008. Primary cortical folding in the human newborn: an early marker of later functional development. Brain 131, 2028–2041.
Eixarch, E., Meler, E., Iraola, A., Illa, M., Crispi, F., Hernandez-Andrade, E., Gratacos, E., Figueras, F., 2008. Neurodevelopmental outcome in 2-year-old infants who

were small-for-gestational age term fetuses with cerebral blood flow redistribution. Ultrasound Obstet. Gynecol. 32, 894–899.
Eliez, S., Reiss, A.L., 2000. MRI neuroimaging of childhood psychiatric disorders: a selective review. J. Child Psychol. Psychiatry 41, 679–694.
Esteban, F.J., Padilla, N., Sanz-Cortes, M., de Miras, J.R., Bargallo, N., Villoslada, P., Gratacos, E., 2010. Fractal-dimension analysis detects cerebral changes in preterm infants with and without intrauterine growth restriction. Neuroimage 53, 1225–1232.
Fagel, D.M., Ganat, Y., Silbereis, J., Ebbitt, T., Stewart, W., Zhang, H., Ment, L.R., Vaccarino, F.M., 2006. Cortical neurogenesis enhanced by chronic perinatal hypoxia. Exp. Neurol. 199, 77–91.
Fan, Y., Shi, F., Smith, J.K., Lin, W., Gilmore, J.H., Shen, D., 2011. Brain anatomical networks in early human brain development. Neuroimage 54, 1862–1871.
Feldman, R., Eidelman, A.I., 2006. Neonatal state organization, neuromaturation, mother-infant interaction, and cognitive development in small-for-gestational-age premature infants. Pediatrics 118, e869–e878.
Figueras, F., Meler, E., Iraola, A., Eixarch, E., Coll, O., Figueras, J., Francis, A., Gratacos, E., Gardosi, J., 2008. Customized birthweight standards for a Spanish population. Eur. J. Obstet. Gynecol. Reprod. Biol. 136, 20–24.
Figueras, F., Oros, D., Cruz-Martinez, R., Padilla, N., Hernandez-Andrade, E., Botet, F., Costas-Moragas, C., Gratacos, E., 2009. Neurobehavior in term, small-for-gestational age infants with normal placental function. Pediatrics 124, e934–e941.
Geva, R., Eshel, R., Leitner, Y., Fattal-Valevski, A., Harel, S., 2006a. Memory functions of children born with asymmetric intrauterine growth restriction. Brain Res. 1117, 186–194.
Geva, R., Eshel, R., Leitner, Y., Valevski, A.F., Harel, S., 2006b. Neuropsychological outcome of children with intrauterine growth restriction: a 9-year prospective study. Pediatrics 118, 91–100.
Ginestet, C.E., Nichols, T.E., Bullmore, E.T., Simmons, A., 2011. Brain network analysis: separating cost from topology using cost-integration. PLoS One 6, e21570.
Gong, G., He, Y., Concha, L., Lebel, C., Gross, D.W., Evans, A.C., Beaulieu, C., 2009. Mapping anatomical connectivity patterns of human cerebral cortex using in vivo diffusion tensor imaging tractography. Cereb. Cortex 19, 524–536.
Gong, G., He, Y., Chen, Z.J., Evans, A.C., 2011. Convergence and divergence of thickness correlations with diffusion connections across the human cerebral cortex. Neuroimage 59, 1239–1248.
Gratacos, E., 2012. Opportunities and challenges of biomedical imaging in fetal and neonatal brain disease. Proceedings of the 9th IEEE International Symposium on Biomedical Imaging: From Nano to Macro, pp. 493–494.
Hagmann, P., 2005. From Diffusion MRI to Brain Connectomics. Signal Processing Institute. Ecole Polytechnique Fédérale de Lausanne (EPFL), Lausanne.
Hagmann, P., Cammoun, L., Gigandet, X., Meuli, R., Honey, C.J., Wedeen, V.J., Sporns, O., 2008. Mapping the structural core of human cerebral cortex. PLoS Biol. 6, e159.
Hagmann, P., Sporns, O., Madan, N., Cammoun, L., Pienaar, R., Wedeen, V.J., Meuli, R., Thiran, J.P., Grant, P.E., 2010. White matter maturation reshapes structural connectivity in the late developing human brain. Proc. Natl. Acad. Sci. U. S. A. 107, 19067–19072.
He, Y., Chen, Z.J., Evans, A.C., 2007. Small-world anatomical networks in the human brain revealed by cortical thickness from MRI. Cereb. Cortex 17, 2407–2419.
He, Y., Chen, Z., Evans, A.C., 2008. Structural insights into aberrant topological patterns of large-scale cortical networks in Alzheimer's disease. J. Neurosci. 28, 8148–8159.
He, Y., Dagher, A., Chen, Z., Charil, A., Zijdenbos, A., Worsley, K., Evans, A., 2009. Impaired small-world efficiency in structural cortical networks in multiple sclerosis associated with white matter lesion load. Brain 132, 3366–3379.
Horsfield, M.A., Jones, D.K., 2002. Applications of diffusion-weighted and diffusion tensor MRI to white matter diseases — a review. NMR Biomed. 15, 570–577.
Iturria-Medina, Y., Sotero, R.C., Canales-Rodríguez, E.J., Alemán-Gómez, Y., Melie-García, L., 2008. Studying the human brain anatomical network via diffusion-weighted MRI and graph theory. Neuroimage 40, 1064–1076.
Kennedy, D.N., Lange, N., Makris, N., Bates, J., Meyer, J., Caviness Jr., V.S., 1998. Gyri of the human neocortex: an MRI-based analysis of volume and variance. Cereb. Cortex 8, 372–384.
Kim, K., Habas, P.A., Rousseau, F., Glenn, O.A., Barkovich, A.J., Studholme, C., 2010. Intersection based motion correction of multislice MRI for 3-D in utero fetal brain image formation. IEEE Trans. Med. Imaging 29, 146–158.
Kuklisova-Murgasova, M., Quaghebeur, G., Rutherford, M.A., Hajnal, J.V., Schnabel, J.A., 2012. Reconstruction of fetal brain MRI with intensity matching and complete outlier removal. Med. Image Anal. 16, 1550–1564.
Latora, V., Marchiori, M., 2001. Efficient behavior of small-world networks. Phys. Rev. Lett. 87, 198701.
Leitner, Y., Fattal-Valevski, A., Geva, R., Eshel, R., Toledano-Alhadef, H., Rotstein, M., Bassan, H., Radianu, B., Bitchonsky, O., Jaffa, A.J., Harel, S., 2007. Neurodevelopmental outcome of children with intrauterine growth retardation: a longitudinal, 10-year prospective study. J. Child Neurol. 22, 580–587.
Li, Y., Liu, Y., Li, J., Qin, W., Li, K., Yu, C., Jiang, T., 2009. Brain anatomical network and intelligence. PLoS Comput. Biol. 5, e1000395.
Liu, Y., Liang, M., Zhou, Y., He, Y., Hao, Y., Song, M., Yu, C., Liu, H., Liu, Z., Jiang, T., 2008. Disrupted small-world networks in schizophrenia. Brain 131, 945–961.
Lo, C.Y., Wang, P.N., Chou, K.H., Wang, J., He, Y., Lin, C.P., 2010. Diffusion tensor tractography reveals abnormal topological organization in structural cortical networks in Alzheimer's disease. J. Neurosci. 30, 16876–16885.
Lodygensky, G.A., Seghier, M.L., Warfield, S.K., Tolsa, C.B., Sizonenko, S., Lazeyras, F., Huppi, P.S., 2008. Intrauterine growth restriction affects the preterm infant's hippocampus. Pediatr. Res. 63, 438–443.
Martinussen, M., Fischl, B., Larsson, H.B., Skranes, J., Kulseng, S., Vangberg, T.R., Vik, T., Brubakk, A.M., Haraldseth, O., Dale, A.M., 2005. Cerebral cortex thickness in 15-year-old adolescents with low birth weight measured by an automated MRI-based method. Brain 128, 2588–2596.
McCarton, C.M., Wallace, I.F., Divon, M., Vaughan Jr., H.G., 1996. Cognitive and neurologic development of the premature, small for gestational age infant through age 6: comparison by birth weight and gestational age. Pediatrics 98, 1167–1178.
McCowan, L.M., Pryor, J., Harding, J.E., 2002. Perinatal predictors of neurodevelopmental outcome in small-for-gestational-age children at 18 months of age. Am. J. Obstet. Gynecol. 186, 1069–1075.
Padilla, N., Falcon, C., Sanz-Cortes, M., Figueras, F., Bargallo, N., Crispi, F., Eixarch, E., Arranz, A., Botet, F., Gratacos, E., 2011. Differential effects of intrauterine growth restriction on brain structure and development in preterm infants: a magnetic resonance imaging study. Brain Res. 1382, 98–108.
Padilla, N., Botet, F., Gratacos, E., 2012. MRI at 12 ± 2 months' corrected age without sedation. Pediatr. Radiol. 42, 385.
Paus, T., Collins, D.L., Evans, A.C., Leonard, G., Pike, B., Zijdenbos, A., 2001. Maturation of white matter in the human brain: a review of magnetic resonance studies. Brain Res. Bull. 54, 255–266.
Raj, A., Mueller, S.G., Young, K., Laxer, K.D., Weiner, M., 2010. Network-level analysis of cortical thickness of the epileptic brain. Neuroimage 52, 1302–1313.
Rees, S., Harding, R., Walker, D., 2011. The biological basis of injury and neuroprotection in the fetal and neonatal brain. Int. J. Dev. Neurosci. 29, 551–563.
Robinson, H.P., Fleming, J.E., 1975. A critical evaluation of sonar "crown-rump length" measurements. Br. J. Obstet. Gynaecol. 82, 702–710.
Rubinov, M., Sporns, O., 2009. Complex network measures of brain connectivity: uses and interpretations. Neuroimage 52, 1059–1069.
Scherjon, S.A., Smolders-DeHaas, H., Kok, J.H., Zondervan, H.A., 1993. The "brain-sparing" effect: antenatal cerebral Doppler findings in relation to neurologic outcome in very preterm infants. Am. J. Obstet. Gynecol. 169, 169–175.
Shi, F., Yap, P.T., Wu, G., Jia, H., Gilmore, J.H., Lin, W., Shen, D., 2011. Infant brain atlases from neonates to 1- and 2-year-olds. PLoS One 6, e18746.
Shu, N., Liu, Y., Li, J., Li, Y., Yu, C., Jiang, T., 2009. Altered anatomical network in early blindness revealed by diffusion tensor tractography. PLoS One 4, e7228.
Shu, N., Liu, Y., Li, K., Duan, Y., Wang, J., Yu, C., Dong, H., Ye, J., He, Y., 2011. Diffusion tensor tractography reveals disrupted topological efficiency in white matter structural networks in multiple sclerosis. Cereb. Cortex 21, 2565–2577.
Smith, S.M., 2002. Fast robust automated brain extraction. Hum. Brain Mapp. 17, 143–155.
Sporns, O., Tononi, G., Kotter, R., 2005. The human connectome: a structural description of the human brain. PLoS Comput. Biol. 1, e42.
Studholme, C., 2011. Mapping fetal brain development in utero using magnetic resonance imaging: the Big Bang of brain mapping. Annu. Rev. Biomed. Eng. 13, 345–368.
Tijms, B.M., Series, P., Willshaw, D.J., Lawrie, S.M., 2012. Similarity-based extraction of individual networks from gray matter MRI scans. Cereb. Cortex 22, 1530–1541.
Tijms, B.M., Moller, C., Vrenken, H., Wink, A.M., de Haan, W., van der Flier, W.M., Stam, C.J., Scheltens, P., Barkhof, F., 2013. Single-subject grey matter graphs in Alzheimer's disease. PLoS One 8, e58921.
Tolsa, C.B., Zimine, S., Warfield, S.K., Freschi, M., Sancho Rossignol, A., Lazeyras, F., Hanquinet, S., Pfizenmaier, M., Huppi, P.S., 2004. Early alteration of structural and functional brain development in premature infants born with intrauterine growth restriction. Pediatr. Res. 56, 132–138.
Tristan-Vega, A., Arribas, J.I., 2007. A fast B-spline pseudo-inversion algorithm for consistent image registration. Proceedings of the International Conference on Computer Analysis Images and Patterns (CAIP), Vienna, Austria, pp. 768–775.
Tymofiyeva, O., Hess, C.P., Ziv, E., Tian, N., Bonifacio, S.L., McQuillen, P.S., Ferriero, D.M., Barkovich, A.J., Xu, D., 2012. Towards the "baby connectome": mapping the structural connectivity of the newborn brain. PLoS One 7, e31029.
Tzourio-Mazoyer, N., Landeau, B., Papathanassiou, D., Crivello, F., Etard, O., Delcroix, N., Mazoyer, B., Joliot, M., 2002. Automated anatomical labeling of activations in SPM using a macroscopic anatomical parcellation of the MNI MRI single-subject brain. Neuroimage 15, 273–289.
Van Essen, D.C., 1997. A tension-based theory of morphogenesis and compact wiring in the central nervous system. Nature 385, 313–318.
van Wijk, B.C.M., Stam, C.J., Daffertshofer, A., 2010. Comparing brain networks of different size and connectivity density using graph theory. PLoS One 5, e13701.
Wang, L., Zhu, C., He, Y., Zang, Y., Cao, Q., Zhang, H., Zhong, Q., Wang, Y., 2009. Altered small-world brain functional networks in children with attention-deficit/hyperactivity disorder. Hum. Brain Mapp. 30, 638–649.
Warfield, S.K., Guimond, A., Roche, A., Bharatha, A., Tei, A., Talos, F., Rexilius, J., Ruiz-Alzola, J., Westin, C.F., Haker, S., Angenent, S., Tannenbaum, A., Jolesz, F., Kilkinis, R., 2002. Advanced nonrigid registration algorithms for image fusion. In: Mazziotta, J.C., Toga, A.W. (Eds.), Brain Mapping: The Methods. Elsevier, pp. 661–690.
Wee, C.-Y., Yap, P.-T., Li, W., Denny, K., Browndyke, J.N., Potter, G.G., Welsh-Bohmer, K.A., Wang, L., Shen, D., 2010. Enriched white matter connectivity networks for accurate identification of MCI patients. Neuroimage 54, 1812–1822.
Wen, W., Zhu, W., He, Y., Kochan, N.A., Reppermund, S., Slavin, M.J., Brodaty, H., Crawford, J., Xia, A., Sachdev, P., 2011. Discrete neuroanatomical networks are associated with specific cognitive abilities in old age. J. Neurosci. 31, 1204–1212.
WHO, 2012. World Health Statistics 2012. World Health Organization, Geneva.
Wu, T., Wang, L., Chen, Y., Zhao, C., Li, K., Chan, P., 2009. Changes of functional connectivity of the motor network in the resting state in Parkinson's disease. Neurosci. Lett. 460, 6–10.
Yap, P.T., Fan, Y., Chen, Y., Gilmore, J.H., Lin, W., Shen, D., 2011. Development trends of white matter connectivity in the first years of life. PLoS One 6, e24678.
Zhou, L., Wang, Y., Li, Y., Yap, P.T., Shen, D., 2011. Hierarchical anatomical brain networks for MCI prediction: revisiting volumetric measures. PLoS One 6, e21935.

Supplementary Material

1.- Relationship with diffusion MRI based brain networks

In order to assess the relationship of the brain networks obtained with the proposed methodology based on gray matter morphology similarity with those obtained with diffusion MRI, we selected a sample of 10 controls which have available a diffusion MRI acquisition. Specifically, we used a subset of controls used in this paper that was also part of the study previously published in (Batalle et al., 2012). Briefly, diffusion images were acquired by using a single-shot Echo-Planar Imaging (SE-EPI) sequence covering 30 diffusion directions with a b-value of 1000 s/mm^2, all acquired images covered the whole brain, with 3-mm slice thickness with no interslice gap, 40 axial slices and in-plane acquisition matrix of 122 x 122 with a field of view (FoV) set to 200 x 200 mm which resulted in a voxel dimension of 1.64 x 1.64 x 3 mm^3. Anatomical T1 acquisition was parceled with Anatomical Automatic Labeling (AAL) atlas (Tzourio-Mazoyer et al., 2002), adapted to one year old population (Shi et al., 2011). A deterministic tractography was performed and integrated to the anatomical parcellation in diffusion space in order to construct inter-cortical measures. Network edge weights were defined according to two different criteria: fiber number (FN) connecting each pair of regions, and mean FA along all the fibers connecting a pair of regions, hence obtaining two weighted adjacency matrices in addition to the binary one. Global graph theory measures assessed included global efficiency and local efficiency of each subject, calculated in both their binary and weighted versions. More details are available in (Batalle et al., 2012).

In the present analysis we assess the cross-subject correlations of the graph theory measures obtained from the gray matter morphology approach proposed with those obtained from the networks generated with diffusion MRI data. As it can be observed in Supplementary Table 2, for the tested population we find high correlations between gray matter morphology similarity based weighted global and local efficiency and diffusion MRI based binary and FA weighted global and local efficiency. No significant correlations were found between cost integrated global and local efficiencies and diffusion MRI based graph features, suggesting that these measures are capturing a different aspect of the brain network topology than the one described with diffusion MRI based features. However, the exact meaning of these results must be deeply assessed with bigger sample size.

2.- Effects of minor head rotations on the networks

Although the brain anatomical acquisition was, previously to any further analyses, manually reoriented following an established criteria and hence minimizing the effects of head rotations in the acquisition, in this complementary analysis we assessed the effects of the possible remaining head orientation difference on the generation of brain networks with the method proposed. To do so, one arbitrary selected control was rotated +/- 10 degrees (at 2 degrees steps) in x, y, and z axis, and then resliced accordingly, in order to observe which effect would have minor rotation due to the acquisition scheme in the resulting brain networks. The brain network was generated for each rotated and resliced brain based on the gray matter morphology similarity method proposed in the present paper.

In order to compare the rotated networks we defined a metric of graph dissimilarity as the Euclidean distance between its adjacency matrices (Frobenius Norm of the difference between matrices). The dissimilarity of the original networks obtained after head rotation (intra-subject distance) was compared with the dissimilarity of the original network with the network obtained for the rest of the subjects (inter-subject distance) (Supplementary Figure 1), showing for all the tested rotations lower intra-subject than inter-subject distance.

References

Batalle, D., Eixarch, E., Figueras, F., Munoz-Moreno, E., Bargallo, N., Illa, M., Acosta-Rojas, R., Amat-Roldan, I., Gratacos, E., 2012. Altered small-world topology of structural brain networks in infants with intrauterine growth restriction and its association with later neurodevelopmental outcome. Neuroimage 60, 1352-1366.

Shi, F., Yap, P.T., Wu, G., Jia, H., Gilmore, J.H., Lin, W., Shen, D., 2011. Infant brain atlases from neonates to 1- and 2-year-olds. PLoS ONE 6, e18746.

Tzourio-Mazoyer, N., Landeau, B., Papathanassiou, D., Crivello, F., Etard, O., Delcroix, N., Mazoyer, B., Joliot, M., 2002. Automated anatomical labeling of activations in SPM using a macroscopic anatomical parcellation of the MNI MRI single-subject brain. Neuroimage 15, 273-289.

Supplementary Figure 1. Dissimilarity (Euclidian distance) of the reconstructed brain network of an arbitrary subject with (A) the brain network reconstructed for the same subject after rotation in each axis of -10 to 10 degrees at 2 degrees steps (intra-subject dissimilarity), and (B) with the rest of subjects included in the study (inter-subject similarity). For better comparison dotted lines of intra-subject dissimilarity for all the tested rotations have also been overlaid in B.

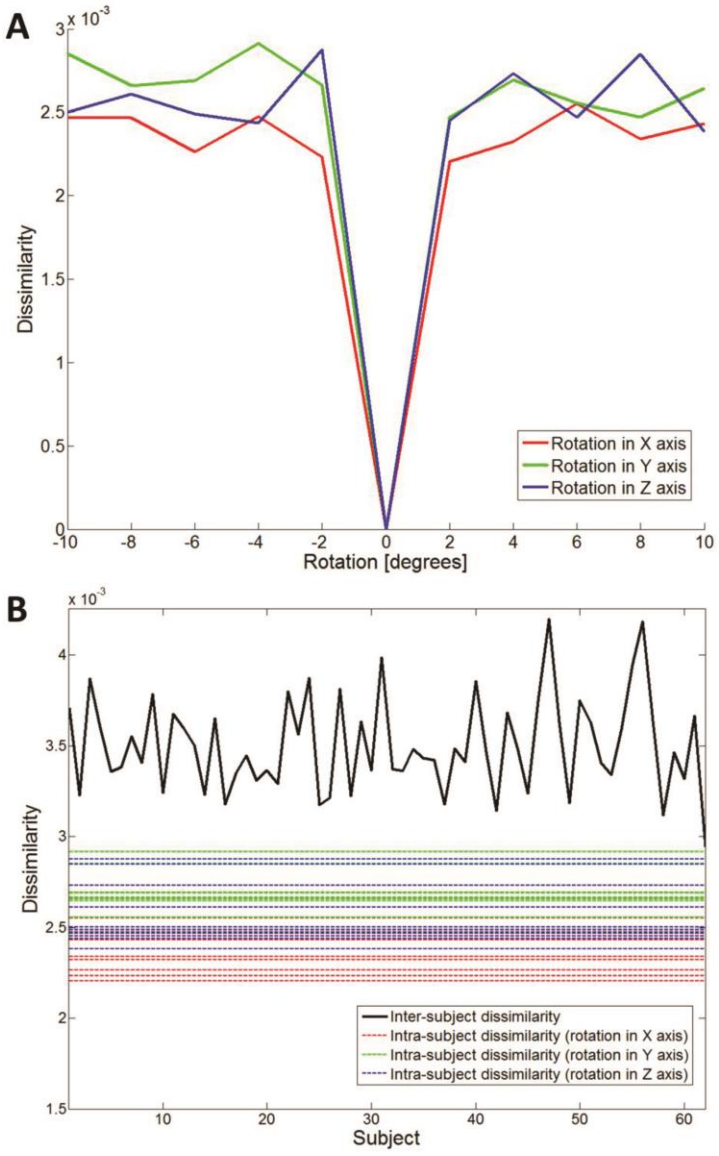

Supplementary Table 1. Analysis of the relative regional volume (normalized by total GM volume) of the parcellated AAL regions in IUGR and control group. Results expressed as mean (standard deviation) in %.

ROI	Controls	IUGR	p
PRE (L)	2.118 (0.154)	2.141 (0.164)	N.S.
PRE (R)	2.118 (0.199)	2.147 (0.196)	N.S.
F1 (L)	1.545 (0.121)	1.584 (0.137)	N.S.
F1 (R)	1.783 (0.144)	1.841 (0.145)	N.S.
F1O (L)	0.494 (0.038)	0.502 (0.046)	N.S.
F1O (R)	0.557 (0.052)	0.56 (0.043)	N.S.
F2 (L)	2.966 (0.242)	3.006 (0.197)	N.S.
F2 (R)	2.811 (0.227)	2.833 (0.226)	N.S.
F2O (L)	0.493 (0.038)	0.499 (0.048)	N.S.
F2O (R)	0.532 (0.06)	0.544 (0.051)	N.S.
F3OP (L)	0.572 (0.067)	0.549 (0.054)	N.S.
F3OP (R)	**0.78 (0.077)**	**0.747 (0.071)**	**p=0.003**
F3T (L)	1.482 (0.155)	1.446 (0.142)	N.S.
F3T (R)	**1.097 (0.108)**	**1.081 (0.112)**	**p=0.002**
F3O (L)	1.271 (0.086)	1.269 (0.114)	N.S.
F3O (R)	1.283 (0.103)	1.289 (0.107)	N.S.
RO (L)	0.655 (0.049)	0.646 (0.038)	N.S.
RO (R)	0.927 (0.062)	0.908 (0.072)	N.S.
SMA (L)	1.304 (0.12)	1.328 (0.128)	N.S.
SMA (R)	1.385 (0.126)	1.384 (0.133)	N.S.
OC (L)	0.229 (0.021)	0.232 (0.023)	N.S.
OC (R)	0.231 (0.022)	0.231 (0.02)	N.S.
F1M (L)	1.529 (0.135)	1.577 (0.163)	N.S.
F1M (R)	1.006 (0.085)	1.059 (0.106)	N.S.
F1MO (L)	0.388 (0.032)	0.397 (0.043)	N.S.
F1MO (R)	0.547 (0.061)	0.553 (0.039)	N.S.
GR (L)	0.545 (0.043)	0.556 (0.051)	N.S.
GR (R)	0.474 (0.036)	0.486 (0.037)	N.S.
IN (L)	1.257 (0.063)	1.26 (0.076)	N.S.
IN (R)	1.214 (0.046)	1.233 (0.085)	N.S.
ACIN (L)	1.12 (0.098)	1.118 (0.099)	N.S.
ACIN (R)	1.005 (0.095)	1.009 (0.09)	N.S.
MCIN (L)	1.552 (0.093)	1.531 (0.099)	N.S.
MCIN (R)	1.676 (0.086)	1.674 (0.116)	N.S.
PCIN (L)	0.239 (0.024)	0.247 (0.029)	N.S.
PCIN (R)	**0.153 (0.017)**	**0.156 (0.015)**	**p=0.007**
HIP (L)	0.518 (0.034)	0.533 (0.034)	N.S.
HIP (R)	0.523 (0.034)	0.528 (0.031)	N.S.
PHIP (L)	0.662 (0.037)	0.687 (0.044)	N.S.
PHIP (R)	0.652 (0.038)	0.675 (0.047)	N.S.
AMYG (L)	0.161 (0.017)	0.165 (0.017)	N.S.
AMYG (R)	0.153 (0.016)	0.162 (0.013)	N.S.
V1 (L)	1.738 (0.118)	1.749 (0.13)	N.S.
V1 (R)	1.323 (0.108)	1.313 (0.088)	N.S.
Q (L)	**1.413 (0.104)**	**1.39 (0.098)**	**p=0.042**
Q (R)	1.166 (0.073)	1.141 (0.06)	N.S.

ROI	Controls	IUGR	p
LING (L)	1.454 (0.073)	1.482 (0.072)	N.S.
LING (R)	1.455 (0.075)	1.462 (0.077)	N.S.
O1 (L)	0.894 (0.066)	0.896 (0.074)	N.S.
O1 (R)	0.92 (0.065)	0.905 (0.062)	N.S.
O2 (L)	2.26 (0.14)	2.297 (0.141)	N.S.
O2 (R)	1.552 (0.158)	1.544 (0.11)	N.S.
O3 (L)	0.599 (0.034)	0.605 (0.043)	N.S.
O3 (R)	0.794 (0.067)	0.805 (0.096)	N.S.
FUSI (L)	1.7 (0.089)	1.72 (0.071)	N.S.
FUSI (R)	1.722 (0.097)	1.727 (0.097)	N.S.
POST (L)	2.291 (0.11)	2.321 (0.166)	N.S.
POST (R)	2.437 (0.144)	2.44 (0.167)	N.S.
P1 (L)	**0.941 (0.096)**	**0.936 (0.071)**	**p=0.030**
P1 (R)	1.211 (0.104)	1.175 (0.098)	N.S.
P2 (L)	1.841 (0.116)	1.811 (0.158)	N.S.
P2 (R)	1.331 (0.104)	1.326 (0.141)	N.S.
SMG (L)	0.774 (0.096)	0.773 (0.089)	N.S.
SMG (R)	1.465 (0.181)	1.463 (0.166)	N.S.
AG (L)	1.131 (0.092)	1.168 (0.112)	N.S.
AG (R)	1.706 (0.14)	1.72 (0.146)	N.S.
PQ (L)	2.979 (0.169)	2.947 (0.171)	N.S.
PQ (R)	**2.372 (0.108)**	**2.354 (0.13)**	**p=0.043**
PCL (L)	0.746 (0.073)	0.741 (0.088)	N.S.
PCL (R)	0.36 (0.03)	0.359 (0.034)	N.S.
CAU (L)	0.584 (0.048)	0.585 (0.051)	N.S.
CAU (R)	0.614 (0.057)	0.616 (0.054)	N.S.
PUT (L)	0.718 (0.035)	0.725 (0.04)	N.S.
PUT (R)	0.744 (0.027)	0.737 (0.044)	N.S.
PAL (L)	0.181 (0.013)	0.184 (0.016)	N.S.
PAL (R)	0.192 (0.013)	0.191 (0.014)	N.S.
THA (L)	0.729 (0.046)	0.739 (0.06)	N.S.
THA (R)	0.719 (0.053)	0.727 (0.056)	N.S.
HES (L)	0.158 (0.014)	0.159 (0.011)	N.S.
HES (R)	0.178 (0.017)	0.175 (0.018)	N.S.
T1 (L)	2.073 (0.163)	2.044 (0.129)	N.S.
T1 (R)	2.267 (0.143)	2.245 (0.122)	N.S.
T1P (L)	**0.967 (0.066)**	**0.928 (0.069)**	**p=0.002**
T1P (R)	0.95 (0.07)	0.944 (0.079)	N.S.
T2 (L)	3.651 (0.271)	3.679 (0.251)	N.S.
T2 (R)	**3.586 (0.188)**	**3.535 (0.204)**	**p=0.039**
T2P (L)	**0.406 (0.044)**	**0.38 (0.045)**	**p=0.019**
T2P (R)	0.506 (0.051)	0.496 (0.053)	N.S.
T3 (L)	1.907 (0.131)	1.919 (0.112)	N.S.
T3 (R)	2.403 (0.151)	2.429 (0.143)	N.S.
CER (L)	1.838 (0.173)	1.891 (0.162)	N.S.
CER (R)	1.759 (0.146)	1.809 (0.154)	N.S.
VER	1.15 (0.121)	1.176 (0.129)	N.S.

(L) refers to left hemisphere, (R) to right hemisphere. N.S. for non-significant. in bold those regions with $p<0.05$ (uncorrected).

Supplementary Table 2. Pearson correlation of graph theory features obtained with morphology based similarity approach with those obtained with diffusion MRI in 10 control subjects.

Gray matter morphology based graph theory features	Diffusion MRI based graph theory features	Pearsons' Rho	p
Weighted Global Efficiency	**Binary Global Efficiency**	**0.765**	**0.010**
	Weighted Global Efficiency FN	0.139	0.702
	Weighted Global Efficiency FA	**0.782**	**0.007**
Weighted Local Efficiency	**Binary Local Efficiency**	**0.806**	**0.005**
	Weighted Local Efficiency FN	0.049	0.893
	Weighted Local Efficiency FA	**0.686**	**0.028**
Cost Integrated Global Efficiency	Binary Global Efficiency	0.040	0.912
	Weighted Global Efficiency FN	0.012	0.973
	Weighted Global Efficiency FA	0.554	0.097
Cost Integrated Local Efficiency	Binary Local Efficiency	0.348	0.324
	Weighted Local Efficiency FN	-0.062	0.864
	Weighted Local Efficiency FA	0.600	0.067

In bold those correlations reaching statistical significance ($p<0.05$).

5.3. PROJECT 3: COPY OF PUBLISHED PAPER

Long-term reorganization of structural brain networks in a rabbit model of intrauterine growth restriction

Batalle D, Muñoz-Moreno E, Arbat-Plana A, Illa M, Figueras F, Eixarch E, Gratacos E

2014, Neuroimage, *In press*

ARTICLE IN PRESS

YNIMG-11406; No. of pages: 15; 4C: 3, 9, 10, 11

NeuroImage xxx (2014) xxx–xxx

Contents lists available at ScienceDirect

NeuroImage

journal homepage: www.elsevier.com/locate/ynimg

Long-term reorganization of structural brain networks in a rabbit model of intrauterine growth restriction

Dafnis Batalle [a,*], Emma Muñoz-Moreno [a], Ariadna Arbat-Plana [a], Miriam Illa [a,b], Francesc Figueras [a,b,c], Elisenda Eixarch [a,b,c], Eduard Gratacos [a,b,c]

[a] Fetal and Perinatal Medicine Research Group, Institut d'Investigacions Biomediques August Pi i Sunyer (IDIBAPS), Barcelona, Spain
[b] Maternal–Fetal Medicine Department, ICGON, Hospital Clínic, Universitat de Barcelona, Barcelona, Spain
[c] Centro de Investigación Biomédica en Red de Enfermedades Raras (CIBERER), Barcelona, Spain

ARTICLE INFO

Article history:
Accepted 25 May 2014
Available online xxxx

Keywords:
Fetal growth restriction
Connectomics
Connectome
Animal model
Low birth weight
Diffusion magnetic resonance imaging
Q-Ball
Neurobehavior
Object Recognition Task
Open Field Behavioral Test

ABSTRACT

Characterization of brain changes produced by intrauterine growth restriction (IUGR) is among the main challenges of modern fetal medicine and pediatrics. This condition affects 5–10% of all pregnancies and is associated with a wide range of neurodevelopmental disorders. Better understanding of the brain reorganization produced by IUGR opens a window of opportunity to find potential imaging biomarkers in order to identify the infants with a high risk of having neurodevelopmental problems and apply therapies to improve their outcomes. Structural brain networks obtained from diffusion magnetic resonance imaging (MRI) is a promising tool to study brain reorganization and to be used as a biomarker of neurodevelopmental alterations. In the present study this technique is applied to a rabbit animal model of IUGR, which presents some advantages including a controlled environment and the possibility to obtain high quality MRI with long acquisition times. Using a Q-Ball diffusion model, and a previously published rabbit brain MRI atlas, structural brain networks of 15 IUGR and 14 control rabbits at 70 days of age (equivalent to pre-adolescence human age) were obtained. The analysis of graph theory features showed a decreased network infrastructure (degree and binary global efficiency) associated with IUGR condition and a set of generalized fractional anisotropy (GFA) weighted measures associated with abnormal neurobehavior. Interestingly, when assessing the brain network organization independently of network infrastructure by means of normalized networks, IUGR showed increased global and local efficiencies. We hypothesize that this effect could reflect a compensatory response to reduced infrastructure in IUGR. These results present new evidence on the long-term persistence of the brain reorganization produced by IUGR that could underlie behavioral and developmental alterations previously described. The described changes in network organization have the potential to be used as biomarkers to monitor brain changes produced by experimental therapies in IUGR animal model.

Introduction

Intrauterine growth restriction (IUGR) affects 5–10% of all pregnancies and is a major public health issue, being a prevalent condition that has been associated with a wide range of short- and long-term neurodevelopmental and cognitive dysfunctions (Arcangeli et al., 2012; Baschat, 2013), even in adulthood (Løhaugen et al., 2013). With the significant advance of magnetic resonance imaging (MRI) in the recent years, the brain alterations and reorganization underlying these neurofunctional alterations are starting to be elucidated. It has been suggested that brain reorganization starts in utero, where different patterns of cortical development (Egaña-Ugrinovic et al., 2013) and altered quantitative MRI texture predictive of altered neurodevelopment (Sanz-Cortes et al., 2013) have been shown in IUGR. At neonatal period IUGR has been reported to have decreased volume in gray matter (GM) (Tolsa et al., 2004) and hippocampus (Lodygensky et al., 2008) and discordant patterns of gyrification (Dubois et al., 2008). At one year of age, persistence of structural changes has been demonstrated, including reduced volumes of GM (Padilla et al., 2011) and decreased fractal dimension in both GM and white matter (WM) that correlate with abnormal neurodevelopment (Esteban et al., 2010). Studies on IUGR at later ages have reported changes in regional brain volumes and cortical

Abbreviations: DI, discrimination index; DWI, diffusion-weighted images; FA, fractional anisotropy; FD, fiber density; FDR, false discovery rate; GFA, generalized fractional anisotropy; GLM, general linear model; GM, gray matter; IQR, inter-quartile range; IUGR, intrauterine growth restriction; MRI, magnetic resonance imaging; OFBT, Open Field Behavioral Test; ORT, Object Recognition Task; SD, standard deviation; WM, white matter.

* Corresponding author at: Fetal and Perinatal Medicine Research Group, Hospital Clínic, IDIBAPS, Sabino de Arana 1, Helios III, 08028 Barcelona, Spain. Fax: +34 93 227 9336.

E-mail addresses: dbatalle@clinic.ub.es (D. Batalle), emunozm@clinic.ub.es (E. Muñoz-Moreno), aarbat@clinic.ub.es (A. Arbat-Plana), miriamil@clinic.ub.es (M. Illa), ffiguera@clinic.ub.es (F. Figueras), eixarch@clinic.ub.es (E. Eixarch), gratacos@clinic.ub.es (E. Gratacos).

http://dx.doi.org/10.1016/j.neuroimage.2014.05.065
1053-8119/

thickness in 4 to 7-year-old children (De Bie et al., 2011), reduced volumes for thalamus and cerebellar white matter (Martinussen et al., 2009), and thinning of corpus callosum and general WM reduction (Skranes et al., 2005) in adolescents. There is a need to better characterize the brain reorganization underlying neurodevelopmental and cognitive dysfunctions in IUGR. Likewise, the development of imaging biomarkers is an urgent clinical and experimental need (Ment et al., 2009).

The study of brain connectivity holds great promise for the development of pathophysiological insights and biomarkers of human disease characterized by subtle brain changes that are not reflected in conventional MRI techniques (Gratacos, 2012). Indeed, one of the major recent advances in the application of new MRI modalities has been the emerging technique of "connectomics" (Hagmann, 2005), opening the possibility to extract macroscopic circuitry of the connections of the brain, in what has been called "the connectome" (Sporns et al., 2005). In particular, the use of graph theory analyses on brain networks has been demonstrated to be a useful tool to characterize brain organization by a few comprehensible parameters (Bassett and Bullmore, 2009). Different sets of data, including functional MRI and diffusion MRI, have been used to extract macroscopic brain networks and analyze network features in healthy adults, adolescents and infants (Gong et al., 2009a; Hagmann et al., 2008, 2010; Iturria-Medina et al., 2008; Yap et al., 2011) and to report altered group connectivity parameters in a wide range of neurological, neurobehavioral and neurodegenerative diseases (Alexander-Bloch et al., 2010; Liu et al., 2008; Lo et al., 2010; Shu et al., 2009, 2011; Wang et al., 2009; Wu et al., 2009). Importantly, connectomics and graph theory features have been shown to be potential tools to develop biomarkers to predict neurological outcomes in adult (He et al., 2009; Li et al., 2009; Wee et al., 2010; Wen et al., 2011) and perinatal diseases (Batalle et al., 2012, 2013; Tymofiyeva et al., 2012). Particularly, brain networks of one-year-old infants obtained from diffusion MRI have been reported to have reduced level of weighted organization and a pattern of altered regional network features that is associated with latter neurodevelopmental problems (Batalle et al., 2012), showing their potential to develop imaging biomarkers to detect infants at high risk of having neurodevelopmental problems one year later. Nonetheless, whether persistent brain reorganization produced by IUGR persists at long-term (adolescence and adult period) and whether connectomic analysis could be a suitable tool to characterize the patterns induced by this conditions are still unknown.

Assessing long-term effects of IUGR in the human brain is a challenging task, limited by the influence of uncontrolled environmental factors (Hall and Perona, 2012) and the difficulty of obtaining sufficiently large sample sizes. The induction of IUGR in rabbit models has been proven to reproduce major features of human IUGR (Bassan et al., 2000; Eixarch et al., 2009, 2011). Furthermore, white matter maturation process in rabbit is closer to humans than other species, since it starts in intrauterine period (Derrick et al., 2007). Hence, albeit their obvious limitations, rabbit model may be a useful tool to analyze long-term brain remodeling in IUGR. They could play a key role in the definition of image biomarkers for early diagnosis that are critical to demonstrate changes after the application of experimental therapies, especially when those should be tested in fetuses or neonates. Besides the highly reproducible experimental conditions, high quality MRI with long acquisition times can be performed in isolated whole brain preparations. Using this model, regional brain changes in fractional anisotropy, correlated with poorer outcome in neurobehavioral tests have been reported in newborns (Eixarch et al., 2012), some of them persisting in preadolescent period (Illa et al., 2013), where changes in the connectivity of anxiety, attention and memory networks have been shown. Due to the recent development of an MRI rabbit brain atlas (Muñoz-Moreno et al., 2013), the possibility to obtain whole brain structural networks based on diffusion MRI arises. This opens the opportunity to assess long-term network reorganization associated with functional impairments without a priori hypothesis, taking advantage of the huge potential of graph theory measures to characterize brain functioning and organization (Bassett and Bullmore, 2009) that have been previously used to characterize one-year-old infants with IUGR (Batalle et al., 2012, 2013).

In the present study, graph theory features from diffusion MRI brain networks were calculated in 15 rabbits with surgically induced IUGR and 14 controls at equivalent preadolescent age, in order to assess the long-term impact of IUGR in brain organization that could underlie behavioral and developmental alterations. The results showed a specific pattern of global network features altered in IUGR, characterized by an impaired network infrastructure, but an increase in the relative terms of organizational efficiency that we hypothesize to be associated with a compensatory effect in IUGR. An exploratory analysis of the regional features altered by IUGR condition was also performed. Both global and regional network features were associated with neurobehavioral test results. The results here presented contribute to the knowledge on long-term brain changes associated with neurobehavioral dysfunctions in IUGR, showing the feasibility of using brain network features from diffusion MRI as biomarkers to assess and potentially monitor treatment of IUGR using experimental models.

Methods

The design of the study and each of the steps of the procedures are shown in Fig. 1. A detailed description of the methodology used is included in this section.

Animals, study protocol and surgical model

Animal experimentation of this study was approved by the Animal Experimental Ethics Committee of the University of Barcelona (permit number: 206/10-5440), and all efforts were made to avoid or minimize suffering.

Part of the animals used in this study has been previously used in a recent study (Illa et al., 2013). From 13 New Zealand pregnant rabbits provided by a certified breeder, we selected two cases and two controls of each dam at birth. At the 70th postnatal day, all surviving cases and one control for each case were included resulting in a total population of 30 rabbits (15 with induced IUGR and 15 sham controls). Dams were housed for 1 week before surgery in separate cages on a reversed 12/12 h light cycle, with free access to water and standard chow. At 25 days of gestation (term at 31 days), a ligation of 40–50% of uteroplacental vessels was performed following a previously described protocol (Eixarch et al., 2009). Briefly, after midline abdominal laparotomy, the gestational sacs of both horns were counted and numbered. Afterwards, only one uterine horn was kept outside the abdomen and the induction of IUGR was performed by ligating 40–50% of the uteroplacental vessels of all the gestational sacs from this horn. After the procedure, the abdomen was closed in two layers and postoperative analgesia (meloxicam) was administered for 48 h. After surgery, the animals were allowed free access to water and standard chow for 5 days until delivery. Cesarean section was performed at 30 days of gestation and living pups were obtained. All living newborns were weighed and identified by a subcutaneous microchip inserted in their back (Microchip MUSICC, Avid Microchip S.L., Barcelona, Spain). Cases were considered those pups delivered from the ligated horn, whereas controls were those delivered from the contralateral horn (non-ligated). Both cases and controls were housed with a wet nurse rabbit with part of the offspring until the 30th postnatal day when they were weaned. Thereafter both groups of rabbits were housed in groups of three with a reversed 12/12 h light cycle with free access to water and standard chow. On the 70th postnatal day, which is considered to be equivalent to preadolescence period in humans in terms of sexual maturity (Moorman et al., 2000), functional tests were applied and the rabbits were anesthetized and sacrificed thereafter. The left and right common carotid arteries were cannulated and the brains were perfused with phosphate-buffered saline (PBS) followed by 4% paraformaldehyde PBS. Then,

Please cite this article as: Batalle, D., et al., Long-term reorganization of structural brain networks in a rabbit model of intrauterine growth restriction, NeuroImage (2014), http://dx.doi.org/10.1016/j.neuroimage.2014.05.065

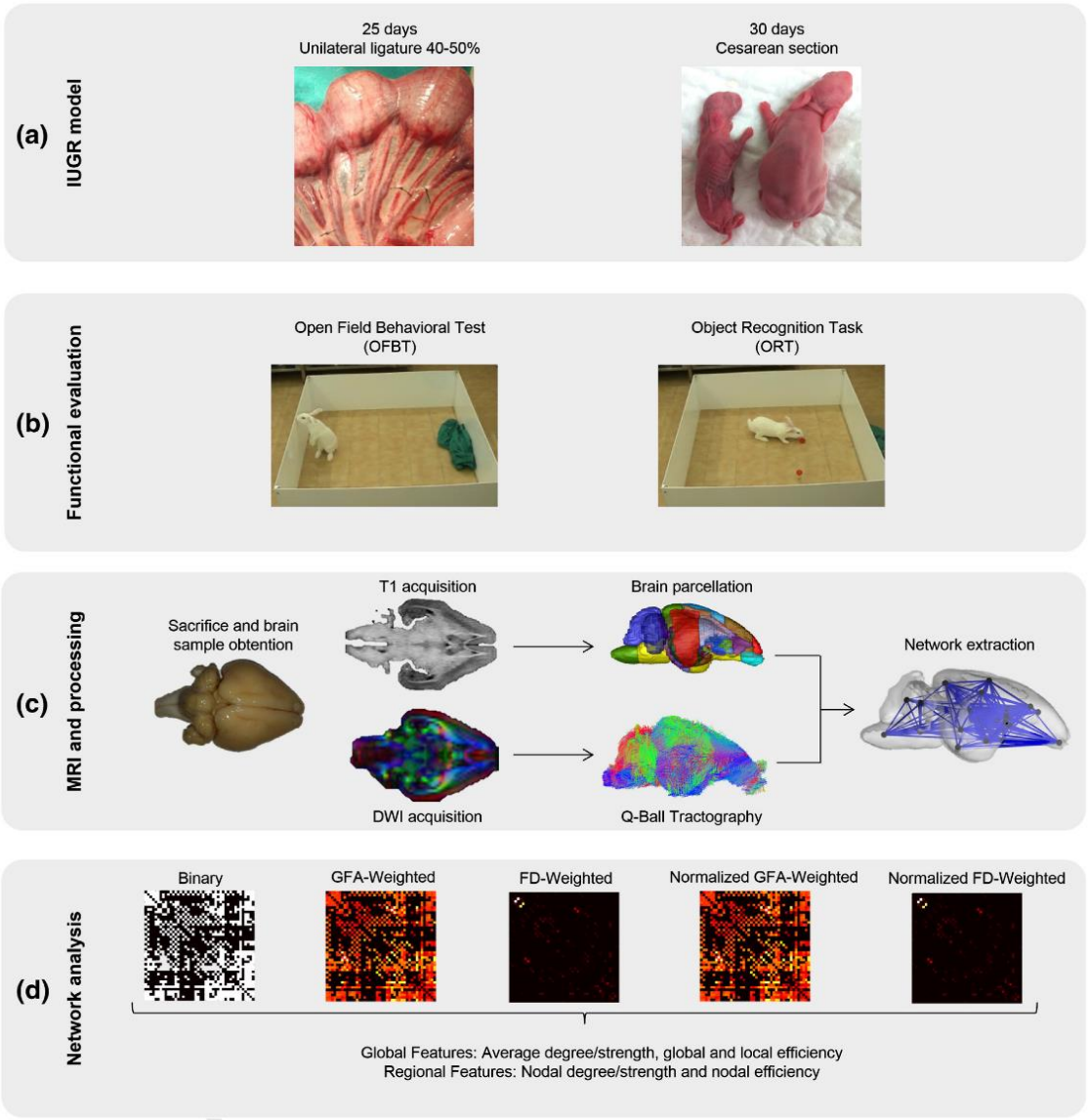

Fig. 1. Methodological scheme. (a) IUGR induction by means of a unilateral ligature at 25 days of gestation in a pregnant rabbit. At 30 days of gestation neonatal rabbits with and without IUGR are obtained by means of a cesarean section. (b) Functional evaluation of 70-day-old rabbits is performed by means of Open Field Behavioral Test (OFBT) and Object Recognition Task (ORT). Note that the blue object in the left panel corresponds to the blanket used to bring the subjects to the open field, serving also as the starting familiar point for the animal. (c) Subjects are sacrificed and brain samples are obtained. MRI acquisition consisting of 126 directions DWI and anatomical T1 volumes is performed. Brain parcellation is performed in T1 volume and Q-Ball reconstruction and tractography is performed on DWI volumes. Parcellation is registered to DWI space by means of an affine registration and brain networks are extracted. (d). Binary, GFA-weighted and FD-weighted networks are obtained, as well as normalized GFA-weighted and normalized FD-weighted versions. Global and regional graph theory features are used to characterize the five brain networks obtained for each subject.

brains were excised from the skull and immersed in 4% paraformaldehyde PBS at 4 °C for 48 h.

Neurobehavioral tests and cognitive evaluation

In order to assess neurobehavioral changes related to emotion and cognition, two standard tests used extensively in rodents and recently adapted to rabbits (Illa et al., 2013) were used: Open Field Behavioral Test (OFBT) and Object Recognition Task (ORT). Neurobehavioral tests were performed in a subset of rabbits. Particularly, of the total sample of 29 subjects, 20 rabbits were selected to perform OFBT and ORT.

OFBT evaluates locomotion and exploratory activities competing against fear, anxiety and attention (Bouet et al., 2003; Walsh and Cummins, 1975), based on the procedures originally described by Hall (1934). Briefly, the testing area was divided into 36 squares of 23 × 23 cm, the four central squares were considered as the internal area and the remaining squares were defined as the external (peripheral) area. The rabbits were taken out of their cage wrapped with a cloth

Please cite this article as: Batalle, D., et al., Long-term reorganization of structural brain networks in a rabbit model of intrauterine growth restriction, NeuroImage (2014), http://dx.doi.org/10.1016/j.neuroimage.2014.05.065

and placed close to one of the lateral walls (starting point) and behavior was assessed during 10 min. In order to minimize interference due to human contact, each session was videotaped and later evaluated by two blinded observers. Rabbits that escaped from the testing area were excluded from the analysis. The main parameters were recorded including latency of leaving the starting point (seconds) and number of squares explored (total, internal and external). In order to obtain a single dichotomic value summarizing a normal or an abnormal performance of a given subject, normality of the control population was established at the 25th centile for each of the four main parameters recorded. Having two or more of these items below this 25th centile was considered to be an abnormal exploration. OFBT was performed successfully in 10 controls and 9 IUGR.

ORT assesses short-term memory, especially recognition (Olton and Feustle, 1981) and attention capacity (Cowan et al., 1999), based on the tendency of rodents to explore new stimuli for a longer time compared to familiar stimuli (Dere et al., 2006; Ennaceur and Aggleton, 1997; Mumby, 2001). The test was adapted from the original description (Ennaceur and Delacour, 1988), including some modifications in the stimulus used (instead of a visual stimulus, an odor-based stimulus was used). Briefly, after a familiarization phase where the rabbit was presented with two boxes containing the same odor-based stimuli (apple), the animal was returned to its cage for a 30-minute retention interval and returned to the testing area for a 5 minute testing phase, where one of the boxes was removed and replaced by a novel stimulus (orange). Cumulative time exploring each object was recorded and discrimination index (DI) was calculated. DI represents the ability to discriminate the novel from the familiar object and was calculated as follows:

$$DI = \frac{\text{Novel Object Exploration Time} - \text{Familiar Object Exploration Time}}{\text{Novel Object Exploration Time} + \text{Familiar Object Exploration Time}}$$

Learning criteria were considered when DI was above 0, and dichotomized version of the score was generated accordingly. ORT was performed in all animals with a successful OFBT test. Animals that did not explore the familiar object at least once in the testing phase or did not explore any of the objects in the familiarization phase were excluded from the analysis, as previously suggested (De Bie et al., 2011; Illa et al., 2013). ORT was performed successfully in 8 controls and 6 IUGR. Further details on the specifics of both tests can be consulted at Illa et al. (2013).

MRI acquisition

MRI was performed on fixed brains using a 7 T animal MRI scanner (BrukerBioSpin MRI GmbH). High-resolution three-dimensional T1 weighted images were obtained in the brain samples by a Modified Driven Equilibrium Fourier Transform (MDEFT) sequence with the following parameters: Time of Echo (TE) = 3.5 ms, Time of Repetition (TR) = 4000 ms, 0.7-mm slice thickness with no interslice gap, 70 coronal slices, in-plane acquisition matrix of 188 × 188 and Field of View (FoV) of 28 × 28 mm^2, resulting in a voxel dimension of 0.15 × 0.15 × 0.7 mm^3. Diffusion-weighted images (DWI) were acquired using a standard diffusion sequence covering 126 gradient directions with a b-value of 3000 s/mm^2 together with a reference (b = 0) image. Other experimental parameters were: TE = 26 ms, TR = 250 ms, slice thickness = 0.7 mm with no interslice gap, 70 coronal slices, in-plane acquisition matrix of 40 × 40, FoV of 28 × 28 mm^2, resulting in a voxel dimension of 0.7 × 0.7 × 0.7 mm^3. The total scan time for both acquisitions was 13 h 56 min 40 s. Any potential tissue alteration, mainly significant tissue loss, was considered as exclusion criteria, being one control of the total population excluded for this reason.

Pre-processing and tractography

Brain tissue was segmented from the background in the T1 volume by means of an Otsu threshold method (Otsu, 1975). In the case of DWI, brain tissue was segmented from the background by means of an in-house algorithm previously described (Eixarch et al., 2012) based on the high SNR of the brain tissue on the average diffusion volume. The orientation diffusion function (ODF) of each voxel was reconstructed by means of a Q-Ball approach (Tuch, 2004) and used to reconstruct fiber tracts by means of a deterministic tractography algorithm with an angle threshold of 30° implemented in Diffusion Toolkit (http://trackvis.org/dtk/) (Wang et al., 2007). Extracted brain volume size and number of fibers reconstructed for each subject were assessed.

Brain parcellation

Automatic brain parcellation of the subjects' brain was performed taking advantage of a recently published New Zealand Rabbit MRI atlas (Muñoz-Moreno et al., 2013) available online (http://medicinafetalbarcelona.org/rabbitbrainatlas). The parcellation was performed on the T1 volume of each subject by means of an elastic registration of the template atlas to each subject's brain performed with a customized software implementing a consistent version (Tristan-Vega and Arribas, 2007) of a block matching algorithm (Warfield et al., 2002). The elastic transformation obtained matching the template atlas and each subject's T1 was applied to the ROI labels, obtaining a parcellation of each brain in 60 ROIs. In order to align the labels obtained for each subject in the T1 volume to its corresponding DWI, affine registration (Studholme et al., 1999) between T1 and the baseline image was performed with IRTK (www.doc.ic.ac.uk/~dr/software/). Discrete values of the labels were preserved by nearest neighbor interpolation in both transformations. ROIs comprising only WM tissue were discarded, leaving a total of 44 regions for each subject (Table 1), each of which was considered as a node in the brain networks obtained.

Network extraction

Brain network of each subject was extracted by means of an in-house algorithm combining the fiber tracts obtained by Q-Ball tractography and the ROIs resulting from the automatic brain parcellation previously

Table 1
Regions of interest used as nodes in the structural brain networks obtained.

ID	Label	Name	ID	Label	Name
1	FCx-L	Frontal cortex left	23	Len-L	Lenticular nucleus left
2	FCx-R	Frontal cortex right	24	Len-R	Lenticular nucleus right
3	MFCx-L	Medial frontal cortex left	25	Th-L	Thalamus left
4	MFCx-R	Medial frontal cortex right	26	Th-R	Thalamus right
5	CiCx-L	Cingulate cortex left	27	Am-L	Amygdala left
6	CiCx-R	Cingulate cortex right	28	Am-R	Amygdala right
7	PiCx-L	Piriform cortex left	29	OlB-L	Olfactory bulb left
8	PiCx-R	Piriform cortex right	30	OlB-R	Olfactory bulb right
9	ECx-L	Entorhinal cortex left	31	Hc-L	Hippocampus left
10	ECx-R	Entorhinal cortex right	32	Hc-R	Hippocampus right
11	PaCx-L	Parietal cortex left	33	FB-L	Forebrain left
12	PaCx-R	Parietal cortex right	34	FB-R	Forebrain right
13	OcCx-L	Occipital cortex left	35	CeH-L	Cerebellar hemisphere left
14	OcCx-R	Occipital cortex right	36	CeH-R	Cerebellar hemisphere right
15	InCx-L	Insular cortex left	37	Ht	Hypothalamus
16	InCx-R	Insular cortex right	38	Ve	Vermis
17	TeCx-L	Temporal cortex left	39	BF	Basal forebrain
18	TeCx-R	Temporal cortex right	40	De	Diencephalon
19	Cl-L	Claustrum left	41	Me	Mesencephalon
20	Cl-R	Claustrum right	42	Po	Pons
21	Cau-L	Caudate nucleus left	43	MO	Medulla oblongata
22	Cau-R	Caudate nucleus right	44	Spt	Septal nuclei

performed. Two nodes (regions) i and j were considered to be connected by an edge e_{ij} when there existed at least one fiber bundle f with endpoints in i and j regions, with self-loops excluded. In addition to the binary network produced with this approach, weights were also assigned to each edge e_{ij}. There is still not a gold standard in the literature to assign connectivity weight between two regions, hence, two of the most used approaches in the literature were followed to weight the connectivity between each pair of regions, w_{GFA}, average generalized fractional anisotropy (GFA) along all the fibers connecting a pair of regions; and w_{FD}, fiber density (FD) as defined by Hagmann et al. (2008) with slight modifications: $w_{FD}(i,j) = \frac{2}{V_i+V_j} \sum_{f \in F_{ij}} 1/l(f)$; where $w_{FD}(i,j)$ is the FD-weight given to the connection between nodes i and j, V_i is the volume of the ROI i, F_{ij} is the set of all fibers connecting ROIs i and j, and l(f) is the length of fiber f along its trajectory, introduced in the denominator to eliminate the linear bias towards longer fibers introduced by the tractography algorithm. In addition, the resulting weighted networks were normalized by the total weight of all the connections in the network, to assess the brain organization independently of the network average strength.

In summary, five networks were extracted for each subject: binary, GFA-weighted, FD-Weighted, normalized GFA-weighted and normalized FD-weighted.

Network analysis

Network analysis by means of graph theory allows obtaining a set of features that summarize the organization of a brain network, represented as an adjacency matrix (binary or weighted). In the present study, we applied graph theory features over each of the five brain network classes computed for each subject. All the features were computed using Brain Connectivity Toolbox (Rubinov and Sporns, 2009).

Global functioning of each network was assessed by its infrastructure (average degree for binary networks and average strength for weighted networks), integration (binary and weighted global efficiency) and segregation (binary and weighted local efficiency). In addition, binary and weighted characteristic path lengths and average clustering coefficient were also assessed.

Regional characteristics were evaluated by means of nodal degree and strength, features that assess the total connectivity of a node in a network in its binary and weighted versions respectively. In addition, nodal efficiency was also assessed in its binary and weighted version. Nodal efficiency measures the efficiency of the sub-network associated with a given node. Nodes with a high nodal efficiency indicate a high fault tolerance of the network to the elimination of the given node, which is given by a high clustering of the neighborhood of this node (Achard and Bullmore, 2007).

In order to assess the small-world behavior of the computed networks (Watts and Strogatz, 1998), binary characteristic path length (L_p) and binary clustering coefficient (C_p) were compared with the average characteristic path length and clustering coefficient of one hundred equivalent random networks with the same size and degree distribution of each subject's network. The ratio of the values obtained for the original subject network and its equivalent random version allowed obtaining the normalized values $\lambda = L_p/L_p^{rand}$, $\gamma = C_p/C_p^{rand}$, and $\sigma = \gamma/\lambda$. Small-worldness value (σ) is above 1 in small-world regimes (Humphries and Gurney, 2008).

Formulation of the graph theory features used to assess each network is based on the definitions compiled by Rubinov and Sporns (2009).

Levels of analysis: raw, cost-corrected, cost-integrated and normalized strength

We analyzed the obtained networks with different approaches in order to catch different aspects of their organization. The first straightforward approach is to directly apply binary and weighted graph theory measures to the raw binary, GFA- and FD-weighted networks obtained for each subject. However, some of these measures could be closely associated with the measured infrastructure of the network, i.e., their average network strength and degree (Ginestet et al., 2011; van Wijk et al., 2010). In order to assess organization independently from network density (i.e., average network degree), a cost-thresholding approach was followed (Achard and Bullmore, 2007) obtaining binary networks for a set of costs in the rank from 0 to 0.39 at 0.01 steps, using GFA- and FD-weighted networks to select the "strongest" connections that yield a network with the desired network cost for each subject. 0.39 is the smallest network density value of any subject included in the study, hence being the largest network density value that is possible to study for all subjects fairly. This approach allows comparing network features independently of differences in the raw number of connections (cost) between subjects. However, it increases the number of comparisons and the complexity of the result interpretation. In order to disentangle network density from topology in a single value for each graph theory feature, a cost-integrated version of each topological version was calculated as the mean value across the assessed rank. In addition, this cost-correction approach has an additional shortcoming that in fact leads to different connections sets across subjects. In order to assess the behavior of the networks using the same set of connections for all the subjects, an experimental approach is used in the Supplementary materials inspired by the methodology used by Gong et al. (2009b).

With the goal to assess the pure weighted organizational characteristic of the network topology, normalized weighted networks were also calculated for each subject in their GFA and FD versions. This normalization was performed by means of dividing each connection weight by the total weight on the network. Hence, normalized weights were calculated as $w_X^N(i,j) = w_X(i,j)/\sum_{\forall i,j} w_X(i,j)$, where "X" is GFA or FD. By this means, each normalized weight $w_{GFA}^N(i,j)$ and $w_{FD}^N(i,j)$ corresponds to the percentage of connection weight used in the link between i and j relative to the total amount of weights in the network. This way the measures performed on normalized GFA- and FD-weighted networks were independent to the total amount of connectivity strength each subject had, and then assessing only its distribution of weights.

Statistics

Comparisons among groups were performed by general linear models (GLM) with gender as co-factor. Interaction of group and gender was first included into the model, but as it did not show any significant effect it was excluded from the final model. Significance was declared at $p < 0.05$ (uncorrected). Normality was assessed with Shapiro–Wilk Test and homoscedasticity with Levene's Test, and when the null hypothesis was rejected, log-transformation was performed prior to GLM analysis. Descriptives of the variables were expressed as mean (standard deviation) for normal distributions and median (interquartile range) for non-normal distributions. Differences between cases and controls of dichotomized values of OFBT and ORT were assessed with a binary logistic regression with group and gender as co-factors. Association of network features with OFBT and ORT was performed by means of a partial correlation controlling the effect of gender. Association with dichotomized OFBT and ORT was performed by a GLM with gender as co-factor. The most discriminative network features of dichotomized OFBT and ORT were assessed by means of a conditional step forward binary logistic regression with an entry probability of 5%. Note that the population available with OFBT and ORT was 19 subjects (10 controls and 9 IUGR) and 14 subjects (8 controls and 6 IUGR) respectively. Regional features were corrected for multiple comparisons with a False Discovery Rate (FDR) approach (Benjamini et al., 2006), controlling alpha error to 10% and 5% for each feature calculated among all 44 regions. Regional alterations were shown in the rabbit brain atlas template using BrainNet

Please cite this article as: Batalle, D., et al., Long-term reorganization of structural brain networks in a rabbit model of intrauterine growth restriction, NeuroImage (2014), http://dx.doi.org/10.1016/j.neuroimage.2014.05.065

viewer (www.nitrc.org/projects/bnv/) (Xia et al., 2013). The software package SPSS 18.0 (SPSS, Chicago, IL) was used for the statistical analyses. Computational algorithms were implemented using MATLAB (2009b, The MathWorks Inc., Natick, MA).

Results

Population

After applying the exclusion criteria, the final population under study consisted of 14 controls and 15 subjects with induced IUGR. As expected, birth weight in IUGR subjects was significantly decreased (controls vs. IUGR: 47.7 g (IQR 7.7 g) vs. 37.4 g (IQR 10.1 g), $p < 0.001$) (controls vs. IUGR: 50.2 g (SD 7.3 g) vs. 38.8 g (SD 6.5 g), $p < 0.001$), however, at 70 days of life the difference in weight disappeared (controls vs. IUGR: 2850 g (IQR 400 g) vs. 2700 g (IQR 675 g), $p = 0.423$) (controls vs. IUGR: 2744 g (SD 438 g) vs. 2596 g (SD 635 g), $p = 0.485$). Concerning brain volume at 70 days, there was not a statistical difference between cases and controls (controls vs. IUGR: 9467 mm^3 (SD 449 mm^3) vs. 9308 mm^3 (SD 615 mm^3), $p = 0.450$), neither concerning the total amount of fibers reconstructed by the tractography algorithm (controls vs. IUGR: 34493 (SD 1595) vs. 33800 (SD 2328), $p = 0.371$). The distribution of gender was also not significantly different between cases (8 males/7 females) and controls (7 males/7 females).

Concerning functional exploration, results showed similar results to those obtained in a very similar sample (Illa et al., 2013). In OFBT, IUGR showed a decreased number of internal boxes crossed (controls vs. IUGR: 9.2 (SD 4.8) vs. 3.7 (SD 3.2), $p = 0.011$), and increased latency (controls vs. IUGR: 2.5 s (IQR 17 s) vs. 52 s (IQR 241 s), $p = 0.042$). Total boxes crossed (controls vs. IUGR: 103.1 (SD 35.6) vs. 73.1 (SD 36.5), $p = 0.105$) and external boxes crossed (controls vs. IUGR: 97.2 (SD 36.7) vs. 69.4 (SD 34.7), $p = 0.120$) did not show statistically significant differences between groups. In ORT, reduced discriminatory index was found in IUGR group (controls vs. IUGR: 0.30 (SD 0.24) vs. −0.25 (SD 0.46), $p = 0.016$). Similarly, binary logistic regression of dichotomized values of OFBT with gender as a co-factor showed a significantly increased percentage of abnormal values in IUGR (controls vs. IUGR: 20.0% vs. 77.8%, $p = 0.021$) and a tendency in dichotomized ORT (controls vs. IUGR: 12.5% vs. 66.7%, $p = 0.059$). In summary, these results showed that IUGR rabbits have a significant degree of anxiety, attention and memory problems when compared to controls.

Global network features

As shown in Fig. 2, the analysis of the basic infrastructure of the network showed a decreased average degree ($p = 0.039$) in IUGR cases. The analysis of the average strength of the weighted networks did not show any significant effect, although a tendency towards significance is found in FD-weighted average strength ($p = 0.084$).

Analysis of small-world characteristics (Fig. 3) showed that both cases and controls have a small-worldness σ value higher than one for all subjects, a typical characteristic of small-world networks, however, no significant differences were found between cases and controls.

The assessment of brain network organization by means of the analysis of global and local efficiencies (Fig. 4) demonstrated several differences between controls and IUGR. Having a significantly reduced average degree it is expectable to find that IUGR also had a reduced binary global efficiency ($p = 0.041$). The IUGR group did not show significant differences in any weighted measure of efficiency, however, the analysis of normalized brain networks, independent of differences in the average strength of each subject, showed that the IUGR group had a significantly increased normalized GFA-weighted global efficiency ($p = 0.018$), normalized GFA-weighted local efficiency ($p = 0.039$) and normalized FD-weighted local efficiency ($p = 0.010$). Note that while FD indirectly measures the axonal density connecting two regions, GFA measures have been related to the integrity of these axonal connections. These results were also confirmed when looking directly into normalized characteristic path length and average clustering coefficient (Supplementary material). Finally, when forcing all the subjects' networks to have the same density (cost-corrected approach), differences between cases and controls were found for several cost values in GFA-weighted global efficiency and FD-weighted local efficiency (Fig. 5) and GFA cost-integrated measure of global efficiency was found to have a tendency of being increased in IUGR ($p = 0.070$). Overall, global network features obtained suggested an altered brain

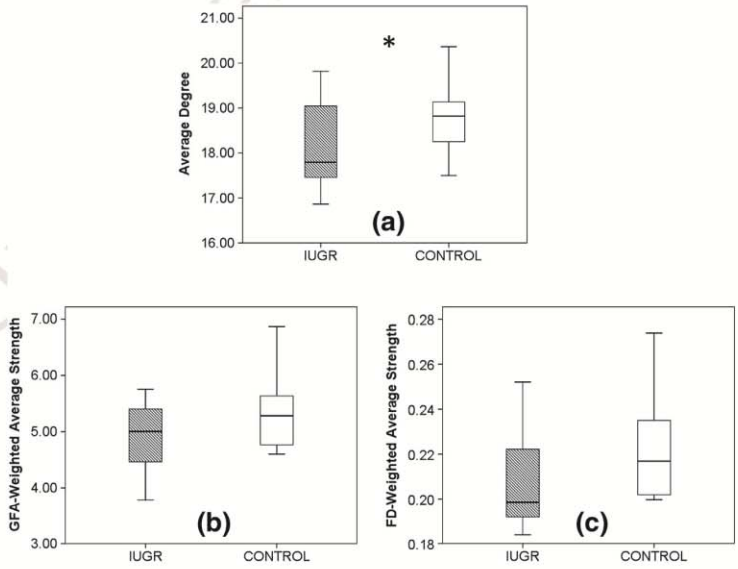

Fig. 2. Basic infrastructure of the brain networks obtained compared between controls and IUGR, including average degree (a), GFA-weighted average strength (b) and FD-weighted average strength (c). *$p < 0.05$.

Please cite this article as: Batalle, D., et al., Long-term reorganization of structural brain networks in a rabbit model of intrauterine growth restriction, NeuroImage (2014), http://dx.doi.org/10.1016/j.neuroimage.2014.05.065

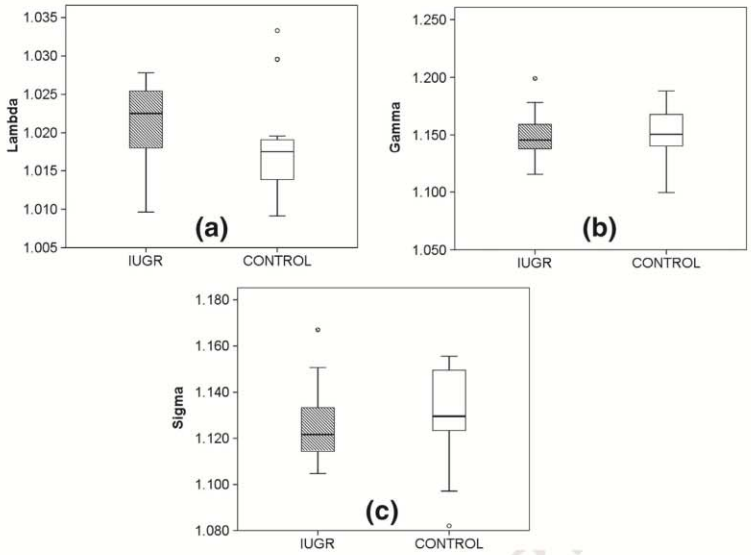

Fig. 3. Small-world characteristics of controls and IUGR obtained from comparison with random equivalent networks. Lambda (a) is the normalized path length, gamma (b) is the normalized average clustering coefficient and sigma (c) is the small-worldness parameter, obtained as the ratio of gamma to lambda.

network organization characterized by a reduced level of network connectivity and a compensatory effect after assessing pure organizational features by means of different normalization approaches. Although a compensatory effect in local efficiency was observed with both GFA and FD weighting approaches, statistically increased global efficiency was only observed for GFA-weights.

Regional network features

The analysis of regional network features showed a pattern of alterations in IUGR group (Fig. 6, Inline Supplementary Table S1). Particularly, IUGR is characterized by a significantly lower nodal degree in several brain regions, although vermis is the only region withstanding a 5% FDR correction. Interestingly, right cingulate cortex, lenticular nucleus and vermis also showed a significantly decreased GFA-weighted strength, both in absolute and relative terms (normalized), vermis also resisting a 5% FDR correction. In line with the results obtained for global network features, regions with a higher degree or strength in IUGR group were only found in relative terms.

Concerning binary nodal efficiency, IUGR showed a significant decrease in right parietal cortex and right frontal cortex, but an increase in vermis. FD-weighted network efficiency also showed a significant increase in the left cerebellar hemisphere and vermis. In line with the significant increase found in global normalized weighted features, IUGR showed a wide pattern of regions with a significantly increased normalized efficiency, including basal forebrain, piriform cortex, cerebellar hemisphere and amygdala in normalized GFA-weighted networks (right piriform cortex and cerebellar hemisphere withstanding a FDR correction at 10%). Efficiencies of mesencephalon, pons, right parietal and cingulate cortex, hippocampus, cerebellar hemisphere and vermis were also increased in normalized FD-weighted networks; with the left cerebellar hemisphere resisting a 10% FDR correction and vermis resisting a 5% FDR correction.

In summary, IUGR mainly showed a pattern of decreased features in raw networks, especially in binary nodal efficiency and degree and GFA-weighted strength, and a pattern of increased features in normalized GFA- and FD-weighted networks, especially in nodal efficiency.

Inline Supplementary Table S1 can be found online at http://dx.doi.org/10.1016/j.neuroimage.2014.05.065.

Association of network characteristics with altered neurobehavior

The analysis of dichotomized OFBT normal/abnormal status with GLM showed significantly decreased GFA-weighted average strength ($p = 0.039$), GFA-weighted global efficiency ($p = 0.035$) and GFA-weighted local efficiency ($p = 0.017$) in the abnormal group. A tendency to have increased normalized FD-weighted global efficiency ($p = 0.058$) and cost-integrated GFA global efficiency ($p = 0.083$) was also found in the group with an abnormal exploration. Analysis of ORT normal/abnormal exploration showed only significantly increased cost-integrated GFA global efficiency ($p = 0.007$) in the abnormal group.

The association with normal/abnormal exploration in OFBT and ORT was confirmed by partial correlation of OFBT continuous values and global features (Inline Supplementary Table S2). Briefly, OFBT scores showed significant correlations with several GFA-weighted measures (average strength, characteristic path length, average clustering, global efficiency and local efficiency) and with normalized FD-weighted global efficiency. ORT, however, only showed some tendencies towards significance with GFA-weighted clustering coefficient and GFA cost-integrated local efficiency. Interestingly, the results showed that for all significant correlations, and for those showing a tendency towards significance, absolute GFA-weighted measures had a significant correlation with neurobehavioral scores in the opposite direction of cost-integrated and normalized measures.

Inline Supplementary Table S2 can be found online at http://dx.doi.org/10.1016/j.neuroimage.2014.05.065.

Regional features associated with abnormal neurobehavior were assessed by means of a GLM with dichotomized OFBT/ORT and gender as co-factor (Fig. 7). The results showed a significant association of several regional features with neurobehavioral tests. As it could be expected from the strong association with global GFA-weighted network features, abnormal OFBT exploration was associated with a wide rank of GFA-weighted nodal measures, particularly with nodal efficiency features. The association of regional features with abnormal ORT was not so spread, but some consistent patterns of alterations across different kinds of networks were also observed, as it is the case of right thalamus and right caudate nodal strength and efficiency features.

Further analysis to find the network features with a higher potential as an image biomarker of altered neurodevelopment was performed by

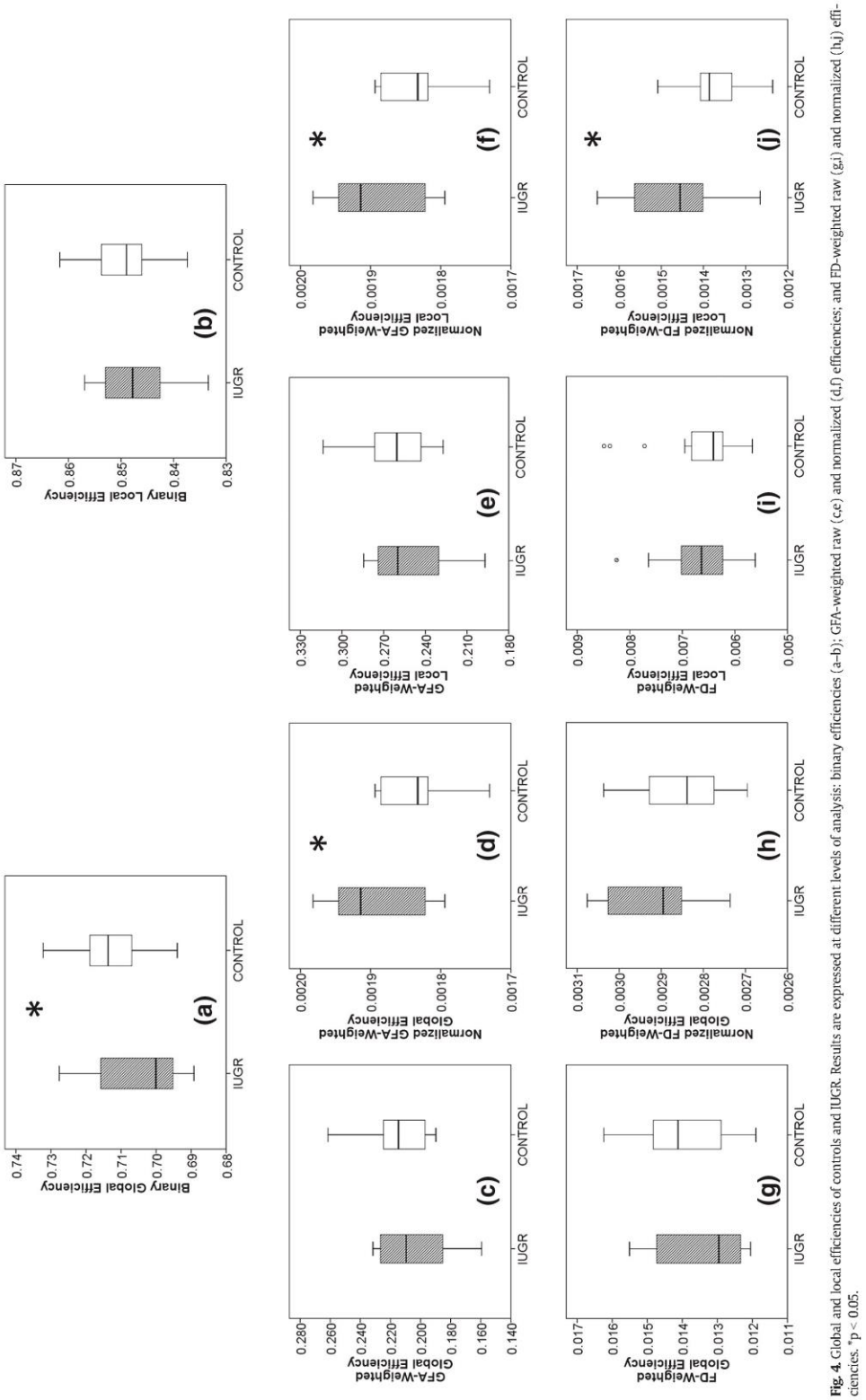

Fig. 4. Global and local efficiencies of controls and IUGR. Results are expressed at different levels of analysis: binary efficiencies (a–b); GFA-weighted raw (c,e) and normalized (d,f) efficiencies; and FD-weighted raw (g,i) and normalized (h,j) efficiencies. *$p < 0.05$.

Please cite this article as: Batalle, D., et al., Long-term reorganization of structural brain networks in a rabbit model of intrauterine growth restriction, NeuroImage (2014), http://dx.doi.org/10.1016/j.neuroimage.2014.05.065

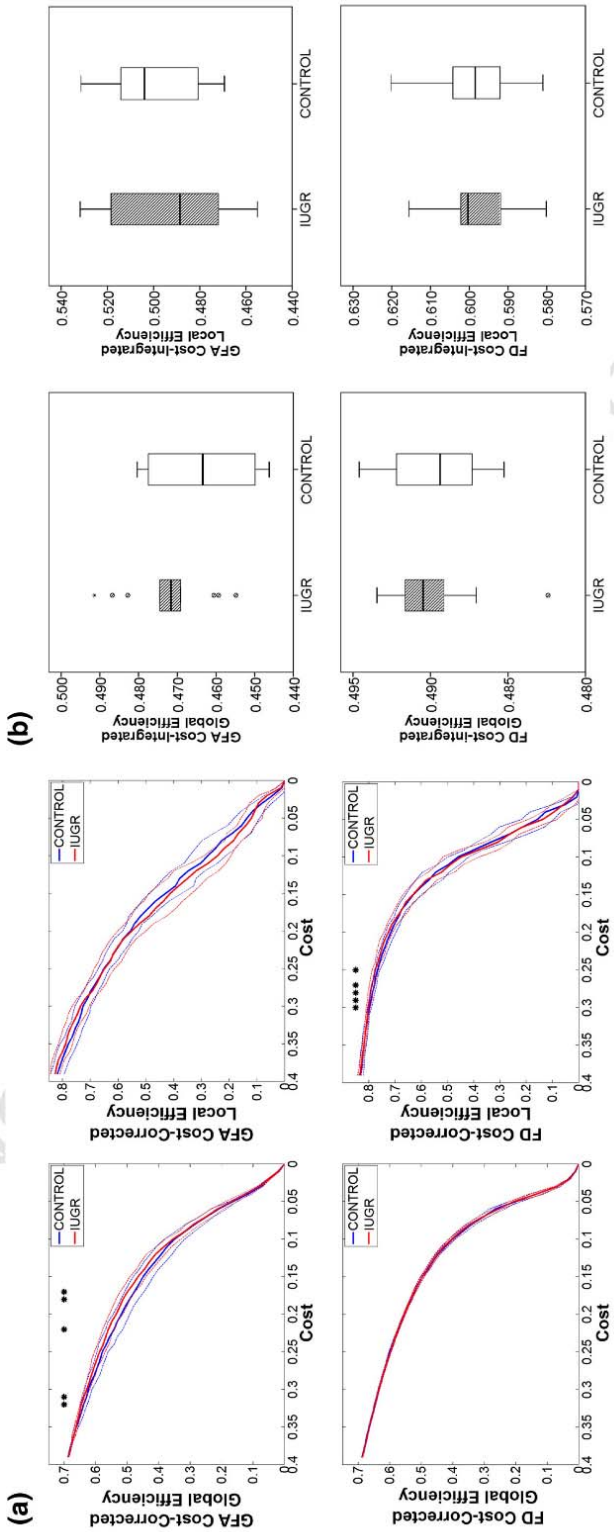

Fig. 5. Cost-corrected (a) and cost-integrated (b) global and local efficiencies compared between controls and IUGR. *$p < 0.05$.

Please cite this article as: Batalle, D., et al., Long-term reorganization of structural brain networks in a rabbit model of intrauterine growth restriction, NeuroImage (2014), http://dx.doi.org/10.1016/j.neuroimage.2014.05.065

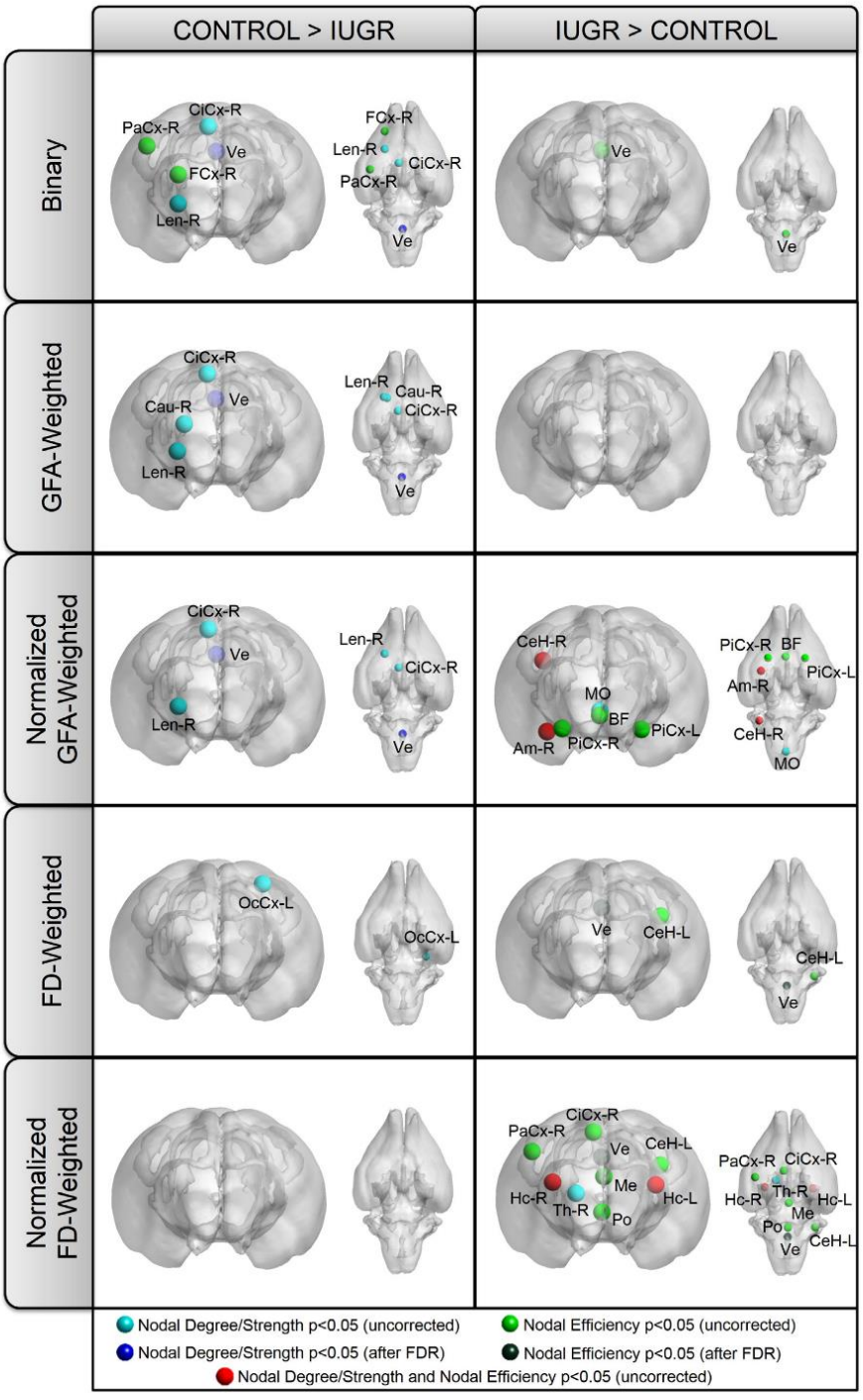

Fig. 6. Pattern of regional network features altered in IUGR group. Significance was declared at $p < 0.05$ (uncorrected). Those regions withstanding a False Discovery Rate (FDR) controlling alpha error to 5% were indicated with dark blue (nodal degree/strength) and dark green (nodal efficiency).

means of a step forward binary logistic regression. All the assessed global network features were entered in a first analysis, selecting GFA-weighted local efficiency as the more discriminative in OFBT (90% sensitivity, 66.7% specificity, Nagelkerke $R^2 = 0.335$, $Chi^2 = 5.494$, $p = 0.019$). The most discriminative global feature in ORT was cost-integrated global efficiency (88.9% sensitivity, 80% specificity,

Please cite this article as: Batalle, D., et al., Long-term reorganization of structural brain networks in a rabbit model of intrauterine growth restriction, NeuroImage (2014), http://dx.doi.org/10.1016/j.neuroimage.2014.05.065

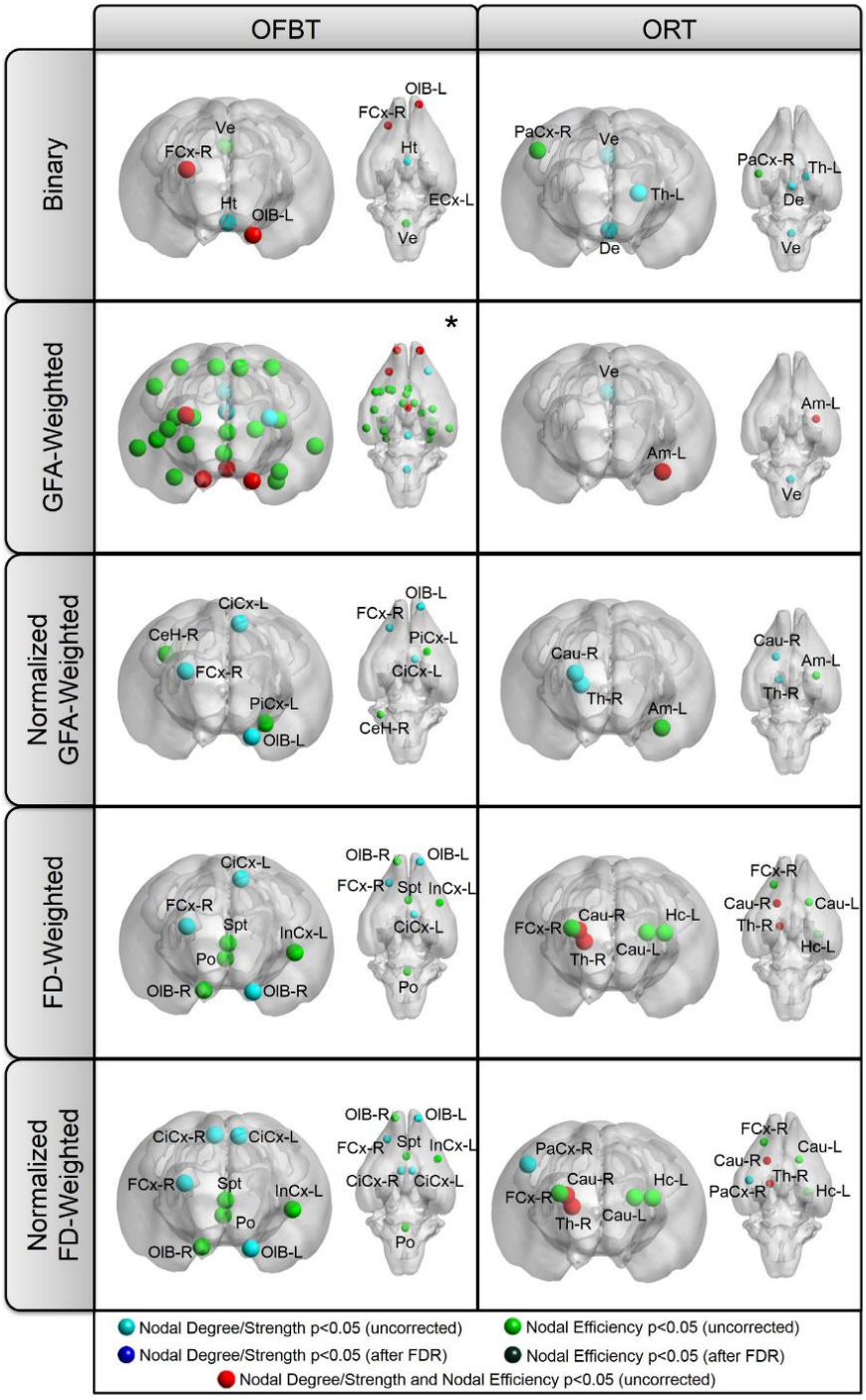

Fig. 7. Pattern of regional network features associated with abnormal Open Field Behavioral Test (OFBT) and Object Recognition Task (ORT). Significance was declared at $p < 0.05$ (uncorrected). Those regions withstanding a False Discovery Rate (FDR) controlling alpha error to 5% were indicated with dark blue (nodal degree/strength) and dark green (nodal efficiency). *GFA-weighted nodal features associated with OFBT included nodal efficiency of right frontal cortex, right and left cingulate cortex, right and left entorhinal cortex, right parietal cortex, right and left occipital cortex, right insular cortex, right and left temporal cortex, right claustrum, right caudate nucleus, right lenticular nucleus, left thalamus, left amygdala, right and left olfactory bulb, right and left hippocampus, hypothalamus, basal forebrain and septum; and nodal strength of right and left frontal cortex, right and left olfactory bulb, hypothalamus, vermis and mesencephalon.

Please cite this article as: Batalle, D., et al., Long-term reorganization of structural brain networks in a rabbit model of intrauterine growth restriction, NeuroImage (2014), http://dx.doi.org/10.1016/j.neuroimage.2014.05.065

Nagelkerke R2 = 0.623, Chi^2 = 8.467, p = 0.004), selecting also normalized FD-weighted local efficiency which allowed a full separation of normal/abnormal ORT (Chi^2 = 18.249, p < 0.001). In a second analysis, all the assessed regional network features were introduced. Regional features more discriminative of OFBT were GFA-weighted right insular cortex strength and normalized FD-weighted septal nuclei nodal efficiency (90% sensitivity, 89.5% specificity, Nagelkerke R^2 = 0.939, Chi^2 = 23.101, p < 0.001). In the case of ORT, the most discriminant regional network feature was normalized FD-weighted nodal strength of right thalamus, which also fully separated by itself normal/abnormal ORT (Chi^2 = 18.249, p < 0.001).

Discussion

This study describes the use of diffusion MRI brain networks to analyze the brain reorganization in a rabbit model of IUGR at 70 days of age, equivalent to pre-adolescence in humans. The results show that IUGR brain reorganization persists into pre-adolescence equivalent age with significant differences at various levels in network infrastructure. GFA-weighted features and regional network features were associated with poor neurobehavioral performance. Furthermore, the increased efficiency of normalized GFA-weighted networks associated with IUGR suggests the existence of reorganizational compensatory processes in postnatal life.

Global network features

Comparison of the brain networks obtained with random equivalent networks showed small-world characteristics. This result is coherent with previously found in humans, animals and a wide range of networks (Bullmore and Sporns, 2009). Small-world networks are suggested to be a balance between random and lattice networks, having a high level of organization but also allowing to communicate any given pair of nodes with relatively few intermediate steps. No differences in small-world features were found in IUGR, but the analysis of other global network features showed a pattern of brain reorganization persisting at preadolescent equivalent age. Particularly, reduced average degree is found in IUGR, supporting the idea that IUGR have an impaired network infrastructure. As expected, having a reduced network infrastructure may be producing a dysfunctional connectivity, expressed by a reduced binary global efficiency. Supporting this concept, we observed also a trend of IUGR to have reduced FD-weighted average strength. Note that strength can be understood as the total power of brain connections between regions. However, although having a less connected brain network, GFA- and FD-weighted efficiencies were not found significantly decreased in IUGR. Broadly, global efficiency assess how easy is on average to connect a pair of regions, while local efficiency has been related with the level of clusterization of the network. The results obtained in raw GFA-weighted efficiencies are in contraposition with previous findings suggesting significantly reduced fractional anisotropy (FA) weighted global and local efficiency found at one year of age in human IUGR (Batalle et al., 2012). One possible explanation could be related with changes in postnatal brain maturation after IUGR. Previous studies have reported that there is a compensation in the long-term myelination and WM volume in a guinea pig model of IUGR (Tolcos et al., 2011). In this line, previous studies assessing WM alterations in a rabbit animal model of IUGR using voxel-based analysis have reported a less prominent pattern of alterations in pre-adolescence age (Illa et al., 2013) than in neonatal age (Eixarch et al., 2012). On the other hand, in this study we could not reproduce previous observations in one-year-old infants' networks showing reduced average degree in IUGR subjects (Batalle et al., 2012). We hypothesize that this apparent discrepancy could be explained by evolutionary changes of brain network reorganization associated with IUGR at different ages. Alternatively, we cannot exclude that this effect could be specific of IUGR in this rabbit animal model.

An interesting finding of this study was the observation of increased efficiencies in the normalized networks of IUGR compared with controls. Consistent with this finding, the evolution of graph theory measures in a cost-thresholding approach showed a discordant pattern in IUGR, particularly an increased FD local efficiency and an increased GFA global efficiency for several network costs. We hypothesize that this effect might reflect a compensatory mechanism in IUGR subjects, whereby available network resources seem to be optimized and reorganized more efficiently from a network perspective. This compensatory effect in brain connectivity could also explain some other intuitively non-expected findings in IUGR in the long-term, such as the reported, regional cortical thickening in small for gestational age children (De Bie et al., 2011; Martinussen et al., 2005).

Regional network features

Concerning regional differences found in IUGR, only vermis features withstood a FDR correction at 5%, while only features of cerebellar hemispheres and piriform cortex withstood a FDR correction at 10% (Inline Supplementary Table S1). Particularly, degree and normalized GFA-weighted strength of vermis were significantly reduced in IUGR, and nodal efficiency of both raw and normalized FD-weighted vermis were significantly increased in IUGR. We could interpret that IUGR subjects have a vermis with reduced neighborhood but with a stronger connectivity (higher clustering). Again, this would support the hypothesis of a compensatory effect and goes in line with the results obtained on global network features. Interestingly, alterations in cerebellum and vermis connectivity in infants with IUGR have previously been reported by network analysis (Batalle et al., 2012, 2013), as well as reduced WM volumes in cerebellar areas in short- (Padilla et al., 2011) and long-term follow-up studies (De Bie et al., 2011; Martinussen et al., 2009). Interestingly, cerebellar areas are implicated in motor learning, memory, cognition and behavior (Baillieux et al., 2008), and have been reported to increase their volume in infants with IUGR after intervention by means of individualized intensive care nursery associated with an improvement in executive function (McAnulty et al., 2013). Considering other animal models of IUGR, in guinea pig it also has been reported a reduction in cerebellar WM volume (Tolcos et al., 2011), and a reduction in Purkinje neuronal population (Mallard et al., 2000). However, we must note that in previous voxel-based analysis studies in IUGR rabbit model (Eixarch et al., 2012; Illa et al., 2013) we only observed mild differences in cerebellar areas. We hypothesize that this could be partially explained by stronger alterations in the sub-network associated with cerebellum (described by network features), than in the structure of cerebellum by itself. Another factor that could explain this discrepancy can be the technical characteristics of voxel-based analysis technique, especially in cerebellar areas, where the limited resolution is especially critical for cerebellar WM.

Beside those associated with cerebellar areas, other regional features were also significantly different in IUGR, although only normalized FD-weighted efficiency of right piriform cortex withstood a 10% FDR correction. It seems interesting that regional features of normalized networks were found significantly increased in IUGR mainly in specific basal and deep gray matter areas, such as amygdala, hippocampus, thalamus, medulla oblongata, and some of the cortical areas controlling essential functions for the rabbit, as is the case of piriform cortex, which has been strongly associated with the smelling processing (Kadohisa and Wilson, 2006). One possible interpretation of these results could be that a compensatory reorganization in IUGR brain might occur preferentially in brain areas regulating function with critical importance in survival, such as memory, attention or smelling processing. Considering other features that did not withstood FDR correction, we must note that the regional features altered in IUGR were coherent with the global results obtained, mainly showing reduced values in binary and raw GFA-weighted measures (especially in degree/strength) and increased values in normalized measures (especially in efficiency). Interestingly,

Please cite this article as: Batalle, D., et al., Long-term reorganization of structural brain networks in a rabbit model of intrauterine growth restriction, NeuroImage (2014), http://dx.doi.org/10.1016/j.neuroimage.2014.05.065

changes in regional features of raw networks were manly identified in brain regions located in the right hemisphere of the brain, suggesting a certain asymmetry in the reorganization associated with IUGR. Reports on asymmetrical brain alterations produced by IUGR are scarce in the literature, and further long-term studies in humans would be required to confirm this effect and discard that is exclusive to animal models. Another interesting finding was left cingulate cortex and right lenticular nucleus decreased nodal degree and relative and absolute GFA-weighted nodal strength. Cingulate cortex features were also correlated with OFBT performance, which is in line with previous results in a similar sample of IUGR rabbit model, where FA changes in the cingulate cortex were found to be correlated to a series of neurobehavioral domains, especially those of OFBT (Illa et al., 2013). Note that cingulate cortex has been strongly associated with anxiety processes (Kim and Whalen, 2009), which is thought to have an important role on the behavioral response in OFBT. In addition, cingulate cortex volumetric differences in humans (Emond et al., 2009; Spampinato et al., 2009) as well as histological changes in rodents (Miller et al., 2012) have been associated with traits of attention deficit and anxiety. Concerning the alterations in lenticular nucleus, FA changes have been previously reported in the putamen of neonatal (Eixarch et al., 2012) and long-term rabbit model of IUGR (Illa et al., 2013), as well as disrupted regional network features associated with putamen and globus pallidum in 1-year-old infants (Batalle et al., 2012). Moreover, features associated with other subcortical GM nuclei including caudate and thalamus were also found affected in IUGR rabbits in this study. These findings are in line with previous evidence suggesting the important role of striatal injury as a risk factor of behavioral disturbances associated with IUGR (Toft, 1999), and alterations in cortico-striato-thalamic network has been associated with cognitive disorders such as attention deficit hyperactivity disorder (Castellanos et al., 1994; Faraone and Biederman, 1998), which in turn is more prevalent in IUGR (Heinonen et al., 2010). Concerning the specific associations with OFBT and ORT by means of a step forward binary logistic regression, features of insular cortex and septal nuclei were found strongly associated with OFBT and features of thalamus with ORT. Septal nuclei participation in the regulation of anxiety and depression in experimental models has been extensively documented (Estrada-Camarena et al., 2002), as well as insular cortex, which has been proposed to have a key role in anxiety proneness (Paulus and Stein, 2006). Importantly, thalamus has been previously associated with memory impairments in animal models (Mitchell and Dalrymple-Alford, 2005) and with poor performance in object recognition tasks in patients with schizophrenia (Heckers et al., 2000), disorder that has also been associated with low birth weight (Nilsson et al., 2005).

In summary, a pattern of regional network features altered in IUGR were identified, some of them being specifically associated with abnormal neurobehavior. Noteworthy, alterations in network features of cerebellum stand out as the more strongly associated with IUGR condition, and septal nuclei, insular cortex and thalamus with poor performance in neurobehavioral tests. These results, and its association with previous literature, reinforce the potential of network features based on these regions to be used as biomarkers of altered neurodevelopment.

Methodological issues and future work

Although the study of brain networks in animal models has been seminal to the field (Sporns et al., 2005), brain networks obtained from diffusion MRI in small animals are scarce. To the best of our knowledge, this is the second study of this kind in small mammals (Iturria-Medina et al., 2011), and the first showing brain networks in rabbits. This animal model has some specific methodological difficulties that had to be overcome. The recent successful development of an MRI atlas for the rabbit brain (Muñoz-Moreno et al., 2013), allowed for automatically segmenting and analyzing brain networks from this model. It is common in human studies to confine deterministic tractography only to WM tissue. However, due to the difficulty of properly defining a WM mask in rabbits, the deterministic tractography was computed for the whole brain. This could create some redundant fibers, and increase tractography noise, but it was partially overcome by the use of a high angular resolution diffusion MRI acquisition, and the use of graph theory, particularly weighted measures, to analyze the results obtained. This limitation also ramifies in the calculation of FD-weighted networks. Instead of the formulation proposed by Hagmann et al. (2008) to calculate FD between two regions (using the surface of the WM-GM interface of the regions involved in a given link in the denominator), we modified this formula introducing the volume of each region instead of the surface of the WM–GM interface. In addition to specific limitations of the rabbit model, some others common to the study of brain networks must be discussed. Using weighted measures of the brain networks obtained has a series of advantages, including a better management of weak and potentially non-significant links (Rubinov and Sporns, 2009); however, how the connectivity between regions must be quantified and its correlation with the underlying anatomical substrate is still an open question that has been approached in very different ways (Griffa et al., 2013). To this regard, instead of selecting a single approach, we decided to use two very different ways of quantifying the weight of brain connectivity: average GFA along the fibers, and fiber density between regions; characterizing different aspects of connectivity that we expected to be complementary. Furthermore, we also computed normalized versions of the networks, allowing disentangling the measures obtained from the variability of absolute weighted strength of each individual network. Notwithstanding this, connectivity could still be dependent to some extent to the variability in network density (average degree). To obtain measures independent of network density, analyzing the evolution of a brain network across a set of network costs is a common approach, although part of the intrinsic connectivity patterns of a network are lost by forcing all the subjects to have the same network density. This issue is especially important when isolated nodes in the network of subjects start appearing at some levels of cost. Although the effect of isolated nodes is partially mitigated by the use of efficiency network features instead of characteristic path length and clustering coefficient measures (Rubinov and Sporns, 2009), brain networks with isolated nodes seem to be biologically implausible. Note that to address this issue some authors decide to restrict the range of network costs assessed in order to ensure fully connected networks without isolated nodes (Bassett et al., 2008). However, we decided to report the whole range of comparable network costs, given that even if this may lead to implausible brain networks at certain costs, the evolution of efficiencies in restrictive network costs is still giving relevant useful information about the weighted topology of the networks under study, directly associated with the backbone structure of each subject brain network. It is also important to note that although different normalization approaches might be capturing different aspects of brain network organization, compensatory effects found in normalized weighted networks (increased global and local efficiencies in IUGR group) were confirmed by the cost-corrected approach, hence minimizing the chance of the reorganizational patterns being dependent of the variability in network density. In addition, we acknowledge that in order to support some of the results, especially the compensatory effect found after normalization of brain networks, it would be very advisable to report the evolution of the network features at previous ages, being of special interest the neonatal period. If the rabbit MRI atlas is successfully adapted to neonatal age, research on the brain networks of neonatal population of IUGR rabbit model will be the likely focus of future studies. Finally, we acknowledge that the relatively reduced sample size used might be reducing the statistical power of the comparisons between cases and controls, preventing to generalize some of the findings obtained, especially concerning regional characteristics that did not withstand a FDR correction.

Finally, we would like to stress the opportunity that represents the study of different neurological conditions with brain networks from

Please cite this article as: Batalle, D., et al., Long-term reorganization of structural brain networks in a rabbit model of intrauterine growth restriction, NeuroImage (2014), http://dx.doi.org/10.1016/j.neuroimage.2014.05.065

animal models. In the specific case of IUGR, animal models are crucial not only to the better characterization of the pathophysiology of the condition, which is intrinsically difficult to assess, but also to the development of reliable image biomarkers of altered neurodevelopment. Hence, the application of brain networks in animal models might allow assessing and monitoring changes after possible interventions consisting of experimental drugs or enriched environment, in line with the recent reports showing that IUGR long-term prognosis significantly improves after intensive care nursing (McAnulty et al., 2013). Further work will involve the deeper characterization of changes in brain network organization by means of the analysis of differences in individual links between regions (Meskaldji et al., 2011; Zalesky et al., 2010), the study of the predictive power of network features using machine learning, and the assessment of the results in long-term effects produced by IUGR in humans.

Conclusions

The evidences presented here support the hypothesis that previously described neurodevelopmental changes produced by IUGR in the long-term could be associated with underlying brain reorganization. This reorganization was characterized by an impaired network infrastructure, which was accompanied by an increase of the relative organization of GFA- and FD-weighted networks. In addition, a pattern of altered regional features was identified, among which changes in cerebellar areas stand out. Furthermore, global and regional network features were associated with behavioral and cognitive tests especially designed for a rabbit model. We hypothesize that IUGR at long-term might result in compensatory effects to deal with an impaired network. The results obtained open the opportunity of developing imaging biomarkers of altered neurodevelopment based network features, which can assess and monitor experimental therapies in an animal model that could later be used in the clinical practice for a better management of human IUGR.

Funding

This work was supported by grants: Obra Social "la Caixa", Barcelona, Spain; Fondo de Investigación Sanitaria (PI12/00851); Rio Hortega grant (grant number CM11/00032 to M.I.) and Sara Borrell grants from Carlos III Institute of Health, Spain (grant number CD11/00048 to E.M.).

Acknowledgments

We would like to acknowledge Guadalupe Soria, Raul Tudela and 7 T MR animal platform of IDIBAPS for the diligent and careful performance of MRI acquisitions. The Image Registration Toolkit was used under License from Ixico Ltd.

Conflict of interest statement

The authors do not have conflicts of interest to declare.

Appendix A. Supplementary data

Supplementary data to this article can be found online at http://dx.doi.org/10.1016/j.neuroimage.2014.05.065.

References

Achard, S., Bullmore, E., 2007. Efficiency and cost of economical brain functional networks. PLoS Comput. Biol. 3, e17.
Alexander-Bloch, A.F., Gogtay, N., Meunier, D., Birn, R., Clasen, L., Lalonde, F., Lenroot, R., Giedd, J., Bullmore, E.T., 2010. Disrupted modularity and local connectivity of brain functional networks in childhood-onset schizophrenia. Front. Syst. Neurosci. 4, 147.
Arcangeli, T., Thilaganathan, B., Hooper, R., Khan, K.S., Bhide, A., 2012. Neurodevelopmental delay in small babies at term: a systematic review. Ultrasound Obstet. Gynecol. 40, 267–275.
Baillieux, H., De Smet, H.J., Paquier, P.F., De Deyn, P.P., Marien, P., 2008. Cerebellar neurocognition: insights into the bottom of the brain. Clin. Neurol. Neurosurg. 110, 763–773.
Baschat, A.A., 2013. Neurodevelopment after fetal growth restriction. Fetal Diagn. Ther. (E-pub ahead of print). Q3
Bassan, H., Trejo, L.L., Kariv, N., Bassan, M., Berger, E., Fattal, A., Gozes, I., Harel, S., 2000. Experimental intrauterine growth retardation alters renal development. Pediatr. Nephrol. 15, 192–195.
Bassett, D.S., Bullmore, E.T., 2009. Human brain networks in health and disease. Curr. Opin. Neurol. 22, 340–347.
Bassett, D.S., Bullmore, E., Verchinski, B.A., Mattay, V.S., Weinberger, D.R., Meyer-Lindenberg, A., 2008. Hierarchical organization of human cortical networks in health and schizophrenia. J. Neurosci. 28, 9239–9248.
Batalle, D., Eixarch, E., Figueras, F., Munoz-Moreno, E., Bargallo, N., Illa, M., Acosta-Rojas, R., Amat-Roldan, I., Gratacos, E., 2012. Altered small-world topology of structural brain networks in infants with intrauterine growth restriction and its association with later neurodevelopmental outcome. Neuroimage 60, 1352–1366.
Batalle, D., Munoz-Moreno, E., Figueras, F., Bargallo, N., Eixarch, E., Gratacos, E., 2013. Normalization of similarity-based individual brain networks from gray matter MRI and its association with neurodevelopment in infants with intrauterine growth restriction. Neuroimage 83C, 901–911.
Benjamini, Y., Krieger, A.M., Yekutieli, D., 2006. Adaptive linear step-up procedures that control the false discovery rate. Biometrika 93, 491–507.
Bouet, V., Gahery, Y., Lacour, M., 2003. Behavioural changes induced by early and long-term gravito-inertial force modification in the rat. Behav. Brain Res. 139, 97–104.
Bullmore, E., Sporns, O., 2009. Complex brain networks: graph theoretical analysis of structural and functional systems. Nat. Rev. Neurosci. 10, 186–198.
Castellanos, F.X., Giedd, J.N., Eckburg, P., Marsh, W.L., Vaituzis, A.C., Kaysen, D., Hamburger, S.D., Rapoport, J.L., 1994. Quantitative morphology of the caudate nucleus in attention deficit hyperactivity disorder. Am. J. Psychiatry 151, 1791–1796.
Cowan, N., Nugent, L.D., Elliott, E.M., Ponomarev, I., Saults, J.S., 1999. The role of attention in the development of short-term memory: age differences in the verbal span of apprehension. Child Dev. 70, 1082–1097.
De Bie, H.M., Oostrom, K.J., Boersma, M., Veltman, D.J., Barkhof, F., Delemarre-van de Waal, H.A., van den Heuvel, M.P., 2011. Global and regional differences in brain anatomy of young children born small for gestational age. PLoS One 6, e24116.
Dere, E., Kart-Teke, E., Huston, J.P., De Souza Silva, M.A., 2006. The case for episodic memory in animals. Neurosci. Biobehav. Rev. 30, 1206–1224.
Derrick, M., Drobyshevsky, A., Ji, X., Tan, S., 2007. A model of cerebral palsy from fetal hypoxia–ischemia. Stroke 38, 731–735.
Dubois, J., Benders, M., Borradori-Tolsa, C., Cachia, A., Lazeyras, F., Ha-Vinh Leuchter, R., Sizonenko, S.V., Warfield, S.K., Mangin, J.F., Hüppi, P.S., 2008. Primary cortical folding in the human newborn: an early marker of later functional development. Brain 131, 2028–2041.
Egaña-Ugrinovic, G., Sanz-Cortes, M., Figueras, F., Bargallo, N., Gratacos, E., 2013. Differences in cortical development assessed by fetal MRI in late-onset intrauterine growth restriction. Am. J. Obstet. Gynecol. 209 (126), e121–e128.
Eixarch, E., Figueras, F., Hernandez-Andrade, E., Crispi, F., Nadal, A., Torre, I., Oliveira, S., Gratacos, E., 2009. An experimental model of fetal growth restriction based on selective ligature of uteroplacental vessels in the pregnant rabbit. Fetal Diagn. Ther. 26, 203–211.
Eixarch, E., Hernandez-Andrade, E., Crispi, F., Illa, M., Torre, I., Figueras, F., Gratacos, E., 2011. Impact on fetal mortality and cardiovascular Doppler of selective ligature of uteroplacental vessels compared with undernutrition in a rabbit model of intrauterine growth restriction. Placenta 32, 304–309.
Eixarch, E., Batalle, D., Illa, M., Munoz-Moreno, E., Arbat-Plana, A., Amat-Roldan, I., Figueras, F., Gratacos, E., 2012. Neonatal neurobehavior and diffusion MRI changes in brain reorganization due to intrauterine growth restriction in a rabbit model. PLoS One 7, e31497.
Emond, V., Joyal, C., Poissant, H., 2009. Structural and functional neuroanatomy of attention-deficit hyperactivity disorder (ADHD). Encéphale 35, 107–114.
Ennaceur, A., Aggleton, J.P., 1997. The effects of neurotoxic lesions of the perirhinal cortex combined to fornix transection on object recognition memory in the rat. Behav. Brain Res. 88, 181–193.
Ennaceur, A., Delacour, J., 1988. A new one-trial test for neurobiological studies of memory in rats. 1: Behavioral data. Behav. Brain Res. 31, 47–59.
Esteban, F.J., Padilla, N., Sanz-Cortes, M., de Miras, J.R., Bargallo, N., Villoslada, P., Gratacos, E., 2010. Fractal-dimension analysis detects cerebral changes in preterm infants with and without intrauterine growth restriction. Neuroimage 53, 1225–1232.
Estrada-Camarena, E., Contreras, C.M., Saavedra, M., Luna-Baltazar, I., Lopez-Rubalcava, C., 2002. Participation of the lateral septal nuclei (LSN) in the antidepressant-like actions of progesterone in the forced swimming test (FST). Behav. Brain Res. 134, 175–183.
Faraone, S.V., Biederman, J., 1998. Neurobiology of attention-deficit hyperactivity disorder. Biol. Psychiatry 44, 951–958.
Ginestet, C.E., Nichols, T.E., Bullmore, E.T., Simmons, A., 2011. Brain network analysis: separating cost from topology using cost-integration. PLoS One 6, e21570.
Gong, G., He, Y., Concha, L., Lebel, C., Gross, D.W., Evans, A.C., Beaulieu, C., 2009a. Mapping anatomical connectivity patterns of human cerebral cortex using in vivo diffusion tensor imaging tractography. Cereb. Cortex 19, 524–536.
Gong, G., Rosa-Neto, P., Carbonell, F., Chen, Z.J., He, Y., Evans, A.C., 2009b. Age- and gender-related differences in the cortical anatomical network. J. Neurosci. 29, 15684–15693.

Please cite this article as: Batalle, D., et al., Long-term reorganization of structural brain networks in a rabbit model of intrauterine growth restriction, NeuroImage (2014), http://dx.doi.org/10.1016/j.neuroimage.2014.05.065

Gratacos, E., 2012. Opportunities and challenges of biomedical imaging in fetal and neonatal brain disease. Proceedings of the 9th IEEE International Symposium on Biomedical Imaging: From Nano to Macro, pp. 493–494.
Griffa, A., Baumann, P.S., Thiran, J.P., Hagmann, P., 2013. Structural connectomics in brain diseases. Neuroimage 80, 515–526.
Hagmann, P., 2005. From Diffusion MRI to Brain Connectomics. Signal Processing Institute. Ecole Polytechnique Fédérale de Lausanne (EPFL), Lausane.
Hagmann, P., Cammoun, L., Gigandet, X., Meuli, R., Honey, C.J., Wedeen, V.J., Sporns, O., 2008. Mapping the structural core of human cerebral cortex. PLoS Biol. 6, e159.
Hagmann, P., Sporns, O., Madan, N., Cammoun, L., Pienaar, R., Wedeen, V.J., Meuli, R., Thiran, J.P., Grant, P.E., 2010. White matter maturation reshapes structural connectivity in the late developing human brain. Proc. Natl. Acad. Sci. U. S. A. 107, 19067–19072.
Hall, C.S., 1934. Drive and emotionality: factors associated with adjustment in the rat. J. Comp. Psychol. 17, 89.
Hall, F.S., Perona, M.T., 2012. Have studies of the developmental regulation of behavioral phenotypes revealed the mechanisms of gene-environment interactions? Physiol. Behav. 107, 623–640.
He, Y., Dagher, A., Chen, Z., Charil, A., Zijdenbos, A., Worsley, K., Evans, A., 2009. Impaired small-world efficiency in structural cortical networks in multiple sclerosis associated with white matter lesion load. Brain 132, 3366–3379.
Heckers, S., Curran, T., Goff, D., Rauch, S.L., Fischman, A.J., Alpert, N.M., Schacter, D.L., 2000. Abnormalities in the thalamus and prefrontal cortex during episodic object recognition in schizophrenia. Biol. Psychiatry 48, 651–657.
Heinonen, K., Räikkönen, K., Pesonen, A.-K., Andersson, S., Kajantie, E., Eriksson, J.G., Wolke, D., Lano, A., 2010. Behavioural symptoms of attention deficit/hyperactivity disorder in preterm and term children born small and appropriate for gestational age: a longitudinal study. BMC Pediatr. 10, 91.
Humphries, M.D., Gurney, K., 2008. Network 'small-world-ness': a quantitative method for determining canonical network equivalence. PLoS One 3, e0002051.
Illa, M., Eixarch, E., Batalle, D., Arbat-Plana, A., Muñoz-Moreno, E., Figueras, F., Gratacos, E., 2013. Long-term functional outcomes and correlation with regional brain connectivity by MRI diffusion tractography metrics in a near-term rabbit model of intrauterine growth restriction. PLoS One 8, e76453.
Iturria-Medina, Y., Sotero, R.C., Canales-Rodríguez, E.J., Alemán-Gómez, Y., Melie-García, L., 2008. Studying the human brain anatomical network via diffusion-weighted MRI and graph theory. Neuroimage 40, 1064–1076.
Iturria-Medina, Y., Perez Fernandez, A., Valdes Hernandez, P., Garcia Penton, L., Canales-Rodriguez, E.J., Melie-Garcia, L., Lage Castellanos, A., Ontivero Ortega, M., 2011. Automated discrimination of brain pathological state attending to complex structural brain network properties: the shiverer mutant mouse case. PLoS One 6, e19071.
Kadohisa, M., Wilson, D.A., 2006. Separate encoding of identity and similarity of complex familiar odors in piriform cortex. Proc. Natl. Acad. Sci. U. S. A. 103, 15206–15211.
Kim, M.J., Whalen, P.J., 2009. The structural integrity of an amygdala-prefrontal pathway predicts trait anxiety. J. Neurosci. 29, 11614–11618.
Li, Y., Liu, Y., Li, J., Qin, W., Li, K., Yu, C., Jiang, T., 2009. Brain anatomical network and intelligence. PLoS Comput. Biol. 5, e1000395.
Liu, Y., Liang, M., Zhou, Y., He, Y., Hao, Y., Song, M., Yu, C., Liu, H., Liu, Z., Jiang, T., 2008. Disrupted small-world networks in schizophrenia. Brain 131, 945–961.
Lo, C.Y., Wang, P.N., Chou, K.H., Wang, J., He, Y., Lin, C.P., 2010. Diffusion tensor tractography reveals abnormal topological organization in structural cortical networks in Alzheimer's disease. J. Neurosci. 30, 16876–16885.
Lodygensky, G.A., Seghier, M.L., Warfield, S.K., Tolsa, C.B., Sizonenko, S., Lazeyras, F., Huppi, P.S., 2008. Intrauterine growth restriction affects the preterm infant's hippocampus. Pediatr. Res. 63, 438–443.
Løhaugen, G.C., Østgård, H.F., Andreassen, S., Jacobsen, G.W., Vik, T., Brubakk, A.M., Skranes, J., Martinussen, M., 2013. Small for gestational age and intrauterine growth restriction decreases cognitive function in young adults. J. Pediatr. 163, 447–453.
Mallard, C., Loeliger, M., Copolov, D., Rees, S., 2000. Reduced number of neurons in the hippocampus and the cerebellum in the postnatal guinea-pig following intrauterine growth-restriction. Neuroscience 100, 327–333.
Martinussen, M., Fischl, B., Larsson, H.B., Skranes, J., Kulseng, S., Vangberg, T.R., Vik, T., Brubakk, A.M., Haraldseth, O., Dale, A.M., 2005. Cerebral cortex thickness in 15-year-old adolescents with low birth weight measured by an automated MRI-based method. Brain 128, 2588–2596.
Martinussen, M., Flanders, D.W., Fischl, B., Busa, E., Lohaugen, G.C., Skranes, J., Vangberg, T.R., Brubakk, A.M., Haraldseth, O., Dale, A.M., 2009. Segmental brain volumes and cognitive and perceptual correlates in 15-year-old adolescents with low birth weight. J. Pediatr. 155 (848–853), e841.
McAnulty, G., Duffy, F.H., Kosta, S., Weisenfeld, N.I., Warfield, S.K., Butler, S.C., Alidoost, M., Bernstein, J.H., Robertson, R., Zurakowski, D., Als, H., 2013. School-age effects of the newborn individualized developmental care and assessment program for preterm infants with intrauterine growth restriction: preliminary findings. BMC Pediatr. 13, 25.
Ment, L.R., Hirtz, D., Huppi, P.S., 2009. Imaging biomarkers of outcome in the developing preterm brain. Lancet Neurol. 8, 1042–1055.
Meskaldji, D.E., Ottet, M.C., Cammoun, L., Hagmann, P., Meuli, R., Eliez, S., Thiran, J.P., Morgenthaler, S., 2011. Adaptive strategy for the statistical analysis of connectomes. PLoS One 6, e23009.
Miller, M.M., Morrison, J.H., McEwen, B.S., 2012. Basal anxiety-like behavior predicts differences in dendritic morphology in the medial prefrontal cortex in two strains of rats. Behav. Brain Res. 229, 280–288.
Mitchell, A.S., Dalrymple-Alford, J.C., 2005. Dissociable memory effects after medial thalamus lesions in the rat. Eur. J. Neurosci. 22, 973–985.
Moorman, W.J., Cheever, K.L., Skaggs, S.R., Clark, J.C., Turner, T.W., Marlow, K.L., Schrader, S.M., 2000. Male adolescent exposure to endocrine-disrupting pesticides: vinclozolin exposure in peripubertal rabbits. Andrologia 32, 285–293.
Mumby, D.G., 2001. Perspectives on object-recognition memory following hippocampal damage: lessons from studies in rats. Behav. Brain Res. 127, 159–181.
Muñoz-Moreno, E., Arbat-Plana, A., Batalle, D., Soria, G., Illa, M., Prats-Galino, A., Eixarch, E., Gratacos, E., 2013. A magnetic resonance image based atlas of the rabbit brain for automatic parcellation. PLoS One 8, e67418.
Nilsson, E., Stalberg, G., Lichtenstein, P., Cnattingius, S., Olausson, P.O., Hultman, C.M., 2005. Fetal growth restriction and schizophrenia: a Swedish twin study. Twin Res. Hum. Genet. 8, 402–408.
Olton, D.S., Feustle, W.A., 1981. Hippocampal function required for nonspatial working memory. Exp. Brain Res. 41, 380–389.
Otsu, N., 1975. A threshold selection method from gray-level histograms. Automatica 11, 23–27.
Padilla, N., Falcon, C., Sanz-Cortes, M., Figueras, F., Bargallo, N., Crispi, F., Eixarch, E., Arranz, A., Botet, F., Gratacos, E., 2011. Differential effects of intrauterine growth restriction on brain structure and development in preterm infants: a magnetic resonance imaging study. Brain Res. 1382, 98–108.
Paulus, M.P., Stein, M.B., 2006. An insular view of anxiety. Biol. Psychiatry 60, 383–387.
Rubinov, M., Sporns, O., 2009. Complex network measures of brain connectivity: uses and interpretations. Neuroimage 52, 1059–1069.
Sanz-Cortes, M., Ratta, G.A., Figueras, F., Bonet-Carne, E., Padilla, N., Arranz, A., Bargallo, N., Gratacos, E., 2013. Automatic quantitative MRI texture analysis in small-for-gestational-age fetuses discriminates abnormal neonatal neurobehavior. PLoS One 8, e69595.
Shu, N., Liu, Y., Li, J., Li, Y., Yu, C., Jiang, T., 2009. Altered anatomical network in early blindness revealed by diffusion tensor tractography. PLoS One 4, e7228.
Shu, N., Liu, Y., Li, K., Duan, Y., Wang, J., Yu, C., Dong, H., Ye, J., He, Y., 2011. Diffusion tensor tractography reveals disrupted topological efficiency in white matter structural networks in multiple sclerosis. Cereb. Cortex 21, 2565–2577.
Skranes, J.S., Martinussen, M., Smevik, O., Myhr, G., Indredavik, M., Vik, T., Brubakk, A.M., 2005. Cerebral MRI findings in very-low-birth-weight and small-for-gestational-age children at 15 years of age. Pediatr. Radiol. 35, 758–765.
Spampinato, M.V., Wood, J.N., De Simone, V., Grafman, J., 2009. Neural correlates of anxiety in healthy volunteers: a voxel-based morphometry study. J. Neuropsychiatry Clin. Neurosci. 21, 199–205.
Sporns, O., Tononi, G., Kotter, R., 2005. The human connectome: a structural description of the human brain. PLoS Comput. Biol. 1, e42.
Studholme, C., Hill, D.L.G., Hawkes, D.J., 1999. An overlap invariant entropy measure of 3D medical image alignment. Pattern Recogn. 32, 71–86.
Toft, P.B., 1999. Prenatal and perinatal striatal injury: a hypothetical cause of attention-deficit-hyperactivity disorder? Pediatr. Neurol. 21, 602–610.
Tolcos, M., Bateman, E., O'Dowd, R., Markwick, R., Vrijsen, K., Rehn, A., Rees, S., 2011. Intrauterine growth restriction affects the maturation of myelin. Exp. Neurol. 232, 53–65.
Tolsa, C.B., Zimine, S., Warfield, S.K., Freschi, M., Sancho Rossignol, A., Lazeyras, F., Hanquinet, S., Pfizenmaier, M., Huppi, P.S., 2004. Early alteration of structural and functional brain development in premature infants born with intrauterine growth restriction. Pediatr. Res. 56, 132–138.
Tristan-Vega, A., Arribas, J.I., 2007. A fast B-spline pseudo-inversion algorithm for consistent image registration. Proceedings of the International Conference on Computer Analysis Images and Patterns (CAIP), Vienna, Austria, pp. 768–775.
Tuch, D.S., 2004. Q-ball imaging. Magn. Reson. Med. 52, 1358–1372.
Tymofiyeva, O., Hess, C.P., Ziv, E., Tian, N., Bonifacio, S.L., McQuillen, P.S., Ferriero, D.M., Barkovich, A.J., Xu, D., 2012. Towards the "baby connectome": mapping the structural connectivity of the newborn brain. PLoS One 7, e31029.
van Wijk, B.C.M., Stam, C.J., Daffertshofer, A., 2010. Comparing brain networks of different size and connectivity density using graph theory. PLoS One 5, e13701.
Walsh, R.N., Cummins, R.A., 1975. Mechanisms mediating the production of environmentally induced brain changes. Psychol. Bull. 82, 986–1000.
Wang, R., Benner, T., Sorensen, A.G., Wedeen, V.J., 2007. Diffusion toolkit: a software package for diffusion imaging data processing and tractography. Proc Intl Soc Mag Reson Med, p. 3720.
Wang, L., Zhu, C., He, Y., Zang, Y., Cao, Q., Zhang, H., Zhong, Q., Wang, Y., 2009. Altered small-world brain functional networks in children with attention-deficit/hyperactivity disorder. Hum. Brain Mapp. 30, 638–649.
Warfield, S.K., Guimond, A., Roche, A., Bharatha, A., Tei, A., Talos, F., Rexilius, J., Ruiz-Alzola, J., Westin, C.F., Haker, S., Angenent, S., Tannenbaum, A., Jolesz, F., Kikkinis, R., 2002. In: Mazziotta, J.C., Toga, A.W. (Eds.), Advanced nonrigid registration algorithms for image fusion. Brain Mapping: The Methods. Elsevier, pp. 661–690.
Watts, D.J., Strogatz, S.H., 1998. Collective dynamics of 'small-world' networks. Nature 393, 440–442.
Wee, C.-Y., Yap, P.-T., Li, W., Denny, K., Browndyke, J.N., Potter, G.G., Welsh-Bohmer, K.A., Wang, L., Shen, D., 2010. Enriched white matter connectivity networks for accurate identification of MCI patients. Neuroimage 54, 1812–1822.
Wen, W., Zhu, W., He, Y., Kochan, N.A., Reppermund, S., Slavin, M.J., Brodaty, H., Crawford, J., Xia, A., Sachdev, P., 2011. Discrete neuroanatomical networks are associated with specific cognitive abilities in old age. J. Neurosci. 31, 1204–1212.
Wu, T., Wang, L., Chen, Y., Zhao, C., Li, K., Chan, P., 2009. Changes of functional connectivity of the motor network in the resting state in Parkinson's disease. Neurosci. Lett. 460, 6–10.
Xia, M., Wang, J., He, Y., 2013. BrainNet Viewer: a network visualization tool for human brain connectomics. PLoS One 8, e68910.
Yap, P.T., Fan, Y., Chen, Y., Gilmore, J.H., Lin, W., Shen, D., 2011. Development trends of white matter connectivity in the first years of life. PLoS One 6, e24678.
Zalesky, A., Fornito, A., Bullmore, E.T., 2010. Network-based statistic: identifying differences in brain networks. Neuroimage 53, 1197–1207.

Please cite this article as: Batalle, D., et al., Long-term reorganization of structural brain networks in a rabbit model of intrauterine growth restriction, NeuroImage (2014), http://dx.doi.org/10.1016/j.neuroimage.2014.05.065

Long-term reorganization of structural brain networks in a rabbit model of intrauterine growth restriction: supplementary material

Dafnis Batalle[a], Emma Muñoz-Moreno[a], Ariadna Arbat-Plana[a], Miriam Illa [a,b], Francesc Figueras[a,b,c], Elisenda Eixarch[a,b,c], Eduard Gratacos[a,b,c]

a) Fetal and Perinatal Medicine Research Group, Institut d'Investigacions Biomediques August Pi i Sunyer (IDIBAPS), Barcelona, Spain b) Maternal-Fetal Medicine Department, ICGON, Hospital Clínic, Universitat de Barcelona, Barcelona, Spain c) Centro de Investigación Biomédica en Red de Enfermedades Raras (CIBERER), Barcelona, Spain

1. Characteristic path length and average clustering coefficient

Characteristic path length, which is inversely associated to global efficiency, was significantly increased in IUGR binary raw network (p=0.048), but significantly decreased in its normalized GFA version (p=0.017). Average clustering coefficient, which is closely related to local efficiency, was also significantly increased in IUGR normalized networks in its FD version (p=0.016) and had a tendency towards significance in its normalized GFA-weighted version (p=0.072).

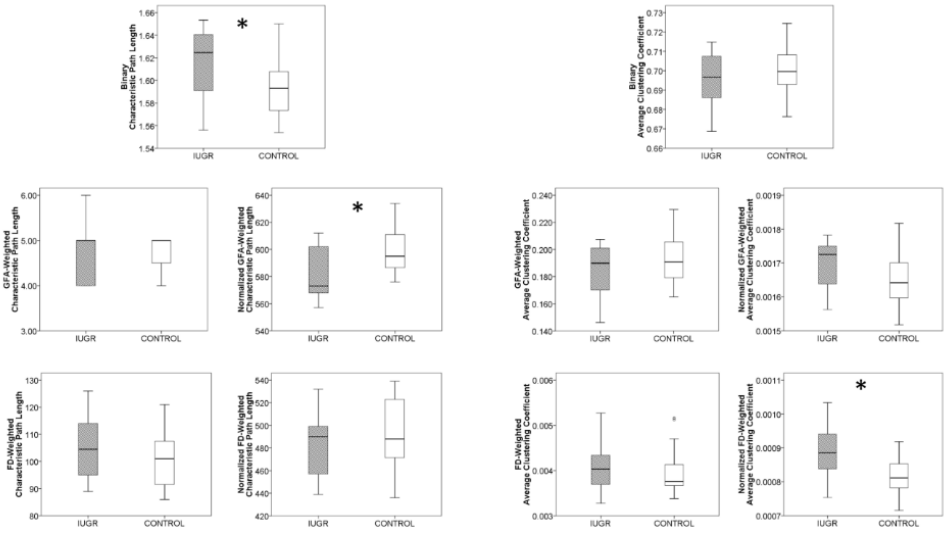

Figure S1. Characteristic path length and average clustering of IUGR and controls

2. Cost-correction of the networks using the same set of nodes for all subjects

Inherent to characteristics of the approach of using individual thresholding to cost-correct each of the networks under study there is a direct shortcoming: while the total number of connections is guaranteed, this approach leads to a different number of connection sets across subjects. Hence, inspired by the idea of assessing the same sub-set of connections at a given cost (Gong et al., 2009), we calculated the connectivity backbone of our population as the connections that are present in all the subjects.

This approach lead to a binary connected network with a network density of 22%. Multiplying this binary network for each subject GFA- or FD-weighted network we obtained individual networks with the same network cost and the same position of connections, only changing the individual weight of each connection.

Assessing the differences between cases and controls, we observed a tendency of IUGR to have a decreased FD-weighted average strength and global efficiency (p=0.079 and p=0.096 respectively). Note that with this approach we are assessing the differences in the average connection weight of the network most plausible connections (i.e. the network "backbone"). This result is coherent with previously reported tendency of IUGR to have decreased FD-weighted average strength in their raw networks, supporting the hypothesis that there is a reduced infrastructure in the "backbone" network of these subjects independently of their network density. Varying the threshold to generate this backbone binary network at different levels of network density we observe similar results than obtained for the maximum set of networks at 22% of network density (see Figure S2).

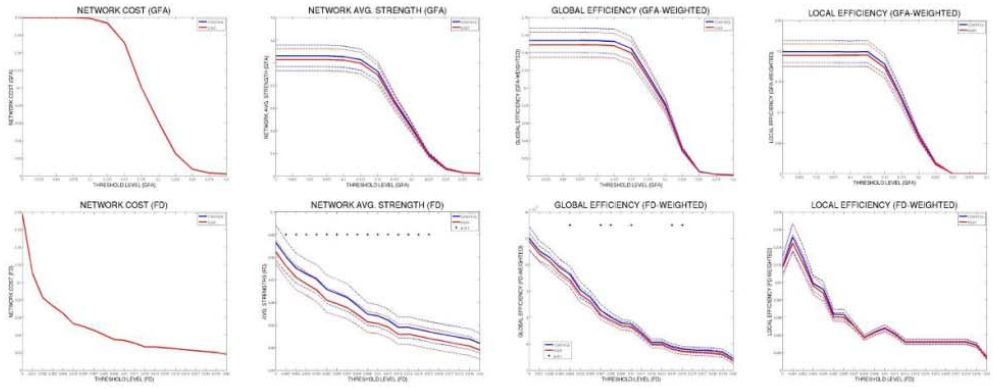

Figure S2. Network cost, average strength, global efficiency and local efficiency of the network "backbone" compared between cases (red) and controls (blue) as a function of GFA- and FD-weighted connectivity. $^{+}$ p<0.1.

REFERENCES

Gong, G., Rosa-Neto, P., Carbonell, F., Chen, Z.J., He, Y., Evans, A.C., 2009. Age- and gender-related differences in the cortical anatomical network. J Neurosci 29, 15684-15693.

Supplementary Table 1. Regions with IUGR statistically significant differences in regional network features

ROI	Binary Degree	Binary Efficiency	GFA-weighted Strength	GFA-weighted Efficiency	FD-weighted Strength	FD-weighted Efficiency	Normalized GFA-weighted Strength	Normalized GFA-weighted Efficiency	Normalized FD-weighted Strength	Normalized FD-weighted Efficiency
FCx-L	n.s.	n.s.	n.s.	n.s.	n.s.	n.s.	n.s.	n.s.	n.s.	n.s.
FCx-R	n.s.	p=0.018	n.s.	n.s.	n.s.	n.s.	n.s.	n.s.	n.s.	n.s.
MFCx-L	n.s.	n.s.	n.s.	n.s.	n.s.	n.s.	n.s.	n.s.	n.s.	n.s.
MFCx-R	n.s.	n.s.	n.s.	n.s.	n.s.	n.s.	n.s.	n.s.	n.s.	n.s.
CiCx-L	n.s.	n.s.	n.s.	n.s.	n.s.	n.s.	n.s.	n.s.	n.s.	n.s.
CiCx-R	p=0.017	n.s.	p=0.020	n.s.	n.s.	n.s.	p=0.046	n.s.	n.s.	p=0.014
PiCx-L	n.s.	n.s.	n.s.	n.s.	n.s.	n.s.	n.s.	p=0.033	n.s.	n.s.
PiCx-R	n.s.	n.s.	n.s.	n.s.	n.s.	n.s.	n.s.	**p=0.003**	n.s.	n.s.
ECx-L	n.s.	n.s.	n.s.	n.s.	n.s.	n.s.	n.s.	n.s.	n.s.	n.s.
ECx-R	n.s.	n.s.	n.s.	n.s.	n.s.	n.s.	n.s.	n.s.	n.s.	n.s.
PaCx-L	n.s.	n.s.	n.s.	n.s.	n.s.	n.s.	n.s.	n.s.	n.s.	n.s.
PaCx-R	n.s.	p=0.035	n.s.	n.s.	n.s.	n.s.	n.s.	n.s.	n.s.	p=0.029
OcCx-L	n.s.	n.s.	n.s.	n.s.	p=0.025	n.s.	n.s.	n.s.	n.s.	n.s.
OcCx-R	n.s.	n.s.	n.s.	n.s.	n.s.	n.s.	n.s.	n.s.	n.s.	n.s.
InCx-L	n.s.	n.s.	n.s.	n.s.	n.s.	n.s.	n.s.	n.s.	n.s.	n.s.
InCx-R	n.s.	n.s.	n.s.	n.s.	n.s.	n.s.	n.s.	n.s.	n.s.	n.s.
TeCx-L	n.s.	n.s.	n.s.	n.s.	n.s.	n.s.	n.s.	n.s.	n.s.	n.s.
TeCx-R	n.s.	n.s.	n.s.	n.s.	n.s.	n.s.	n.s.	n.s.	n.s.	n.s.
CI-L	n.s.	n.s.	n.s.	n.s.	n.s.	n.s.	n.s.	n.s.	n.s.	n.s.
CI-R	n.s.	n.s.	n.s.	n.s.	n.s.	n.s.	n.s.	n.s.	n.s.	n.s.
Cau-L	n.s.	n.s.	n.s.	n.s.	n.s.	n.s.	n.s.	n.s.	n.s.	n.s.
Cau-R	n.s.	n.s.	p=0.025	n.s.	n.s.	n.s.	n.s.	n.s.	n.s.	n.s.
Len-L	n.s.	n.s.	n.s.	n.s.	n.s.	n.s.	n.s.	n.s.	n.s.	n.s.
Len-R	p=0.017	n.s.	p=0.028	n.s.	n.s.	n.s.	p=0.036	n.s.	n.s.	n.s.
Th-L	n.s.	n.s.	n.s.	n.s.	n.s.	n.s.	n.s.	n.s.	n.s.	n.s.
Th-R	n.s.	n.s.	n.s.	n.s.	n.s.	n.s.	n.s.	n.s.	p=0.004	n.s.
Am-L	n.s.	n.s.	n.s.	n.s.	n.s.	n.s.	n.s.	n.s.	n.s.	n.s.
Am-R	n.s.	n.s.	n.s.	n.s.	n.s.	n.s.	p=0.040	p=0.010	n.s.	n.s.
OlB-L	n.s.	n.s.	n.s.	n.s.	n.s.	n.s.	n.s.	n.s.	n.s.	n.s.
OlB-R	n.s.	n.s.	n.s.	n.s.	n.s.	n.s.	n.s.	n.s.	n.s.	n.s.
Hc-L	n.s.	n.s.	n.s.	n.s.	n.s.	n.s.	n.s.	n.s.	p=0.007	p=0.018
Hc-R	n.s.	n.s.	n.s.	n.s.	n.s.	n.s.	n.s.	n.s.	p=0.024	p=0.019
FB-L	n.s.	n.s.	n.s.	n.s.	n.s.	n.s.	n.s.	n.s.	n.s.	n.s.
FB-R	n.s.	n.s.	n.s.	n.s.	n.s.	n.s.	n.s.	n.s.	n.s.	n.s.
CeH-L	n.s.	n.s.	n.s.	n.s.	n.s.	p=0.010	n.s.	n.s.	n.s.	**p=0.003**
CeH-R	n.s.	n.s.	n.s.	n.s.	n.s.	n.s.	p=0.023	**p=0.003**	n.s.	n.s.
Ht	n.s.	n.s.	n.s.	n.s.	n.s.	n.s.	n.s.	n.s.	n.s.	n.s.
Ve	**p<0.001**	p=0.031	**p<0.001**	n.s.	n.s.	**p=0.001**	**p=0.001**	n.s.	n.s.	**p<0.001**
BF	n.s.	n.s.	n.s.	n.s.	n.s.	n.s.	n.s.	p=0.045	n.s.	n.s.
De	n.s.	n.s.	n.s.	n.s.	n.s.	n.s.	n.s.	n.s.	n.s.	n.s.
Me	n.s.	n.s.	n.s.	n.s.	n.s.	n.s.	n.s.	n.s.	n.s.	p=0.011
Po	n.s.	n.s.	n.s.	n.s.	n.s.	n.s.	n.s.	n.s.	n.s.	p=0.026
MO	n.s.	n.s.	n.s.	n.s.	n.s.	n.s.	p=0.035	n.s.	n.s.	n.s.
Spt	n.s.	n.s.	n.s.	n.s.	n.s.	n.s.	n.s.	n.s.	n.s.	n.s.

Supplementary Table 2. Correlation of neurobehavioral scores with the main global network features obtained

		OPEN FIELD BEHAVIORAL TEST [a]				OBJECT RECOGNITION TASK [b]
		Latency	Total Boxes Crossed	Number External Boxes	Number Internal Boxes	Discriminatory Index
Average degree	p	*-0.427*	0.308	0.265	0.353	-0.065
	p	*0.077*	0.214	0.288	0.151	0.833
GFA-weighted Average strength	p	**-0.561**	**0.607**	**0.548**	**0.492**	0.329
	p	**0.015**	**0.008**	**0.019**	**0.038**	0.272
FD-weighted Average strength	p	-0.330	0.319	0.249	0.215	0.011
	p	0.181	0.197	0.320	0.392	0.972
Binary Characteristic Path Length	p	0.297	-0.173	-0.141	-0.264	0.177
	p	0.231	0.493	0.576	0.290	0.563
GFA-weighted Characteristic Path Length	p	**0.491**	**-0.496**	***-0.456***	-0.269	-0.277
	p	**0.039**	**0.036**	***0.057***	0.281	0.360
Normalized GFA-weighted Characteristic Path Length	p	**-0.490**	**0.503**	*0.455*	**0.469**	0.167
	p	**0.039**	**0.033**	*0.058*	**0.049**	0.586
FD-weighted Characteristic Path Length	p	-0.074	-0.056	-0.044	-0.019	0.079
	p	0.770	0.825	0.864	0.940	0.799
Normalized FD-weighted Characteristic Path Length	p	0.256	-0.042	-0.010	-0.342	-0.382
	p	0.306	0.869	0.970	0.165	0.197
Binary Average Clustering	p	-0.390	0.298	0.225	-0.100	0.328
	p	0.110	0.229	0.370	0.692	0.274
GFA-weighted Average Clustering	p	**-0.598**	**0.686**	**0.625**	**0.460**	*0.515*
	p	**0.009**	**0.002**	**0.006**	**0.055**	*0.072*
Normalized GFA-weighted Average Clustering	p	0.266	-0.204	-0.183	-0.343	0.136
	p	0.287	0.416	0.467	0.163	0.659
FD-weighted Average Clustering	p	-0.042	0.217	0.183	-0.057	-0.211
	p	0.870	0.387	0.466	0.822	0.489
Normalized FD-weighted Average Clustering	p	0.256	-0.042	-0.010	-0.342	-0.382
	p	0.306	0.869	0.970	0.165	0.197
Binary Global Efficiency	p	-0.377	0.254	0.216	0.319	-0.113
	p	0.123	0.309	0.390	0.197	0.713
GFA-weighted Global Efficiency	p	**-0.563**	**0.634**	**0.576**	**0.473**	0.412
	p	**0.015**	**0.005**	**0.012**	**0.047**	0.162
Normalized GFA-weighted Global Efficiency	p	**0.511**	*-0.465*	*-0.420*	*-0.463*	-0.043
	p	**0.030**	*0.052*	*0.083*	*0.053*	0.890
Cost-integrated GFA-weighted Global Efficiency	p	0.028	-0.097	-0.055	-0.067	*-0.504*
	p	0.912	0.700	0.829	0.793	*0.079*
FD-weighted Global Efficiency	p	-0.041	0.080	0.032	0.099	0.094
	p	0.870	0.751	0.899	0.696	0.760
Normalized FD-weighted Global Efficiency	p	**0.560**	**-0.596**	**-0.534**	-0.369	-0.092
	p	**0.016**	**0.009**	**0.022**	0.132	0.766
Cost-integrated FD-weighted Global Efficiency	p	0.210	-0.045	-0.003	-0.089	-0.124
	p	0.403	0.859	0.991	0.725	0.687
Binary Local Efficiency	p	-0.391	0.291	0.217	-0.102	0.335
	p	0.109	0.241	0.388	0.687	0.264
GFA-weighted Local Efficiency	p	**-0.576**	**0.677**	**0.621**	**0.486**	*0.501*
	p	**0.012**	**0.002**	**0.006**	**0.041**	*0.081*
Normalized GFA-weighted Local Efficiency	p	*0.407*	-0.314	-0.273	-0.354	0.062
	p	*0.094*	0.204	0.274	0.150	0.840
Cost-integrated GFA-weighted Local Efficiency	p	-0.150	-0.215	-0.276	0.113	0.465
	p	0.554	0.391	0.267	0.655	0.109
FD-weighted Local Efficiency	p	-0.015	0.164	0.140	-0.040	-0.169
	p	0.953	0.515	0.579	0.873	0.580
Normalized FD-weighted Local Efficiency	p	0.373	-0.187	-0.122	*-0.402*	-0.390
	p	0.127	0.457	0.631	*0.098*	0.187
Cost-integrated FD-weighted Local Efficiency	p	0.215	-0.039	-0.038	-0.174	0.167
	p	0.391	0.876	0.880	0.489	0.585

[a] 10 controls and 9 IUGR. [b] 8 controls and 6 IUGR. Highlighted in bold those correlations statistically significant (p<0.05), in italics those with a tendency towards significance (p<0.1).

5.4. PROJECT 4: COPY OF PRE-SUBMITTED PAPER

Altered resting-state whole-brain functional brain networks of neonates with intrauterine growth restriction

Batalle D, Muñoz-Moreno E, Tornador C, Bargallo N, Deco G, Eixarch E, Gratacos E

Ready to be submitted

Altered resting-state whole-brain functional networks of neonates with intrauterine growth restriction

Dafnis Batalle a, 1, Emma Muñoz-Moreno a, Cristian Tornador b, Nuria Bargallo c,d, Gustavo Deco b,e, Elisenda Eixarch a,f,g, Eduard Gratacos a,f,g

a) Fetal and Perinatal Medicine Research Group, Institut d'Investigacions Biomediques August Pi i Sunyer (IDIBAPS), Barcelona, Spain b) Center for Brain and Cognition, Computational Neuroscience Group, Department of Information and Communication Technologies, Universitat Pompeu Fabra, Barcelona, Spain c) Department of Radiology, Centre de Diagnòstic per la Imatge Clínic (CDIC), Hospital Clínic, Barcelona, Spain d) Magnetic Resonance core facility, Institut d'Investigacions Biomediques August Pi i Sunyer (IDIBAPS), Barcelona, Spain e) Institució Catalana de la Recerca i Estudis Avançats (ICREA), Universitat Pompeu Fabra, Barcelona, Spain f) Maternal-Fetal Medicine Department, ICGON, Hospital Clínic, Universitat de Barcelona, Barcelona, Spain g) Centro de Investigación Biomédica en Red de Enfermedades Raras (CIBERER), Barcelona, Spain

Submitted to Proceedings of the National Academy of Sciences of the United States of America

Intrauterine growth restriction (IUGR) is a prevalent prenatal condition that affects up to 10% of pregnancies. It has been associated with alterations in short- and long-term neurodevelopment, but its etiology and pathophysiology are still largely unknown. Although different studies have demonstrated an association of IUGR with mild structural brain changes, its effect on functional brain organization has never been assessed. In the present study, we filled this gap in the literature analyzing low-frequency fluctuations of functional MRI signal of a population of 20 neonates with IUGR and comparing them with 13 controls. Based on partial correlations of blood oxygen level-dependent (BOLD) signal averaged on 90 gray matter regions of an established anatomical atlas (AAL) we obtained whole-brain functional networks at neonatal age. Characterization of the obtained networks with graph theoretical features showed increased network infrastructure and raw efficiencies but reduced efficiency after normalization, demonstrating hyper-connected but sub-optimally organized IUGR functional brain networks. In addition, a significant association of functional network features with neurobehavioral scores was found, improving the association obtained with main clinical characteristics. Regional features were also analyzed, showing a pattern of alterations in IUGR group. Further assessment of spatio-temporal dynamics of BOLD signals displayed a tendency of an increased level of overall synchronization in IUGR as well as showing alterations into a set of features associated to frontal, cingulate and lingual cortices.

neuroimaging | *graph theory* | *resting state* | *functional MRI*

INTRODUCTION

Intrauterine growth restriction (IUGR) affects 5-10% of all pregnancies in developed countries and it is a major public health issue, being associated with short- and long-term neurodevelopmental and cognitive dysfunctions (1-3). The characterization of underlying brain alterations supporting these dysfunctions and the prediction of the subset of the population with a higher risk of altered neurodevelopmental outcomes are among the challenges of modern fetal medicine and pediatrics. Magnetic resonance imaging (MRI) has been used to characterize structural brain alterations underlying neurodevelopmental dysfunctions of subjects with IUGR at different stages of development, starting in-utero (4, 5), persisting at neonatal and early infancy (6-11) and at adolescence (12, 13). In the recent years, the knowledge of structural brain organization has significantly advanced with the assessment of the macroscopic circuitry of connections of the brain with structural brain networks obtained from MRI (14, 15). Importantly, graph theoretical features have been used to characterize brain networks (16), allowing to comprehensibly describe with a few network features the underlying brain connectivity organization. This approach has been demonstrated to be useful to characterize a wide-range of pathologies and conditions that affect brain connectivity (17). Based on anatomical and diffusion MRI, this technique has been promising in the study of IUGR, allowing to demonstrate alterations in the structural brain network organization and its association with altered neurodevelopment (18, 19). However, it remains unknown if there exists a functional brain reorganization in this population.

Since the seminal study of Biswal et al. (20), the potential of low-frequency components of resting-state functional MRI (rs-fMRI) to obtain whole-brain functional brain networks based on partial correlations of blood oxygen level-dependent (BOLD) signal (21) has been demonstrated. Several studies have demonstrated the feasibility to use rs-fMRI to characterize the functional organization of the healthy neonatal brain, opening the opportunity to characterize also the alterations in brain organization due to prenatal condition such as IUGR. Using independent component analysis (ICA), the emergence of synchronized spontaneous low-frequency rs-fMRI BOLD signals exhibiting resting state networks (RSN) has been demonstrated in studies of cross-sectional term and preterm infants both during light sedation and natural sleep (22, 23). Both ICA and seed-based correlation approaches have also been used in longitudinal studies showing the emergence of connections partially or completely matching several RSN during neonatal development, including the default mode network (24-27). However, studies considering whole-brain

Significance

The feasibility to use functional MRI during natural sleep to assess low-frequency basal brain activity fluctuations in neonates has been well demonstrated, although its potential to characterize pathologies of prenatal origin has not yet been exploited. In the present study, we used intrauterine growth restriction (IUGR) as a model of altered neurodevelopment due to prenatal condition to show the suitability of brain networks to characterize functional brain organization at neonatal age. Using graph theory features, we demonstrated a pattern of alterations in IUGR functional brain organization associated with neurodevelopmental performance. These findings show the potential of brain networks based on functional MRI to characterize brain reorganization from an early age, and their potential to develop biomarkers of altered neurodevelopment.

Reserved for Publication Footnotes

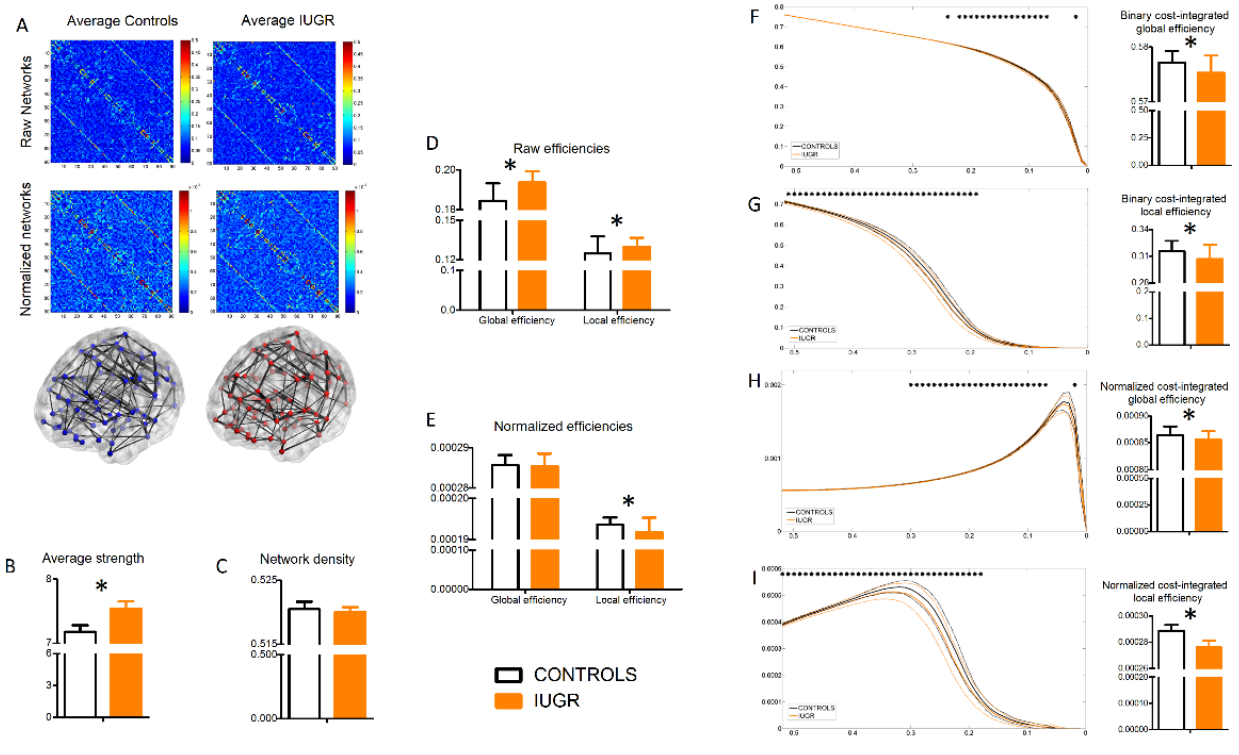

Fig. 1. Representation of control and IUGR raw and normalized functional brain networks (A). Comparison of average strength (B), network density (C), raw global and local efficiency (F) and normalized global and local efficiency between controls and IUGR. Cost-corrected values and its integration in the valid cost range (0.51-0) of binary global efficiency (F), binary local efficiency (G), normalized global efficiency (H) and normalized local efficiency (I). * p<0.05.

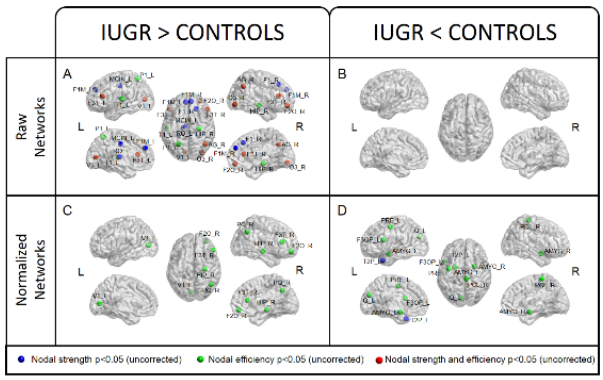

Fig. 2. Pattern of alterations in IUGR nodal weighted efficiency and nodal strength of raw and normalized networks. Raw features increased (A) and decreased (B) in IUGR group. Normalized features increased (C) and decreased (D) in IUGR group. L and R indicate left and right side of the brain respectively. Abbreviations of altered features can be consulted in Table S1.

functional brain networks of the neonatal brain are scarce in the literature. Neonatal networks composed of selected regions of interest (ROIs) were studied by Gao et al. (26), while voxel-wise networks obtained in a normalized space were obtained by Fransson et al. (28), showing the presence of cortical hubs and sub-networks associated with these hubs.

In the present study we used partial correlations of the rs-fMRI BOLD signals averaged into 90 brain regions corresponding to the anatomical automatic labeling (AAL) atlas (29) in 13 controls and 20 subjects with IUGR scanned at 44 weeks equivalent post menstrual age (PMA). We demonstrated the feasibility

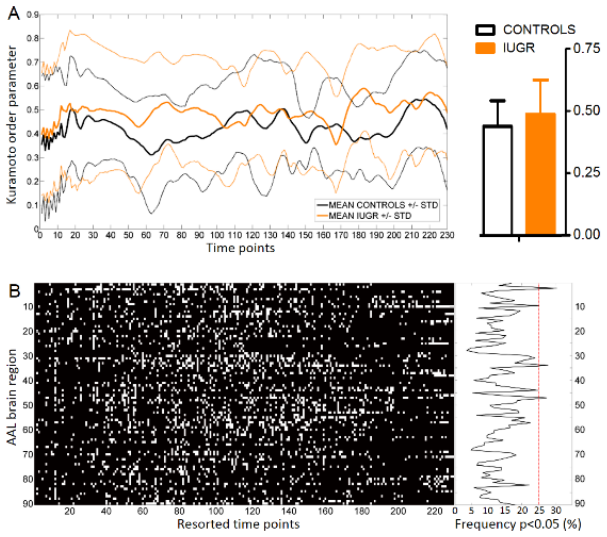

Fig. 3. (A) Kuramoto order parameter at each time point and its average value compared between cases and controls. (B) Time points where nodal efficiency is significantly different in IUGR when compared with controls and its frequency of appearance among time points. Red dotted line is set at 25.1%, corresponding to two standard deviations above mean. Regions significantly different during more than 25.1 % are left superior frontal gyrus dorsolateral part (3), right middle frontal gyrus, orbital part (10), right median cingulate and paracingulate gyri (34), and left lingual gyrus (47). $^{+}$p<0.10

to obtain whole-brain functional brain networks of the neonatal brain based on an anatomical atlas and used graph theory features to characterize alterations in the individual functional brain networks of IUGR neonates. We further characterized dynamic functional connectivity (DFC) to assess differences in temporal network synchronization to confirm previously obtained results and determine a set of nodes with altered graph theory characteristics during a significant amount of time. In addition, association of individual network features with neonatal neurobehavioral outcomes was also assessed.

RESULTS

Resting-state networks in IUGR neonates

BOLD time-series of the rs-fMRI obtained during natural sleep of 20 one-month-old neonates who suffered IUGR and 13 one-month-old controls were analyzed. Particularly, low frequency band of the time-series (0.01-0-15 Hz) was used (30). Brain was parcelled in 90 ROIs corresponding to an AAL atlas (29) adapted to the neonatal brain (31). Whole-brain functional network for each subject was obtained by means of partial correlations of the pre-processed BOLD signal averaged in each ROI. The correlation between each pair of ROIs excluding the effect of the signal common to the rest of ROIs (introduced as confounders into the partial correlation) was therefore inferred to be proportional to the connectivity of each given pair of ROIs, obtaining connectome matrices that represent RSN, as shown in Fig. 1A. See Methods section and S.I. for detailed information on the pre-processing steps and extraction of brain networks.

Infrastructure of the raw weighted partial correlation functional brain networks obtained (Fig. 1 B-D) was assessed by graph theory analysis, showing significantly increased values of IUGR average strength ($p=0.013$), global ($p=0.015$) and local efficiency ($p=0.028$). Network density, however, did not significantly differ between cases and controls.

Analysis of the pure organizational components of brain networks could be strongly influenced by differences in the network infrastructure among subjects (32). Hence, in order to isolate organization from infrastructure three different approaches were followed. Firstly, the effect of different average strength among subjects was neutralized by means of normalization of each subject's brain network by its total energy, taking into account only its relative organization to calculate global and local weighted efficiencies (Fig. 1E). As a result significantly reduced local efficiency was observed in IUGR group ($p=0.003$). Secondly, differences among subjects in network density (cost) were neutralized by means of a cost-corrected analysis (33), obtaining binary global and local efficiency features at each network cost from 0 to 0.51 at 0.01 steps (Fig. 1F-G). The maximum value of the range was fixed at 0.51 as it is the lower network density for any subject included. Using this approach, IUGR showed significantly reduced values for several costs, and importantly, when integrated among the whole valid cost-range (32), significantly reduced global efficiency ($p=0.008$) and local efficiency ($p=0.013$) were also observed. Finally, the differences in strength and network density were neutralized simultaneously by means of a combination of both methods: the weighted network obtained at each network cost was normalized by its remaining energy and weighted global and local efficiency were calculated. Using this approach, reduced values for cost-corrected weighted global and local efficiency were observed again at several network costs (Fig. 1H-I), being their cost-integrated values also significantly reduced for global and local efficiencies ($p=0.013$ and $p=0.016$ respectively). In summary, all three different approaches of normalization yielded the same conclusion: although IUGR had an increased RSN infrastructure characterized by increased average strength yielding to increased raw efficiencies, its organization was sub-optimal when compared with controls.

In addition to the analysis of global network features, in order to find the regional components that have a higher influence in the network reorganization observed in IUGR group, nodal strength and nodal efficiency were further assessed in its raw and normalized versions (Fig. 2). Nodal features of raw networks showed a pattern of alterations in IUGR for both nodal efficiency and strength in frontal areas, but also on occipital, parietal and sub-cortical regions. Nodal features of normalized networks showed a less spread pattern of alterations in IUGR, but also including some belonging to frontal, temporal and occipital cortices and sub-cortical regions such as amygdala and hippocampus. However, it is important to note that the nodal alterations reported must be considered exploratory, given that the differences observed did not withstand a false discovery rate (FDR) correction.

Dynamic functional network connectivity

Dynamic functional connectivity (DFC) has been defined as the functional connectivity over a sliding time window (34). Recently, phase synchronization has been used to solve the resolution/reliability trade-off of windowing the signal in fMRI time-series by means of conversion of the real signal into a complex analytic version, with techniques such as Hilbert transform (35). In the present study we used similar techniques to study the temporal dynamics of the ROI signals in a narrowband (0.04-0.07 Hz) comparing phase differences pair-wise and obtaining a measure of phase similarity between each pair of ROIs at each instant of time (see Methods and S.I. for a detailed explanation of the methodology used).

In order to assess if there were any notable differences in the DFC of IUGR, we first used Kuramoto order parameter R to analyze the global level of synchronization of each subject's brain at each instant of time (Fig. 3A), being zero for complete asynchrony and 1 for full synchronization. As the subject acquisition was not under specific stimuli, rather than analyzing the results in a temporal basis, the average value over time was compared. A tendency towards significance of having an increased Kuramoto order parameter was observed in IUGR group ($p=0.055$, Fig. 3A), showing that, overall, subjects with IUGR tend to present a more synchronized brain than their control counterparts. The Kuramoto order parameter was further used to sort the acquisition time-points of each individual subject, from the lowest to the highest level of synchronization of each subject's whole-brain DFC. This resorting approach allowed comparing the temporal dynamics among subjects fairly at a similar level of synchronization given a temporal instant. Particularly, we observed significantly increased values of Kuramoto order parameter for several time points in IUGR (Fig. S1A), and as expected, increased global and local efficiency for several time points (Fig. S1B-C) with a marginally non-significant tendency when averaged along all the instants of time ($p=0.060$ and $p=0.059$ respectively). Temporal alterations of nodal efficiency were also assessed, finding a pattern of nodal alterations in IUGR across time (Fig. 3B). Observing the percentage of time that each nodal efficiency is significantly different in IUGR allowed highlighting four regional features altered in IUGR more than two standard deviations above the mean: left superior frontal gyrus dorsolateral part (F1-L), right middle frontal gyrus, orbital part (F2O-R), right median cingulate and paracingulate gyri (MCIN-R), and left lingual gyrus (LIN-L). Analogous analysis of nodal strength yielded similar results, in this case being only left superior frontal gyrus, dorsolateral part (F1-L) and right middle frontal gyrus, orbital part (F2O-R) the regions found to be different during a significant amount of time.

Association with neonatal neurobehavior

Neonatal behavioral assessment scale (NBAS) (36) was used to characterize neurobehavioral outcomes in neonatal period. Association of neurobehavioral scores assessed by NBAS with global network features was assessed by means of partial correlations

controlling for weight centile, gender, gestational age (GA) and smoking status. Network density was found to be significantly correlated with social-interactive cluster (rho=0.409, p=0.042) and attention cluster (rho=0.523, p=0.006). Normalized weighted global efficiency was correlated with organization of the state (rho=0.434, p=0.027).

In addition, each NBAS cluster was normalized to a standard population and considered abnormal if scored one standard deviation below mean value. NBAS severity score was defined as the number of altered clusters (excluding habituation, see Methods and S.I. for details), hence being in a range from 0 to 5. An ordinal regression of NBAS severity score with main clinical data (GA, weight centile, gender and smoking status during pregnancy) was performed, yielding to a non-significant model (p=0.334, Chi^2=4.570, Nagelkerke R^2=0.149, df=4). However, the addition of network features significantly changed the model (p=0.003, Chi^2=28.692, df=11), allowing to obtain a statistically significant model (p=0.004, Chi^2=33.262, Nagelkerke R^2=0.706, df=15), showing significant association of graph theory features based on RSN with the severity of abnormal neurobehavioral outcome and the addition of significant information to main clinical features.

DISCUSSION

The characterization of brain changes underlying IUGR risk of having neurodevelopmental problems is a main challenge in modern fetal and pediatric medicine. A better understanding of the pathophysiology of this condition is essential to start developing early biomarkers to detect the infants at high risk of having altered neurodevelopmental problems. Importantly, it has been shown that early individualized interventions significantly improves IUGR neurobehavioral performance at short- and mid-term (37, 38). However, given the high prevalence of IUGR and the economic cost of individualized care units, selecting those IUGR infants with a higher risk is essential to appropriately advise parents and optimally use clinical resources. With this long-term goal in mind, in the present study we investigated functional brain networks in IUGR for the first time, being also the first study to characterize neonatal whole-brain RSN based on an atlas.

The results obtained showed a very specific pattern of alterations in IUGR whole-brain RSN, characterized by a hyper-connectivity of their raw networks. However, when assessing the pure organizational features by means of three different normalization procedures, we observe a sub-optimal organization in IUGR characterized by decreased global and local efficiency. Further analysis of nodal features showed a spread pattern of regional alterations in IUGR, however, not strong enough to withstand a FDR correction. Spatio-temporal analysis of the signal supported previous results, revealing a tendency of increased overall synchronization in IUGR, and a set of nodal features that might have an important role in the reorganization of functional brain networks obtained. These results, together with previously reported alterations in IUGR structural brain networks (18) support the hypothesis that IUGR is a condition strongly associated with brain organization, as has been suggested to happen with mood and psychiatric disorders. Albeit it is important to note that establishing a causality with the evidence available is still premature, association of network features with neurobehavioral performance is reported in this and other studies (18, 19), postulating IUGR as a candidate to be a brain-network disorder (39).

Interestingly, in a previous study of structural brain networks in one-year-old population, reduced fractional anisotropy (FA) weighted global and local efficiency was found in IUGR (18). Intuitively one would expect to obtain reduced efficiencies in functional brain networks because of a weaker structural connectivity, but in contrary, we obtained significantly increased raw efficiencies in IUGR neonates. A possible explanation for this discord could be the difference of age in the population under study, as it is a critical period in terms of brain connectivity changes (40). Functional and structural brain networks might also be capturing different aspects of brain organization, and they do not necessarily need to behave in the same manner. In fact, although the constraining of functional connectivity to the structural substrate has been demonstrated (41, 42), in line with our results theoretical models suggest that reduced structural connectivity could induce increased efficiency in functional brain networks (43, 44).

IUGR has been suggested to be a risk factor of developing disorders such as attention deficit hyperactive disorder (ADHD) (45, 46), autism spectrum disorders (ASD) (47, 48) and schizophrenia (49). Although there are some contradictory reports, generally ASD has been characterized by having functional hyper-connectivity of salience and default mode network (50). However, whole-brain RSN have been reported to show reduced raw local efficiency but increased global efficiency after cost-correction (51). In adult schizophrenia patients, reduced global and local efficiency after cost-correction of RSN has been reported (52), but also decreased average functional connectivity (53). RSN of children with ADHD have been reported to have increased local efficiency for several costs, although raw weighted measures have not been described (54). Overall, after comparison with the body of literature available we note a unique pattern of alterations in neonatal IUGR brain networks. This pattern of alterations must be confirmed at a later age, being the follow-up of IUGR population a crucial aspect for the characterization of the evolution of the alterations and long-term effects of this condition. The specific connectivity fingerprint trajectories that could underlie the increased prevalence of IUGR subjects developing disorders of neural development is not clear, and will also be the likely focus of future prospective studies. We hypothesize that some of the links of IUGR with neurodevelopmental disorders could be partially associated with dysfunctions in some specific regional sub-networks produced by brain reorganization. It is worthwhile to note that although partial correlation networks and temporal dynamics yield to same global functioning conclusions (IUGR has a hyper-connected, hyper-synchronized brain but with a sub-optimal organization), the regional results obtained by each of these techniques showed different altered regions, suggesting that they assess complementary features of brain organization, although both highlighted the role of frontal areas. Particularly, analysis of temporal dynamics allowed to obtain a reduced set of regions altered, comprised by frontal, cingulate and lingual cortices. In agreement with the results obtained, several frontal regions with altered structural brain network features have been previously reported in IUGR (18), while evidence of alterations in frontal-posterior networks in ASD has been reported in several studies (55). Interestingly, altered nodal efficiency of left lingual gyrus has been specifically reported in structural brain networks of IUGR (18, 19) and has also been shown to be decreased in RSN of ADHD patients (54). Concerning cingulate cortical areas, FA measures of this area have been strongly associated with altered neurobehavioral performance in a long-term rabbit model of IUGR (56). In addition, functional alterations of cingulate areas have been reported in different studies of ASD (55), schizophrenia (53) and ADHD (57).

Finding alterations in the brain network features associated to a pathology is by itself relevant for the characterization of its pathophysiology. In the case of IUGR, the results suggest that brain reorganization previously demonstrated in the structural substrate is also present at a functional level since neonatal age. This significantly improves the knowledge of this condition, serving as a potential physiological basis for the neurobehavioral alterations reported in these infants (58). Note that given the

heterogeneity of the etiology and progression of this condition, big samples are needed to find differences in neonatal neurobehavior, being even more crucial to find individualized biomarkers of the long-term prognosis of infants with IUGR in order to be able to clinically intervene. Therefore, the association found between the functional network features and NBAS is especially important, significantly improving the capacity of association obtained with basic clinical features. These results are in line with previous findings reporting an association of structural network features of structural brain networks with neurodevelopment in IUGR (18, 19). In addition, recent reports showing the feasibility to assess fMRI in fetal period reinforces the potential to use functional brain networks as an early biomarker (59). We are confident that combination of multi-modal features of brain networks will significantly improve the assessment of the risk of neurodevelopmental problems of prenatal origin since an early age, being its translation to the clinical practice in the mid-term horizon.

Finally, there are several issues of the study that must be noted. First, we would like to note that the MRI acquisition was performed during natural sleep. Previous reports have associated deepness of sleep with functional connectivity (60, 61); however, although the effects of sedation and sleep in functional connectivity are not fully understood, significant differences have not been found between sedated and non-sedated infants using ICA and seed-based correlation approaches (23, 25, 28). Importantly, neonatal sleep has been suggested to be mainly in active sleep (62), minimizing the possibility that different sleep deepness could be partially explaining some of the results obtained, being also mitigated by the case-control design of the study. Regarding the comparability of the results obtained, only a previous study assessed whole-brain networks in a neonatal population (28), however, it was performed voxel-wise in a normalized space, obtaining very large networks (4966-by-4966 elements). Albeit the use of voxel-wise networks have some advantages, constraining the networks obtained to an anatomical brain atlas allows a more comprehensible and manageable comparison among studies, especially given the broad use of AAL atlas in the literature. However, regional parcellation of the neonatal brain is also a critical issue and could be a source of bias. This was alleviated by the use of T2-weighted anatomical volumes which improve WM contrast in neonatal acquisitions (63), and by the use of a specific neonatal atlas (31). In addition, note that the use of partial correlation (instead of directly correlate the signal averaged in each region), also reduce possible sources of bias, extracting residual motion artifacts and other signal distortions that affect the whole brain.

CONCLUSIONS

In conclusion, the results presented here show for the first time the feasibility to use functional brain networks at neonatal age to characterize alterations of prenatal origin. Particularly, brain networks of a population with IUGR were assessed based on a resting-state acquisition during natural sleep, showing a unique pattern of alterations in the network organization characterized by being hyper-connected and hyper-synchronized but suboptimally organized, associated with neonatal neurobehavioral scores. In addition, dynamic functional connectivity highlighted a set of regions with temporally altered network features that could be related to impairment of specific sub-networks. Overall, the observed functional reorganization could be a potential substrate of high risk of altered neurodevelopment in infants with IUGR, and together with previous findings, postulate IUGR condition as a possible brain-network disorder. Importantly, association of network features with neurobehavior since such an early age opens the opportunity to develop early image biomarkers of altered neurodevelopment, a clinical chance to improve the management of a condition that affects 10% of the population.

MATERIALS AND METHODS

Participants, neurobehavioral assessment and MRI acquisition

The infants of the study were part of a larger prospective research program in IUGR involving fetal assessment and short- and long-term postnatal follow-up at Hospital Clínic (Barcelona, Spain). The local Ethics Comitee approved the study protocol, and written informed consent was obtained from the parents or legal guardians of all the participants (CEIC: 2012/7715). Late-onset IUGR was defined as those fetuses with estimated fetal weight below the 10th centile according to local reference standards (64) confirmed at birth and delivered after 34 weeks of pregnancy. MRI was performed around one month corrected age during natural sleep after feeding the baby. All acquired images were visually inspected for apparent artifacts and anomalies and subjects excluded accordingly. Neonatal neurobehavioral performance was assessed at neonatal age with NBAS (36), which evaluates cortical and subcortical functions in 35 items grouped into 6 clusters: habituation, motor, social-interactive, organization of state, regulation of state, autonomous nervous system and attention (65). Cluster scores were defined as abnormal if they have a z-score below minus one. NBAS severity score was defined as the number of abnormal NBAS clusters for each subject. Functional MRI data was acquired using gradient echo planar imaging (EPI) consisting in volumes of 42 axial slices with a spatial resolution of 2 x 2 x 2 mm^3. Resting-state functional connectivity was assessed during 8 minutes of natural sleep (240 EPI volumes).

Pre-processing, network extraction and analysis

T2-weighted volumes were skull-striped (66) and segmented into WM, gray matter (GM) and cerebrospinal fluid (CSF) (67) using neonatal tissue probability maps (31). AAL atlas (29) adapted to neonatal population in a T2-weighted template (31) was used to parcellate each subject' brain into 90 regions based on an elastic transformation. Image preprocessing included correction of intra-volume time differences and inter-volume geometric displacements, regression of head motion effects in the signal, average of time series corresponding to each ROI and band pass filtering (0.01 – 0.15 Hz). Network edges were calculated as the partial correlation coefficients obtained between the average signals of each pair of ROIs excluding the effects of the signal of the other 88 ROIs. Negative correlation coefficients were excluded. In order to disentangle network infrastructure from network organization, three different normalization approaches were followed: 1) different average strength among subjects was neutralized by means of normalization of each subject's brain network by its total energy; 2) differences of network density (cost) were neutralized by means of a cost-corrected analysis of network features (33); 3) effect of differences in strength and density were neutralized at the same time by means of a combination of both methods, obtaining the weighted network at each network cost and normalizing it as described in the strength normalization approach. Global functioning of each network was assessed by its infrastructure (network density and average strength), integration (global efficiency) and segregation (local efficiency). Regional characteristics were evaluated by means of nodal strength and nodal efficiency. Calculation of the graph theory features used to assess each network was based on the definitions and code compiled by Rubinov and Sporns (68).

Dynamic functional connectivity

Dynamic functional connectivity was characterized in a narrowband (0.04-0.07 Hz), allowing the application of Hilbert transform to extract the phases obtaining an analytic signal representing the narrowband signal $s(t)$ as a rotating vector with an instant phase $\varphi(t)$ and an instant amplitude $A(t)$: $s(t) = A(t)cos(\varphi(t))$. Global level of phase synchrony among all brain areas was quantified with Kuramoto order parameter. Further analysis involved the calculation of phase similarity between each pair of regions for each instant of time, giving a weight $w_{ij}^{H}(t)$ at each instant of time for each pair of regions i and j as $w_{ij}^{H}(t) = \left|\frac{\Delta\varphi_{ij}(t)-\pi}{\pi}\right|$. Using this approach, a weighted connectivity matrix based on the phase similarity was constructed at each instant of time. However, given that the subjects are not receiving comparable stimuli during the acquisition time, Kuramoto order parameter was used to resort temporal axis according to the relative level of global synchronization of each subject, from its lowest to its highest level. The temporal features obtained for each subject were resorted accordingly being comparable as they are obtained based on the same relative level of synchronization.

Statistical analysis

Comparisons among groups were performed by general linear models (GLM) with gender as co-factor and GA and PMA at MRI as co-variables. Significance was declared at p<0.05 (uncorrected). Regional alterations were shown using BrainNet viewer (69). Association of network features obtained with NBAS in IUGR group was performed by means of partial correlations using gender, GA and smoking status as confounder factors. The software package SPSS 18.0 (SPSS, Chicago, IL) was used for the statistical analyses. Computational algorithms were implemented using MATLAB (2009b, The MathWorks Inc., Natick, MA).

ACKNOWLEDGEMENTS.

The authors would like to thank Cesar Garrido for his help and advice in the design and performance of the acquisition scheme. The images used were

acquired in the Magnetic Resonance core facility of Institut d'Investigacions Biomèdiques August Pi I Sunyer (IDIBAPS), Barcelona, Spain. This work was supported by grants: Obra Social "la Caixa", Barcelona, Spain; Fondo de Investigación Sanitaria (PI12/00851) and Sara Borrell grant from Carlos III Institute of Health, Spain (grant number CD11/00048 to E.M.).

1. Arcangeli T, Thilaganathan B, Hooper R, Khan KS, & Bhide A (2012) Neurodevelopmental delay in small babies at term: a systematic review. *Ultrasound Obstet Gynecol* 40(3):267-275.
2. Baschat AA (2013) Neurodevelopment after Fetal Growth Restriction. *Fetal Diagn Ther* E-pub ahead of print.
3. Løhaugen GC, *et al.* (2013) Small for gestational age and intrauterine growth restriction decreases cognitive function in young adults. *J Pediatr* 163(2):447-453.
4. Egaña-Ugrinovic G, Sanz-Cortes M, Figueras F, Bargallo N, & Gratacos E (2013) Differences in cortical development assessed by fetal MRI in late-onset intrauterine growth restriction. *Am J Obstet Gynecol* 209(2):126 e121-128.
5. Sanz-Cortes M, *et al.* (2013) Automatic quantitative MRI texture analysis in small-for-gestational-age fetuses discriminates abnormal neonatal neurobehavior. *PLoS One* 8(7):e69595.
6. Tolsa CB, *et al.* (2004) Early alteration of structural and functional brain development in premature infants born with intrauterine growth restriction. *Pediatr Res* 56(1):132-138.
7. Lodygensky GA, *et al.* (2008) Intrauterine growth restriction affects the preterm infant's hippocampus. *Pediatr Res* 63(4):438-443.
8. Dubois J, *et al.* (2008) Primary cortical folding in the human newborn: an early marker of later functional development. *Brain* 131:2028-2041.
9. Padilla N, *et al.* (2011) Differential effects of intrauterine growth restriction on brain structure and development in preterm infants: a magnetic resonance imaging study. *Brain Res* 1382:98-108.
10. Esteban FJ, *et al.* (2010) Fractal-dimension analysis detects cerebral changes in preterm infants with and without intrauterine growth restriction. *Neuroimage* 53(4):1225-1232.
11. De Bie HM, *et al.* (2011) Global and regional differences in brain anatomy of young children born small for gestational age. *PLoS One* 6(9):e24116.
12. Martinussen M, *et al.* (2009) Segmental brain volumes and cognitive and perceptual correlates in 15-year-old adolescents with low birth weight. *J Pediatr* 155(6):848-853 e841.
13. Skranes JS, *et al.* (2005) Cerebral MRI findings in very-low-birth-weight and small-for-gestational-age children at 15 years of age. *Pediatr Radiol* 35(8):758-765.
14. Hagmann P (2005) From diffusion MRI to brain connectomics. (Ecole Polytechnique Fêdêrale de Lausanne (EPFL), Lausane).
15. Sporns O, Tononi G, & Kotter R (2005) The human connectome: A structural description of the human brain. *PLoS Comput Biol* 1(4):e42.
16. Bullmore E & Sporns O (2009) Complex brain networks: graph theoretical analysis of structural and functional systems. *Nat Rev Neurosci* 10(3):186-198.
17. Bassett DS & Bullmore ET (2009) Human brain networks in health and disease. *Curr Opin Neurol* 22(4):340-347.
18. Batalle D, *et al.* (2012) Altered small-world topology of structural brain networks in infants with intrauterine growth restriction and its association with later neurodevelopmental outcome. *Neuroimage* 60(2):1352-1366.
19. Batalle D, *et al.* (2013) Normalization of similarity-based individual brain networks from gray matter MRI and its association with neurodevelopment in infants with intrauterine growth restriction. *Neuroimage* 83C:901-911.
20. Biswal B, Yetkin FZ, Haughton VM, & Hyde JS (1995) Functional connectivity in the motor cortex of resting human brain using echo-planar MRI. *Magn Reson Med* 34(4):537-541.
21. Salvador R, *et al.* (2005) Neurophysiological architecture of functional magnetic resonance images of human brain. *Cereb Cortex* 15(9):1332-1342.
22. Fransson P, *et al.* (2007) Resting-state networks in the infant brain. *Proc Natl Acad Sci U S A* 104(39):15531-15536.
23. Fransson P, *et al.* (2009) Spontaneous brain activity in the newborn brain during natural sleep--an fMRI study in infants born at full term. *Pediatr Res* 66(3):301-305.
24. Smyser CD, *et al.* (2010) Longitudinal analysis of neural network development in preterm infants. *Cereb Cortex* 20(12):2852-2862.
25. Doria V, *et al.* (2010) Emergence of resting state networks in the preterm human brain. *Proc Natl Acad Sci U S A* 107(46):20015-20020.
26. Gao W, *et al.* (2009) Evidence on the emergence of the brain's default network from 2-week-old to 2-year-old healthy pediatric subjects. *Proc Natl Acad Sci U S A* 106(16):6790-6795.
27. Lin W, *et al.* (2008) Functional connectivity MR imaging reveals cortical functional connectivity in the developing brain. *AJNR Am J Neuroradiol* 29(10):1883-1889.
28. Fransson P, Aden U, Blennow M, & Lagercrantz H (2011) The functional architecture of the infant brain as revealed by resting-state fMRI. *Cereb Cortex* 21(1):145-154.
29. Tzourio-Mazoyer N, *et al.* (2002) Automated anatomical labeling of activations in SPM using a macroscopic anatomical parcellation of the MNI MRI single-subject brain. *NeuroImage* 15:273-289.
30. Braun U, *et al.* (2011) Test-retest reliability of resting-state connectivity network characteristics using fMRI and graph theoretical measures. *Neuroimage* 59(2):1404-1412.
31. Shi F, *et al.* (2011) Infant brain atlases from neonates to 1- and 2-year-olds. *PLoS One* 6(4):e18746.
32. Ginestet CE, Nichols TE, Bullmore ET, & Simmons A (2011) Brain network analysis: separating cost from topology using cost-integration. *PLoS One* 6(7):e21570.
33. Achard S & Bullmore E (2007) Efficiency and cost of economical brain functional networks. *PLoS Comput Biol* 3(2):e17.
34. Sakoglu U, *et al.* (2010) A method for evaluating dynamic functional network connectivity and task-modulation: application to schizophrenia. *MAGMA* 23(5-6):351-366.
35. Glerean E, Salmi J, Lahnakoski JM, Jaaskelainen IP, & Sams M (2012) Functional magnetic resonance imaging phase synchronization as a measure of dynamic functional connectivity. *Brain Connect* 2(2):91-101.
36. Nugent J & Brazelton T (2000) *Preventive mental health: Uses of the Brazelton Scale* (Wiley, New York, NY).
37. Als H, *et al.* (2012) NIDCAP improves brain function and structure in preterm infants with severe intrauterine growth restriction. *J Perinatol* 32(10):797-803.
38. McAnulty G, *et al.* (2013) School-age effects of the newborn individualized developmental care and assessment program for preterm infants with intrauterine growth restriction: preliminary findings. *BMC Pediatr* 13:25.
39. Rubinov M & Bullmore E (2013) Fledgling pathoconnectomics of psychiatric disorders. *Trends Cogn Sci* 17(12):641-647.
40. Yap PT, *et al.* (2011) Development trends of white matter connectivity in the first years of life. *PLoS ONE* 6(9):e24678.
41. Honey CJ, *et al.* (2009) Predicting human resting-state functional connectivity from structural connectivity. *Proc Natl Acad Sci U S A* 106(6):2035-2040.
42. Deco G, *et al.* (2013) Resting-state functional connectivity emerges from structurally and dynamically shaped slow linear fluctuations. *J Neurosci* 33(27):11239-11252.
43. Cabral J, Hugues E, Kringelbach ML, & Deco G (2012) Modeling the outcome of structural disconnection on resting-state functional connectivity. *Neuroimage* 62(3):1342-1353.
44. Cabral J, Kringelbach ML, & Deco G (2012) Functional graph alterations in schizophrenia: a result from a global anatomic decoupling? *Pharmacopsychiatry* 45 Suppl 1:S57-64.
45. Heinonen K, *et al.* (2010) Behavioural symptoms of attention deficit/hyperactivity disorder in preterm and term children born small and appropriate for gestational age: a longitudinal study. *BMC pediatrics* 10:91.
46. Linnet KM, *et al.* (2006) Gestational age, birth weight, and the risk of hyperkinetic disorder. *Arch Dis Child* 91(8):655-660.
47. Moore GS, Kneitel AW, Walker CK, Gilbert WM, & Xing G (2012) Autism risk in small- and large-for-gestational-age infants. *Am J Obstet Gynecol* 206(4):314 e311-319.
48. Gardener H, Spiegelman D, & Buka SL (2011) Perinatal and neonatal risk factors for autism: a comprehensive meta-analysis. *Pediatrics* 128(2):344-355.
49. Nielsen PR, *et al.* (2013) Fetal growth and schizophrenia: a nested case-control and case-sibling study. *Schizophr Bull* 39(6):1337-1342.
50. Menon V (2013) Developmental pathways to functional brain networks: emerging principles. *Trends Cogn Sci* 17(12):627-640.
51. Rudie JD, *et al.* (2012) Altered functional and structural brain network organization in autism. *Neuroimage Clin* 2:79-94.
52. Liu Y, *et al.* (2008) Disrupted small-world networks in schizophrenia. *Brain* 131(Pt 4):945-961.
53. Lynall ME, *et al.* (2010) Functional connectivity and brain networks in schizophrenia. *J Neurosci* 30(28):9477-9487.
54. Wang L, *et al.* (2009) Altered small-world brain functional networks in children with attention-deficit/hyperactivity disorder. *Hum Brain Mapp* 30(2):638-649.
55. Maximo JO, Cadena EJ, & Kana RK (2014) The Implications of Brain Connectivity in the Neuropsychology of Autism. *Neuropsychol Rev*.
56. Illa M, *et al.* (2013) Long-Term Functional Outcomes and Correlation with Regional Brain Connectivity by MRI Diffusion Tractography Metrics in a Near-Term Rabbit Model of Intrauterine Growth Restriction. *PLoS ONE* 8(10):e76453.
57. De La Fuente A, Xia S, Branch C, & Li X (2013) A review of attention-deficit/hyperactivity disorder from the perspective of brain networks. *Front Hum Neurosci* 7:192.
58. Figueras F, *et al.* (2009) Neurobehavior in term, small-for-gestational age infants with normal placental function. *Pediatrics* 124(5):e934-941.
59. Thomason ME, *et al.* (2013) Cross-hemispheric functional connectivity in the human fetal brain. *Science translational medicine* 5(173):173ra124.
60. Larson-Prior LJ, *et al.* (2009) Cortical network functional connectivity in the descent to sleep. *Proc Natl Acad Sci U S A* 106(11):4489-4494.
61. Horovitz SG, *et al.* (2009) Decoupling of the brain's default mode network during deep sleep. *Proc Natl Acad Sci U S A* 106(27):11376-11381.
62. Biagioni E, *et al.* (2005) Distribution of sleep and wakefulness EEG patterns in 24-h recordings of preterm and full-term newborns. *Early Hum Dev* 81(4):333-339.
63. Williams LA, *et al.* (2005) Neonatal brain: regional variability of in vivo MR imaging relaxation rates at 3.0 T--initial experience. *Radiology* 235(2):595-603.
64. Figueras F, *et al.* (2008) Customized birthweight standards for a Spanish population. *Eur J Obstet Gynecol Reprod Biol* 136(1):20-24.
65. Sagiv SK, *et al.* (2008) Prenatal organochlorine exposure and measures of behavior in infancy using the Neonatal Behavioral Assessment Scale (NBAS). *Environ Health Perspect* 116(5):666-673.
66. Smith SM (2002) Fast robust automated brain extraction. *Hum Brain Mapp* 17(3):143-155.
67. Ashburner J & Friston KJ (2005) Unified segmentation. *Neuroimage* 26(3):839-851.
68. Rubinov M & Sporns O (2009) Complex network measures of brain connectivity: uses and interpretations. *Neuroimage* 52(3):1059-1069.
69. Xia M, Wang J, & He Y (2013) BrainNet Viewer: a network visualization tool for human brain connectomics. *PLoS One* 8(7):e68910.

==EndOfDocument==

Supplementary Information: Altered resting-state whole-brain functional brain networks of neonates with intrauterine growth restriction

Dafnis Batalle [a, 1], Emma Muñoz-Moreno [a], Cristian Tornador [b], Nuria Bargallo [c,d], Gustavo Deco [b,e], Elisenda Eixarch [a,f,g], Eduard Gratacos [a,f,g]

a) Fetal and Perinatal Medicine Research Group, Institut d'Investigacions Biomediques August Pi i Sunyer (IDIBAPS), Barcelona, Spain b) Center for Brain and Cognition, Computational Neuroscience Group, Department of Information and Communication Technologies, Universitat Pompeu Fabra, Barcelona, Spain c) Centre de Diagnòstic per la Imatge Clínic (CDIC), Hospital Clínic, Barcelona, Spain d) Clinical Imaging Research, Institut d'Investigacions Biomediques August Pi i Sunyer (IDIBAPS), Barcelona, Spain e) Institució Catalana de la Recerca i Estudis Avançats (ICREA), Universitat Pompeu Fabra, Barcelona, Spain f) Maternal-Fetal Medicine Department, ICGON, Hospital Clínic, Universitat de Barcelona, Barcelona, Spain g) Centro de Investigación Biomédica en Red de Enfermedades Raras (CIBERER), Barcelona, Spain

Participants

The infants of the study were part of a larger prospective research program in IUGR involving fetal assessment and short- and long-term postnatal follow-up at Hospital Clínic (Barcelona, Spain). The local Ethics Comitee approved the study protocol, and written informed consent was obtained from the parents or legal guardians of all the participants (CEIC: 2012/7715). The original sample of the study included a sample of 45 pregnancies with 30 late-onset IUGR and 15 control fetuses. Late-onset IUGR was defined as those fetuses with estimated fetal weigth below the 10^{th} centile according to local reference standards (1) confirmed at birth and delivered after 34 weeks of pregnancy. Control subjects were sampled from general pregnant population and defined as fetuses with fetal estimated weight between 10^{th} and 90^{th} centile confirmed at birth. Infants with chromosomal, genetic or structural defects and signs of intrauterine infection or neonatal onset sepsis were excluded from the study. Neonatal data was prospectively recorded including GA, birth weight, gender, Apgar at 5 min, umbilical artery pH, neonatal complications and maternal smoking status during pregnancy.

MRI was performed around one month corrected age during natural sleep after feeding the baby. An expert neuroradiologist analyzed anatomical images and those infants without overt brain lesions were further analyzed. In addition, all acquired images were visually inspected for apparent artifacts and subjects excluded accordingly. Thus, ten of 30 cases and two of the 15 controls were excluded from the study due to WM lesions, awakening or excessive movement

during acquisition, obtaining a final sample of 13 controls (5 males) and 20 subjects with IUGR (13 males). The average GA at birth was 38 weeks and 5 days (range 34 weeks and 2 days to 42 weeks) and the average PMA at MRI acquisition was 43 weeks and 3 days (range 39 weeks and 6 days to 48 weeks and 3 days). Particular care was taken in order to ensure neonatal welfare during the MR acquisition. A pulseoximetry probe was placed around the baby's wrist to monitor oxygen saturation levels throughout the scan, and acoustic noise was minimized with the use of neonatal ear muffs (MiniMuffs ® Neonatal Noise Attenuators, Natus Medical Incorporated, USA). The infant was swaddled with one or two infant sheets before being placed within a vacuum immobilizer, air was removed from the bag and the infant was contained within a rigid cradle that is shaped to its body, effectively swaddling the infant. The lighting in the scanner room was reduced to aid the infant's sleep but was kept at a level that allows safely monitoring.

Neonatal neurobehavioral performance was assessed at neonatal age with NBAS (2), which evaluates cortical and subcortical functions in 35 items grouped into 6 clusters: habituation, motor, social-interactive, organization of state, regulation of state, autonomous nervous system and attention (3). Cluster scores were transformed to z-scores according to a standard population (3, 4) and defined as abnormal if they have a z-score below minus one. NBAS severity score was defined as the number of abnormal NBAS clusters for each subject. Due to the low successful rate of obtention of habituation cluster (12 out of 33), it was excluded from the calculation of NBAS severity score. Therefore, it was only calculated on 29 out of 33 subjects that had valid estimation of social-interactive, organization of the state, regulation of the state, autonomous nervous system and attention clusters, in a range from 0 to 5.

MRI acquisition

MRI acquisition was performed with a TIM TRIO 3.0 T whole body MR scanner (Siemens, Germany). Anatomical T2-weighted acquisition consisted in 45 axial slices with 2-mm slice thickness, in-plane acquisition matrix of 256 x 256, FoV = 160 x 160 mm^2, resulting in a resolution of 0.625 x 0.625 x 2 mm^3, repetition time (TR) = 5460 ms and echo time (TE) = 91 ms. Functional MRI data were acquired using gradient echo planar imaging (EPI) consisting in volumes of 42 axial slices with 2-mm slice thickness, in-plane acquisition matrix of 80 x 80, FoV

= 160 x 160 mm^2, yielding a spatial resolution of 2 x 2 x 2 mm^3, TR = 2000 ms, TE = 20 ms. Resting-state functional connectivity was assessed during 8 minutes of natural sleep (240 EPI volumes). The first ten volumes were discarded to allow accommodating T1-equilibrium processes. The acquisition protocol included other sequences not used in this study, having a total scanning time of ~30-45 min.

Pre-processing and network extraction

All anatomical T2-weighted volumes were first skull-striped using BET (5). Brain tissue was segmented into WM, gray matter (GM) and cerebrospinal fluid (CSF) with unified segmentation model (6) available with SPM8. The default adult templates were replaced with specific neonatal tissue probability maps (7). AAL atlas (8) recently adapted to neonatal population in a T2-weighted template (7) was used to parcellate each subject into 90 cortical and sub-cortical regions. Particularly, a customized software implementing a consistent version (9) of a block matching algorithm (10) was used to obtain an elastic transformation matching the template with each subject's T2 volume. AAL labels were propagated to each subject using this elastic transformation with discrete labeling preserved by nearest neighbor interpolation.

Image preprocessing of BOLD images was mainly performed with SPM8 package. First, intra-volume time differences between slices were corrected. Inter-volume geometric displacements were corrected using a six-parameter rigid transformation for each acquired volume and spatially smoothed using a Gaussian kernel with 2 mm full width at half maximum. Correction of head motion effects in the signal was performed by regressing out the 6-parameter head motion profiles previously estimated in each voxel across all the acquisition time. GM/WM/CSF segmentation and AAL ROI parcellation obtained in T2 anatomical volume were registered to an averaged BOLD volume using an affine transformation. The representative averaged time series corresponding to each ROI were estimated for those voxels belonging to the GM mask and band pass filtered (0.01 – 0.15 Hz). This "broad band" has been suggested to be the more reliable for graph theory analysis (11). Network edges were calculated as the partial correlation coefficients obtained between each pair of ROI averaged signal excluding the effects of the signal of the other 88 ROIs, obtaining a 90 x 90 partial correlation matrix for each subject. Pearson coefficients were transformed according to Fisher z-

transformation, negative correlation coefficients were excluded. The resulting weighted matrix was considered to represent the raw connectivity of the RSN of each subject.

Network normalization

In order to disentangle network infrastructure from network organization, i.e., evaluate the organization of networks independently of their average strength and density (cost), three different approaches were followed. First, different average strength among subjects was neutralized by means of normalization of each subject's brain network by its total energy, that is, given a network C with weights $w_{i,j}$ for each pair of nodes *i*, *j*, we defined a normalized version of the network C^{norm} with normalized weights defined as $w_{i,j}^{norm} = w_{i,j} / \sum_{\forall i,j} w_{i,j}$. Secondly, differences of network density (cost) were neutralized by means of a cost-corrected analysis of network features (12). Following this approach a binary network was created at different network costs, selecting for each cost-value *x* the connections with a strongest weight that yield to a cost *x*. The cost range was limited by the minimum value of network density for any subject included into the analysis, which is the maximum network cost where is possible to fairly compare among all the subjects. Finally, the effect of differences in strength and density were neutralized at the same time by means of a combination of both methods: instead of obtaining a binary network at each network cost, as it was performed in the second approach, the weighted network obtained at each network cost was considered in this third approach. Given that weighted features are much related to the strength of a network (weighted cost), to obtain pure organizational descriptors, the weighted networks obtained at each network cost were normalized as described in the strength normalization approach. More formally, for a given network $C(i,j) = w_{i,j}$ were $w_{i,j}$ represents the weight of the connection between nodes *i* and *j*, we defined a cost-corrected network $C_w(i,j,x)$ for each value of cost x. Note that $C_w(i,j,x) = w_{i,j}(x)$ were $w_{i,j}(x) = w_{i,j}$ if the link between node *i* and *j* belongs to the subset of strongest connections that ensure a network density of x and $w_{i,j}(x) = 0$ otherwise. In this context, normalized cost-corrected network at cost x was defined as $C_w^{norm}(i,j,x) = w_{i,j}(x) / \sum_{\forall i,j} w_{i,j}(x)$.

Network analysis

Graph theory features allow to summarize infrastructure and organization of a brain network represented as an adjacency matrix (binary or weighted). Global functioning of each network was assessed by its infrastructure (average strength), integration (global efficiency) and segregation (local efficiency). Regional characteristics were evaluated by means of nodal strength, assessing the total connectivity of a node in a given network, and nodal efficiency, measuring the efficiency of the sub-network associated to a given node. Nodes with a high nodal efficiency indicate a high tolerance of the network to the elimination of the given node, which is associated to a high clustering of the neighborhood of this node (12). Formulation and calculation of the graph theory features used to assess each network was based on the definitions and code compilated by Rubinov and Sporns (13).

Dynamic functional connectivity

Dynamic functional connectivity was characterized by means of the analysis of spatio-temporal dynamics of resting state activity in a narrowband (0.04-0.07 Hz) between each pair of ROIs. Narrowband filtering of the signal allows the application of the Hilbert transform to extract the phases obtaining an analytic signal. This analytic signal represent the narrowband signal *s(t)* as a rotating vector with an instant phase *φ(t)* and an instant amplitude *A(t)*, i.e., $s(t) = A(t)\cos(\varphi(t))$. Phase of the signal was obtained from the complex signal $z(t) = s(t) + i.\mathrm{H}[s(t)]$ were *i* is the imaginary unit and H[*s(t)*] is the Hilbert transform of *s(t)*. Global level of phase synchrony among all brain areas was quantified with Kuramoto order parameter *R(t)*, defined as $R(t) = \left|\frac{1}{N}\sum_{j=1}^{N} e^{i\varphi_j(t)}\right|$, where N is the number of ROIs. Kuramoto order parameter quantifies the level of global synchronization of a collection of phase oscillators, being constrained between 0 and 1 increasing monotonically as a function of the level of global synchronization between all pairs of ROIs in the system, 0 representing total asynchrony and 1 representing total asynchrony. As Kuramoto order parameter is defined at each time point, describing the evolution of spatial coherence as a function of time, it was averaged across all time points in order to obtain a global feature characterizing the average level of synchronization of each subject.

Further analysis involved the calculation of a measure of phase similarity between each pair of regions for each instant of time. Hence, the level of synchronization between a pair of brain

areas was considered to be inversely proportional to their phase difference, giving them a weight $w_{ij}^{H}(t)$ at each instant of time as $w_{ij}^{H}(t) = \left|\frac{\Delta\varphi_{ij}(t)-\pi}{\pi}\right|$. Note that as $\Delta\varphi_{ij}(t)$ is constrained between 0 and π, $w_{ij}^{H}(t)$ will be constrained between 0 and 1, being $w_{ij}^{H}(t) = 1$ when the phase of the two regions is identical. Using this approach, a weighted connectivity matrix based on the phase similarity was constructed at each instant of time, allowing to obtain temporal-dependent global and regional network features that assess dynamic functional connectivity organization.

However, given that the subjects are not receiving comparable stimuli during the acquisition time, features obtained at each time point are not easily comparable among subjects. Hence, we used Kuramoto order parameter to resort temporal axis according to the relative level of global synchronization of each subject, from its lowest to its highest level. Therefore, the temporal features obtained for each subject were resorted and can be compared as they are obtained based on the same relative level of synchronization.

Table S1. Regions of interest used as nodes in structural brain networks, corresponding to the regions defined in AAL atlas.

Anatomical regions	Label	Anatomical regions	Label
Precentral gyrus	PRE	Lingual gyrus	LING
Superior frontal gyrus, dorsolateral	F1	Superior occipital gyrus	O1
Superior frontal gyrus, orbital	F1O	Middle occipital gyrus	O2
Middle frontal gyrus	F2	Inferior occipital gyrus	O3
Middle frontal gyrus, orbital part	F2O	Fusiform gyrus	FUSI
Inferior frontal gyrus, opercular part	F3OP	Postcentral gyrus	POST
Inferior frontal gyrus, triangular part	F3T	Superior parietal gyrus	P1
Inferior frontal gyrus, orbital part	F3O	Inferior parietal, but supramarginal and angular gyri	P2
Rolandic operculum	RO	Supramarginal gyrus	SMG
Supplementary motor area	SMA	Angular gyrus	AG
Olfactory cortex	OC	Precuneus	PQ
Superior frontal gyrus, medial	F1M	Paracentral lobule	PCL
Superior frontal gyrus, medial orbital	F1MO	Caudate nucleus	CAU
Gyrus rectus	GR	Lenticular nucleus, putamen	PUT
Insula	IN	Lenticular nucleus, pallidum	PAL
Anterior cingulate and paracingulate gyri	ACIN	Thalamus	THA
Median cingulate and paracingulate gyri	MCIN	Heschl gyrus	HES
Posterior cingulate gyrus	PCIN	Superior temporal gyrus	T1
Hippocampus	HIP	Temporal pole: superior temporal gyrus	T1P
Parahippocampal gyrus	PHIP	Middle temporal gyrus	T2
Amygdala	AMYG	Temporal pole: middle temporal gyrus	T2P
Calcarine fissure and surrounding cortex	V1	Inferior temporal gyrus	T3
Cuneus	Q	Cerebelum	CER
		Vermis	VER

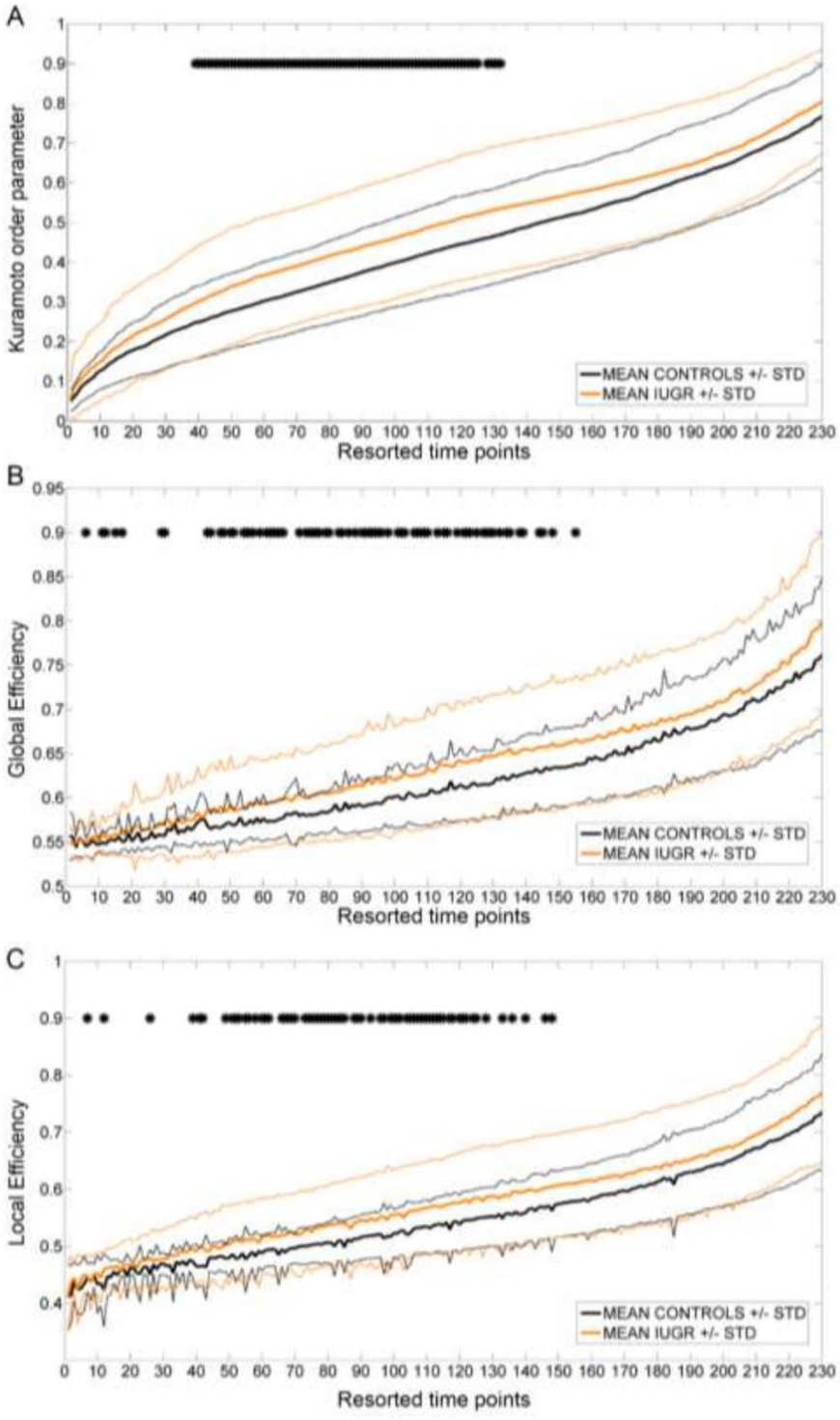

Figure S1. Comparison of control and IUGR Kuramoto order parameter (A), global (B) and local efficiency (C). Time points were resorted according to relative Kuramoto order parameter for each subject, from its lowest to its highest value.

SUPPORTING REFERENCES

1. Figueras F*, et al.* (2008) Customized birthweight standards for a Spanish population. *Eur J Obstet Gynecol Reprod Biol* 136(1):20-24.
2. Nugent J & Brazelton T (2000) *Preventive mental health: Uses of the Brazelton Scale* (Wiley, New York, NY).
3. Sagiv SK*, et al.* (2008) Prenatal organochlorine exposure and measures of behavior in infancy using the Neonatal Behavioral Assessment Scale (NBAS). *Environ Health Perspect* 116(5):666-673.
4. Costas Moragas C, Fornieles Deu A, Botet Mussons F, Boatella Costa E, & de Caceres Zurita ML (2007) [Psychometric evaluation of the Brazelton Scale in a sample of Spanish newborns]. *Psicothema* 19(1):140-149.
5. Smith SM (2002) Fast robust automated brain extraction. *Hum Brain Mapp* 17(3):143-155.
6. Ashburner J & Friston KJ (2005) Unified segmentation. *Neuroimage* 26(3):839-851.
7. Shi F*, et al.* (2011) Infant brain atlases from neonates to 1- and 2-year-olds. *PLoS One* 6(4):e18746.
8. Tzourio-Mazoyer N*, et al.* (2002) Automated anatomical labeling of activations in SPM using a macroscopic anatomical parcellation of the MNI MRI single-subject brain. *NeuroImage* 15:273-289.
9. Tristan-Vega A & Arribas JI (2007) A Fast B-Spline Pseudo-inversion Algorithm for Consistent Image Registration. *Proceedings of the International Conference on Computer Analysis Images and Patterns (CAIP)*, pp 768-775.
10. Warfield SK*, et al.* (2002) Advanced Nonrigid Registration Algorithms for Image Fusion. *Brain Mapping: The Methods*, eds Mazziotta JC & Toga AW (Elsevier), 2nd Ed Vol 24, pp 661-690.
11. Braun U*, et al.* (2011) Test-retest reliability of resting-state connectivity network characteristics using fMRI and graph theoretical measures. *Neuroimage* 59(2):1404-1412.
12. Achard S & Bullmore E (2007) Efficiency and cost of economical brain functional networks. *PLoS Comput Biol* 3(2):e17.
13. Rubinov M & Sporns O (2009) Complex network measures of brain connectivity: uses and interpretations. *Neuroimage* 52(3):1059-1069.

6. SUPPLEMENTARY RESULTS

6.1. Supplementary results of PROJECT 1 (I): normalized structural brain network features of one-year-old infants with IUGR

In the first published paper, the assessment of normalized brain network features was not included, in part given that some key points of the methodology were introduced in the following studies. To solve this issue, and allow a fairly comparison of all the results presented, in this section we present the results of normalizing the structural brain networks assessed in **PROJECT 1**.

Following the methodology introduced in previous sections, structural brain networks of one-year-old infants were normalized following three different approaches. First, the networks obtained were assessed independently of the average network strength, by means of a normalization of the weighted network by the total energy of each individual weighted brain network. With this approach we did not find any statistical significant differences, but a tendency of IUGR to have increased normalized FA-weighted local efficiency was observed ($p=0.094$). The second approach consisting on neutralizing differences in network density with cost-correction did not yield significant differences after cost-integration for FA weights (Figure 1) or FN weights.

The third approach assesses weighted network organization independently to the effects of network cost and differences in average strength by cost-correction and normalization by the energy of each subject network at each level of cost. Using this technique we observed an increased FA-weighted global efficiency at an isolated point of network cost (Figure 2), and a tendency towards significance after integrating among all the network cost range (0 to 0.51 at 0.01 steps), weighted global efficiency ($p=0.095$). No relevant results were obtained using FN weights.

The results presented in this section support the idea that infants that suffered IUGR, albeit having a reduced structural brain network infrastructure, present a tendency to have a more optimal brain network organization consistent with the hypothesis of a compensatory effect.

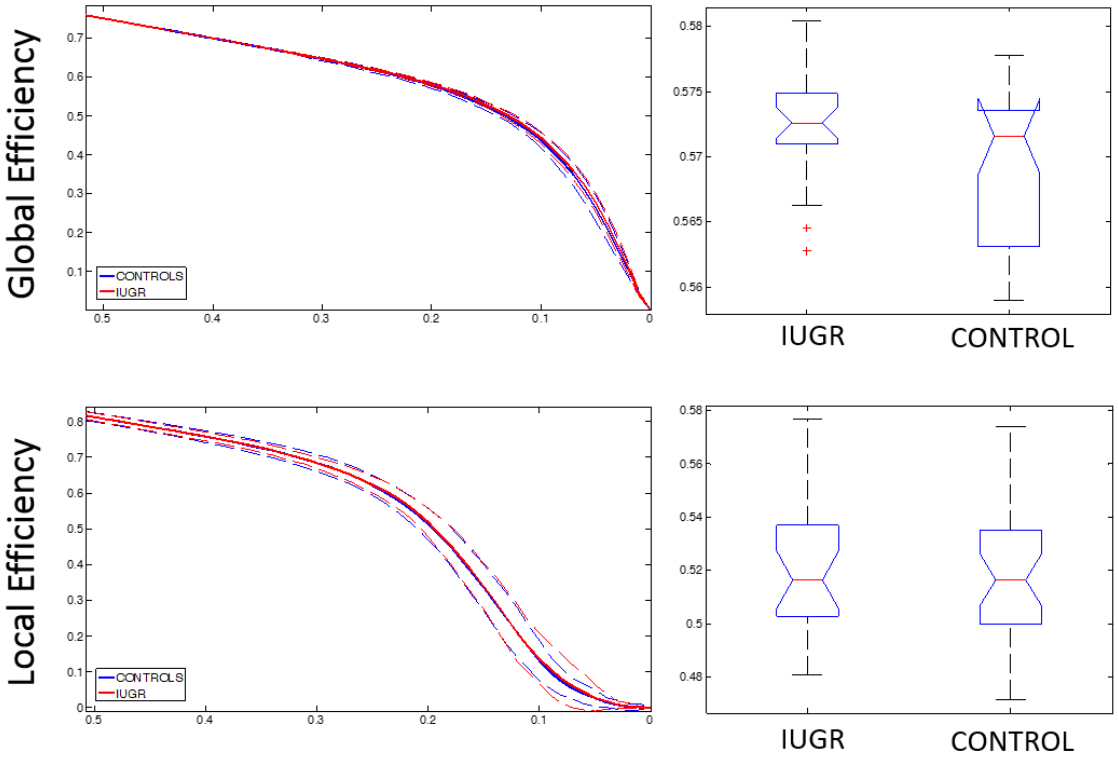

Figure 1. FA-weighted cost-corrected structural brain network features of IUGR compared with controls at one year of age and cost-integrated along the valid cost range

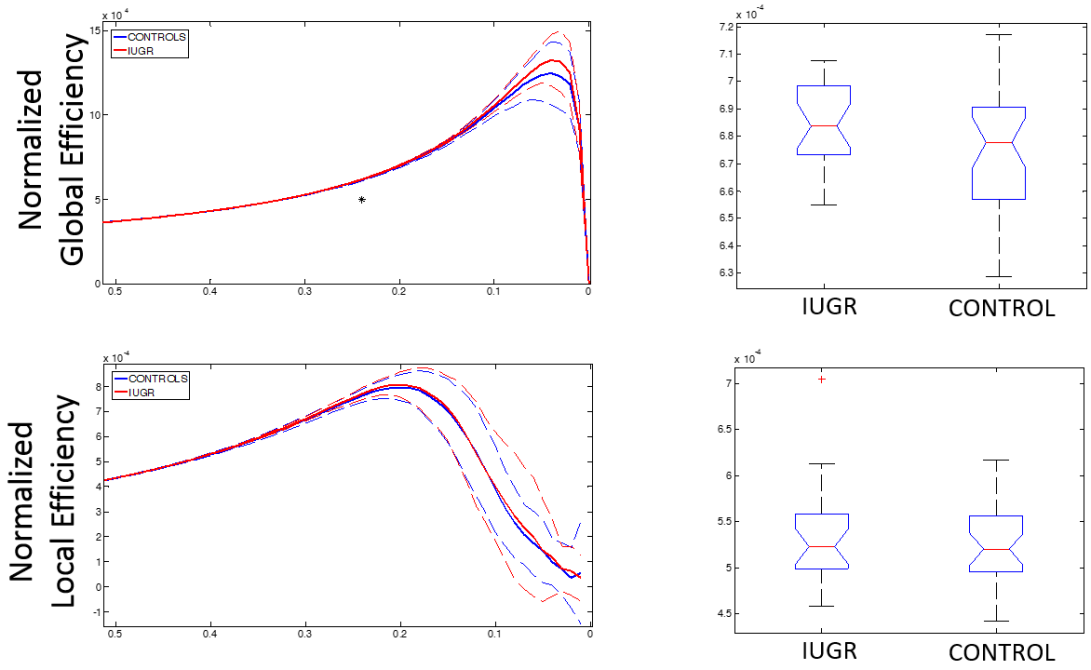

Figure 2. FA-weighted normalized and cost-corrected structural brain network global and local efficiency of IUGR compared with controls at one year of age and cost-integrated among the valid cost range.

6.2. Supplementary results of PROJECT 1 (II): functional brain network features of one-year-old infants with IUGR

For the sake of completeness and comparability with the other projects presented in this PhD Thesis, in this section preliminary results of the resting-state functional brain networks obtained in a similar sub-sample of one-year-old infants with IUGR are also assessed. In addition to the increased complexity of comprehensibly present functional and structural brain networks at the same time, these results were not included in the original publication of **PROJECT 1** given that only a small proportion of the population of **PROJECT 1** had a proper rs-fMRI acquisition (10 controls and 6 IUGR). However, in the last years we were able to increase the population of infants at one year of age with a good quality rs-fMRI acquisition.

In particular, a similar sample than the one analyzed in **PROJECT 1** was considered in this section, consisting on 22 controls and 19 one-year-old infants with IUGR. For all the subjects, a high resolution structural T1 weighted images were obtained by a Magnetization Prepared Rapid Acquisition Gradient Echo (MPRAGE) sequence with the following parameters: 0.9-mm slice thickness with no interslice gap, 192 sagittal slices, in-plane acquisition matrix of 256 x 256, FoV = 220 x 220 mm2, which resulted in a voxel dimension of 0.86 x 0.86 x 0.9 mm3, TR = 2050 ms, TE = 2.41 ms and inversion time (TI) = 1050 ms. Functional MRI data was acquired using gradient echo planar imaging (EPI) consisting in volumes of 42 axial slices with a spatial resolution of 2 x 2 x 2 mm3. Resting-state functional connectivity was assessed during 8 minutes of natural sleep (240 EPI volumes).

The same pre-processing steps followed in **PROJECT 4** were also followed with this data, with the only difference of using T1 anatomical volumes instead of T2-weighted volumes, due to the different state of myelination in one-year-old infants compared with neonates, which allow a better WM-GM differentiation with T1 volumes. Hence, pre-processing steps included skull-striping, segmentation of WM/GM/CSF (Ashburner and Friston, 2005) with specific one-year-old tissue probability maps (Shi et al., 2011), parcellation of the brain in 90 regions using an elastic registration of AAL atlas (Tzourio-Mazoyer et al., 2002) adapted to one-year-old population (Shi et al., 2011). Pre-processing of resting-state fMRI data

included correction of intra-volume time differences and inter-volume geometric displacements, regression of head motion effects in the signal, average of time series corresponding to each ROI and band pass filtering (0.01 – 0.15 Hz). Network edges were calculated as the partial correlation coefficients obtained between the average signals of each pair of ROIs excluding the effects of the signal of the other 88 ROIs and negative correlation coefficients were excluded.

Analysis of the raw network features showed a reduced infrastructure in IUGR functional brain networks, characterized by a significantly reduced network density ($p=0.043$) that is also reflected by a reduced binary global efficiency ($p=0.043$). Notwithstanding, no significant differences were found in any of the weighted features assessed. In the case of normalized weighted network features, which allows to assess differences in network organization independently of network strength, no statistically significant differences were found, but a tendency towards significance was observed for normalized weighted global efficiency ($p=0.053$), showing increased values for IUGR.

Using the cost-correction approach in order to assess the organization of the networks independently of differences in network density (cost), no significant differences were found. However, when assessing weighted normalized features with cost-correction at the same time, increased values of global efficiency were found for several network costs in IUGR group (Figure 3).

The results presented in this section, showed a reduction in some features of functional network infrastructure, which seems in line with the results obtained with structural network features in **PROJECT 1.** Furthermore, after normalization approaches, a tendency of IUGR subjects to have a slightly more optimal organization (global efficiency) for their given infrastructure is also observed.

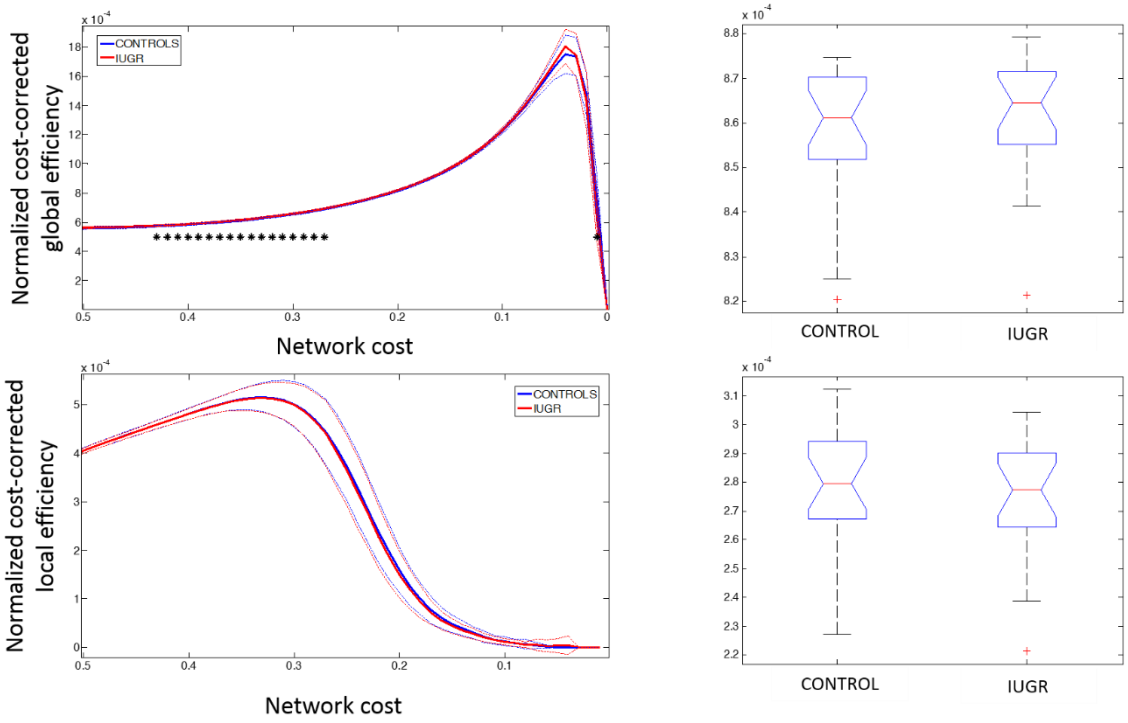

Figure 3. Normalized weighted and cost corrected global and local efficiency of functional brain networks compared between controls and IUGR at one year of age and cost-integrated among the valid cost range. * p<0.05

6.3. Supplementary results of PROJECT 4: structural brain network features of neonates with IUGR

In order to complement the results of the resting-state functional brain networks in neonates, in this section an analysis of a sample with an appropriate diffusion MRI acquisition is assessed and their structural brain network analyzed. These results were not included in the original publication, as it is our opinion that they probably deserve an independent publication when an increased sample size is available. However, we think that this is necessary to include these results in this Thesis to better understand and analyze their implications.

Particularly, in this section a sample of neonates composed by 9 controls and 15 subjects with late-onset IUGR is analyzed, being 5 controls and 12 IUGR part of the population presented in **PROJECT 4**. Diffusion MRI data was acquired using gradient echo planar imaging (EPI) sequence covering 30 diffusion directions with a b-value of 750 s/mm2. Acquired diffusion volumes consisted on 42 axial slices with a spatial resolution of 2 x 2 x 2 mm3, repetition time (TR) = 6000 ms, echo time (TE) = 86 ms. An additional image without diffusion weight (b=0 s/mm2) was also acquired.

An in-home algorithm was used to correct inter-plane movement artifacts by rigid registration of each diffusion volume, and intra-plane movement by the automatic discarding of planes with excessive movement artifacts. With the remaining volumes and planes, a tensor model was applied to each voxel of the brain with a variable amount of diffusion directions (between 20 and 30, depending on the amount of planes discarded for each subject). A deterministic tractography algorithm with an angle threshold of 30 degrees implemented in Diffusion Toolkit (http://trackvis.org/dtk/) (Wang et al., 2007) was used to reconstruct WM tracts of each subject. Brain parcellation into 90 regions based in AAL atlas was performed with an identic protocol as performed in **PROJECT 4**, elastically aligning a neonatal template (Shi et al., 2011) to the T2 anatomical volume of each subject.

Structural brain networks of each subject were obtained by the integration of WM tracts and anatomical regions using an in-home algorithm. Two nodes (regions) *i* and *j* were

considered to be connected by an edge e_{ij} when there existed at least one fiber bundle f with end-points in *i* and *j* regions, with self-loops excluded. In addition to the binary network produced with this approach, weights were also assigned to each edge e_{ij}. Two of the most used approaches in the literature were followed to weight the connectivity between each pair of regions, w_{FA}, average FA along all the fibers connecting a pair of regions; and w_{FD}, fiber density (FD) defined similarly as Hagmann et al. (2008). In addition, the resulting weighted networks were normalized by the total weight of all the connections in the network, to assess the brain organization independently of the network average strength.

Graph theory features of the brain networks obtained were compared between controls and IUGR subjects by means of a GLM analysis with group as a fixed factor, gender as a co-factor and gestational age and post-menstrual age at MRI acquisition as co-variables.

As shown in Figure 4, IUGR structural brain networks at neonatal age had a significantly increased FD-weighted average strength (p=0.025) and a significantly increased FD-weighted global efficiency. None of the other network features, including those of normalized networks, showed a statistically significant difference.

Although hampered by a reduced sample size, the results here presented support the idea that subjects with IUGR, at neonatal age present a hyper-connected structural brain network characterized by increased FD-weighted features.

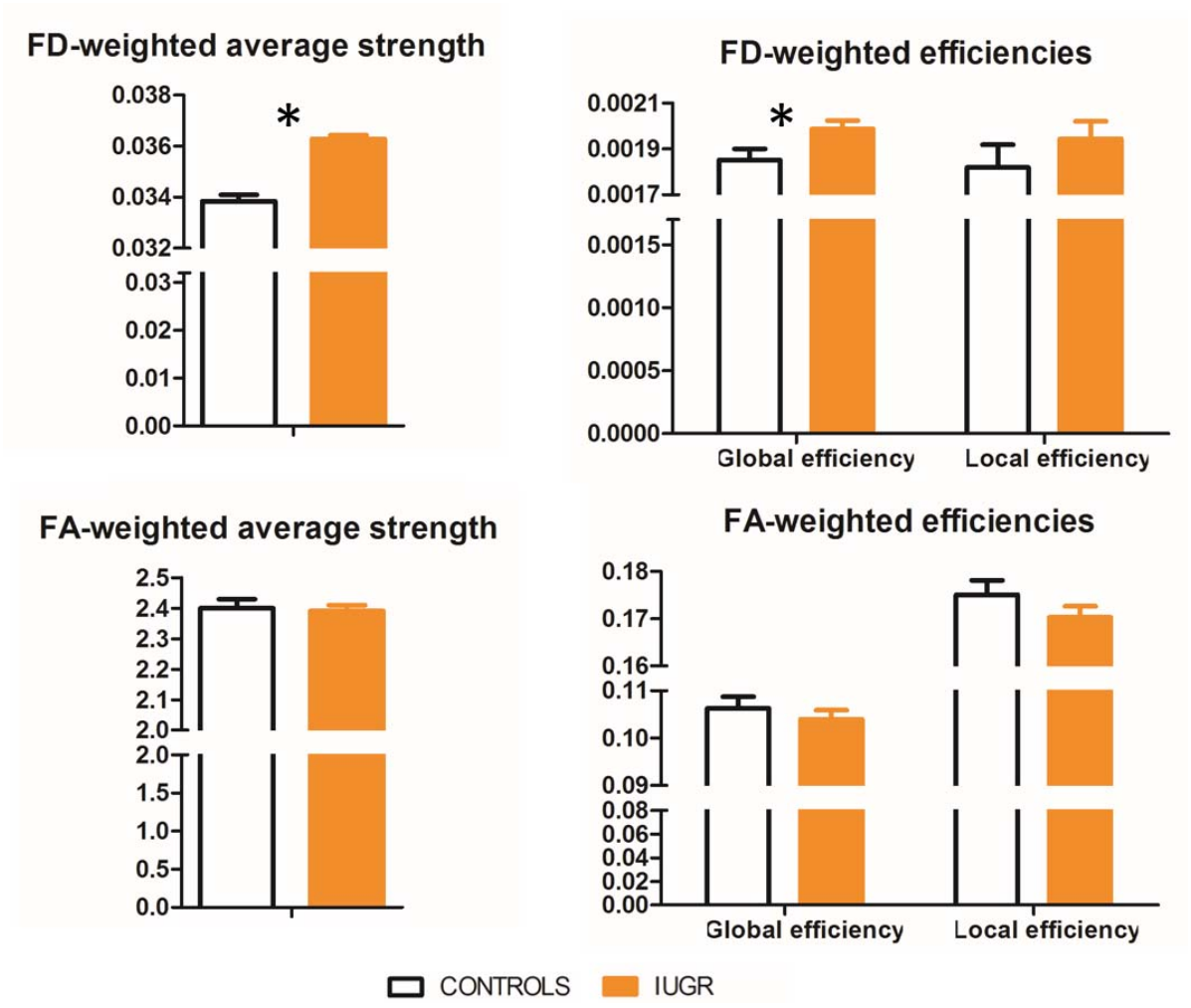

Figure 4. Structural network features of IUGR based on diffusion MRI at neonatal age, compared with controls. * $p<0.05$

7. SUMMARY OF RESULTS

PROJECT 1: Brain networks of diffusion MRI in one-year-old infants with IUGR

- It was feasible to reconstruct one-year-old structural brain networks by means of diffusion MRI.
- There was a reduction in global features of structural brain networks in one-year-old infants with IUGR.
- There was an altered pattern of regional features of structural brain networks in IUGR.
- The altered brain network topology in one-year-old infants with IUGR was associated with abnormal performance in neurodevelopmental scales at two years of age.
- Based on altered brain network features of one-year-old infants with IUGR, a machine learning algorithm was capable of blindly classify abnormal performance in neurodevelopmental scales (BSID-III) at two years of age with an accuracy of 82.4%.

Supplementary results

Normalized structural brain network features of one-year-old infants with IUGR

- Albeit having a reduced structural network infrastructure, with network normalization schemes we observed that one-year-old IUGR subjects had a tendency to have more optimal organization of their structural brain network.

Brain networks of functional MRI in one-year-old infants with IUGR

- IUGR infants presented a reduced infrastructure of their functional brain network at one year of age.
- There was a tendency in IUGR subjects to have increased efficiencies after functional network normalization at one year of age.

In summary, structural and functional brain networks showed decreased network features in IUGR. The reorganization observed is also accompanied by a tendency of having compensatory effects partially compensating this reduced infrastructure. Diffusion MRI network features had a high predictive value of altered neurodevelopment.

PROJECT 2: Brain networks of GM morphology similarity in one-year-old infants with IUGR

- A novel method proposing a solution to the problem of having different network sizes in individual large-scale networks obtained from GM MRI morphology similarities was presented.
- The feasibility of obtaining such kind of networks in a pediatric population was demonstrated.
- There were alterations in the features of structural brain networks based in GM morphology similarities of infants who suffered IUGR.
- There was an association of the brain network features obtained at one year of age with abnormal neurodevelopmental scores at two years of age.

In summary, it was feasible to use network models to analyze GM morphology from MRI in a pediatric population in a case-control study. Particularly, infants at one year of age showed alterations in GM morphology networks that were associated with altered neurodevelopment at two years of age.

PROJECT 3: Brain networks of diffusion MRI in a rabbit model of IUGR at pre-adolescent age

- Reorganization of IUGR rabbit brain was persistent at preadolescent age, showing an overall reduced network infrastructure.
- There was a compensatory effect in IUGR group characterized by higher values of the global features of normalized brain networks.
- There was a spread pattern of alterations in regional network features that resembled some of the results obtained at one year of age in humans.
- Global features were associated with neurobehavioral alterations.

In summary, structural brain networks of the rabbit model of IUGR showed long-term reorganization in IUGR brain, characterized by a decreased infrastructure and a mild compensatory effect at a pure organizational level.

PROJECT 4: Brain networks of functional MRI in neonates with IUGR

- Whole-brain functional brain networks based on an anatomical atlas were obtained for the first time in a neonatal population, showing its potential to characterize functional brain alterations of prenatal origin.
- Raw functional network features of neonates with IUGR presented increased values when compared with controls, suggesting hyper-connectivity in their functional brain organization.
- IUGR showed a sub-optimal pattern of functional organization characterized by significantly reduced normalized network features when assessing its pure organizational components.
- There was a pattern of alterations in the regional features of the functional brain networks of neonates with IUGR.
- Network features were associated with altered neurobehavior.

Supplementary results

Brain networks of structural MRI in neonates with IUGR

- Structural brain network features weighted by fiber density were increased in neonates who suffered IUGR.

In summary, resting-state functional brain networks of neonatal IUGR showed a pattern of increased co-activation and synchronization of brain regions with a sub-optimal organization. This functional reorganization is partially supported by a structural reorganization at the same age.

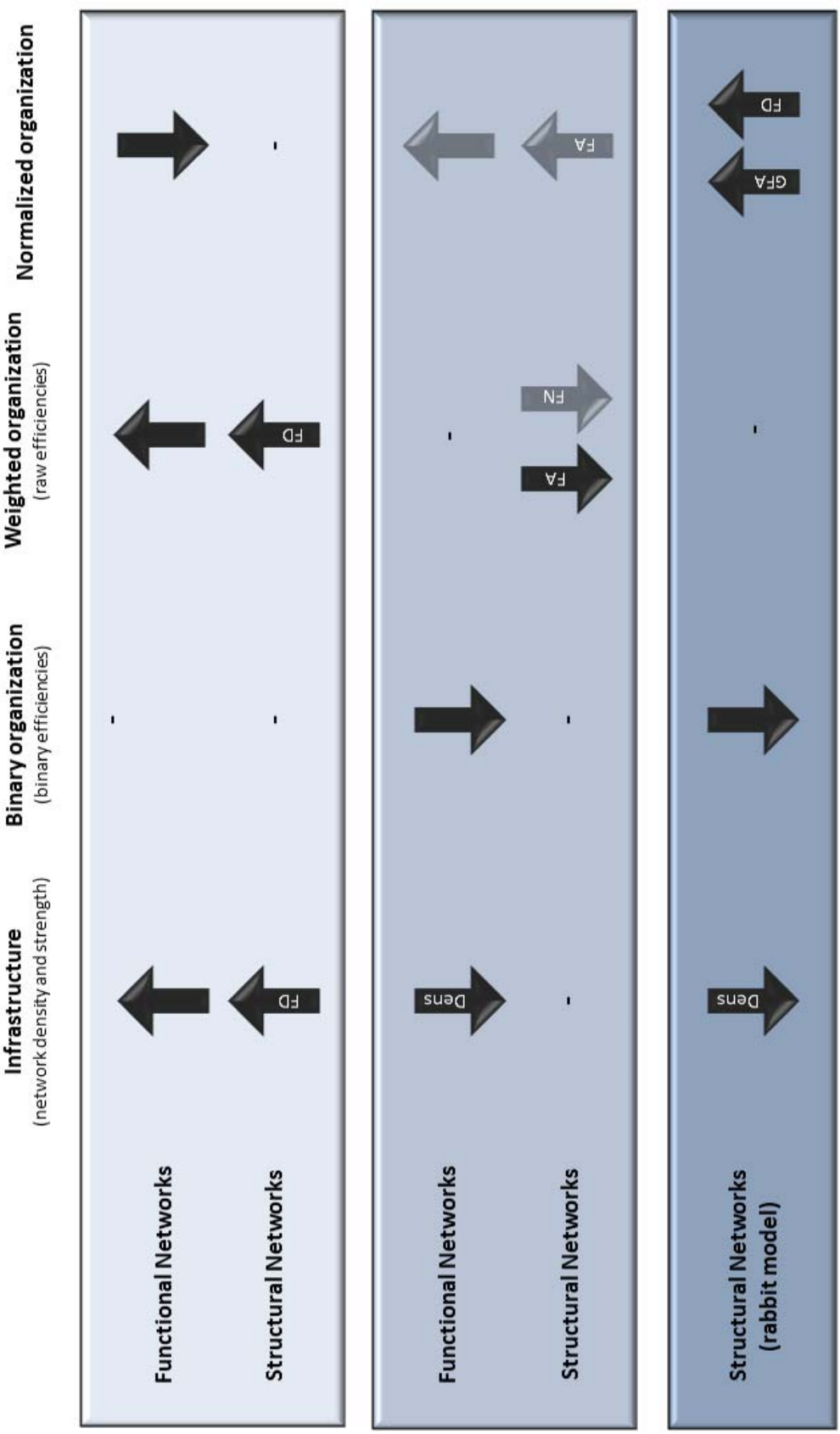

Figure 5. Comprehensible summary of all the results presented. Abbreviations: Dens, network density weighted features; FA, fractional anisotropy weighted features; FD, fiber density weighted features; FN, fiber number weighted features; GFA, generalized fractional anisotropy weighted features.

8. GENERAL DISCUSSION

The characterization of brain changes underlying IUGR risk of having neurodevelopmental problems is a main challenge in modern fetal and pediatric medicine. A better understanding of the pathophysiology of this condition is essential to start developing early biomarkers to detect the infants at high risk of having altered neurodevelopmental problems. Importantly, it has been shown that an early individualized intervention significantly improves IUGR neurobehavioral performance at short- and mid-term (Als et al., 2012; McAnulty et al., 2013). However, given the high prevalence of IUGR and the economic cost of individualized care units, selecting those IUGR infants with a higher risk is essential to appropriately advise parents and optimally use clinical resources.

There is an increasing agreement that brain network features are appropriate to characterize brain organization (Bassett and Bullmore, 2009). Hence, this kind of features has a high potential to be used as image biomarkers for the early detection of a variety of pathologies, including those of perinatal origin. However, the relationships between structural and functional network features are still not clear, and even the different ways of weighting structural brain networks and its implications are still in dispute (Griffa et al., 2013). It is our opinion that different brain networks are capturing complementary aspects of brain organization. Broadly, functional brain networks seem to capture patterns of co-activation of different regions of the brain, directly related to the functional infrastructure necessary to maintain the basic functions of consciousness and cognition (Deco et al., 2010). It is straightforward to see structural brain networks as the underlying infrastructure that allows different layers of communication between different areas of the brain. Intuitively, weighting these connections as a function of their number of fibers or their fiber density seems to be capturing the biological absolute and relative size of WM tracts, while weighting their FA or GFA is associated to the level of myelination and the integrity of those connections.

8.1. Global brain network features

One of the main aims of the present PhD Thesis was to characterize the re-organization in structural and functional brain network features produced by IUGR since neonatal age up to

pre-adolescence in a systematic way, using complementary techniques that give information about different aspects of brain organization and infrastructure. The results suggest that brain reorganization produced by IUGR is characterized at neonatal age by an increase in FD-weighted structural brain network infrastructure together with a hyper-connectivity of functional brain network, but a sub-optimal functional organization. During early infancy (one year of age), the results suggest that both structural and functional brain network infrastructure appears reduced in IUGR, and that there is a mild compensatory effect that slightly optimizes FA-weighted structural organization. The effects of IUGR observed in one-year-old infants are partially confirmed by a long-term rabbit model of this condition, at least at a structural level, suggesting that the reorganization observed at one year of age persist at pre-adolescence, although in this case being characterized by a reduced infrastructure and a compensatory effect when assessing the pure organizational components of the normalized networks.

Overall, the pattern of brain network reorganization assessed at three different stages of IUGR condition obtained in the presented studies is very specific and postulate IUGR condition as a possible brain-network disorder. Particularly intriguing is the evolution observed from neonatal age to early infancy. The evidence obtained suggest that during this short period, both functional and structural brain networks of IUGR subjects evolve from having an increased infrastructure to be reduced when compared with controls. We must note however, that the increased infrastructure in structural brain networks at neonatal age was found in FD-weighted measures while at early infancy the strongest findings where in FA-weighted measures. Increased infrastructure revealed by FD-weighted measure in neonatal period could be related with changes in type and number of connections, since proportion of short and long-range association fibers change during brain maturation (Huang and Vasung, 2014). On the other hand, changes in FA-weighted measures later in life could be more related with an alteration of tract's integrity and myelination process, a process that has its peak during first year of life (Tau and Peterson, 2010).

Regarding functional brain networks, the increased infrastructure and sub-optimal organization at neonatal age seems to be partially mitigated at one year of age. We

hypothesize that adverse fetal environment associated with IUGR produce a re-organization of brain connectivity, especially affecting functional organization. This brain re-organization was strongly observed in perinatal periods, but later in life, the absence of an adverse environment could be alleviating some of the changes observed. In the same line, although having a less connected brain network (decreased network density and binary global efficiency), GFA- and FD-weighted efficiencies were not found significantly decreased in the IUGR long-term animal model (**PROJECT 3**). One possible explanation could be related with changes in postnatal brain maturation after IUGR. Previous studies have reported that there is a compensation in the long-term myelination and WM volume in a guinea pig model of IUGR (Tolcos et al., 2011). In this line, previous studies assessing WM alterations in a rabbit animal model of IUGR using voxel based analysis have reported a less prominent pattern of alterations in pre-adolescence age (Illa et al., 2013) than in neonatal age (Eixarch et al., 2012). Notwithstanding, the results suggest that part of the brain re-organization produced by IUGR persist after perinatal period. Some of the persisting changes observed with brain network features, could be crucial in order to discriminate the IUGR infants with a higher risk of having an abnormal neurodevelopment later in life. Nevertheless, finding alterations in the brain network features associated to an abnormal condition is by itself relevant for the characterization of its pathophysiology. In the case of IUGR, the results suggest that there is a complex pattern of brain reorganization in both the structural and the functional substrate since neonatal age through pre-adolescence. This significantly improves the knowledge of this condition, serving as a potential physiological basis for the neurobehavioral alterations reported in these infants (Figueras et al., 2009). Note that given the heterogeneity of the etiology and progression of this condition, big samples are needed to find differences in neonatal neurobehavior, being even more crucial to find individualized biomarkers of the long-term prognosis of infants with IUGR in order to be able to clinically intervene. In this line, the association found between the functional network features at neonatal age and NBAS is especially relevant, significantly improving the capacity of association obtained with basic clinical features. Prospective studies associating later neurodevelopmental outputs with neonatal network features would help to find the most

sensible network features that will allow predicting altered neurodevelopment. However, we are confident that combination of multi-modal features of brain networks will significantly improve the assessment of the risk of neurodevelopmental problems of prenatal origin since an early age, being its translation to the clinical practice in the mid-term horizon.

While the studies presented in this Ph.D. Thesis show for the first time the brain connectivity reorganization produced by IUGR, and the potential of brain network models to be used as early image biomarkers, in order to have an application into the clinical practice these results should be confirmed by other studies. Although logistically very challenging, especially interesting would be the longitudinal analysis of brain reorganization produced by IUGR from neonatal age to pre-adolescence following a population. However, currently there is only another study in the literature analyzing brain reorganization in IUGR (Fischi-Gomez et al., 2014). This study demonstrate reduced network features of a six-year-old group of infants with IUGR with a combination of FD- and FA-weighted measures, supporting the notion of a reduced structural brain network infrastructure of IUGR during infancy suggested by the results obtained in **PROJECT 1** and **PROJECT 3**.

After further comparison with the body of literature available, we note a unique pattern of alterations in IUGR brain networks. IUGR has been suggested to be a risk factor of developing disorders such as attention deficit hyperactive disorder (ADHD) (Heinonen et al., 2010; Linnet et al., 2006), autism spectrum disorders (ASD) (Gardener et al., 2011; Moore et al., 2012) and schizophrenia (Nielsen et al., 2013). Although there are some contradictory reports, generally ASD has been characterized by having functional hyper-connectivity of salience and default mode network (Menon, 2013). However, whole-brain RSN have been reported to show reduced raw local efficiency but increased global efficiency after cost-correction (Rudie et al., 2012). In adult schizophrenia patients, reduced global and local efficiency after cost-correction of RSN has been reported (Liu et al., 2008), but also decreased average functional connectivity (Lynall et al., 2010). RSN of children with ADHD have been reported to have increased local efficiency for several costs, although raw weighted measures have not been described (Wang et al., 2009). Concerning structural brain

network features, studies in pediatric clinical populations are scarce in the literature, but a pattern of increasing global efficiency and decreasing clustering coefficients with increasing age from 2 to 18 years of age has been described (Hagmann et al., 2010). However, similar global efficiency values but age-increased local efficiencies were observed during the first years of live in neonates, one-year-old and two-year-old infants (Yap et al., 2011). The specific connectivity fingerprint trajectories that could underlie the increased prevalence of IUGR subjects developing disorders of neural development are still not clear, and will be the likely focus of future prospective studies. We hypothesize that some of the links of IUGR with neurodevelopmental disorders could be partially associated with dysfunctions in some specific regional sub-networks produced by brain reorganization.

The results obtained in **PROJECT 2**, deserve a special mention, as their comparability with the other studies here presented is not clear. In this study, we used a novel technique to obtain brain networks based on GM morphology similarity for the first time in a pediatric population. Although no statistically significant differences were found in weighted features, late-onset IUGR showed several differences when compared with controls when binarizing the weighted networks for the whole range of network cost, and these differences were confirmed by the integration of the values along the entire cost regime. We noted insistently in this study that the evidence available is not enough to state that there is an actual underlying brain circuitry explaining the connections obtained with this methodology. We could consider that part of the network reorganization found is related to some aspects of the underlying structural brain networks of the infants assessed, but also could be just simply be reflecting a different organization of GM morphology, independently of their connectivity properties. In fact, the results showed a sub-optimal organization of the networks obtained in IUGR infants, which paradoxically could be associated to a decreased infrastructure of their structural networks as shown in **PROJECT 1**, more than to a sub-optimal organization of the underlying networks, as it is suggested by the normalized brain networks presented in **Supplementary Results (I)**. As stated previously, the main interest of the methodology presented in **PROJECT 2** is to take advantage of graph theory features to assess GM morphology, which could be a useful resource to identify pathological alterations in brain

tissue characteristics in a broad spectrum of conditions of perinatal origin. However, the association of GM morphology reshaping with structural and functional brain connectivity reorganization is an issue that deserves further study.

8.2. Regional brain network features

Analysis of regional brain network features allowed extracting information of the topological changes on each region and its associated network. The analysis of structural brain networks at one year of age in IUGR (**PROJECT 1**) rendered regional alterations following a diffuse pattern along the whole brain, which included multiple areas as frontal, temporal, parietal and occipital lobes, sub cortical GM nuclei, insular cortex and cerebellum. Frontal and temporal areas showed changes in all regional features, although alterations in frontal areas were found mainly in FN-weighted nodal efficiency. Frontal and temporal areas are involved in the regulation of functions previously reported to be abnormal in IUGR children, including short-term memory (Geva et al., 2006a), learning abilities (Geva et al., 2006b), attention (Heinonen et al., 2010) and social skills (Eixarch et al., 2008). Fronto-temporal areas have also been related with ADHD (Kobel et al., 2010), which is present in higher proportion in children who suffered IUGR (Heinonen et al., 2010). Parietal areas showed differences mainly in nodal degree and FA-weighted nodal efficiency. These findings are consistent with the poorer performance in BSID-III motor domain observed in IUGR children. Previous studies have linked worst motor performance with reduced GM in parietal areas of IUGR (Padilla et al., 2011). Occipital areas were altered mainly on FA-weighted nodal efficiency, but also on nodal degree in a less spread pattern. This result is consistent with previous findings where parieto-occipital and inferior occipital regional vulnerability to IUGR has been demonstrated (Thompson et al., 2007). Some sub cortical GM nuclei including amygdala, putamen, pallidum and thalamus were also found altered, by regional features, mainly by FN-weighted nodal efficiency. Interestingly, striatal injury has been related to perinatal disorders, including IUGR, suggesting that it could be a risk factor of behavioral disturbances (Toft, 1999) and specific alterations in the cortico-striato-thalamic network have been associated with cognitive disorders, including Tourette syndrome (Makki et al., 2009), bipolar disorder (Chen et al., 2006) and ADHD (Castellanos

et al., 1994; Faraone and Biederman, 1998). Finally, cerebellum alterations in nodal degree and weighted nodal efficiency were found. These findings are in line with previously described decreases in cerebellar WM in IUGR infants (Padilla et al., 2011) and with alterations in cerebellar neuron population in animal models of IUGR (Mallard et al., 2000).

Interestingly, the analysis of altered regional network features based on GM morphology similarities (**PROJECT 2**), rendered differences consistent with some of the regional alterations found with structural network features based on diffusion MRI at the same age in **PROJECT 1**. This is the case of lingual gyrus, supramarginal gyrus, angular gyrus and vermis. As stated in the previous section, we acknowledge that the meaning of these findings is unclear, but we speculate that these differences could reflect a subtle pattern of alterations in cortical morphology produced by brain reorganization. This notion is in line with previous studies demonstrating structural differences in early and late-onset IUGR. Studies in preterm neonates have reported a decreased volume in cortical GM (Tolsa et al., 2004) and hippocampus (Lodygensky et al., 2008), and major delays in cortical development with discordant patterns of gyrification and a pronounced reduction in cortical expansion (Dubois et al., 2008). Persistence of structural changes at one year of age in IUGR babies has been reported, which demonstrate reduced volumes of GM in the temporal, parietal, frontal and insular regions (Padilla et al., 2011) and decreases in the fractal dimension of both gray and white matter, which correlate with specific neurodevelopmental difficulties in a similar population (Esteban et al., 2010). Note that the importance of the relationship between the network features obtained by individual GM similarity-based networks and fractal dimension has been previously suggested as there is a resemblance in both methodologies (Tijms et al., 2012). Recently published data has also demonstrated a reduced global cortical surface and volume as well as regional changes in cortical thickness, especially in the frontal region, in children after late-onset IUGR (De Bie et al., 2011) such that these regional changes are also present in the adolescent population (Martinussen et al., 2005). In summary, a pattern of regional network features altered in IUGR long-term animal model were identified, some of them being specifically associated with abnormal neurobehavior. Noteworthy, alterations in network features of cerebellum stand out as the

more strongly associated with IUGR condition, and septal nuclei, insular cortex and thalamus with poor performance in neurobehavioral tests.

Concerning regional differences found in structural brain networks of long-term animal model (**PROJECT 3**), only vermis features withstood a FDR correction at 5%, while only features of cerebellar hemispheres and piriform cortex withstood a FDR correction at 10%. Particularly, degree and normalized GFA-weighted strength of vermis were significantly reduced in IUGR, and nodal efficiency of both raw and normalized FD-weighted vermis were significantly increased in IUGR. We could interpret that IUGR subjects at long-term have a vermis with reduced neighborhood but with a stronger connectivity (higher clustering). This would support the hypothesis of a compensatory effect in these subjects and goes in line with the results obtained on global network features. Interestingly, alterations in cerebellum and vermis connectivity in infants are in line with the results previously obtained in infants with IUGR at one year of age (**PROJECT 1** and **PROJECT 2**), as well as reduced WM volumes in cerebellar areas in short- (Padilla et al., 2011) and long-term follow-up studies (De Bie et al., 2011; Martinussen et al., 2009), postulating cerebellar area as a key region in IUGR brain reorganization. Interestingly, cerebellar areas are implicated in motor learning, memory, cognition and behavior (Baillieux et al., 2008), and have been reported to increase their volume in infants with IUGR after intervention by means of individualized intensive care nursery associated with an improvement in executive function (McAnulty et al., 2013). Considering other animal models of IUGR, in guinea pig it also has been reported a reduction in cerebellar WM volume (Tolcos et al., 2011), and a reduction in Purkinje neuronal population (Mallard et al., 2000). However, we must note that in previous voxel-based analysis studies in IUGR rabbit model (Eixarch et al., 2012; Illa et al., 2013) we only observed mild differences in cerebellar areas. We hypothesize that this could be partially explained by stronger alterations in the sub-network associated to cerebellum (described by network features), than in the structure of cerebellum by itself. Another factor that could explain this discrepancy can be the technical characteristics of voxel-based analysis technique, especially in cerebellar areas, where the limited resolution is especially critical for cerebellar WM. Beside those associated with cerebellar areas, other regional features

were also significantly different in IUGR, although only normalized FD-weighted efficiency of right piriform cortex withstood a 10% FDR correction. It seems interesting that regional features of normalized networks were found significantly increased in IUGR mainly in specific basal and deep gray matter areas, such as amygdala, hippocampus, thalamus, medulla oblongata, and some of the cortical areas controlling essential functions for the rabbit, as is the case of piriform cortex, which has been strongly associated to the smelling processing (Kadohisa and Wilson, 2006). One possible interpretation of these results could be that a compensatory reorganization in IUGR brain might occur preferentially in brain areas regulating function with critical importance in survival, such as memory, attention or smelling processing. Considering other features that did not withstood FDR correction, we must note that the regional features altered in IUGR were coherent with the global results obtained, mainly showing reduced values in binary and raw GFA-weighted measures (especially in degree/strength) and increased values in normalized measures (especially in efficiency). Interestingly, changes in regional features of raw networks were manly identified in brain regions located in the right hemisphere of the brain, suggesting a certain asymmetry in the reorganization associated with IUGR. Reports on asymmetrical brain alterations produced by IUGR are scarce in the literature, and further long-term studies in humans would be required to confirm this effect and discard that is exclusive to animal models.

Concerning functional brain networks at neonatal age (**PROJECT 4**), it is worthwhile to note that although partial correlation networks and temporal dynamics yield to same global functioning conclusions (IUGR has a hyper-connected, hyper-synchronized brain but with a sub-optimal organization), the regional results obtained by each of these techniques showed different altered regions, suggesting that they assess complementary features of brain organization, although both highlighted the role of frontal areas. Particularly, analysis of temporal dynamics allowed to obtain a reduced set of regions altered, comprised by frontal, cingulate and lingual cortices. In agreement with these results, several frontal regions with altered structural brain network features have been also found at one year of age (**PROJECT 1**), while evidence of alterations in frontal-posterior networks in ASD has

been reported in several studies (Maximo et al., 2014). Interestingly, altered nodal efficiency of left lingual gyrus has been specifically reported in structural brain networks of IUGR (**PROJECT 1** and **PROJECT 2**) and has also been shown to be decreased in RSN of ADHD patients (Wang et al., 2009). Concerning cingulate cortical areas, FA measures of this area have been strongly associated with altered neurobehavioral performance in a long-term rabbit model of IUGR (Illa et al., 2013). In addition, functional alterations of cingulate areas have been reported in different studies of ASD (Maximo et al., 2014), schizophrenia (Lynall et al., 2010) and ADHD (De La Fuente et al., 2013).

8.3. Association with altered neurobehavior and neurodevelopment

An association between IUGR and long-term neurodevelopmental and cognitive dysfunctions has been previously demonstrated (Bassan et al., 2011; Feldman and Eidelman, 2006; Geva et al., 2006a; Geva et al., 2006b; Leitner et al., 2007; McCarton et al., 1996; Scherjon et al., 1993) as was the case with studies focusing on late-onset cases (Bassan et al., 2011; Eixarch et al., 2008; Figueras et al., 2009; McCowan et al., 2002). In order to develop image biomarkers to find the population with a higher risk of having an altered neurodevelopment, the general association of brain network features with functional behavioral or developmental outcomes is a key point to demonstrate its potential.

The results of **PROJECT 1** provide evidence that graph theory features of structural brain networks at one year of age carry relevant individual information related with adverse neurodevelopment measured one year later by BSID-III. Specifically, we demonstrated that global network connectivity features were associated to abnormal neurodevelopment. In addition, in this population we were able to test a simple machine learning approach that demonstrated the high potential of structural network features at one year of age to predict those infants with a higher risk of altered neurodevelopment. Particularly, regional connectivity features allowed to blindly classify abnormal neurodevelopment in IUGR with an accuracy of 82.4%.

The results of **PROJECT 2** also demonstrated that network features of brain networks extracted from GM standard T1-weighted acquisitions at one--year of age are related with neurodevelopment later in life. In this study, the combination of clinical data with global features was associated with the number of abnormal Bayley's scales, giving additional information about the severity of the neurodevelopmental delay. In our opinion, it is highly relevant that the network features extracted with the present methodology are related with neurodevelopmental outcome in IUGR children, suggesting the potential of this methodology to generate biomarkers able to detect altered neurodevelopment. This is especially relevant to clinical practice, as the early detection of abnormal neurodevelopment would open a window of opportunity to apply interventional strategies based in simple T1 acquisitions. However, we must note that the predictive power of this technique was not so powerful compared with features obtained from diffusion MRI structural brain networks, which allowed blind classification based on a machine learning approach.

Concerning the long-term animal model of IUGR (**PROJECT 3**), we should highlight regional associations as those of cingulate cortex network features, which were correlated with OFBT performance. This is in line with previous results in a similar sample of IUGR rabbit model, where FA changes in the cingulate cortex were found to be correlated to a series of neurobehavioral domains, especially those of OFBT (Illa et al., 2013). Note that cingulate cortex has been strongly associated with anxiety processes (Kim and Whalen, 2009), which is thought to have an important role on the behavioral response in OFBT. In addition, cingulate cortex volumetric differences in humans (Emond et al., 2009; Spampinato et al., 2009) as well as histological changes in rodents (Miller et al., 2012) have been associated with traits of attention deficit and anxiety. Concerning the specific associations with OFBT and ORT by means of a step forward binary logistic regression, features of insular cortex and septal nuclei were found strongly associated with OFBT and features of thalamus with ORT. Septal nuclei participation in the regulation of anxiety and depression in experimental models has been extensively documented (Estrada-Camarena et al., 2002), as well as insular cortex, which has been proposed to have a key role in anxiety proneness (Paulus and Stein,

2006). Importantly, thalamus has been previously associated to memory impairments in animal models (Mitchell and Dalrymple-Alford, 2005) and with poor performance in object recognition tasks in patients with schizophrenia (Heckers et al., 2000), disorder that has also been associated to low birth weight (Nilsson et al., 2005).

Concerning the alterations found in the functional brain network features of IUGR at neonatal age (**PROJECT 4**), those by itself are relevant for the characterization of its pathophysiology, suggesting that brain reorganization previously demonstrated in the structural substrate is also present at a functional level. This significantly improves the knowledge of this condition, serving as a potential physiological basis for the neurobehavioral alterations reported in these infants (Figueras et al., 2009). Note that given the heterogeneity of the etiology and progression of this condition, big samples are needed to find differences in neonatal neurobehavior, being even more crucial to find individualized biomarkers of the long-term prognosis of infants with IUGR in order to be able to clinically intervene. Therefore, the association found between the functional network features and NBAS is especially important, significantly improving the capacity of association obtained with basic clinical features. In addition, recent reports showing the feasibility to assess fMRI in fetal period reinforce the potential to use functional brain networks as an early biomarker (Thomason et al., 2013). However, albeit their potential, it is still unknown the predictive power of these functional brain network features, and follow-up studies of this population will be required in order to assess their capacity to determine the sub-set of the population with IUGR with a higher risk of altered neurodevelopment.

In general, the results of this PhD Thesis are in line with previous studies relating neurofunction with brain network features. Thus, global efficiency has been previously demonstrated to be associated with intelligence (Li et al., 2009), and regional features of brain networks selected by means of a learning algorithm have been related successfully to mild cognitive impairment in studies attempting to develop early biomarkers for Alzheimer's disease (Wee et al., 2010). The data here reported and previous studies suggest that combining global and regional characteristics could help to improve the understanding of neurofunctional mechanisms underlying structural connectivity. In addition, further

studies linking structural and functional networks would be very helpful in order to better understand the intricate link between structural and functional connectivity in the neonatal and infant brain. Combined analysis of both substrates is warranted in future studies to advance in the understanding of brain reorganization and its relation with altered neurobehavior and neurodevelopment due to IUGR and other prenatal conditions.

8.4. Limitations

Some issues must be noted concerning the methodology followed. The techniques used on a series of complex analyses, and due to their relative novelty there is a lack of 'gold standards' in the literature. Brain parcellation in young infants and neonates is a controversial subject and tissue segmentation in infant brains is considered a challenging task due to the isointense developmental pattern which results in a poor differentiation between GM and WM (Paus et al., 2001). To minimize this limitation we used high quality T1 and T2 weighted 3-Tesla Magnetic Resonance images and to guide the segmentation we used appropriate brain tissue probability maps and a pediatric atlas (Shi et al., 2011). In addition, each scan was reviewed to determine if the results of the tissue segmentation were accurate (Knickmeyer et al., 2008).

A specific limitation of **PROJECT 1** is the use of DTI tractography, which reconstruction is highly sensitive to motion artifacts during acquisition. This prevented us to analyze a remarkable number of subjects. It is also well known that DTI is not able to encode multi-directional diffusion information, which may lead to errors in regions with a high amount of crossing fibers. Other techniques such as Q-Ball Imaging (Tuch, 2004) , used in **PROJECT 3**, can be used to solve this issue and provide more accurate WM tractography, but need the acquisition of an increased amount of gradient directions. Current limitations of DTI and (with a lesser extent) Q-Ball based tractography, and the intrinsic noisy nature of MRI acquisitions, may result in the inclusion of spurious connections in individual networks. However, it must be noted that we did not perform an analysis directly based on edges, but measured network topology features. This approach is robust against noise as it integrates overall information of the individual networks, and therefore, minimizes the effect of

spurious connections. The same rationale can be applied to functional resting-state brain networks as those obtained in **PROJECT 4,** in which the analysis of network topology features is also robust to spurious connections inferred due to artificial correlations produced by artifacts of fMRI signal, with the addition that the use of partial correlations (instead of directly correlating the signal averaged in each region), also reduce possible sources of bias, extracting residual motion artifacts and other signal distortions that affect the whole brain.

How the connectivity between regions must be quantified is also an issue to be addressed. Binarization of the obtained network implies a loss of information of the connectivity pattern, and some authors propose different measures to quantify structural connections based on diffusion MRI as the number of fiber bundles, density of fibers or average measures of diffusion along the tract (Hagmann et al., 2007; Li et al., 2009; Wee et al., 2010). However, how the weight of a connection must be quantified, and its correlation with the anatomical substrate in which transfer of neural signals yields is still an open question (Li et al., 2009; Shu et al., 2009). It must be noted that average degree, and therefore the network cost, were non-significantly different between groups in the unthresholded networks, which supports that similar network density of WM connections were calculated throughout all the population, minimizing the chances of differences in network cost causing some of the observed differences.

Concerning **PROJECT 2**, it is important to note that by its design, the methodology presented does not discriminate between GM to CSF or GM to WM boundaries, thus a connection could be considered between two cubes that have similar GM pattern without taking into account if they are adjacent to WM or CSF. However, it must be stressed that, even if the area occupied by WM and/or CSF in a pair of cubes is identical, a connection will not be established if GM pattern between the two cubes is different. Another key issue that can be considered a limitation of **PROJECT 2** is the possible resemblance (or not) of the networks obtained with actual underlying brain circuitry. Some hints on the validity of the networks obtained have been shown in the original article presenting the theoretical base of this methodology (Tijms et al., 2012), comparing the individual networks obtained to resting

state and conventional GM morphology inter-subject correlation networks. In addition, in the present study some correlations of the network features obtained with a reduced sample of 10 subjects with diffusion MRI based networks has also been shown. However, the evidence available is not enough to state that there is an actual underlying brain circuitry explaining the connections obtained with the present methodology. Further studies are necessary to compare the individual networks obtained with morphology similarities to those networks obtained from standard diffusion and/or functional MRI in larger samples to clarify this issue. This is an extremely important remark when interpreting the results obtained, but is not so relevant from the point of view of purely developing neurological outcome biomarkers. Being able to show differences in the network features obtained between controls and cases may not directly indicate a different topology of brain circuitry, but may instead be showing subtle differences in cortical patterns that may not be detected by other less sensitive techniques. We can only hypothesize that the differences found can be partially explained by differences in brain connectivity that modulate cortical morphology (Gong et al., 2011; Van Essen, 1997), but also by differences in cortical structure produced by other reasons, such as changes in the distribution and/or density of neuronal bodies as occurs in animal models of chronic hypoxia (Fagel et al., 2006). In any case, in the sense used in the present paper, networks represent the similarities between regions of the brain (nodes) giving the weight of this similarity to the links connecting them. Whether these links, or what is the same, the morphological similarity between regions of the brain, describe or not an underlying circuitry is certainly unknown. However, to our understanding, the relevance of the technique and results here presented lies on the fact that differences in a pathological group have been demonstrated with this methodology and, importantly, a correlation between the features of the extracted networks from a simple T1 acquisition with the neurodevelopmental tests performed one year later has been found. This data show the potential of the proposed methodology to find image biomarkers in a different set of pathologies, but especially in pediatric population, independently of whether or not the networks obtained with the presented methodology correspond with true underlying brain circuitries.

With respect to the specific limitations of **PROJECT 3**, although the study of brain networks in animal models has been seminal to the field (Sporns et al., 2005), brain networks obtained from diffusion MRI in small animals are scarce. To the best of our knowledge, this is the second study of this kind in small mammals (Iturria-Medina et al., 2011), and the first showing brain networks in rabbits. This animal model has some specific methodological difficulties that had to be overcome. The recent successful development of an MRI atlas for the rabbit brain (Muñoz-Moreno et al., 2013), allowed to automatically segment and analyze brain networks from this model. It is common in human studies to confine deterministic tractography only to WM tissue. However, due to the difficulty of properly defining a WM mask in rabbits, the deterministic tractography was computed for the whole brain. This could create some redundant fibers, and increase tractography noise, but it was partially overcome by the use of a high angular resolution diffusion MRI acquisition, and the use of graph theory, particularly weighted measures, to analyze the results obtained. This limitation also ramifies in the calculation of FD-weighted networks. Instead of the formulation proposed by Hagman et al. (2008) to calculate FD between two regions (using the surface of the WM-GM interface of the regions involved in a given link in the denominator), we modified this formula introducing the volume of each region instead of the surface of the WM-GM interface. Finally, we acknowledge that the relatively reduced sample size used might be reducing the statistical power of the comparisons between cases and controls, preventing to generalize some of the findings obtained, especially concerning regional characteristics that did not withstand a FDR correction.

Concerning functional brain networks (**PROJECT 4**), it is important to note that MRI acquisition was performed during natural sleep. Previous reports have associated deepness of sleep with functional connectivity (Horovitz et al., 2009; Larson-Prior et al., 2009); however, although the effects of sedation and sleep in functional connectivity are not fully understood, significant differences have not been found between sedated and non-sedated infants using ICA and seed-based correlation approaches (Doria et al., 2010; Fransson et al., 2011; Fransson et al., 2009). Importantly, neonatal sleep has been suggested to be mainly in active sleep (Biagioni et al., 2005), minimizing the possibility that different

sleep deepness could be partially explaining some of the results obtained, being also mitigated by the case-control design of the study. Regarding the comparability of the results obtained, only a previous study assessed whole-brain networks in a neonatal population (Fransson et al., 2011), however, it was performed voxel-wise in a normalized space, obtaining very large networks (4966-by-4966 elements). Albeit the use of voxel-wise networks have some advantages, constraining the networks obtained to an anatomical brain atlas allows a more comprehensible and manageable comparison among studies, especially given the broad use of AAL atlas in the literature. However, regional parcellation of the neonatal brain is also an especially critical issue and could be a source of bias. This was alleviated by the use of T2-weighted anatomical volumes which improve WM contrast in neonatal acquisitions (Williams et al., 2005), and by the use of a specific neonatal atlas (Shi et al., 2011).

8.5. Concluding remarks and future work

The use of brain network models based in MRI is an emerging technique that is suitable for the assessment of brain reorganization in IUGR neonates and infants by means of global and regional graph theory based network features, which are related to different levels of organizational complexity. We assessed different modalities of MRI to find different aspects of IUGR physiopathology and their association with altered neurodevelopment measured by NBAS and BSID-III, finding potential biomarkers for early detection of high risk of altered neurodevelopment. In addition, these techniques have also been tested in an animal model of IUGR, which is crucial to assess their reliability in a controlled environment and to assess possible pharmacological therapies. Overall, the observed functional and structural reorganization could be a potential substrate of the altered neurodevelopment described in infants with IUGR, and together with previous findings, postulate IUGR condition as a possible brain-network disorder. Importantly, association of network features with neurobehavior and neurodevelopment since an early age opens the opportunity to develop early image biomarkers of altered neurodevelopment, a clinical chance to improve the management of a condition that affects 10% of the population. Future work will be focused on the feasibility to predict altered neurodevelopment at late infancy and adolescence

based on multi-modal brain networks obtained at neonatal age and the assessment of the impact of network features trajectories across different ages in developing different neurodevelopmental alterations.

9. CONCLUSIONS

Project 1:

- IUGR structural brain networks show a decreased infrastructure producing a sub-optimal raw organization at one year of age.
- Functional brain networks of IUGR at one year of age partially support the results obtained with structural brain networks.
- Brain networks based on diffusion MRI at one year of age have a high predictive value of altered neurodevelopment.

Project 2:

- It is feasible to use network models to analyze GM morphology in a pediatric population.
- IUGR showed alterations in GM morphology networks and there was an association with altered neurodevelopment.

Project 3:

- Structural brain networks of the rabbit model of IUGR showed long-term reorganization in IUGR brain.
- This reorganization is characterized by a decreased infrastructure and a compensatory effect at pure organizational level, and is associated with neurobehavioral scores.

Project 4:

- Resting-state functional brain networks of neonatal IUGR showed a pattern of increased co-activation and synchronization of brain regions together with a sub-optimal organization.
- Features of structural brain networks partially supported the results obtained with functional brain networks.
- Functional brain network features were associated to neurobehavioral alterations.

Our main conclusion is that IUGR condition produces structural and functional brain reorganization since early life that persists postnatally up to pre-adolescence. We hypothesize that the observed functional and structural reorganization could be a potential substrate of high risk of altered neurodevelopment in infants with IUGR, and postulate this condition as a possible brain network disorder. Importantly, the association of network features with neurobehavior and neurodevelopment since an early age opens the opportunity to further develop early image biomarkers of altered neurodevelopment, a clinical chance to improve the management of a condition that affects up to 10% of deliveries.

10. BIBLIOGRAPHY

Achard, S., Bullmore, E., 2007. Efficiency and cost of economical brain functional networks. PLoS Comput Biol 3, e17.
Als, H., Duffy, F.H., McAnulty, G., Butler, S.C., Lightbody, L., Kosta, S., Weisenfeld, N.I., Robertson, R., Parad, R.B., Ringer, S.A., Blickman, J.G., Zurakowski, D., Warfield, S.K., 2012. NIDCAP improves brain function and structure in preterm infants with severe intrauterine growth restriction. J Perinatol 32, 797-803.
Anderson, P.J., De Luca, C.R., Hutchinson, E., Roberts, G., Doyle, L.W., 2010. Underestimation of developmental delay by the new Bayley-III Scale. Arch Pediatr Adolesc Med 164, 352-356.
Ashburner, J., Friston, K.J., 2005. Unified segmentation. Neuroimage 26, 839-851.
Baillieux, H., De Smet, H.J., Paquier, P.F., De Deyn, P.P., Marien, P., 2008. Cerebellar neurocognition: insights into the bottom of the brain. Clin Neurol Neurosurg 110, 763-773.
Bandettini, P.A., Wong, E.C., Hinks, R.S., Tikofsky, R.S., Hyde, J.S., 1992. Time course EPI of human brain function during task activation. Magn Reson Med 25, 390-397.
Baschat, A.A., 2004. Pathophysiology of fetal growth restriction: implications for diagnosis and surveillance. Obstet Gynecol Surv 59, 617-627.
Bassan, H., Stolar, O., Geva, R., Eshel, R., Fattal-Valevski, A., Leitner, Y., Waron, M., Jaffa, A., Harel, S., 2011. Intrauterine growth-restricted neonates born at term or preterm: how different? Pediatr Neurol 44, 122-130.
Bassan, H., Trejo, L.L., Kariv, N., Bassan, M., Berger, E., Fattal, A., Gozes, I., Harel, S., 2000. Experimental intrauterine growth retardation alters renal development. Pediatr Nephrol 15, 192-195.
Basser, P.J., Pierpaoli, C., 1996. Microstructural and physiological features of tissues elucidated by quantitative-diffusion-tensor MRI. J Magn Reson B 111, 209-219.
Bassett, D.S., Bullmore, E., Verchinski, B.A., Mattay, V.S., Weinberger, D.R., Meyer-Lindenberg, A., 2008. Hierarchical organization of human cortical networks in health and schizophrenia. J Neurosci 28, 9239-9248.
Bassett, D.S., Bullmore, E.T., 2009. Human brain networks in health and disease. Curr Opin Neurol 22, 340-347.
Biagioni, E., Boldrini, A., Giganti, F., Guzzetta, A., Salzarulo, P., Cioni, G., 2005. Distribution of sleep and wakefulness EEG patterns in 24-h recordings of preterm and full-term newborns. Early Hum Dev 81, 333-339.
Biswal, B., Yetkin, F.Z., Haughton, V.M., Hyde, J.S., 1995. Functional connectivity in the motor cortex of resting human brain using echo-planar MRI. Magn Reson Med 34, 537-541.
Carr, H.Y., 1953. Free precession techniques in nuclear magnetic resonance.
Castellanos, F.X., Giedd, J.N., Eckburg, P., Marsh, W.L., Vaituzis, A.C., Kaysen, D., Hamburger, S.D., Rapoport, J.L., 1994. Quantitative morphology of the caudate nucleus in attention deficit hyperactivity disorder. Am J Psychiatry 151, 1791-1796.
Chen, C.H., Lennox, B., Jacob, R., Calder, A., Lupson, V., Bisbrown-Chippendale, R., Suckling, J., Bullmore, E., 2006. Explicit and implicit facial affect recognition in manic and depressed States of bipolar disorder: a functional magnetic resonance imaging study. Biol Psychiatry 59, 31-39.
Damadian, R., 1971. Tumor detection by nuclear magnetic resonance. Science 171, 1151-1153.
De Bie, H.M., Oostrom, K.J., Boersma, M., Veltman, D.J., Barkhof, F., Delemarre-van de Waal, H.A., van den Heuvel, M.P., 2011. Global and regional differences in brain anatomy of young children born small for gestational age. PLoS ONE 6, e24116.
De La Fuente, A., Xia, S., Branch, C., Li, X., 2013. A review of attention-deficit/hyperactivity disorder from the perspective of brain networks. Front Hum Neurosci 7, 192.
Deco, G., Jirsa, V.K., McIntosh, A.R., 2010. Emerging concepts for the dynamical organization of resting-state activity in the brain. Nat Rev Neurosci 12, 43-56.

Derrick, M., Drobyshevsky, A., Ji, X., Tan, S., 2007. A model of cerebral palsy from fetal hypoxia-ischemia. Stroke 38, 731-735.
Donaldson, D.I., Buckner, R.L., 2001. Effective Paradigm Design. In: Matthews, P.M., Jezzard, P., Smith, S.M. (Eds.), Functional Magnetic Resonance Imaging: An Introduction to Methods. Oxford University Press, Oxford.
Doria, V., Beckmann, C.F., Arichi, T., Merchant, N., Groppo, M., Turkheimer, F.E., Counsell, S.J., Murgasova, M., Aljabar, P., Nunes, R.G., Larkman, D.J., Rees, G., Edwards, A.D., 2010. Emergence of resting state networks in the preterm human brain. Proc Natl Acad Sci U S A 107, 20015-20020.
Dubois, J., Benders, M., Borradori-Tolsa, C., Cachia, a., Lazeyras, F., Ha-Vinh Leuchter, R., Sizonenko, S.V., Warfield, S.K., Mangin, J.F., Hüppi, P.S., 2008. Primary cortical folding in the human newborn: an early marker of later functional development. Brain 131, 2028-2041.
Egaña-Ugrinovic, G., Sanz-Cortes, M., Figueras, F., Bargallo, N., Gratacos, E., 2013. Differences in cortical development assessed by fetal MRI in late-onset intrauterine growth restriction. Am J Obstet Gynecol 209, 126 e121-128.
Eixarch, E., Batalle, D., Illa, M., Munoz-Moreno, E., Arbat-Plana, A., Amat-Roldan, I., Figueras, F., Gratacos, E., 2012. Neonatal neurobehavior and diffusion MRI changes in brain reorganization due to intrauterine growth restriction in a rabbit model. PLoS ONE 7, e31497.
Eixarch, E., Figueras, F., Hernandez-Andrade, E., Crispi, F., Nadal, A., Torre, I., Oliveira, S., Gratacos, E., 2009. An experimental model of fetal growth restriction based on selective ligature of uteroplacental vessels in the pregnant rabbit. Fetal Diagn Ther 26, 203-211.
Eixarch, E., Hernandez-Andrade, E., Crispi, F., Illa, M., Torre, I., Figueras, F., Gratacos, E., 2011. Impact on fetal mortality and cardiovascular Doppler of selective ligature of uteroplacental vessels compared with undernutrition in a rabbit model of intrauterine growth restriction. Placenta 32, 304-309.
Eixarch, E., Meler, E., Iraola, A., Illa, M., Crispi, F., Hernandez-Andrade, E., Gratacos, E., Figueras, F., 2008. Neurodevelopmental outcome in 2-year-old infants who were small-for-gestational age term fetuses with cerebral blood flow redistribution. Ultrasound Obstet Gynecol 32, 894-899.
Emond, V., Joyal, C., Poissant, H., 2009. Structural and functional neuroanatomy of attention-deficit hyperactivity disorder (ADHD). Encephale 35, 107-114.
Esteban, F.J., Padilla, N., Sanz-Cortes, M., de Miras, J.R., Bargallo, N., Villoslada, P., Gratacos, E., 2010. Fractal-dimension analysis detects cerebral changes in preterm infants with and without intrauterine growth restriction. Neuroimage 53, 1225-1232.
Estrada-Camarena, E., Contreras, C.M., Saavedra, M., Luna-Baltazar, I., Lopez-Rubalcava, C., 2002. Participation of the lateral septal nuclei (LSN) in the antidepressant-like actions of progesterone in the forced swimming test (FST). Behav Brain Res 134, 175-183.
Fagel, D.M., Ganat, Y., Silbereis, J., Ebbitt, T., Stewart, W., Zhang, H., Ment, L.R., Vaccarino, F.M., 2006. Cortical neurogenesis enhanced by chronic perinatal hypoxia. Exp Neurol 199, 77-91.
Fan, Y., Shi, F., Smith, J.K., Lin, W., Gilmore, J.H., Shen, D., 2011. Brain anatomical networks in early human brain development. Neuroimage 54, 1862-1871.
Faraone, S.V., Biederman, J., 1998. Neurobiology of attention-deficit hyperactivity disorder. Biol Psychiatry 44, 951-958.
Feldman, R., Eidelman, A.I., 2006. Neonatal state organization, neuromaturation, mother-infant interaction, and cognitive development in small-for-gestational-age premature infants. Pediatrics 118, e869-878.
Figueras, F., Meler, E., Iraola, A., Eixarch, E., Coll, O., Figueras, J., Francis, A., Gratacos, E., Gardosi, J., 2008. Customized birthweight standards for a Spanish population. Eur J Obstet Gynecol Reprod Biol 136, 20-24.

Figueras, F., Oros, D., Cruz-Martinez, R., Padilla, N., Hernandez-Andrade, E., Botet, F., Costas-Moragas, C., Gratacos, E., 2009. Neurobehavior in term, small-for-gestational age infants with normal placental function. Pediatrics 124, e934-941.

Fischi-Gomez, E., Vasung, L., Meskaldji, D.E., Lazeyras, F., Borradori-Tolsa, C., Hagmann, P., Barisnikov, K., Thiran, J.P., Huppi, P.S., 2014. Structural Brain Connectivity in School-Age Preterm Infants Provides Evidence for Impaired Networks Relevant for Higher Order Cognitive Skills and Social Cognition. Cereb Cortex. In Press,

Fox, M.D., Snyder, A.Z., Vincent, J.L., Corbetta, M., Van Essen, D.C., Raichle, M.E., 2005. The human brain is intrinsically organized into dynamic, anticorrelated functional networks. Proc Natl Acad Sci U S A 102, 9673-9678.

Fransson, P., Aden, U., Blennow, M., Lagercrantz, H., 2011. The functional architecture of the infant brain as revealed by resting-state FMRI. Cereb Cortex 21, 145-154.

Fransson, P., Skiold, B., Engstrom, M., Hallberg, B., Mosskin, M., Aden, U., Lagercrantz, H., Blennow, M., 2009. Spontaneous brain activity in the newborn brain during natural sleep--an fMRI study in infants born at full term. Pediatr Res 66, 301-305.

Fransson, P., Skiold, B., Horsch, S., Nordell, A., Blennow, M., Lagercrantz, H., Aden, U., 2007. Resting-state networks in the infant brain. Proc Natl Acad Sci U S A 104, 15531-15536.

Gao, W., Zhu, H., Giovanello, K.S., Smith, J.K., Shen, D., Gilmore, J.H., Lin, W., 2009. Evidence on the emergence of the brain's default network from 2-week-old to 2-year-old healthy pediatric subjects. Proc Natl Acad Sci U S A 106, 6790-6795.

Gardener, H., Spiegelman, D., Buka, S.L., 2011. Perinatal and neonatal risk factors for autism: a comprehensive meta-analysis. Pediatrics 128, 344-355.

Geva, R., Eshel, R., Leitner, Y., Fattal-Valevski, A., Harel, S., 2006a. Memory functions of children born with asymmetric intrauterine growth restriction. Brain Res 1117, 186-194.

Geva, R., Eshel, R., Leitner, Y., Valevski, A.F., Harel, S., 2006b. Neuropsychological outcome of children with intrauterine growth restriction: a 9-year prospective study. Pediatrics 118, 91-100.

Ginestet, C.E., Nichols, T.E., Bullmore, E.T., Simmons, A., 2011. Brain network analysis: separating cost from topology using cost-integration. PLoS ONE 6, e21570.

Gong, G., He, Y., Concha, L., Lebel, C., Gross, D.W., Evans, A.C., Beaulieu, C., 2009. Mapping anatomical connectivity patterns of human cerebral cortex using in vivo diffusion tensor imaging tractography. Cereb Cortex 19, 524-536.

Gong, G., He, Y., Chen, Z.J., Evans, A.C., 2011. Convergence and divergence of thickness correlations with diffusion connections across the human cerebral cortex. Neuroimage 59, 1239-1248.

Griffa, A., Baumann, P.S., Thiran, J.P., Hagmann, P., 2013. Structural connectomics in brain diseases. Neuroimage 80, 515-526.

Hagmann, P., 2005. From diffusion MRI to brain connectomics., Signal Processing Institute. Ecole Polytechnique Fédérale de Lausanne (EPFL), Lausane.

Hagmann, P., Cammoun, L., Gigandet, X., Meuli, R., Honey, C.J., Wedeen, V.J., Sporns, O., 2008. Mapping the structural core of human cerebral cortex. PLoS Biol 6, e159.

Hagmann, P., Jonasson, L., Maeder, P., 2006. Understanding Diffusion MR Imaging Techniques: From Scalar Diffusion-weighted Imaging to Diffusion Tensor Imaging and Beyond1. RadioGraphics 26, 205-224.

Hagmann, P., Kurant, M., Gigandet, X., Thiran, P., Wedeen, V.J., Meuli, R., Thiran, J.P., 2007. Mapping human whole-brain structural networks with diffusion MRI. PLoS ONE 2, e597.

Hagmann, P., Sporns, O., Madan, N., Cammoun, L., Pienaar, R., Wedeen, V.J., Meuli, R., Thiran, J.P., Grant, P.E., 2010. White matter maturation reshapes structural connectivity in the late developing human brain. Proc Natl Acad Sci U S A 107, 19067-19072.

Hall, F.S., Perona, M.T., 2012. Have studies of the developmental regulation of behavioral phenotypes revealed the mechanisms of gene-environment interactions? Physiol Behav 107, 623-640.
He, Y., Chen, Z., Evans, A.C., 2008. Structural insights into aberrant topological patterns of large-scale cortical networks in Alzheimer's disease. J Neurosci 28, 8148-8159.
He, Y., Chen, Z.J., Evans, A.C., 2007. Small-world anatomical networks in the human brain revealed by cortical thickness from MRI. Cereb Cortex 17, 2407-2419.
Heckers, S., Curran, T., Goff, D., Rauch, S.L., Fischman, A.J., Alpert, N.M., Schacter, D.L., 2000. Abnormalities in the thalamus and prefrontal cortex during episodic object recognition in schizophrenia. Biol Psychiatry 48, 651-657.
Heinonen, K., Räikkönen, K., Pesonen, A.-K., Andersson, S., Kajantie, E., Eriksson, J.G., Wolke, D., Lano, A., 2010. Behavioural symptoms of attention deficit/hyperactivity disorder in preterm and term children born small and appropriate for gestational age: a longitudinal study. BMC pediatrics 10, 91.
Horovitz, S.G., Braun, A.R., Carr, W.S., Picchioni, D., Balkin, T.J., Fukunaga, M., Duyn, J.H., 2009. Decoupling of the brain's default mode network during deep sleep. Proc Natl Acad Sci U S A 106, 11376-11381.
Huang, H., Vasung, L., 2014. Gaining insight of fetal brain development with diffusion MRI and histology. Int J Dev Neurosci 32, 11-22.
Illa, M., Eixarch, E., Batalle, D., Arbat-Plana, A., Muñoz-Moreno, E., Figueras, F., Gratacos, E., 2013. Long-Term Functional Outcomes and Correlation with Regional Brain Connectivity by MRI Diffusion Tractography Metrics in a Near-Term Rabbit Model of Intrauterine Growth Restriction. PLoS ONE 8, e76453.
Iturria-Medina, Y., Perez Fernandez, A., Valdes Hernandez, P., Garcia Penton, L., Canales-Rodriguez, E.J., Melie-Garcia, L., Lage Castellanos, A., Ontivero Ortega, M., 2011. Automated discrimination of brain pathological state attending to complex structural brain network properties: the shiverer mutant mouse case. PLoS ONE 6, e19071.
Iturria-Medina, Y., Sotero, R.C., Canales-Rodríguez, E.J., Alemán-Gómez, Y., Melie-García, L., 2008. Studying the human brain anatomical network via diffusion-weighted MRI and graph theory. Neuroimage 40, 1064-1076.
Jarvis, S., Glinianaia, S.V., Torrioli, M.G., Platt, M.J., Miceli, M., Jouk, P.S., Johnson, A., Hutton, J., Hemming, K., Hagberg, G., Dolk, H., Chalmers, J., 2003. Cerebral palsy and intrauterine growth in single births: European collaborative study. Lancet 362, 1106-1111.
Kadohisa, M., Wilson, D.A., 2006. Separate encoding of identity and similarity of complex familiar odors in piriform cortex. Proc Natl Acad Sci U S A 103, 15206-15211.
Kady, S., Gardosi, J., 2004. Perinatal mortality and fetal growth restriction. Best Pract Res Clin Obstet Gynaecol 18, 397-410.
Kim, M.J., Whalen, P.J., 2009. The structural integrity of an amygdala-prefrontal pathway predicts trait anxiety. J Neurosci 29, 11614-11618.
Knickmeyer, R.C., Gouttard, S., Kang, C., Evans, D., Wilber, K., Smith, J.K., Hamer, R.M., Lin, W., Gerig, G., Gilmore, J.H., 2008. A structural MRI study of human brain development from birth to 2 years. J Neurosci 28, 12176-12182.
Kobel, M., Bechtel, N., Specht, K., Klarhöfer, M., Weber, P., Scheffler, K., Opwis, K., Penner, I.-K., 2010. Structural and functional imaging approaches in attention deficit/hyperactivity disorder: does the temporal lobe play a key role? Psychiatry research 183, 230-236.
Kwong, K.K., Hopkins, A.L., Belliveau, J.W., Chesler, D.A., Porkka, L.M., McKinstry, R.C., Finelli, D.A., Hunter, G.J., Moore, J.B., Barr, R.G., et al., 1991. Proton NMR imaging of cerebral blood flow using H2(17)O. Magn Reson Med 22, 154-158.

Larson-Prior, L.J., Zempel, J.M., Nolan, T.S., Prior, F.W., Snyder, A.Z., Raichle, M.E., 2009. Cortical network functional connectivity in the descent to sleep. Proc Natl Acad Sci U S A 106, 4489-4494.
Latora, V., Marchiori, M., 2001. Efficient behavior of small-world networks. Phys Rev Lett 87, 198701.
Lauterbur, P.C., 1973. Image Formation by Induced Local Interactions: Examples Employing Nuclear Magnetic Resonance. Nature 242, 190-191.
Le Bihan, D., Breton, E., 1985. Imagerie de Diffusion In Vivo par Résonance Magnétique Nucléaire. XXX CR Académie des Sciences de Paris 301, 1109-1112.
Leitner, Y., Fattal-Valevski, A., Geva, R., Eshel, R., Toledano-Alhadef, H., Rotstein, M., Bassan, H., Radianu, B., Bitchonsky, O., Jaffa, A.J., Harel, S., 2007. Neurodevelopmental outcome of children with intrauterine growth retardation: a longitudinal, 10-year prospective study. J Child Neurol 22, 580-587.
Li, Y., Liu, Y., Li, J., Qin, W., Li, K., Yu, C., Jiang, T., 2009. Brain anatomical network and intelligence. PLoS Comput Biol 5, e1000395.
Lin, W., Zhu, Q., Gao, W., Chen, Y., Toh, C.H., Styner, M., Gerig, G., Smith, J.K., Biswal, B., Gilmore, J.H., 2008. Functional connectivity MR imaging reveals cortical functional connectivity in the developing brain. AJNR Am J Neuroradiol 29, 1883-1889.
Linnet, K.M., Wisborg, K., Agerbo, E., Secher, N.J., Thomsen, P.H., Henriksen, T.B., 2006. Gestational age, birth weight, and the risk of hyperkinetic disorder. Arch Dis Child 91, 655-660.
Liu, Y., Liang, M., Zhou, Y., He, Y., Hao, Y., Song, M., Yu, C., Liu, H., Liu, Z., Jiang, T., 2008. Disrupted small-world networks in schizophrenia. Brain 131, 945-961.
Lo, C.Y., Wang, P.N., Chou, K.H., Wang, J., He, Y., Lin, C.P., 2010. Diffusion tensor tractography reveals abnormal topological organization in structural cortical networks in Alzheimer's disease. J Neurosci 30, 16876-16885.
Lodygensky, G.A., Seghier, M.L., Warfield, S.K., Tolsa, C.B., Sizonenko, S., Lazeyras, F., Huppi, P.S., 2008. Intrauterine growth restriction affects the preterm infant's hippocampus. Pediatr Res 63, 438-443.
Logothetis, N.K., Pauls, J., Augath, M., Trinath, T., Oeltermann, A., 2001. Neurophysiological investigation of the basis of the fMRI signal. Nature 412, 150-157.
Løhaugen, G.C., Østgård, H.F., Andreassen, S., Jacobsen, G.W., Vik, T., Brubakk, A.M., Skranes, J., Martinussen, M., 2013. Small for gestational age and intrauterine growth restriction decreases cognitive function in young adults. J Pediatr 163, 447-453.
Lynall, M.E., Bassett, D.S., Kerwin, R., McKenna, P.J., Kitzbichler, M., Muller, U., Bullmore, E., 2010. Functional connectivity and brain networks in schizophrenia. J Neurosci 30, 9477-9487.
Makki, M.I., Govindan, R.M., Wilson, B.J., Behen, M.E., Chugani, H.T., 2009. Altered fronto-striato-thalamic connectivity in children with Tourette syndrome assessed with diffusion tensor MRI and probabilistic fiber tracking. J Child Neurol 24, 669-678.
Mallard, C., Loeliger, M., Copolov, D., Rees, S., 2000. Reduced number of neurons in the hippocampus and the cerebellum in the postnatal guinea-pig following intrauterine growth-restriction. Neuroscience 100, 327-333.
Mansfield, P., Maudsley, A.A., 1977. Medical imaging by NMR. Br J Radiol 50, 188-194.
Martinussen, M., Fischl, B., Larsson, H.B., Skranes, J., Kulseng, S., Vangberg, T.R., Vik, T., Brubakk, A.M., Haraldseth, O., Dale, A.M., 2005. Cerebral cortex thickness in 15-year-old adolescents with low birth weight measured by an automated MRI-based method. Brain 128, 2588-2596.
Martinussen, M., Flanders, D.W., Fischl, B., Busa, E., Lohaugen, G.C., Skranes, J., Vangberg, T.R., Brubakk, A.M., Haraldseth, O., Dale, A.M., 2009. Segmental brain volumes and cognitive and perceptual correlates in 15-year-old adolescents with low birth weight. J Pediatr 155, 848-853 e841.

Maslov, S., Sneppen, K., 2002. Protein interaction networks beyond artifacts. FEBS Lett 530, 255-256.
Maximo, J.O., Cadena, E.J., Kana, R.K., 2014. The Implications of Brain Connectivity in the Neuropsychology of Autism. Neuropsychol Rev.
McAnulty, G., Duffy, F.H., Kosta, S., Weisenfeld, N.I., Warfield, S.K., Butler, S.C., Alidoost, M., Bernstein, J.H., Robertson, R., Zurakowski, D., Als, H., 2013. School-age effects of the newborn individualized developmental care and assessment program for preterm infants with intrauterine growth restriction: preliminary findings. BMC Pediatr 13, 25.
McCarton, C.M., Wallace, I.F., Divon, M., Vaughan, H.G., Jr., 1996. Cognitive and neurologic development of the premature, small for gestational age infant through age 6: comparison by birth weight and gestational age. Pediatrics 98, 1167-1178.
McCowan, L.M., Pryor, J., Harding, J.E., 2002. Perinatal predictors of neurodevelopmental outcome in small-for-gestational-age children at 18 months of age. Am J Obstet Gynecol 186, 1069-1075.
Menon, V., 2013. Developmental pathways to functional brain networks: emerging principles. Trends Cogn Sci 17, 627-640.
Ment, L.R., Hirtz, D., Huppi, P.S., 2009. Imaging biomarkers of outcome in the developing preterm brain. Lancet Neurol 8, 1042-1055.
Miller, M.M., Morrison, J.H., McEwen, B.S., 2012. Basal anxiety-like behavior predicts differences in dendritic morphology in the medial prefrontal cortex in two strains of rats. Behav Brain Res 229, 280-288.
Mitchell, A.S., Dalrymple-Alford, J.C., 2005. Dissociable memory effects after medial thalamus lesions in the rat. Eur J Neurosci 22, 973-985.
Moore, G.S., Kneitel, A.W., Walker, C.K., Gilbert, W.M., Xing, G., 2012. Autism risk in small- and large-for-gestational-age infants. Am J Obstet Gynecol 206, 314 e311-319.
Muñoz-Moreno, E., Arbat-Plana, A., Batalle, D., Soria, G., Illa, M., Prats-Galino, A., Eixarch, E., Gratacos, E., 2013. A magnetic resonance image based atlas of the rabbit brain for automatic parcellation. PLoS ONE 8, e67418.
Nielsen, P.R., Mortensen, P.B., Dalman, C., Henriksen, T.B., Pedersen, M.G., Pedersen, C.B., Agerbo, E., 2013. Fetal growth and schizophrenia: a nested case-control and case-sibling study. Schizophr Bull 39, 1337-1342.
Nilsson, E., Stalberg, G., Lichtenstein, P., Cnattingius, S., Olausson, P.O., Hultman, C.M., 2005. Fetal growth restriction and schizophrenia: a Swedish twin study. Twin Res Hum Genet 8, 402-408.
Nugent, J., Brazelton, T., 2000. Preventive mental health: Uses of the Brazelton Scale. Wiley, New York, NY.
Ogawa, S., Lee, T.M., Nayak, A.S., Glynn, P., 1990. Oxygenation-sensitive contrast in magnetic resonance image of rodent brain at high magnetic fields. Magn Reson Med 14, 68-78.
Padilla, N., Falcon, C., Sanz-Cortes, M., Figueras, F., Bargallo, N., Crispi, F., Eixarch, E., Arranz, A., Botet, F., Gratacos, E., 2011. Differential effects of intrauterine growth restriction on brain structure and development in preterm infants: a magnetic resonance imaging study. Brain Res 1382, 98-108.
Paulus, M.P., Stein, M.B., 2006. An insular view of anxiety. Biol Psychiatry 60, 383-387.
Paus, T., Collins, D.L., Evans, A.C., Leonard, G., Pike, B., Zijdenbos, A., 2001. Maturation of white matter in the human brain: a review of magnetic resonance studies. Brain Res Bull 54, 255-266.
Pierpaoli, C., Basser, P.J., 1996. Toward a quantitative assessment of diffusion anisotropy. Magn Reson Med 36, 893-906.
Raj, A., Mueller, S.G., Young, K., Laxer, K.D., Weiner, M., 2010. Network-level analysis of cortical thickness of the epileptic brain. Neuroimage 52, 1302-1313.
Rees, S., Harding, R., Walker, D., 2011. The biological basis of injury and neuroprotection in the fetal and neonatal brain. Int J Dev Neurosci 29, 551-563.

Robinson, H.P., Fleming, J.E., 1975. A critical evaluation of sonar "crown-rump length" measurements. Br J Obstet Gynaecol 82, 702-710.
Rubinov, M., Sporns, O., 2009. Complex network measures of brain connectivity: uses and interpretations. Neuroimage 52, 1059-1069.
Rudie, J.D., Brown, J.A., Beck-Pancer, D., Hernandez, L.M., Dennis, E.L., Thompson, P.M., Bookheimer, S.Y., Dapretto, M., 2012. Altered functional and structural brain network organization in autism. Neuroimage Clin 2, 79-94.
Sagiv, S.K., Nugent, J.K., Brazelton, T.B., Choi, A.L., Tolbert, P.E., Altshul, L.M., Korrick, S.A., 2008. Prenatal organochlorine exposure and measures of behavior in infancy using the Neonatal Behavioral Assessment Scale (NBAS). Environ Health Perspect 116, 666-673.
Salvador, R., Suckling, J., Coleman, M.R., Pickard, J.D., Menon, D., Bullmore, E., 2005. Neurophysiological architecture of functional magnetic resonance images of human brain. Cereb Cortex 15, 1332-1342.
Sandrone, S., Bacigaluppi, M., Galloni, M.R., Cappa, S.F., Moro, A., Catani, M., Filippi, M., Monti, M.M., Perani, D., Martino, G., 2014. Weighing brain activity with the balance: Angelo Mosso's original manuscripts come to light. Brain 137, 621-633.
Sanz-Cortes, M., Ratta, G.A., Figueras, F., Bonet-Carne, E., Padilla, N., Arranz, A., Bargallo, N., Gratacos, E., 2013. Automatic quantitative MRI texture analysis in small-for-gestational-age fetuses discriminates abnormal neonatal neurobehavior. PLoS ONE 8, e69595.
Scherjon, S., Briet, J., Oosting, H., Kok, J., 2000. The discrepancy between maturation of visual-evoked potentials and cognitive outcome at five years in very preterm infants with and without hemodynamic signs of fetal brain-sparing. Pediatrics 105, 385-391.
Scherjon, S.A., Smolders-DeHaas, H., Kok, J.H., Zondervan, H.A., 1993. The "brain-sparing" effect: antenatal cerebral Doppler findings in relation to neurologic outcome in very preterm infants. Am J Obstet Gynecol 169, 169-175.
Shi, F., Yap, P.T., Wu, G., Jia, H., Gilmore, J.H., Lin, W., Shen, D., 2011. Infant brain atlases from neonates to 1- and 2-year-olds. PLoS ONE 6, e18746.
Shu, N., Liu, Y., Li, J., Li, Y., Yu, C., Jiang, T., 2009. Altered anatomical network in early blindness revealed by diffusion tensor tractography. PLoS ONE 4, e7228.
Shu, N., Liu, Y., Li, K., Duan, Y., Wang, J., Yu, C., Dong, H., Ye, J., He, Y., 2011. Diffusion tensor tractography reveals disrupted topological efficiency in white matter structural networks in multiple sclerosis. Cereb Cortex 21, 2565-2577.
Skranes, J.S., Martinussen, M., Smevik, O., Myhr, G., Indredavik, M., Vik, T., Brubakk, A.M., 2005. Cerebral MRI findings in very-low-birth-weight and small-for-gestational-age children at 15 years of age. Pediatr Radiol 35, 758-765.
Smith, S.M., 2002. Fast robust automated brain extraction. Hum Brain Mapp 17, 143-155.
Smyser, C.D., Inder, T.E., Shimony, J.S., Hill, J.E., Degnan, A.J., Snyder, A.Z., Neil, J.J., 2010. Longitudinal analysis of neural network development in preterm infants. Cereb Cortex 20, 2852-2862.
Smyser, C.D., Snyder, A.Z., Neil, J.J., 2011. Functional connectivity MRI in infants: exploration of the functional organization of the developing brain. Neuroimage 56, 1437-1452.
Sobradillo, B., Aguirre, A., Aresti, U., Bilbao, C., Fernandez-Ramos, C., Lizarraga, A., Lorenzo, H., Madariaga, L., Rica, I., Ruiz, I., Sanchez, E., Santamaria, C., Serrano, J., Zabala, A., Zurimendi, B., Hernandez, M., 2004. Curvas y tablas de crecimiento (Estudios longitudinal y transversal). Fundacion Faustino Orbegozo Eizaguirre Bilbao.
Spampinato, M.V., Wood, J.N., De Simone, V., Grafman, J., 2009. Neural correlates of anxiety in healthy volunteers: a voxel-based morphometry study. J Neuropsychiatry Clin Neurosci 21, 199-205.

Sporns, O., Tononi, G., Kotter, R., 2005. The human connectome: A structural description of the human brain. PLoS Comput Biol 1, e42.
Stejskal, E.O., Tanner, J.E., 1965. Spin Diffusion Measurements: Spin Echoes in the Presence of a Time-Dependent Field Gradient. The Journal of Chemical Physics 42, 288-292.
Tau, G.Z., Peterson, B.S., 2010. Normal development of brain circuits. Neuropsychopharmacology 35, 147-168.
Thomason, M.E., Dassanayake, M.T., Shen, S., Katkuri, Y., Alexis, M., Anderson, A.L., Yeo, L., Mody, S., Hernandez-Andrade, E., Hassan, S.S., Studholme, C., Jeong, J.W., Romero, R., 2013. Cross-hemispheric functional connectivity in the human fetal brain. Sci Transl Med 5, 173ra124.
Thompson, D.K., Warfield, S.K., Carlin, J.B., Pavlovic, M., Wang, H.X., Bear, M., Kean, M.J., Doyle, L.W., Egan, G.F., Inder, T.E., 2007. Perinatal risk factors altering regional brain structure in the preterm infant. Brain 130, 667-677.
Tijms, B.M., Moller, C., Vrenken, H., Wink, A.M., de Haan, W., van der Flier, W.M., Stam, C.J., Scheltens, P., Barkhof, F., 2013. Single-subject grey matter graphs in Alzheimer's disease. PLoS ONE 8, e58921.
Tijms, B.M., Series, P., Willshaw, D.J., Lawrie, S.M., 2012. Similarity-based extraction of individual networks from gray matter MRI scans. Cereb Cortex 22, 1530-1541.
Toft, P.B., 1999. Prenatal and perinatal striatal injury: a hypothetical cause of attention-deficit-hyperactivity disorder? Pediatr Neurol 21, 602-610.
Tolcos, M., Bateman, E., O'Dowd, R., Markwick, R., Vrijsen, K., Rehn, A., Rees, S., 2011. Intrauterine growth restriction affects the maturation of myelin. Exp Neurol 232, 53-65.
Tolsa, C.B., Zimine, S., Warfield, S.K., Freschi, M., Sancho Rossignol, A., Lazeyras, F., Hanquinet, S., Pfizenmaier, M., Huppi, P.S., 2004. Early alteration of structural and functional brain development in premature infants born with intrauterine growth restriction. Pediatr Res 56, 132-138.
Tristan-Vega, A., Arribas, J.I., 2007. A Fast B-Spline Pseudo-inversion Algorithm for Consistent Image Registration. Proceedings of the International Conference on Computer Analysis Images and Patterns (CAIP), Vienna, Austria, pp. 768-775.
Tuch, D.S., 2004. Q-ball imaging. Magn Reson Med 52, 1358-1372.
Tzourio-Mazoyer, N., Landeau, B., Papathanassiou, D., Crivello, F., Etard, O., Delcroix, N., Mazoyer, B., Joliot, M., 2002. Automated anatomical labeling of activations in SPM using a macroscopic anatomical parcellation of the MNI MRI single-subject brain. Neuroimage 15, 273-289.
Van Essen, D.C., 1997. A tension-based theory of morphogenesis and compact wiring in the central nervous system. Nature 385, 313-318.
Wang, L., Zhu, C., He, Y., Zang, Y., Cao, Q., Zhang, H., Zhong, Q., Wang, Y., 2009. Altered small-world brain functional networks in children with attention-deficit/hyperactivity disorder. Hum Brain Mapp 30, 638-649.
Wang, Q., Su, T.P., Chou, K.H., Chen, I.Y., Jiang, T., Lin, C.P., 2012. Anatomical insights into disrupted small-world networks in schizophrenia. Neuroimage 59, 1085-1093.
Wang, R., Benner, T., Sorensen, A.G., Wedeen, V.J., 2007. Diffusion toolkit: a software package for diffusion imaging data processing and tractography. Proc Intl Soc Mag Reson Med, p. 3720.
Warfield, S.K., Guimond, A., Roche, A., Bharatha, A., Tei, A., Talos, F., Rexilius, J., Ruiz-Alzola, J., Westin, C.F., Haker, S., Angenent, S., Tannenbaum, A., Jolesz, F., Kilkinis, R., 2002. Advanced Nonrigid Registration Algorithms for Image Fusion. In: Mazziotta, J.C., Toga, A.W. (Eds.), Brain Mapping: The Methods. Elsevier, pp. 661-690.
Watts, D.J., Strogatz, S.H., 1998. Collective dynamics of 'small-world' networks. Nature 393, 440-442.
Wedeen, V.J., Hagmann, P., Tseng, W.Y., Reese, T.G., Weisskoff, R.M., 2005. Mapping complex tissue architecture with diffusion spectrum magnetic resonance imaging. Magn Reson Med 54, 1377-1386.

Wee, C.-Y., Yap, P.-T., Li, W., Denny, K., Browndyke, J.N., Potter, G.G., Welsh-Bohmer, K.a., Wang, L., Shen, D., 2010. Enriched white matter connectivity networks for accurate identification of MCI patients. Neuroimage 54, 1812-1822.

Wen, W., Zhu, W., He, Y., Kochan, N.A., Reppermund, S., Slavin, M.J., Brodaty, H., Crawford, J., Xia, A., Sachdev, P., 2011. Discrete neuroanatomical networks are associated with specific cognitive abilities in old age. J Neurosci 31, 1204-1212.

Williams, L.A., Gelman, N., Picot, P.A., Lee, D.S., Ewing, J.R., Han, V.K., Thompson, R.T., 2005. Neonatal brain: regional variability of in vivo MR imaging relaxation rates at 3.0 T--initial experience. Radiology 235, 595-603.

Yan, C., Gong, G., Wang, J., Wang, D., Liu, D., Zhu, C., Chen, Z.J., Evans, A., Zang, Y., He, Y., 2010. Sex- and brain size-related small-world structural cortical networks in young adults: a DTI tractography study. Cereb Cortex 21, 449-458.

Yap, P.T., Fan, Y., Chen, Y., Gilmore, J.H., Lin, W., Shen, D., 2011. Development trends of white matter connectivity in the first years of life. PLoS ONE 6, e24678.

Zeng, L.L., Shen, H., Liu, L., Wang, L., Li, B., Fang, P., Zhou, Z., Li, Y., Hu, D., 2012. Identifying major depression using whole-brain functional connectivity: a multivariate pattern analysis. Brain 135, 1498-1507.

Zhou, L., Wang, Y., Li, Y., Yap, P.T., Shen, D., 2011. Hierarchical anatomical brain networks for MCI prediction: revisiting volumetric measures. PLoS ONE 6, e21935.

11. ACKNOWLEDGEMENTS

First of all, I would like to express my sincere gratitude to my thesis director, Eduard Gratacós, who trusted in me since the beginning and supported, guided and advised me during all these years of PhD. My greatest gratitude also to my other thesis director, Elisenda Eixarch, who introduced me to the clinical world, and has always been there when I needed her, helping and advising me in many things in this road to obtain a PhD. My sincere thanks also to Emma Muñoz, whose advice is inestimable for me, and always provided a smile when needed (and codes, and revisions, and suggestions…). I would also like to thank Ivan Amat, who introduced me to the world of brain networks, for his help and advice during the first years of the PhD. My gratitude also to the technicians that performed and helped to design MRI acquisitions, in special Cesar Garrido from the IDIBAPS imaging core facilities, and to Guadalupe Soria and Raul Tudela from 7T MR animal platform of IDIPABS. My thanks also to all the co-authors of the articles presented in this thesis, from whom I have learned so much. And of course, to all the infants who kindly allowed us to use their brain images to perform the studies presented in this thesis.

Vull expressar el meu agraïment també a tots els companys de feina, cafès, dinars, riures i after-works, ha estat un plaer compartir tots aquests anys amb vosaltres. M'agradaria recordar també als enginyers amb els que vam començar aquesta aventura, l'Alvaro, la Senda i la Patri, m'heu acompanyat i ajudat durant tots aquests anys i espero no perdre-us de vista.

Per suposat, no em puc oblidar dels amics de Barcelona i de l'Empordà (Luchi, Pericu, Carlus, Etu, Hare, Nat, Esteve, Pep, Alfredo, Emma, Txetxu, Àlvaro,...) que han estat molt a prop meu durant tots aquest anys de tesi, donant-me moral, i sobretot, salut mental.

Per tot, però en especial per ensenyar-me a estimar el coneixement, vull expressar molt especialment la meva gratitud a la meva família, la meva àvia Victoria i els meus pares, en Narcis i la Salomé.

Finally, I would like to deeply acknowledge all the great men and women that, all through human history, dedicated their life to science, knowledge and enlightenment:

Nanos gigantum humeris insidentes.

12. APPENDIX I: SUMMARY IN CATALAN (RESUM EN CATALÀ)

12.1. Introducció

12.1.1. Restricció de creixement intrauterí

La restricció de creixement intrauterí (RCIU) deguda a insuficiència placentària afecta entre el 5 i el 10% de tots els embarassos i és una de les principals causes de morbiditat i mortalitat fetal (Jarvis et al., 2003; Kady and Gardosi, 2004). En concret, la reducció del flux sanguini placentari resulta en una exposició sostinguda a hipoxèmia i malnutrició (Baschat, 2004) que té conseqüències severes en el cervell en desenvolupament (Rees et al., 2011). Un nombre substancial d'estudis ha descrit associacions entre RCIU i problemes cognitius i del neurodesenvolupament en període neonatal (Bassan et al., 2011; Figueras et al., 2009), infància (Bassan et al., 2011; Eixarch et al., 2008; Feldman and Eidelman, 2006; Geva et al., 2006a; Geva et al., 2006b; Leitner et al., 2007; McCarton et al., 1996; Scherjon et al., 2000), i etapa adulta (Løhaugen et al., 2013). Per aquest motiu, la caracterització de les alteracions cerebrals subjacents a aquests problemes de neurodesenvolupament representa un dels principals reptes de la medicina fetal i pediàtrica moderna ja que és la base per a poder desenvolupar biomarcadors d'imatge per a la identificació de la població amb risc elevat de tenir problemes de neurodesenvolupament (Ment et al., 2009).

12.1.2. Imatge per ressonància magnètica

Aquesta necessitat d'obtenir biomarcadors precoços s'ha vist acompanyada per l'evolució dels biomarcadors basats en imatge, i l'avanç radical de les tècniques d'imatge per ressonància magnètica (MRI). La MRI és una tècnica no invasiva que permet estudiar les propietats i estructures dels teixits del cos humà sota un fort camp magnètic, basant-se en la seva resposta a polsós de radiofreqüència. Les tècniques típicament emprades en la pràctica clínica permeten una reconstrucció anatòmica detallada de diferents teixits, especialment sensible als que formen el cervell, com la matèria blanca i la matèria grisa. Això ha permès que en els últims anys aquesta tècnica es converteixi en una de les eines més emprades per millorar el coneixement científic de l'estructura i la funció del cervell.

Però més enllà de les tècniques clàssiques utilitzades per obtenir reconstruccions anatòmiques detallades del teixit cerebral, altres subtècniques de MRI s'han desenvolupat, permetent obtenir informació complementària de l'estructura i la funció del cervell. D'aquestes destaquen en especial la ressonància magnètica per difusió (*diffusion MRI*) i la ressonància magnètica funcional (*fMRI*). Per una banda, la *diffusion MRI*, basant-se en la difusió de l'aigua en cada punt del cervell, i en que aquesta difusió està restringida per les característiques del teixit, en especial per la matèria blanca mielinitzada, permet obtenir una reconstrucció dels tractes de matèria blanca que formen el cervell, en el que es coneix com a *tractografia*. Diferents tècniques són emprades amb l'objectiu de modelar la difusió de l'aigua en cada punt (vòxel) del cervell, essent la imatge de tensor de difusió (DTI) la més utilitzada. Tot i això, la DTI presenta algunes limitacions tècniques que són superades per altres tipus de model més avançats com són la *Q-Ball imaging* (Tuch, 2004), que a diferència de la DTI permet la caracterització de fibres de matèria blanca que creuen pel mateix punt al cervell i ofereixen una resolució angular molt superior. Però independentment de la tècnica emprada, la ressonància magnètica per difusió i les tractografies obtingudes amb aquesta eina, són especialment rellevants ja que la informació que aporten sobre l'organització dels tractes de matèria blanca, unida amb informació anatòmica que permet identificar diferents regions del cervell, fa possible modelar el cervell com una xarxa de comunicacions que descriu com cadascuna de les regions del cervell està connectada de manera estructural amb la resta de regions. Per altra banda, la *fMRI* utilitza models estadístics per caracteritzar canvis en la magnetització que permeten diferenciar teixits amb un alt o un baix nivell d'oxigen. En especial, la *fMRI* permet obtenir un senyal anomenat *blood-oxygen-level dependent* (*BOLD*) en diversos instants de temps, permetent veure l'evolució de l'oxigenació-desoxigenació dels teixits en cada punt del cervell, típicament durant diversos minuts. La rellevància de la tècnica és que aquesta oxigenació-desoxigenació del teixit que permet veure el senyal BOLD està associada amb l'activitat neuronal (Logothetis et al., 2001). Diferents estudis basats en *fMRI* han proliferat en els últims anys, utilitzant diverses tècniques per modelar i avaluar l'activitat cerebral de manera individual i grupal. De les tècniques desenvolupades destaca la utilització de contrastos

basats en dissenys de blocs d'estímuls, que permeten comparar l'activitat basal respecte l'activitat sota un estímul determinat. No obstant, mitjançant l'anàlisi detallat de l'activitat basal, és a dir, amb el cervell en repòs, s'ha demostrat que existeixen fluctuacions a baixa freqüència amb un alt nivell de correlació temporal, fortament associades amb la connectivitat funcional subjacent del cervell (Biswal et al., 1995). Estudis posteriors d'aquesta activitat del cervell en repòs mitjançant anàlisis de components independents (ICA) demostraren una anticorrelació espacial molt diferenciada entre diferents àrees del cervell, suggerint l'existència de xarxes funcionals actives en el cervell en repòs, incloent la rellevant *default mode network* (Fox et al., 2005). En els últims anys, aquestes fluctuacions de baixa freqüència s'han utilitzat també per modelar la xarxa funcional del cervell en repòs de manera exhaustiva, mitjançant l'anàlisi de les correlacions de el senyal BOLD de cadascuna de les regions del cervell amb la resta (Salvador et al., 2005), permetent obtenir xarxes funcionals comparables a les xarxes estructurals obtingudes amb ressonància magnètica per difusió.

12.1.3. Imatge per ressonància magnètica en la restricció de creixement intrauterí

Amb l'avanç significatiu de la MRI, les alteracions cerebrals subjacents als problemes de neurodesenvolupament associats a la restricció de creixement intrauterí estan començant a ésser dilucidades. En especial, s'ha suggerit que la restricció del creixement està associada a una reorganització cerebral que comença *in utero*, caracteritzada per l'existència de patrons diferenciats de desenvolupament cortical (Egaña-Ugrinovic et al., 2013) i per alteracions en les textures quantitatives de MRI (Sanz-Cortes et al., 2013) associades a alteracions al neurodesenvolupament posterior. En període neonatal, la restricció de creixement intrauterí s'ha associat a reduccions en el volum de matèria grisa (Tolsa et al., 2004) i de l'hipocamp (Lodygensky et al., 2008), i amb patrons discordants en la girificació del còrtex (Dubois et al., 2008). La persistència de canvis estructurals a l'any de vida també s'ha descrit, demostrant volums reduïts de matèria grisa en àrees temporals, parietals, frontals i insulars (Padilla et al., 2011), i amb reduccions en la dimensió fractal de la matèria grisa i en la matèria blanca que correlen amb alteracions en el neurodesenvolupament

(Esteban et al., 2010). Estudis sobre els efectes d'aquesta condició en períodes posteriors de la vida han demostrat canvis en els volums de diverses regions i en el gruix cortical en nens de 4 a 7 anys d'estat (De Bie et al., 2011), reduccions en el volum cerebelar i de la matèria blanca (Martinussen et al., 2009), així com un escurçament del cos callós junt amb una reducció general de la matèria blanca en adolescents (Skranes et al., 2005). No obstant, tot i que tots aquests estudis són útils en la demostració de diferències associades amb una condició determinada, la possibilitat d'utilitzar informació provinent de la ressonància magnètica per generar biomarcadors d'imatge predictius d'alteracions en el desenvolupament és encara limitada, existint doncs la necessitat d'una millor caracterització de la reorganització cerebral subjacent a problemes cognitius i del neurodesenvolupament associats a la restricció de creixement intrauterí.

12.1.4. Xarxes cerebrals basades en imatge per ressonància magnètica

La utilització de models de xarxa cerebrals basats en ressonància magnètica és una tècnica emergent que permet extraure informació associada a l'organització cerebral de manera no invasiva. Basant-se en informació anatòmica i ressonància magnètica per difusió és possible obtenir xarxes cerebrals estructurals, mentre que combinant aquesta informació anatòmica amb ressonància magnètica funcional és possible obtenir xarxes cerebrals funcionals. Molt rellevant resulta també la possibilitat d'utilitzar teoria del graf per caracteritzar aquestes xarxes cerebrals, podent caracteritzar l'organització cerebral amb uns pocs paràmetres. Mitjançant aquesta branca de les matemàtiques és possible caracteritzar diferents característiques de les xarxes estudiades, de les quals destaca la infraestructura (grau mig i força mitjana), la integració (eficiència global) i la segregació (eficiència local) (Rubinov and Sporns, 2009). A més a més, la teoria del graf també permet l'anàlisi regional de diferències entre casos i controls mitjançant l'anàlisi de característiques corresponents a les xarxes regionals associades a cadascuna de les regions del cervell.

L'anàlisi exhaustiva de la connectivitat del cervell mitjançant xarxes estructurals i les seves característiques de teoria del graf, també s'ha anomenat amb el terme "connectòmica" (Hagmann, 2005), cadascuna de les xarxes cerebrals essent anomenades "connectomes"

(Sporns et al., 2005). Aquesta tècnica s'ha emprat amb èxit en l'anàlisi de l'estructura de la connectivitat en poblacions control (Gong et al., 2009; Hagmann et al., 2008; Iturria-Medina et al., 2008), essent les seves propietats associades a diferents característiques incloent el gènere, la mida cerebral, la intel·ligència i les capacitats cognitives en l'edat avançada (Li et al., 2009; Wen et al., 2011; Yan et al., 2010). A més a més també s'han reportat diferències significatives en grups patològics diversos tals com malaltia d'Alzheimer, esclerosi múltiple, esquizofrènia i ceguesa precoç (Wang et al., 2012; Lo et al., 2010; Wee et al., 2010; Shu et al., 2011; Shu et al., 2009). Respecte a la utilització d'aquesta tècnica en grups pediàtrics, s'ha aplicat amb èxit en la caracterització del desenvolupament normal del cervell humà des del naixement fins l'adolescència (Yap et al., 2011; Hagmann et al., 2010), però fins a la publicació dels articles associats a aquesta tesi no s'havia emprat mai en la caracterització de grups pediàtrics amb condicions d'origen prenatal com la restricció de creixement intrauterí, justificant la realització del **PROJECTE 1** d'aquesta tesi. No obstant, la caracterització de la reorganització cerebral produïda per la restricció de creixement intrauterí a llarg termini té associades diverses dificultats, en especial la dificultat d'obtenir una bona mostra poblacional ben caracteritzada amb unes condicions d'entorn similars. Per això resulta d'especial interès la utilització de models animals. En especial, un model animal de la restricció de creixement basat en el conill s'ha demostrat que reprodueix les principals característiques d'aquesta condició en humans (Bassan et al., 2000; Eixarch et al., 2009; Eixarch et al., 2011). La utilització d'aquest model presenta tota una sèrie d'avantatges per l'estudi de la restricció del creixement a llarg termini, incloent la seva alta reproductibilitat i la possibilitat d'obtenir imatges per ressonància magnètica de moltíssima qualitat mitjançant llargs temps d'adquisició. A més a més, el recent desenvolupament d'un atles anatòmic del conill en ressonància magnètica permet el desenvolupament i l'anàlisi de xarxes cerebrals en aquesta espècie. Així doncs, utilitzant aquest model animal, en la present tesi analitzem l'efecte de la restricció de creixement intrauterí a llarg termini en la reorganització estructural de la connectivitat cerebral (**PROJECTE 3**).

Tot i que la utilització de la ressonància magnètica per difusió cada vegada és més habitual en l'entorn de recerca, el seu ús en la pràctica clínica és molt escàs comparat amb les

adquisicions de contrast anatòmic (T1 i T2). Per això, basat en el concepte que correlacions de característiques de la matèria grisa (com volum o gruix cortical) a nivell grupal estan associats amb la connectivitat cerebral (He et al., 2007), adquisicions anatòmiques convencionals han estat emprades per obtenir xarxes estructurals de grup, que han permès una millor comprensió dels circuits cerebrals en poblacions sanes i patològiques (Bassett et al., 2008; Fan et al., 2011; He et al., 2008). No obstant, aquest tipus de tècnica no és útil per desenvolupar biomarcadors individuals, ja que es basen en correlacions a nivell poblacional. Tot i això, recentment apareixen una sèrie d'articles que proposen tècniques per obtenir xarxes cerebrals estructurals a partir de correlacions de característiques de matèria grisa a nivell individual, permetent doncs la utilització de models de xarxa per l'estudi de característiques de matèria grisa (Raj et al., 2010; Tijms et al., 2013; Tijms et al., 2012; Zhou et al., 2011). Aquestes metodologies, però, presenten una sèrie de problemes que inclouen l'obtenció d'una xarxa de mida variable per cada individu. La modificació d'aquest tipus de tècniques per obtenir xarxes cerebrals de mida fixa, basada en un atles anatòmic motiva la realització del **PROJECTE 2**, en que a més a més s'avalua la possibilitat d'utilitzar aquest tipus de tècnica per caracteritzar diferències produïdes per la restricció de creixement intrauterí en una població d'un any d'edat, i l'associació d'aquestes diferències en les característiques de xarxa amb alteracions en el neurodesenvolupament posterior.

Finalment, diversos estudis han demostrat la possibilitat d'utilitzar la ressonància magnètica funcional per caracteritzar l'organització cerebral normal en època neonatal, obrint la possibilitat d'utilitzar aquesta tècnica per caracteritzar la reorganització cerebral funcional produïda per patologies d'origen prenatal. Així doncs, mitjançant tècniques estadístiques com l'anàlisi de components independents, a partir de ressonàncies magnètiques funcionals de nounats en són natural, s'ha demostrat l'existència de xarxes cerebrals que es corresponen amb aquelles trobades en adults en repòs, incloent connexions similars a la *default mode network* (Dòria et al., 2010; Fransson et al., 2009; Fransson et al., 2007; Gaó et al., 2009; Lín et al., 2008; Smyser et al., 2010). Tot i això, mai s'han desenvolupat xarxes completes del cervell neonatal basades en un atles anatòmic. En la present tesi es desenvolupen per primer cop aquest tipus de xarxa en nounats, adaptant

tècniques emprades anteriorment amb èxit en adults (Zeng et al., 2012), i s'avalua la seva capacitat per caracteritzar diferències en l'organització cerebral funcional causades per la restricció de creixement intrauterí i la seva associació amb tests de neurocomportament (**PROJECTE 4**).

12.2. Hipòtesis i objectius

12.2.1. Hipòtesis

La principal hipòtesi d'aquesta tesi és que el neurodesenvolupament alterat produït per la RCIU té un substrat en l'organització estructural i funcional del cervell.

Les hipòtesis específiques són:

1. Les xarxes cerebrals estructurals obtingudes a partir de MRI de difusió permeten caracteritzar la reorganització estructural produïda per la RCIU en nens d'un any, estant aquesta associada amb alteracions al neurodesenvolupament observats en etapes posteriors.
    a. Les tècniques per obtenir xarxes cerebrals estructurals a partir de MRI de difusió es poden adaptar a poblacions pediàtriques.
    b. Els infants amb RCIU presenten una reorganització cerebral estructural que pot ser caracteritzada mitjançant característiques globals i regionals de teoria del graf.
    c. Els canvis en la connectivitat estructural a l'any de vida produïts per RCIU estan associats amb neurodesenvolupament alterat observat en etapes posteriors de la vida.

2. Les xarxes cerebrals estructurals individuals obtingudes a partir de similitud de característiques morfològiques de matèria grisa permeten demostrar diferències en infants amb RCIU, essent aquestes associades amb alteracions al neurodesenvolupament observats en etapes posteriors.

a. Les tècniques existents per obtenir xarxes estructurals individuals basades en característiques morfològiques de matèria grisa poden ésser adaptades a poblacions pediàtriques.
b. Aquestes tècniques poden ser modificades per tal d'obtenir xarxes de mida fixa per tots els individus, basant-se en un atles anatòmic.
c. Les xarxes cerebrals obtingudes mitjançant aquesta tècnica permeten caracteritzar la reorganització cerebral produïda per la RCIU.
d. Els canvis en les característiques de xarxa obtinguts amb aquesta tècnica estan associats amb alteracions al neurodesenvolupament observats en etapes posteriors.

3. Les xarxes cerebrals estructurals basades en MRI de difusió permeten caracteritzar la reorganització estructural persistent a llarg termini en un model animal de conill amb RCIU, essent aquesta reorganització associada a resultats de neurocomportament en aquest animal.
    a. Les tècniques per obtenir xarxes cerebrals estructurals a partir de MRI de difusió poden ser adaptades al cervell del conill en edat pre-adolescent.
    b. La reorganització cerebral estructural produïda per la RCIU a llarg termini pot ser caracteritzada amb un model animal de conill amb RCIU.
    c. Els canvis en les característiques de xarxa obtinguts en edat pre-adolescent estan associats a resultats en el neurocomportament en el model animal de conill amb RCIU.

4. La reorganització cerebral funcional produïda per la RCIU pot ésser caracteritzada en etapa neonatal mitjançant xarxes cerebrals funcionals obtingudes a partir d'adquisicions de MRI funcional durant són natural, essent aquesta reorganització funcional associada als resultats de neurocomportament obtinguts en aquests nens.

a. Els mètodes per obtenir xarxes cerebrals funcionals complertes basades en un atles anatòmic poden ser adaptats a poblacions neonatals.
b. Les característiques globals i regionals de les xarxes funcionals permeten caracteritzar la reorganització cerebral funcional produïda per la RCIU en nounats.
c. Els canvis en les característiques de les xarxes funcionals produïts per la RCIU poden ésser associats a resultats de neurocomportament alterats.

12.2.2. Objectius

El principal objectiu d'aquesta tesi és la caracterització de la reorganització cerebral produïda per la RCIU mitjançant característiques de teoria del graf obtingudes a partir de xarxes cerebrals, i la seva associació amb alteracions del neurodesenvolupament.

Els objectius específics són:

1. Caracteritzar la reorganització estructural en infants d'un any que sofriren RCIU, i la seva associació amb alteracions en el neurodesenvolupament observades als dos anys d'edat.
    a. Adaptar les tècniques de l'estat de l'art per obtenir xarxes cerebrals estructurals en una població pediàtrica.
    b. Caracteritzar les alteracions en les característiques globals i regionals de les xarxes estructurals obtingudes en una població de nens d'un any amb RCIU.
    c. Associar les característiques de les xarxes estructurals obtingudes en nens d'un any amb alteracions en el neurodesenvolupament als dos anys de vida.
2. Caracteritzar les alteracions en les xarxes estructurals basades en similitud de característiques de matèria grisa obtingudes a partir de MRI en nens d'un any amb RCIU i la seva associació amb alteracions en el neurodesenvolupament als dos anys de vida.
    a. Adaptar les tècniques existents a poblacions pediàtriques.

b. Modificar les tècniques existents perquè permetin obtenir xarxes amb una mida fixa per tots els individus basant-se en un atles anatòmic.
c. Caracteritzar les diferencies en les característiques globals i regionals de les xarxes cerebrals obtingudes mitjançant aquesta tècnica en una població de nens d'un any amb RCIU.
d. Associar les característiques de xarxa obtingudes a l'any de vida amb alteracions en el neurodesenvolupament als dos anys de vida.

3. Caracteritzar alteracions en la xarxa cerebral estructural obtinguda a partir de MRI de difusió en un model animal de conill amb RCIU a llarg termini i associar aquestes alteracions als resultats de neurocomportament.
    a. Adaptar les tècniques existents al cervell del conill en període pre-adolescent.
    b. Caracteritzar les alteracions en les característiques de xarxa globals i regionals obtingudes de les xarxes cerebrals estructurals del model animal de conill amb RCIU en edat pre-adolescent.
    c. Associar les característiques de xarxa obtingudes en el model animal de conill amb RCIU amb alteracions en els resultats de neurocomportament.

4. Caracteritzar la reorganització funcional produïda per la RCIU en període neonatal i associar-la a alteracions en el neurocomportament.
    a. Adaptar la metodologia emprada en etapa adulta a població neonatal per tal d'obtenir xarxes cerebrals funcionals complertes de tot el cervell basades en un atles anatòmic.
    b. Caracteritzar les alteracions en les característiques globals i regionals de les xarxes funcionals obtingudes en nounats amb RCIU.
    c. Associar les característiques de xarxa obtingudes amb alteracions en el neurocomportament.

12.3. Resum dels articles publicats

12.3.1. PROJECTE 1: Xarxes cerebrals estructurals basades en MRI de difusió en infants d'un any de vida amb restricció de creixement intrauterí

Corresponent a l'article:

Altered small-world topology of structural brain networks in infants with intrauterine growth restriction and its association with later neurodevelopmental outcome

Batalle D, Eixarch E, Figueras F, Muñoz-Moreno E, Bargalló N, Illa M, Acosta-Rojas R, Amat-Roldan I, Gratacos E

2012, Neuroimage 60, 1352-1366

Resum:

La restricció de creixement intrauterí (RCIU) deguda a insuficiència placentària afecta al 5-10% de tots els embarassos i està associat a un ampli espectre d'alteracions en el neurodesenvolupament a curt i llarg termini. Així doncs la predicció dels resultats de neurodesenvolupament en subjectes amb RCIU està entre els reptes clínics de la medicina fetal i pediàtrica moderna. En els últims anys, diversos estudis han utilitzat tècniques

d'imatge per ressonància magnètica (MRI) per demostrar diferències en l'estructura cerebral de subjectes amb RCIU, però la capacitat d'utilitzar MRI amb un propòsit predictiu individualitzat és molt limitada. Resultats de recerca recents suggereixen que l'accés *in vivo* a la connectivitat cerebral que permet la MRI podria tenir un gran potencial per ajudar a comprendre processos cognitius i del neurodesenvolupament. De manera especial, la connectòmica basada en MRI és una tècnica emergent que permet extraure informació de la MRI, podent analitzar de manera exhaustiva el mapa de connectivitat cerebral i construir un model de graf dels circuits neuronals en el que es coneix com una xarxa cerebral. En el present estudi hem utilitzat tècniques de connectòmica basada en MRI per difusió per tal d'obtenir la xarxa cerebral estructural d'una cohort prospectiva d'infants a un any de vida (32 controls i 24 RCIU) i hem analitzat l'existència de reorganització cerebral quantificable en els circuits de matèria blanca en el grup de RCIU, mitjançant mesures de teoria del graf globals i regionals que caracteritzen les xarxes cerebrals. Basant-se en l'anàlisi global i regional de la topologia d'aquestes xarxes cerebrals demostrem reorganització en infants amb RCIU a l'any de vida. De manera específica, els infants amb RCIU presenten una reducció en els seus valors ponderats per anisotropia fraccional en eficiència global i local, i presenten un patró d'alteracions en les característiques de teoria del graf regionals. A més a més, mitjançant una regressió logística binomial, també demostrem que les mesures de connectivitat estan associades amb un comportament anormal en un test de neurodesenvolupament (*Bayley Scale for Infant and Toddler Development, Third Edition*) realitzat als dos anys d'edat. Aquestes troballes demostren el potencial de la connectòmica basada en MRI de difusió i de les característiques de teoria del graf de les xarxes cerebrals obtingudes per estimar diferències en l'arquitectura dels circuits neuronals i desenvolupar biomarcadors basats en imatge de risc de problemes en el neurodesenvolupament en infants amb patologies d'origen prenatal.

12.3.2. PROJECTE 2: Xarxes cerebrals estructurals basades en característiques morfològiques de matèria grisa en infants d'un any de vida amb restricció de creixement intrauterina

Corresponent a l'article:

Normalization of similarity-based individual brain networks from gray matter MRI and its association with neurodevelopment in infants with intrauterine growth restriction

Batalle D, Muñoz-Moreno E, Figueras F, Bargalló N, Eixarch E, Gratacos E

2013, Neuroimage 83C, 901-911.

Resum:

L'obtenció de biomarcadors individuals per la predicció d'alteracions neurològiques és un repte per la medicina moderna i la neurociència. La connectòmica basada en la ressonància magnètica per imatge (MRI) representa una bona eina per extreure informació de la MRI mitjançant la integració de la informació obtinguda en unes poques característiques que poden ser emprades com a biomarcadors individuals de resultats neurològics. Tot i això, aquesta estratègia típicament requereix la utilització de MRI per difusió o MRI funcional per extreure xarxes cerebrals individuals, requerint llargs temps d'adquisició i presentant una alta sensitivitat a artefactes de moviment, problemes especialment crítics quan s'adquireixen imatges de fetus i infants. L'extracció de xarxes individuals basades en la similitud morfològica de la matèria grisa és una nova estratègia que es beneficia del poder d'anàlisi de la teoria del graf per descriure la morfologia de la matèria grisa com una xarxa morfològica a gran escala a partir d'una adquisició clínica típica, com les imatges de MRI ponderades en T1. En el present article proposem una nova metodologia per normalitzar aquestes xarxes morfològiques de gran escala a una xarxa cerebral de mida estandarditzada basada en un esquema de parcel·lació anatòmica. La metodologia proposada és aplicada

per reconstruir xarxes cerebrals individuals de 63 infants amb un any de vida, 41 amb restricció de creixement intrauterí (RCIU) i 22 controls, demostrant característiques de xarxa alterades en el grup amb RCIU, i la seva associació amb els resultats de neurodesenvolupament obtinguts als dos anys de vida mitjançant una regressió ordinal de les característiques de xarxa obtingudes amb un test de neurodesenvolupament (*Bayley Scale for Infant and Toddler Development, Third Edition*). Tot i que cal una caracterització més profunda d'alguns aspectes de la metodologia utilitzada, aquesta es presenta com a un bon candidat per desenvolupar biomarcadors de neurodesenvolupament alterat en població pediàtrica.

12.3.3. PROJECTE 3: Xarxes cerebrals estructurals basades en MRI de difusió en un model animal de conill amb restricció de creixement en edat pre-adolescent.

Corresponent a l'article:

Long-term reorganization of structural brain networks in a rabbit model of intrauterine growth restriction

Batalle D, Muñoz-Moreno E, Arbat-Plana A, Illa M, Figueras F, Eixarch E, Gratacos E

2014, Neuroimage, *In Press*

Resum:

La caracterització dels canvis cerebrals produïts per la restricció de creixement intrauterí (RCIU) representa un dels principals reptes de la medicina fetal moderna i la pediatria. Aquesta condició afecta entre un 5 i un 10 % dels embarassos i està associada a un ampli espectre de problemes del neurodesenvolupament. Una millor comprensió de la

reorganització cerebral produïda per la RCIU obriria una finestra d'oportunitat per trobar biomarcadors d'imatge potencials que permetin identificar els infants amb un alt risc de presentar problemes en el neurodesenvolupament i aplicar teràpies adequades per millorar els seus resultats. Les xarxes cerebrals estructurals obtingudes a partir d'imatge per ressonància magnètica (MRI) de difusió es presenten com a una eina prometedora en l'estudi de la reorganització cerebral que podria ser usada com a biomarcadors d'alteracions en el neurodesenvolupament. En el present estudi aquesta tècnica és aplicada a un model animal de conill amb RCIU, que presenta certs avantatges incloent un entorn controlat i la possibilitat d'obtenir MRI d'alta qualitat amb llargs temps d'adquisició. Utilitzant el model de difusió *Q-Ball*, i un atles del cervell del conill per MRI, obtenim les xarxes cerebrals estructurals de 15 conills amb RCIU i 14 controls, a 70 dies d'edat (equivalent a la pre-adolescència humana). L'anàlisi de les característiques de teoria del graf demostren una reducció en la infraestructura de xarxa (grau mig i força mitja) associada amb la condició de RCIU i un conjunt de mesures ponderades per anisotropia fraccional generalitzada (GFA) associades amb un neurocomportament anormal. Resulta especialment interessant que al caracteritzar l'organització de les xarxes cerebrals de manera independent a la infraestructura individual de cada xarxa, mitjançant una estratègia de normalització, el grup RCIU mostra un increment en la seva eficiència global i local. A partir d'aquest resultat hipotetitzem que aquest efecte es podria explicar degut a una resposta compensatòria a la infraestructura reduïda en RCIU. Aquests resultats presenten noves evidències en la persistència a llarg termini de la reorganització cerebral produïda per la RCIU que podria ésser subjacent a problemes de comportament i neurodesenvolupament prèviament descrits. A més, els canvis demostrat en l'organització de xarxa tenen el potencial d'ésser emprats com a biomarcadors per monitoritzar canvis cerebrals produïts en teràpies experimentals en el model animal de RCIU.

12.3.4. PROJECTE 4: Xarxes cerebrals funcionals en nounats amb restricció de creixement intrauterí

Corresponent a l'article:

Altered resting-state whole-brain functional brain networks of neonates with intrauterine growth restriction

Batalle D, Muñoz-Moreno E, Tornador C, Bargalló N, Deco G, Eixarch E, Gratacos E

Ready to be submitted.

Resum:

La restricció de creixement intrauterina (RCIU) és una condició prenatal prevalent que afecta fins al 10% dels embarassos. S'ha associat amb alteracions a curt i llarg termini en el neurodesenvolupament, però la seva etiologia i fisiopatologia són encara majorment desconegudes. Tot i que diferents estudis han demostrat l'associació de RCIU amb canvis moderats en l'estructura del cervell, el seu efecte en l'organització cerebral funcional mai ha estat caracteritzat. En el present estudi pretenem omplir aquest forat en la literatura, analitzant fluctuacions de baixa freqüència en el senyal de ressonància magnètica funcional d'una població de 20 nounats amb RCIU comparats amb 13 controls. Basant-nos en la correlació parcial del senyal *blood oxygen level-dependent* (*BOLD*) mitjà en 90 regions de matèria blanca, obtenim una xarxa cerebral funcional completa per cada nounat. La caracterització de les xarxes obtingudes en el grup RCIU amb característiques de teoria del graf mostren un increment en la infraestructura de xarxa i en les eficiències calculades de manera directa però una reducció en l'eficiència després de normalitzacions en aquest grup. Aquests resultats suggereixen xarxes cerebrals hiperconnectades però subòptimament organitzades en el grup amb RCIU. A més a més, una associació de les xarxes cerebrals funcionals obtingudes amb els resultats obtinguts en neurocomportament també és demostrada, millorant l'associació obtinguda només amb característiques clíniques.

Característiques regionals de xarxa també són analitzades, mostrant un patró d'alteracions en el grup amb RCIU. Mitjançant una caracterització addicional de la dinàmica espacio-temporal del senyal BOLD, es demostra una tendència a tenir un nivell de sincronització general augmentada en els subjectes amb RCIU, i també es troben una sèrie d'alteracions en característiques associades als còrtexs frontals, cingulats i linguals.

12.4. Resum esquemàtic dels resultats

PROJECTE 1: Xarxes cerebrals estructurals basades en MRI de difusió en infants d'un any de vida amb restricció de creixement intrauterina

- Es demostra la viabilitat de reconstruir la xarxa cerebral estructural en nens d'un any mitjançant MRI de difusió.
- Existeix una reducció de les característiques de xarxa estructurals globals en els nens d'un any amb RCIU.
- Es troba un patró d'alteració en les característiques de xarxa regionals en els infants amb RCIU.
- L'alteració en la topologia de xarxa dels nens d'un any amb RCIU està associada amb alteracions en el neurodesenvolupament als dos anys de vida.
- Les característiques de xarxa dels nens amb RCIU a l'any de vida serveixen per entrenar un algoritme d'aprenentatge que permet classificar a cegues aquells subjectes que tindran un resultat de neurodesenvolupament alterat als dos anys de vida amb un encert del 82.4%.

Resultats suplementaris

Normalització de les xarxes cerebrals estructurals de nens d'un any amb RCIU

- Els nens amb RCIU a l'any de vida tenen una tendència a tenir una organització lleugerament més òptima quan aquesta s'avalua de manera independent a la seva infraestructura reduïda

Xarxes cerebrals funcionals en nens d'un any amb RCIU

- Els nens d'un any amb RCIU presenten unes xarxes cerebrals funcionals amb una certa disminució en alguns dels paràmetres d'infraestructura de xarxa.
- Existeix una certa tendència estadística en els subjectes amb RCIU a tenir unes eficiències augmentades quan es comparen les seves xarxes cerebrals funcionals normalitzades de manera que siguin independents a la seva infraestructura.

En resum, les xarxes cerebrals estructurals i funcionals dels nens d'un any de vida amb RCIU presenten una disminució en alguns dels paràmetres de la seva infraestructura i la seva organització de xarxa bàsica. La reorganització observada està acompanyada d'una certa tendència compensatòria a ser més òptima organitzativament tot i aquesta reducció de la infraestructura de xarxa. Cal destacar l'alt potencial predictiu d'alteracions en el neurodesenvolupament demostrat per les xarxes cerebrals estructurals a aquesta edat.

PROJECTE 2: Xarxes cerebrals estructurals basades en característiques morfològiques de matèria grisa en infants d'un any de vida amb restricció de creixement intrauterina

- Es presenta una nova metodologia que permet resoldre fixar la mida de les xarxes de gran escala individuals obtingudes a partir de similituds en la morfologia de la matèria gris obtinguda amb MRI.
- S'adapta la metodologia existent a una població pediàtrica per primer cop.
- Es demostren diferències en l'organització de les xarxes obtingudes en nens d'un any amb RCIU.
- Es demostra l'associació de les característiques de xarxa obtingudes a l'any de vida amb alteracions en el neurodesenvolupament als dos anys de vida.

En resum, en aquest projecte es demostra la viabilitat d'utilitzar models de xarxa per analitzar la similitud de la morfologia de matèria grisa obtinguda a partir de MRI en poblacions pediàtriques. A més, la població de nens d'un any amb RCIU mostra alteracions en les característiques de les xarxes obtingudes que es relacionen amb alteracions en el neurodesenvolupament als dos anys de vida.

PROJECTE 3: Xarxes cerebrals estructurals basades en MRI de difusió en un model animal de conill amb restricció de creixement en edat pre-adolescent.

- Es demostra que la reorganització cerebral estructural produïda per la RCIU en un model animal de conill és persistent fins a la pre-adolescència, caracteritzant-se per una infraestructura de xarxa reduïda.
- Es demostra un efecte compensatori en els subjectes amb RCIU caracteritzat per un increment de l'eficiència quan les xarxes són normalitzades de manera que els resultats siguin independents a la seva infraestructura.
- Es troba un patró d'alteracions en les característiques regionals de les xarxes cerebrals estructurals que té certes similituds amb l'obtingut en humans amb nens d'un any.
- Les característiques de xarxa globals estan associades als resultats de neurocomportament obtinguts.

En resum, les xarxes cerebrals estructurals del model animal de conill amb RCIU demostren una reorganització estructural a llarg termini causada per aquesta condició prenatal caracteritzada per una reducció en la infraestructura de xarxa i un efecte compensatori a un nivell purament organitzatiu.

PROJECTE 4: Xarxes cerebrals funcionals en nounats amb restricció de creixement intrauterí

- Xarxes cerebrals funcionals de tot el cervell basades en un atles anatòmic són obtingudes per primer cop en una població neonatal.
- Diverses característiques de la xarxa funcional presenten valors augmentats en nounats amb RCIU, mostrant una hiperconnectivitat en la seva organització funcional.
- El grup amb RCIU mostra un patró d'organització funcional sub-òptim caracteritzar per una disminució en l'eficiència de la xarxa cerebral funcional normalitzada.

- Es mostra un patró d'alteracions en les característiques de xarxa regionals del grup amb RCIU.
- Les característiques de la xarxa cerebral funcional obtinguda s'associen amb alteracions en el neurocomportament.

Resultats suplementaris

Xarxes cerebrals estructurals basades en MRI de difusió en nounats amb RCIU

- Les xarxes cerebrals estructurals obtingudes en el grup amb RCIU mostren un increment en les característiques de xarxa obtingudes a partir d'una ponderació per densitat de fibres.

En resum, les xarxes cerebrals funcionals de nounats mostren un patró de co-activació i sincronització de les diferents regions del cervell augmentat en els subjectes amb RCIU, acompanyat no obstant d'una organització sub-òptima. Aquesta reorganització funcional està parcialment recolzada per una reorganització estructural observada en la mateixa edat.

12.5. Discussió

La caracterització dels canvis cerebrals subjacents als problemes en el neurodesenvolupament causats per la RCIU és un dels reptes de la medicina fetal moderna i de la pediatria. De fet, una millor comprensió de la fisiopatologia d'aquesta condició prenatal és essencial per iniciar el desenvolupament de biomarcadors precoços que permetin detectar aquell subgrup d'infants amb un alt risc de tenir problemes en el neurodesenvolupament. En aquest respecte, és important destacar que intervencions precoces individualitzades han demostrat ser una eina molt útil per millorar els resultats funcionals a curt i mig termini en subjectes amb RCIU (Als et al., 2012; McAnulty et al., 2013). Tot i això, donada l'alta prevalença de la RCIU i l'alt cost econòmic de les unitats d'atenció individualitzades, la selecció d'aquells subjectes amb RCIU amb un major risc de problemes de neurodesenvolupament és essencial per aconsellar de manera adient a la família i utilitzar de manera òptima els recursos sanitaris.

Així doncs, un dels principals objectius de la present tesis doctoral és la caracterització sistemàtica i objectiva de la reorganització cerebral estructural i funcional produïda per la RCIU des del període neonatal fins a la pre-adolescència, utilitzant diverses tècniques complementàries que aporten informació sobre diferents aspectes de l'organització i la infraestructura cerebral. En concret, els resultats obtinguts suggereixen que la reorganització produïda per la RCIU està caracteritzada en període neonatal per un increment en les característiques directes de la xarxa cerebral estructural ponderada per densitat de fibres, acompanyada d'una hiperconnectivitat de la xarxa cerebral funcional, tot i demostrar també una organització sub-òptima en termes purament organitzatius. Durant la primera infància (a l'any de vida), els resultats suggereixen que tant la xarxa cerebral estructural com la funcional dels subjectes amb RCIU evolucionen de manera que la seva infraestructura es mostra disminuïda al comparar-la amb controls en aquesta edat, en especial en les xarxes estructurals ponderades per anisotropia fraccional (FA), existint també un efecte compensatori invers al demostrat en etapa neonatal, caracteritzat per un cert increment en l'eficiència de les xarxes cerebrals normalitzades. Aquests efectes de la RCIU a l'any de vida són parcialment confirmats a llarg termini mitjançant l'estudi d'un model

animal de conill amb RCIU, al menys a nivell estructural, suggerint que la reorganització observada a l'any de vida persisteix fins a la pre-adolescència. En resum, el patró de reorganització cerebral estructural i funcional observat en aquesta tesi resulta molt específic quan es compara amb la reorganització produïda per altres patologies, i postula la RCIU com un possible trastorn de la connectivitat cerebral.

Per ser traslladades a la pràctica clínica, les conclusions presentades en aquesta tesi doctoral per primer cop, haurien d'ésser confirmades per altres estudis independents. En aquest sentit, tot i la seva gran dificultat logística, d'especial interès resultarien estudis longitudinals de la RCIU seguint una mateixa població clínica des de l'etapa neonatal fins a l'adolescència. Tot i això, només existeix en la literatura un altre estudi que analitzi la reorganització en les xarxes cerebrals causada per la RCIU (Fischi-Gomez et al., 2014). Aquest estudi demostra la reducció de les característiques de la xarxa cerebral estructural en un grup d'infants amb RCIU als sis anys d'edat, mitjançant una ponderació de la xarxa basada en una combinació de FA i densitat de fibres, recolzant la noció presentada en aquesta tesi que la xarxa cerebral estructural durant la infància presenta una infraestructura reduïda en els subjectes amb RCIU, tal com es mostra en el **PROJECTE 1** i el **PROJECTE 3**.

A més a més, en general, els resultats d'aquesta tesi estan en línia amb altres estudis relacionant neurofunció i xarxes cerebrals. Així doncs, l'eficiència global s'ha demostrat que està associada amb la intel·ligència (Li et al., 2009), i característiques regionals de xarxes cerebrals s'han associat amb èxit amb alteracions cognitives en l'estudi de biomarcadors precoços de malaltia d'Alzheimer (Wee et al., 2010). Els resultats aquí reportats, juntament amb els mostrats per altres estudis en la literatura, suggereixen el potencial d'unir informació global i regional per millorar la comprensió dels mecanismes neurofuncionals subjacents a la connectivitat estructural. A més a més, l'estudi de la connexió entre estructura i la funció cerebral resulta especialment interessant, i estudis posteriors d'aquest aspecte de ben segur aportaran una millor comprensió del cervell durant la infància tant en la salut com sota condicions patològiques. De fet, la combinació del substrat estructural i funcional, sembla tenir un gran potencial per avançar en la comprensió de l'organització

cerebral i la seva relació amb el comportament i el neurodesenvolupmant patològics causats per la RCIU i d'altres condicions prenatals.

12.6. Conclusions

Projecte 1:

- Les xarxes cerebrals estructurals de nens d'un any amb RCIU mostren una infraestructura de xarxa disminuïda produint una organització sub-òptima.
- Les xarxes cerebrals funcionals de nens d'un any amb RCIU confirmen parcialment els resultats obtinguts amb xarxes estructurals.
- Les xarxes cerebrals estructurals a l'any d'edat tenen un alt poder predictiu de nerurodesenvolupament alterat.

Projecte 2:

- És viable utilitzar models de xarxa per analitzar les similituds de la morfologia de matèria grisa en poblacions pediàtriques.
- Els nens d'un any amb RCIU mostren alteracions en la seva xarxa de similitud de morfologia de matèria grisa, associades amb alteracions del neurodesenvolupament.

Projecte 3:

- Les xarxes cerebrals estructurals del model animal de conill amb RCIU mostren una reorganització a llarg termini produïda per aquesta condició.
- Aquesta reorganització es caracteritza per una infraestructura de xarxa disminuïda i un efecte compensatori a un nivell purament organitzatiu, estant associada als resultats de neurocomportament.

Projecte 4:

- La xarxa cerebral funcional en nounats amb RCIU presenta un patró de co-activació i sincronització augmentat, juntament amb una organització sub-òptima.
- Les característiques de la xarxa cerebral estructural de nounats amb RCIU confirmen parcialment els resultats obtinguts en les xarxes funcionals.
- Les característiques de xarxa funcional en nounats estan associades amb alteracions en el neurocomportament.

La conclusió principal d'aquesta tesi és que la RCIU produeix una reorganització de la connectivitat cerebral estructural i funcional des de període neonatal que persisteix fins a la pre-adolescència. Hipotetitzem que aquesta reorganització pot ser un potencial substrat que expliqui l'alt risc de problemes en el neurodesenvolupament en infants amb RCIU. A més, els resultats obtinguts postulen la RCIU com un possible trastorn de la connectivitat cerebral. L'associació de les característiques de xarxa amb alteracions del neurocomportament i el neurodesenvolupament des d'una edat tan precoç és especialment rellevant, doncs obre l'oportunitat a desenvolupar biomarcadors precoços de neurodesenvolupament alterat. Això representaria una oportunitat molt important per millorar la gestió clínica d'una condició que afecta fins al 10% dels embarassos.

13. APPENDIX II: CURRICULUM VITAE

CURRICULUM VITAE

DAFNIS BATALLÉ

Pre-doctoral researcher
Fetal and Perinatal Medicine Research Group
IDIBAPS – Hospital Clínic – University of Barcelona
Barcelona, Spain

Email: dbatalle@clinic.ub.es / dbatalle@gmail.com
Phone: +34 932275400 (ext. 7286) / +34 660805284

EDUCATION

2011 – 2014 (expected)
Ph.D. in Biomedicine (Neuroscience), University of Barcelona (UB)
Fetal and Perinatal Medicine Research Group, Hospital Clínic of Barcelona
Supervisors: Dr. Elisenda Eixarch & Prof. Eduard Gratacós
Dissertation Title: *Brain connectivity network models based on multi-modal MRI to study brain reorganization of prenatal origin using intrauterine growth restriction as a model*

2009 – 2011
M.Sc. in Neuroscience, University of Barcelona (UB)
Master Thesis in Fetal and Perinatal Medicine Research Group, Hospital Clínic of Barcelona
Dissertation Advisors: Dr. Ivan Amat-Roldan & Prof. Eduard Gratacós
Dissertation Title: *Towards diffusion MRI connectomic imaging biomarkers for 1-year old children to quantify brain reorganization in low birth weight*

2001 – 2008
B.Sc. & M.Sc. in Telecommunications Engineering, Polytechnic University of Catalonia (UPC)
Master Thesis in the Image Processing Group, Department of Signal Theory and Communications
Dissertation Advisor: Prof. Montse Pardàs
Dissertation Title: *Foreground extraction and object tracking in video processing and their application for unusual event detection*

RESEARCH EXPERIENCE

2009 – 2014
PhD Candidate & Research Assistant
Fetal and Perinatal Medicine Research Group
University of Barcelona – Hospital Clínic, Barcelona, Spain

- Image and signal processing of structural, diffusion and functional MRI
- Generation of brain networks of pediatric population (neonates and one year old)
- Analysis of alterations produced by pathophysiology in brain network organization
- Machine learning to predict high risk of altered neurodevelopment

2012 – 2012
Guest PhD Student
Signal Processing Laboratory 5 (LTS5)
École Polytechnique Fédérale de Lausanne (EPFL), Switzerland

- 3 months exchange, working on novel graph theory network features

2008 – 2009
Scientific Software Developer
Faculty of Physics, University of Barcelona, Spain

- Software developing (Java) for the Data Processing and Analysis Consortium (DPAC) of the European Space Agency Gaia Spacecraft mission
- Development of tools to validate data processing and simulations

2007 – 2008
Undergraduate Research Assistant
Image Processing Group, Signal Processing Department
Polytechnic University of Catalonia, Barcelona, Spain

- Foreground extraction and object tracking in video processing
- Video feature extraction to detect suspicious events in security monitoring
- Image processing with OpenCV libraries (C/C++)

JOURNAL ARTICLES

Long-term reorganization of structural brain networks in a rabbit model of intrauterine growth restriction
Batalle D, Muñoz-Moreno E, Arbat-Plana A, Illa M, Figueras F, Eixarch E, Gratacos E
NeuroImage, 2014, *In Press* Link

Normalization of similarity-based individual brain networks from gray matter MRI and its association with neurodevelopment in infants with intrauterine growth restriction
Batalle D, Muñoz-Moreno E, Figueras F, Bargallo N, Eixarch E, Gratacos E
NeuroImage, 2013, 83, pp. 901-911 Link

Long-term neurofunctional outcomes and correlation with brain regional connectivity by MRI diffusion tractography metrics in a rabbit model of intrauterine growth restriction
Illa M, Eixarch E, **Batalle D**, Arbat-Plana A, Muñoz-Moreno E, Figueras F, Gratacos E
PLOS ONE, 2013, 8(10): e76453. doi:10.1371/journal.pone.0076453 Link

A Magnetic Resonance Image Based Atlas of the Rabbit Brain for Automatic Segmentation
Muñoz-Moreno E, Arbat-Plana A, **Batalle D**, Soria G, Illa M, Prats-Galino A, Eixarch E, Gratacos E
PLOS ONE, 2013, 8(7): e67418. doi:10.1371/journal.pone.0067418 Link

The ins and outs of the BCCAo model for chronic hypoperfusion: a multimodal and longitudinal MRI approach
Soria G, Tudela R, Márquez-Martín A, Camon L, **Batalle D**, Muñoz-Moreno E, Eixarch E, Puig J, Pedraza S, Vila E, Prats-Galino A, Planas A
PLOS ONE, 2013, 8(9): e74631. doi:10.1371/journal.pone.0074631 Link

Altered small-world topology of structural brain networks in infants with intrauterine growth restriction and its association with later neurodevelopmental outcome (cover art of the issue)
Batalle D, Eixarch E, Figueras F, Muñoz-Moreno E, Illa M, Bargallo N, Acosta-Rojas R, Amat-Roldan I, Gratacos E
NeuroImage, 2012, 60(2), pp. 1352-1366 Link

Neonatal Neurobehavior and Diffusion MRI Changes in Brain Reorganization Due to Intrauterine Growth Restriction in a Rabbit Model
Eixarch E, **Batalle D**, Illa M, Muñoz-Moreno E, Arbat-Plana A, Amat-Roldan I, Figueras F, Gratacos E
PLOS ONE, 2012, 7(2): e31497. doi:10.1371/journal.pone.0031497 Link

MANUSCRIPTS IN PREPARATION

Altered resting-state whole-brain functional brain networks of neonates with intrauterine growth restriction
Batalle D, Muñoz-Moreno E, Tornador C, Deco G, Eixarch E, Gratacos E
In preparation

Evolution of brain network reorganization in preterm IUGR during childhood: a longitudinal study
Muñoz-Moreno E, Fischi-Gomez E, Meskaldji D, **Batalle D**, Vasung L, Eixarch E, Thiran J-P, Gratacos E, Huppi PS
In preparation

CONFERENCE PAPERS

Fiber-tract based analysis of brain damage and neurodevelopment disorders due to intrauterine growth restriction
Muñoz-Moreno E, Eixarch E, **Batalle D**, Gratacos E
Proceedings of the MICCAI workshop on Perinatal and Paediatric Imaging (PaPI 2012)
1 October 2012, Nice, France Link

Altered structural brain network topology in infants with intrauterine growth restriction
Batalle D, Eixarch E, Muñoz-Moreno E, Figueras F, Amat-Roldan I, Gratacos E
Proceedings of the 9th IEEE Inernational Symposium on Biomedical Imaging (ISBI 2012), Pages 554-557
2-5 May 2012, Barcelona, Spain Link

CONFERENCE ABSTRACTS

Functional and structural brain connectivity re-organization assessed by MRI in neonates after intrauterine growth restriction (selected for oral presentation)
Eixarch E, **Batalle D**, Muñoz-Moreno E, Gratacos E
24th World congress on Ultrasound in Obstetrics and Gynecology (ISUOG 2014)
14-17 September 2014, Barcelona, Spain

Longitudinal analysis of brain network reorganization in preterm IUGR children at 1, 6 and 9 years of age
(selected for oral presentation)
Muñoz-Moreno E, Fischi-Gomez E, **Batalle D**, Vasung L, Eixarch E, Thiran J-P, Gratacos E, Huppi PS
22nd Annual Meeting of the International Society for Magnetic Resonance in Medicine (ISMRM-ESMRMB 2014)
10-16 May 2014, Milano, Italy

Resting state brain networks: First evidence demonstrating different functional organization in neonates after intrauterine growth restriction (selected for oral presentation)
Eixarch E, **Batalle D**, Muñoz-Moreno E, Gratacos E
12th World congress in Fetal Medicine
23-27 June 2013, Marbella, Spain

Animal models of intrauterine growth restriction: comparison of neurobehavioral consequences in neonatal and long-term period
Illa M, Eixarch E, **Batalle D**, Muñoz-Moreno E, A Arbat-Plana, Figueras F, Gratacos E
12th World congress in Fetal Medicine
23-27 June 2013, Marbella, Spain

Brain connectivity in one-year-old intrauterine growth restricted infants is abnormal and correlates with neurodevelopment at two years of age (selected for oral presentation)
Eixarch E, **Batalle D**, Muñoz-Moreno E, Figueras F, Gratacos E
22nd World congress on Ultrasound in Obstetrics and Gynecology (ISUOG 2012)
9-12 September 2012, Copenhagen, Denmark

Short and long-term impact of intrauterine growth restriction on neurobehavior, white matter diffusion and connectivity in a rabbit model
Illa M, Eixarch E, **Batalle D**, Muñoz-Moreno E, A Arbat-Plana, Figueras F, Gratacos E
22nd World congress on Ultrasound in Obstetrics and Gynecology (ISUOG 2012)
9-12 September 2012, Copenhagen, Denmark

Altered brain networks and prediction of altered neurodevelopment in infants with IUGR
Batalle D, Eixarch E, Muñoz-Moreno E, Figueras F, Amat-Roldan I, Gratacos E
18th Annual Meeting of the Organization for Human Brain Mapping (OHBM 2012)
10-14 June 2012, Beijing, China

Neurobehaviour and structural brain changes due to intrauterine growth restriction in a rabbit model in neonatal and adult period
Eixarch E, Illa M, **Batalle D**, Muñoz-Moreno E, Arbat-Plana A, Figueras F, Gratacos E
18th Annual Meeting of the Organization for Human Brain Mapping (OHBM 2012)
10-14 June 2012, Beijing, China

Multimodal Brain Atlas of the New Zealand Rabbit based on Diffusion and Structural MRI
Muñoz-Moreno E, Arbat-Plana A, Eixarch E, **Batalle D**, Illa M, Gratacos E
18th Annual Meeting of the Organization for Human Brain Mapping (OHBM 2012)
10-14 June 2012, Beijing, China

Neonatal and long-term neurodevelopment and neurostructure in a rabbit model of Fetal Growth Restriction
Illa M, Eixarch E, **Batalle D**, Arbat-Plana A, Acosta-Rojas R, Figueras F, Gratacos E
43rd European Brain and Behaviour Society Meeting (EBBS 2011)
9-12 September 2011, Sevilla, Spain

Fetal growth restriction: MRI connectomics and neurodevelopment (selected for oral presentation)
Eixarch E, **Batalle D**, Figueras F, Amat-Roldan I, Gratacos E
10th World congress in Fetal Medicine
26-30 June 2011, St. Julian's, Malta

Fetal growth restriction: Evaluation of the fetal rabbit as a model to evaluate neurostructural and neurodevelopmental changes
Illa M, Eixarch E, **Batalle D**, Arbat-Plana A, Acosta-Rojas R, Figueras F, Gratacos E
10th World congress in Fetal Medicine
26-30 June 2011, St. Julian's, Malta

MRI brain connectomics to demonstrate brain reorganization in 1-year-old children with intrauterine growth restriction (selected for oral presentation)
4th CIBERER Scientific Annual Meeting
Batalle D, Amat-Roldan I, Eixarch E, Acosta-Rojas R, Figueras F, Gratacos E
28-29 October 2010, Madrid, Spain

Comparison of Statistical Methods for Studying Brain Regional Connections in Weighted Brain Networks
Batalle D, Calderero F, Gratacos E, Amat-Roldan I
16th Annual Meeting of the Organization for Human Brain Mapping (OHBM 2010)
6-10 June 2010, Barcelona, Spain

OTHER CONTRIBUTIONS

Teaching of "Medical Applications of Engineering I" laboratory (12h), 4th grade of Biomedical Engineering degree
University of Barcelona

Invited speaker to the educational conference ***"Una esperanza para los problemas de origen prenatal"*** **(Hope for prenatal origin problems)**, presenting the results obtained in brain network analysis of IUGR children to a broad audience.
22th November 2011, Cosmocaixa Venue, Barcelona, Spain